Design, Set up and Commissioning of a Test Facility for Smokeless Rich Diesel Combustion Research

Timothy Cole King

Thesis presented for the degree of
Master of Science in Engineering

Sasol Advanced Fuels Laboratory
Department of Mechanical Engineering
University of Cape Town

July 2015

Plagiarism Declaration

1. I know that plagiarism is wrong. Plagiarism is to use another's work and pretend that it is one's own.
2. Each contribution to, and quotation in, this thesis from the work(s) of other people has been attributed, and has been cited and referenced.
3. This thesis is my own work.
4. I have not allowed, and will not allow, anyone to copy my work with the intention of passing it off as his or her own work.
5. I acknowledge that copying someone else's work, or part of it, is wrong, and declare that this is my own work.

_____

Name Surname

Acknowledgements

The author of this report would like to extend his thanks to the following people who have assisted him throughout the project and report:

To Ian and Kim King, my parents, for their on-going support throughout the project. Special thanks must go forward to Gerhard Lourens from SAFL, for his input on design features and continued assistance through the project in his capacity as an electronic instrumentation technician.

Dr Gareth Floweday, for his enthusiastic manner in presenting material and guidance, in his capacity as project supervisor. I would like to thank Paul Schaberg for his expert input into best testing practices used in this project and his general involvement as the project co-supervisor. In addition, I would like to thank Mark Wattrus for his assistance with the control system development. A further thanks to Glen Newins, manager of the UCT workshop, his son Tyrone, and the exceptional workshop team, with special mention to Pierre Smith, for their input in designing for manufacture and various other manufacturing techniques to ensure economical design.

Thanks to my colleagues Dylan Smit, Ross Burnham and Aidan Ehrenreich for their assistance during my time at the Sasol Advanced Fuels Laboratory. I would like to especially thank Dr Toby Rockstroh for his consistent valuable input and mentoring throughout the course of this research project.

Special thanks must be given to my friends, Liam Williams, Liam Burke, Jean Jordaan and Sheldon Yoko for their continued moral support throughout the project. In addition, I would like to thank three other people, critical in the editing and proofing of this report, namely James Boonzaier, Cait Black and Richard King.

Finally I would like to thank the UCT teaching staff for equipping me with tools to systematically solve the design problem presented in this report. Furthermore, I would like to thank them for equipping me with the knowledge that will be valuable in my engineering career.

Abstract

Low Temperature Combustion (LTC)[1] is a strategy that harnesses the properties of exhaust gas, through the use of large quantities of exhaust gas recirculation (EGR), to reduce the peak combustion temperatures below that favoured by the formation processes of oxides of nitrogen (NOx) and those of soot. There is interest within the fuels research community in investigating the effects of diesel fuel formulations on LTC, using a suitable engine test platform. The objective of this study was to design and set up a test apparatus capable of achieving LTC in a diesel research engine, that could subsequently be used to study LTC behaviour with different fuels. In addition, it was necessary to present test data demonstrating the engine's performance, in terms of engine-out emissions and indicated specific fuel consumption (ISFC), transitioning between conventional diesel combustion (CDC) and LTC.

The mechanical, electrical and control requirements for attaining CDC and LTC conditions were investigated in the literature and through consultations with experts in the fuels research field. These requirements were distilled into a definitive System Requirement Specification.

Where possible, off-the-shelf equipment that met the performance requirements stipulated, was chosen for the test apparatus. Components that were beyond the project budget were designed in accordance with their individual requirement specifications. A state-of-the-art single cylinder diesel research engine (AVL5402), representative of a modern-day light duty vehicle, was integrated with various ancillary systems. These systems performed tasks such as conditioning and metering of the intake air and fuel, as well as the analysis of exhaust gas emissions. A custom-built air supply and exhaust system was implemented for accurate control of EGR rate, the facilitation of measurements of important temperatures, pressures, intake and exhaust gas species, as well as minimisation of gas pressure pulsations in the system.

The apparatus was integrated with a control system necessary for managing the operation

[1]There are many LTC strategies that exist. For the purposes of this project, LTC will refer to the smokeless rich diesel combustion strategy.

of the engine and its ancillary systems, as well as recording user-specified data. In addition, custom engine maps were constructed for injection pressure, intake boost pressure and exhaust back pressure (to simulate the back pressure generated by a turbocharger) in an attempt to achieve operating conditions representative of those in a commercial vehicle.

The project culminated in a fully-functional test facility that addresses the requirements of CDC and those of the LTC operating regime. Experimental investigations were conducted using the designed test apparatus in conventional diesel combustion mode, with user control of the relevant diesel engine and fuel research parameters.

The results of a parametric investigation, which involved transitioning the engine operation mode between CDC and LTC at different operating conditions (by individually changing intake boost pressure, intake air mixture temperature and fuel injection pressure) at nominally constant fuelling, demonstrated heightened emissions sensitivity at EGR rates between approximately 45 % and 58 % (this is before the LTC zone). In addition, it was discovered that the peak engine-out soot levels during the transition between CDC and LTC were most effectively reduced by increasing the injection pressure. Furthermore, it became apparent by the contradictions between some of the results presented in this project and what was demonstrated in literature, that the effects of different operating parameters on combustion characteristics and corresponding engine-out emissions cannot be generalised for all operating conditions.

Control and general test apparatus operational challenges experienced at certain stages of this study were documented, and many of them were resolved. However, some of the suggested modifications were not implemented, and are therefore presented as recommendations in this report. The chief recommendations include the implementation of closed loop control of combustion phasing and EGR rate in order to improve combustion control and the efficiency of obtaining setpoint stability for data capturing during test work.

Table of Contents

List of Figures

List of Tables

List of Abbreviations

°ATDC	Degrees after top-dead-centre
°CA	Degrees crank angle
BMEP	Brake mean effective pressure
BP	Boost pressure
BTDC	Before top dead centre
CDC	Conventional diesel combustion
CoV	Coefficient of variance
CP	Cam phase sensor
DI	Direct injection
DPF	Diesel particulate filter
EBP	Exhaust back pressure
EGR	Exhaust gas recirculation
FSN	Filter smoke number
GUI	Graphical user interface
HCCI	Homogeneous charge compression ignition
HP	High pressure
HPL	High pressure EGR Loop
IBDC	Intake bottom dead centre
IC	Internal combustion
ID	Injection duration
IMEP	Indicated mean effective pressure
IMP	Inlet manifold pressure
$ISCO_2$	Indicated specific carbon-dioxide
ISCO	Indicated specific carbon-monoxide
ISFC	Indicated specific fuel consumption
ISFC	Indicated specific fuel consumption
ISHC	Indicated specific hydro-carbons
ISNOx	Indicated specific NOx
ISSoot	Indicated specific soot
LPL	Low Pressure EGR Loop
LTC	Low temperature combustion
LTC	Low temperature combustion

MeUn	Metering unit
MK	Modulated kinetics
PCCI	Premixed charge compression ignition
PCV	Pressure control valve
PPCI	Partial premixed compression ignition
RCCI	Reactivity controlled compression ignition
RP	Rail pressure
SAFL	Sasol advanced fuels laboratory
SoC	Start of combustion
SoD	Start of de-energisation
SoE	Start of energisation
SoI	Start of injection
TDC	Top dead centre
UI	User interface
VFD	Variable frequency driver
VGT	Variable geometry turbochargers

Chapter 1

Introduction

1.1 Current state of diesel engine technology

In the past, diesel engines have typically been viewed by the public in a negative light, due to their large black clouds of particulate matter (PM), oxides of nitrogen (NOx) and sulphurous emissions. With increased recognition and usage of the diesel engine in the 1990s came public pressure to mandate stricter regulations of emissions. Since then, with the ever increasing diesel legislations focussing on emissions of NOx and soot, the need for advanced methods of reducing engine-out emissions has been on the rise.

European vehicle emissions are representative of international best practice. Furthermore, the South African automotive industry standards are aligned with those in Europe [7]. It is therefore appropriate that South African vehicle emissions follow European standards. South Africa is currently compliant with the requirements of Euro 2. Furthermore, the South African Petroleum Industry Association (SAPIA) stipulated in 2011 that they are in support of a quantum leap from Euro 2 to Euro 5 by 2017 [8]; however, since then the department of energy has announced that this deadline will be delayed [9].

Over the past few decades, reduction in exhaust emissions from diesel engines has been achieved using a combination of cleaner fuels, improved combustion strategies and innovative mechanical design. Some of these methods include uncooled Exhaust Gas Recirculation (EGR), widely accepted as the primary Euro 2[1] light-duty vehicle NOx reduction strategy in 1996 [10], and cooled EGR which became the standard in light-duty engines after

[1]The different stages of the European light-duty standards are commonly referred to as Euro 1, Euro 2 etc, where the number is applied chronologically. For heavy-duty European emissions standards, the number is replaced by Roman numerals.

Euro 4 (after 2005) [10]. With Euro 2 and Euro 3 emissions legislations (1996 and 2000) came the widespread use of oxidation catalysts primarily to reach the required reduction in carbon monoxide (CO) and hydrocarbon (HC) emissions [11]. In addition, the use of after-treatment systems such as NOx reduction catalysts and diesel particulate filters were used after Euro 3, in an attempt to meet regulated emissions standards. However, the high fuel sulphur content (50 ppm and greater) prior to 2004 (before the launch of the *Euro 4 enabling fuel specifications*) [12] caused a reduction in DPF and NOx catalyst efficiencies, as well as increased PM. Consequently, in some cases, the expensive exhaust after-treatment systems, have a fuel consumption penalty (cost of regeneration at reduced operating intervals due to high fuel sulphur content) [11]. This issue hyped the much anticipated launch of EU Directive's 2009.01 'Sulphur-free' diesel specification (10 ppm) for vehicle manufacturers in 2009 [12]. Similar sulphur-content specification diesel standards were implemented in Japan [13] and North America [14] over the same time period. The rest of the world began to follow suit, including South Africa. With Sasol's launch of *Sasol turbdiesel^{TM} ULS* [2] *10ppm* in 2013, they have already reached the South African Clean Fuels 2 sulphur restriction standard, which was originally set to be implemented in 2017, but has since been delayed [9].

1.2 Pressures on future engine development

With Euro 6c emissions legislations set to take effect on 01 September 2017 and corresponding potential for tightened NOx, CO and HC emissions (still to be confirmed [15]), new and innovative ideas are required. As combustion understanding and technology has improved, researchers have increasingly been using in-cylinder approaches for investigating means of reducing emissions to meet regulatory requirements. The result of this could have the potential to eliminate the need for, or reduce the complexity of, after-treatment systems. In addition, after-treatment catalysts, such as diesel particulate filters (DPF) require regeneration, typically using fuel, therefore, improvements of engine-out emissions can in some cases indirectly improve fuel consumption. An example of an in-cylinder approach for achieving cleaner emissions is Low Temperature Combustion (LTC). If successfully implemented, LTC could provide engine manufacturers with an alternative method to conventional diesel combustion (CDC) for achieving future emissions legislations.

[2] Ultra-low sulphur diesel is a globally recognised term referring to low sulphur-content diesel fuel. There is no single standard set of specifications and the definition is permanently evolving with stricter government mandated standards

1.3 Low temperature combustion

The phrase 'low temperature combustion' encapsulates numerous combustion strategies which share a common characteristic, specifically that the majority of the fuel is premixed before the start of ignition. This form of combustion is typically characterised by low peak cylinder temperatures, reduced NOx and PM emissions, and generally increased HCs and CO.

Due to the need for advanced injection timing, and the corresponding low in-cylinder charge density and temperature that exists at this point, there is typically a longer liquid jet penetration which can result in fuel accumulation on the cylinder surfaces. Consequently, only partial burning of the fuel occurs, combustion efficiency deteriorates, and HC and CO emissions rise. Normally oxidation catalysts could be used as a counter measure, however LTC exhaust gas temperatures are often too low for them to work effectively [16]. Therefore, a significant technical challenge with LTC is improving the combustion efficiency, whilst simultaneously reducing the NOx and PM emissions.

Additionally, unlike conventional diesel cycles, where phasing controlled combustion is precise and directly related to start of injection (SoI) [17], LTC cycles have less authority on phasing control, especially in homogeneous charge compression ignition (HCCI). Significant cycle-to-cycle variations in EGR-induced LTC, such as the smokeless rich diesel combustion strategy, is common. This is predominantly caused by the increased ignition delay due to raised CO_2 and lowered O_2 concentrations present in the combustion chamber. The lengthened ignition delays typically increase air-fuel mixture homogeneity before combustion starts. This makes predicting the start of combustion (SoC) challenging, therefore adding a degree of complexity to combustion phasing control. Combustion efficiency deteriorates with increased ignition delay and as a result there is a fluctuation in the combustion products. This causes enhanced consecutive cycle variation due to varying cylinder charge temperature, pressure and composition [18].

In summation, it has been demonstrated in the literature that LTC is effective in reducing NOx and soot emissions. However, it would appear that there are still many challenges associated with LTC that are yet to be addressed. Until such a time as these challenges have been sufficiently resolved, implementation of LTC strategies into production engines does not seem to be a viable option.

1.4 Project scope

The project entailed the design, construction and commissioning of a test facility, which utilises a light duty single cylinder diesel research engine, capable of operating under CDC as well as in the LTC regime. For the purposes of this work the *test facility* will refer to the room and all of the testing apparatuses included in the room. The project objectives were to:

i. understand diesel combustion and emissions characteristics under LTC conditions induced by EGR,

ii. perform, where necessary the mechanical design, fabrication and construction of some of the contents of the facility,

iii. integrate the mechanical and electrical aspects of the test apparatus,

iv. design and integrate aspects of the control system,

v. perform proof of design tests on the facility for commissioning and to assess whether LTC (as defined in Chapter 5) could be achieved with the designed test apparatus, without the need for exhaust gas after-treatment systems,

vi. perform a basic repeatability study illustrating the effects of transitioning between CDC and the LTC regime, on emissions and engine performance, and

vii. undertake a simple parametric assessment of the engine's operational characteristics as EGR rates are increased, focusing on the operational areas of LTC transition and LTC mode.

The operation of the engine needed to be representative of a light duty, commercially available vehicle, and so it was assumed that fuel injection pressure maps, as well as inlet air boost pressure and exhaust gas back pressure maps based on existing data were to be designed and implemented into the control system. The aim of the objectives was to develop a practical and theoretical understanding of LTC and the challenges involved, as well as to provide Sasol with a tool to further their fuels research in LTC.

Chapter 2

Literature review

Understanding the pollutant formation processes and what factors affect their production rates during combustion is key for understanding the reasoning behind existing combustion strategies and the development of alternative ones. The combustion process is largely impacted by in-cylinder conditions such as intake temperature, boost pressure, degree of fuel atomisation and oxygen. Thus, understanding how they affect engine-out emissions is critical for emissions reduction.

Due to the large demand for high-performance and fuel-efficient vehicles, as well as the increasingly stringent emissions legislations on the horizon, technologies for the control of in-cylinder conditions have been and continue to be developed. These technologies have the potential to improve fuel efficiency and reduce emissions. After-treatment systems currently play a major roll in reducing tail-pipe emissions; however, alternative in-cylinder approaches are becoming increasingly attractive.

The aim of this chapter is to summarise key literature and concepts pertaining to CDC and LTC technology. Alternative LTC combustion strategies will also be discussed along with their benefits and shortcomings.

2.1 Diesel engine emissions

Regulated diesel emissions are the emissions discharged from the exhaust which have legal upper limits attached to them specified by various standards such as Euro and EPA emissions legislation. These include [19]:

i. Diesel particulate matter (PM), comprising predominantly carbon molecules with ad-

sorbed HC's.

ii. Nitrogen oxides (NOx), composed of nitrogen dioxide (NO_2) and nitric oxide (NO). Other nitrogen containing oxides, such as N_2O, are not regulated.

iii. Hydrocarbons (HC), regulated as either total hydrocarbon emissions (THC) or as non-methane hydrocarbons (NMHC). In some cases a combined limit for HC and NOx is used in place of the separate limits.

iv. Carbon monoxide (CO).

Additionally, internal combustion (IC) engines emit H_2O and carbon dioxide (CO_2). The significant quantities of the greenhouse gas, CO_2, being pumped into the atmosphere draws extensive attention to engines. Diesel combustion noise pollution is also an area of concern with relation to vehicle comfort and overall refinement. This noise is related to the pressure rise rate within the cylinder. The maximum rate of pressure rise is a constraint on diesel operation and studies have shown that this operating parameter is typically limited to 10 bar/°CA (bar per degree crank angle) [20,21]. However, since a single injection strategy (typically resulting in greater peak pressure rise rates) was employed for this project, the maximum allowable rate of pressure rise was increased to 15 bar/°CA. However, this is not a focal area for the purposes of this project and will therefore not be discussed at length.

The primary aim of the subsequent sections is to provide the reader with background on the various emissions and how they are formed (as a means of contextualising the purpose of this particular study)

2.1.1 Nitrogen oxides (NOx)

Nitrogen oxide pollutants contribute to the production of acid rain, photochemical smog and nitrate chemicals [22]. These resulting substances are acidifying the earth's waters, detrimental to the rain forests, and adding to the tropospheric smog, thus causing damage to human health and the environment.

There are many different nitrogen oxides emitted as a result of diesel combustion; however, the two most important are NO and nitrogen dioxide (NO_2). Collectively these two molecules are referred to as NOx. 70 % to 90 % of engine-out NOx is comprised of NO [23]. NOx is a direct result of high temperature combustion, where as other emissions are due to incomplete combustion. NO formation can be described by the extended *Zeldovich Mechanism* (also referred to as the *thermal mechanism* [24]) as follows:

$$O + N_2 \leftrightarrow NO + N \tag{2.1.1}$$
$$N + O_2 \leftrightarrow NO + O \tag{2.1.2}$$
$$N + OH \leftrightarrow NO + H \tag{2.1.3}$$

At temperatures above 2200 K molecular oxygen forms elementary oxygen [24]. In lean areas and temperatures generally above 2000 K this elementary oxygen reacts with N_2 to form NO and N. The N formed in the initial reaction then reacts with O_2 to form NO and O. This process repeats itself, forming NO. Thus two prerequisites for NO formation are:

i. High localised peak temperatures

ii. Excess air, especially in these peak temperature regions

Gases burnt before compression top dead centre[1] (TDC) are of great importance. This hot burnt gas is compressed to higher temperatures and pressures. The temperatures reached are higher than that of any other region of the charge. It is for this reason that almost all of the NOx formation occurs within the first 20 °CA (degrees crank angle) after the start of combustion [24]. It is therefore typically the focus area when trying to minimise NO formation.

There are other mechanism of NO formation such as:

i. *Prompt NO*, otherwise known as the Fenimore NO mechanism [25], resulting from the reaction of N_2 with fuel radicals

ii. NO from the reactions of fuel-based nitrogen

iii. The formation of NO from N_2O

These mechanisms tend to be considered as secondary and less important in conventional diesel combustion. However, Fenimore discovered that there is NO being promptly formed in the diffusion flame of a hydrocarbon fuel [25], before that formed by the Zeldovich Mechanism [26]. He called this *promt NO*. The most critical pathway for this means of NO formation is the rapid reaction of hydrocarbon radicals, from fuel, with molecular nitrogen. The resulting amine species react to form NO. Prompt NO is most prevalent in rich flames, and at temperatures lower than 2000 K it dominates the thermal NO formation rate [26]. Therefore, for LTC, where richer overall air-fuel ratios exist and temperatures are lower, relative to conventional diesel combustion, and thermal NO formation is practically non existent, promt NO becomes important.

[1]Compression top dead centre (or compression TDC) refers to the instantaneous point at which the piston is at the top of its compression stroke, i.e. just before the commencement of the expansion stroke

2.1.2 Particulate matter (PM)

Particulate matter comprises an insoluble fraction (ISF) and soluble organic fraction (SOF). Carbonaceous compounds (soot) make up the bulk of the ISF. Diesel particulate matter contains a variable quantity of soot, but typically exceeds 50 % [27].

Soot formation has been commonly accepted to take place in five steps, namely:

i pyrolysis,

ii nucleation,

iii coalescence,

iv agglomeration, and

v oxidation.

Pyrolysis involves the changing of an organic compound's (fuel) molecular structure at elevated temperatures (typically $>$ 750 K [28]) and limited oxygen availability, without significant oxidation. Since these reactions are generally endothermic, their rates can be temperature dependent. When a fuel pyrolysizes, polycyclic aromatic hydrocarbons form (PAH) form and these species are soot precursors. The presence of these precursors are a result of competing fuel pyrolysis with precursor and pure fuel oxidation. The rates of pyrolysis and oxidation increase with temperature; however, oxidation increases faster [27]. The condensation of PAH's and other unsaturated hydrocarbons lead to the appearance of minuscule soot particles (diameter $<$ 2nm [17]), these are commonly referred to as nuclei [17]. The nucleation process is temperature dependent and nominally begins to occur between 1300 K and 1600 K [27]. Whilst the presence of these nuclei add negligible soot mass; they provide a hot reactive surface to which gas phase hydrocarbons can attach themselves. Typically, during this process, the number of particles remain constant and only the particle mass increases [27,29]. This process is commonly known as surface growth. Coalescence and agglomeration both involve the combining of particles. Their point of difference is that coalescence involves the combining of two spherical shaped masses to form a single spherical shape of combined mass, whereas agglomeration is when individual particles stick together, each keeping their original shape.

Soot and soot precursor oxidation can take place at any point where both soot and oxidising species are present in temperatures exceeding 1300 K [25]. Soot oxidation rates are very dependent on temperature, pressure and equivalence ratio. Tree and Svensson found that soot oxidation will effectively cease at temperatures below 1300 K and soot formation rates favour temperatures above 1500 K [27]. From the well known $\phi - T$ map (illustrated in Figure 2.2 and discussed in more detail in Section 2.3) which illustrates the conditions

for NOx formation, soot formation and soot oxidation, it can be seen that combustion processes containing high equivalence ratios and temperatures favour all phases of diesel soot formation. Combustion pressures also have a significant effect on soot formation rates. Tree and Svensson found that an increase in pressure increases soot formation at a rate which could be as high as the square of the pressure [27].

During diesel combustion, both soot formation and soot oxidation take place. The nett result of these two reactions is the soot emitted from the engine. Refined mixing between the fuel and charge typically has a result of lowering the local equivalence ratios resulting in less soot formation. The impact temperature has on soot formation and oxidation is somewhat complex, the extent of which is dependent on local air-fuel ratios ($\phi - T$ map [3]). The presence of elevated temperatures, soot, and their oxidisers in the later part of combustion can improve the efficacy of the oxidation reactions, typically reducing the emitted soot. Furthermore, these conditions are somewhat undesirable as they increase NO formation rates. However, if local temperatures are reduced to below the soot formation temperature at corresponding equivalence ratios ($\phi - T$ diagram), soot oxidation reactions would become less critical, and thus both NOx and soot engine-out emissions could be reduced. This fact facilitates the concept of LTC for combined soot and NOx reduction.

2.1.3 NOx-soot trade-off

The preceding section has highlighted that conditions that have adverse effects on engine-out soot, promote NOx formation, and that the converse applies. Reducing combustion temperatures by means of retarded start of injection (SoI) or exhaust gas recirculation (EGR) can be effective in reducing NOx; however, the lowered cylinder temperatures in the later parts of combustion slow oxidation rates, subsequently increasing engine emitted soot. Advancing SoI typically results in a larger premixed phase of combustion and thus elevates peak cylinder temperatures, as well as shortening the overall combustion duration. As mentioned in Section 2.1.2, soot oxidation increases faster with temperature than the soot formation process, therefore reducing soot emissions. Although higher injection pressures can also be an effective means of reducing soot emissions, by promoting mixing and increasing premixed combustion, the resulting elevated temperatures and lean environment are favourable for NOx formation rates.

There are a few strategies that exist to effectively reduce both the NOx and soot emissions simultaneously. Two of these are outlined below:

i. Homogeneous charge compression ignition (HCCI) involves producing a very lean and homogeneous charge, the effect of which both reduces the peak in-cylinder temperatures below that required for the formation of NOx, and lowers the local air equivalence ratio inhibiting soot formation.

ii. Smokeless rich diesel combustion is a strategy that uses high EGR rates (typically greater than 50 %) to reduce the peak combustion temperatures below that favoured by soot and NOx formation processes.

2.1.4 Hydrocarbons and carbon monoxide

Engine-out hydrocarbons in diesel engines comprise of unburned fuel and partially oxidised fuel species. The magnitude of these emissions vary greatly with engine operating conditions, and it is probable that a wide variety of different formation mechanisms will be at work. The two primary conditions in conventional diesel combustion that result in HC formation are *over-mixing* and *under-mixing* within the cylinder [17]. *Over-mixing* is when the air fuel mixture becomes leaner than the lean combustion limit ($\phi \approx 0.3$). In swirling flow, the auto-ignition point is typically located in-between the rich core and lean outer boundary of the injected plume. The lean outer boundary zone contains fuel that has been mixed beyond its combustion limit, and is unable to auto-ignite, generally resulting in partial oxidation via thermal oxidation reactions. The quantity of HC's formed in these lean regions is dependent on ignition delay, fuel injection quantity during the ignition delay period, rate of mixing during this period and how conducive the prevailing cylinder conditions are to auto-ignition [17]. Experimental data from a DI, naturally aspirated engine, demonstrates that there is a strong correlation between ignition delay and engine emitted HC's [17]. As ignition delay increases, HC emissions rise at an increasing rate. Hence, fuel injected during the ignition delay period has a significant contribution to HC emissions.

The sources of HC emissions due to *under-mixing* have been limited to two mechanisms. The first is the low velocity fuel which leaves the injector (injector dribbling), most importantly the nozzle sac volume (volume in the tip of the injector after the needle seats), and the second being the quantity of excess fuel when the engine is over-fuelled [17, 23]. An additional source of hydrocarbon emissions exist and is said to be due to quenching outside the piston bowl, in the squish volume. Heywood refers to an experiment in a direct injection engine that showed a 30 % decrease in hydrocarbon emissions when the oil and coolant temperatures were increased from 40 °C to 90 °C [17]. Since ignition delay was kept constant, the possible change in HC emissions due to over-mixing can be considered negligible, therefore leaving the primary source of increased HC's to the quenching phenomena.

The CO emitted from IC engines is primarily controlled by the equivalence ratio [17], and is a direct outcome of incomplete combustion. Any CO formed in a diesel engine is due to insufficient mixing, and therefore higher peak local equivalence ratios exist during combustion which increases the tendency for incomplete combustion [30]. Since diesel engines run lean, CO formation is not commonly a concern with respect to regulated emissions. However, in the case of LTC where EGR rates are high, the air-fuel ratios can become too

rich, resulting in incomplete combustion.

HC and CO are transitional species, and given high enough temperatures and mixture rates, will oxidise almost completely before being pumped out the engine. Thus, in conventional diesel combustion these emissions are not of great concern. However, using strategies such as LTC, where ignition delays are substantial, peak combustion temperatures and over all equivalence ratios are lower, typically result in THC and CO being unable to oxidise sufficiently. Since the use of LTC to achieve regulated emissions limits can be used at loads up to 50 % [31], HC emissions caused by injector dribbling will be dominant as far as under-mixing mechanisms are concerned. This is due to low combustion temperatures, especially later-on in combustion, being unable to fully vaporise and oxidise the fuel from the sac volume (to a greater extent than usual). Additionally, it is necessary to substantially advance injection timing, sometimes as much as -25 °ATDC (depending on the EGR rate), in order to maintain optimum combustion phasing in terms of best indicated specific fuel consumption (ISFC). The cool, low density mixture formed during early injection results in a longer liquid jet penetration relative to that present during conventional diesel combustion SoI. Dec illustrated that in conventional diesel combustion, liquid jet penetration length is in the region of 25 mm [25]. Musculus demonstrated that typical liquid jet penetration when operating under LTC operating conditions, is lengthened (35 mm or greater) [32]. The extended penetration suggests a likelihood of wall wetting and possible flame quenching, resulting in increased CO and unburned hydrocarbons.

2.2 Current diesel engine technologies

2.2.1 Fuel injection systems

Fuel injection systems have advanced extensively since the 1990s. The objectives have been to provide driver comfort in terms of engine noise and vibration comparable to that of a gasoline fuelled engine, future emissions compliance and improved fuel consumption [33]. Systems, including electronically controlled distributor pumps, electronically controlled unit injectors and common rail systems have all been an area of focus to varying degrees.

Common rail injection systems have distinct advantages over other fuel system architectures. These include the:

i possibility of multiple injection events used for:

- pre-injections (1 or 2) for NOx and noise control,
- rapid injection rates for heat release control,
- post injection for soot burn-up and additional post injection for exhaust catalyst heating or regeneration when needed.

ii decoupling of rail pressure from engine speed,

iii smoothing of torque fluctuation on the drive-shaft.

In the case of globally higher equivalence ratios, such as the high EGR LTC conditions, high injection pressures improve the air utilisation with enhanced mixing and better fuel vaporisation and thus optimising the combustion efficiency. Han et al. demonstrated successful reduction in peak soot levels across the EGR range when comparing tests conducted at 400 bar and 1200 bar injection pressure [34]. Many studies have shown a reduction in peak soot levels across the EGR range with little or no effect on NOx (depending on EGR rate) at similar high injection pressures (typically over 800 bar) [1,35].

2.2.2 Turbocharging

Turbochargers consist of a compressor wheel and an exhaust gas turbine wheel coupled by a solid shaft. The exhaust gas turbine extracts energy from the exhaust stream, ultimately resulting in the rotation of the compressor wheel. Consequently, inlet air is drawn into the compressor wheel and pumped into the engine under pressure. This increases the mass of oxygen in the cylinder allowing for greater quantities of fuel to be injected whilst still operating the engine at favourable air-fuel ratio [36]. That is to say, turbochargers increase the engine's power density (power per unit of engine volume) by utilising the exhaust gas mass flow rate and enthalpy. The main incentives behind turbocharging include [37]:

i. maintaining power at different altitudes,

ii. the ability to use smaller and lighter engines to provide output power equivalent to that of larger capacity naturally aspirated engines,

iii. raising the engines peak torque and power output, and

iv. improving the fuel efficiency of engines, particularly the such engines that operate predominantly under full-load conditions.

Simple fixed geometry turbochargers have to make a compromise between maximum power and the shape of the torque speed curve. If a turbocharger of this type is matched to an engine such that it provides high torque at low speeds, it is probable that at high engine speeds, large exhaust back pressures, over spinning of the turbine and over boosting of the engine will occur. As a counter-measure, a waste-gate is generally utilised to by-pass excess exhaust mass flow at high engine speeds. However, this is not very efficient and results in large quantities of potentially usable hot exhaust gas being wasted. A potential means of eliminating the inherent compromise is through the use of variable geometry turbochargers (VGTs) which utilise servo-controlled guide-vanes to control the angle of the air-flow onto the turbine blades. This enables improved control of the exhaust back pressure (EBP) and inlet boost pressure. Therefore, VGT's can indirectly reduce pumping losses, fuel consumption and result in enhanced engine transient response [30, 38].

In addition to being used for charge densification, modern day VGTs are also play a major role in the combustion process control. With the added element of nozzle size control, VGTs are being used to control the EBP, and thus EGR rate, in conjunction with boost pressures. Compared to naturally aspirated engines, intercooled turbocharging, where the boosted air is cooled using an intercooler before it enters the cylinder, has the ability to increase the air-fuel ratio (for a given fuelling condition) and reduce soot [38]. NOx is typically reduced through the use of EGR and once again can benefit from the VGT's functionality. It follows that the turbocharger's role within and transitioning to the LTC regime is critical.

2.2.3 Exhaust gas recirculation (EGR)

EGR is a process by which a portion of the exhaust gas is recycled and mixed with fresh charge before entering the cylinder. This process results in in-cylinder O_2 reduction and exhaust gas species increase, specifically CO_2 and H_2O. There are two ways that EGR is typically achieved [10, 24], via a:

i high pressure loop (HPL or high pressure EGR), or

ii low pressure loop (LPL or low pressure EGR).

The HPL extracts exhaust gas upstream of the turbine and generally cools the gas in a dedicated EGR cooler before mixing it with the fresh charge (atmospheric air), typically just before the intake plenum chamber where the intake charge is at boost pressure. In order to support EGR flow, the EGR has to be at a pressure above the boost pressure. The LPL extracts exhaust gas down stream of the turbocharger and passes it to the inlet, upstream of the compressor. This form of EGR involves a longer pathway and therefore

results in a decreased transient response rate [10,24]. Using a LPL also puts added stresses on the compressor and dedicated EGR cooler system in terms of corrosion and/or erosion due to the presence of sulphur dioxide and sulphuric acid typically expected in the exhaust stream [24]. However, improved mixing with the fresh charge and cylinder to cylinder uniformity is generally achieved.

When exhaust gas is mixed with the fresh charge, it can either replace a portion of the fresh air that would typically enter the cylinder "replaced EGR" or be additional air to the mixture "additional EGR" (where the words 'replaced' and 'additional' are referring to the fresh charge) [24]. For the purposes of this project, only "replaced EGR" will be used and will henceforth be referred to as "EGR".

In the 1990s, Ladommatos et al. worked extensively toward the description of the effect of EGR on diesel combustion. The mechanisms, according to Ladommatos et al. [10, 39–42] are:

i. The *dilution effect* describes how the replacement of oxygen with exhaust gas results in flame temperature and NOx reductions. This effect is the most significant for NOx emissions reduction.

ii. The *added-mass effect* describes how by adding a denser diluent (exhaust gas) to the intake air, the engine-in (into the cylinder) mass flow rate is increased. The change in heat capacity due to the additional mass flow can be termed the added-mass effect. This effect works hand-in-hand with the *thermal effect.*

iii. The *thermal effect* is typically a direct consequence of the addition of the tri-atomic molecules CO_2 and H_2O, present in exhaust gas, to the intake charge, both of which have significantly greater specific heat capacities than fresh air. This effect is only as a result of increased specific heat capacity in the combustion zones. It has been shown that this effect is secondary to that from lowering the O_2 concentration. The equation shown below describes the increase in heat absorption (ΔQ) of the non-reacting gasses, where Δm_0 is the increase in mass entering the cylinder, c_p is the average specific heat capacity at constant pressure and ΔT is the temperature differential between that of combustion and the EGR.

$$\Delta Q = \Delta m_0 c_p (T_{combustion} - T_{EGR}) \tag{2.2.1}$$

iv. The *chemical effect* (EGR species affecting chemical reactions and peak cylinder temperatures) is due to the reactions that may take place as a result of intake exhaust gas. For example, the heat absorption due to the endothermic dissociation reactions of CO_2 and H_2O. However, these effects have been shown to be very small relative to the other mechanisms at work. It is suspected that at high EGR rates the partially cracked HCs, CO and OH radicals in LTC could have a significant effect on auto-ignition time-scales.

These mechanisms all cause a reduction in combustion temperatures, thus having a large effect on emissions. Thermal NO formation effectively ceases and if temperatures drop below 1600 K, soot formation will slow and potentially stop [27]. However, the temperature reduction is not sufficient to stop the prompt NO formation, which then becomes the dominant NOx contributor at high levels of EGR. As a consequence of the lower temperatures, THC and CO oxidation rates slow.

Uncooled EGR can result in an increased mixture temperature in the manifold. There is an inherent lower density and therefore less mass is able to enter the cylinder. The effect of this is called *thermal throttling* [43] and is dependent on EGR rate, exhaust gas temperature and rate of heat transfer from the EGR system. However, at low loads, uncooled EGR can cause improved combustion stability, shorter engine warm-up time and prevent condensation in the intake manifold [10]. Cooled EGR results in both an increased mass in the cylinder and a greater difference between combustion temperature and EGR temperature. Therefore as seen in Equation 2.2.1, the resulting effect is greater heat absorption and even lower combustion temperatures, leading to lower NOx emissions. At high EGR rates combustion becomes very sensitive to small changes in EGR, and can impact phasing, emissions and cycle-to-cycle variation.

2.3 Low temperature diesel combustion

In literature there are many strategies that fall under the LTC umbrella term, such as HCCI, partial premixed compression ignition (PPCI) and premixed charge compression ignition (PCCI). These strategies use methods such as EGR that result in lowered peak flame temperatures which inhibit thermal NO formation. However, different means are used for the reduction in PM, such as ultra lean combustion in the case of HCCI; improved air-fuel mixing as in the case of PPCI; or lower local equivalence ratio by not using EGR and increasing the premixed burn rate via controlling injection timing and pressure as in PCCI [4]. Another LTC combustion strategy termed *smokeless rich diesel combustion* [3], uses additional EGR (typically more than 50 %) to further lower the peak flame temperatures to below the soot formation temperature. For the purposes of this project LTC will refer to smokeless rich diesel combustion, and abbreviations corresponding to other 'LTC' strategies will be used when referring to them.

The point at which LTC is achieved is typically defined by target NOx and soot engine-out emissions. However, these values tend to vary among researchers; for example, Yao et al. used 1.5 g/kWh and 0.1 g/kWh for indicated specific[2] NOx (ISNOx) and indicated specific soot (ISSoot) respectively [1], whereas Asad et al. used 0.2 g/kWh and 0.01 g/kWh (also

[2]Indicated specific emissions are reported in terms of mass flow rate of the exhaust species over indicated power (calculated from cylinder pressure) in g/kWh.

on an indicated basis) [2]. In this project a similar approach is used to frame LTC relative to typical emissions standards and is discussed in more detail in Section 5.1.

Figure 2.1 shows data from EGR sweeps performed by Yao et al. [1] and Asad et al. [2]. It demonstrates ISNOx and ISSoot as a function of EGR and the trade off that exists between ISNOx and ISSoot as discussed in Section 2.1.3. Two of the data sets are of tests performed by Yao et al. and illustrated by the blue and black curves. The orange curve is the test performed by Asad et al. and only included an EGR sweep from 45 % EGR. All three tests show how ISNOx decreases with EGR and how ISSoot initially increases to a maximum with increasing EGR before dropping off. Until the ISSoot maximum turning point all three tests show the trade-off between reducing ISNOx and increasing ISSoot. The different data magnitudes and peak soot values and location relative to EGR rate can be attributed to the different test conditions.

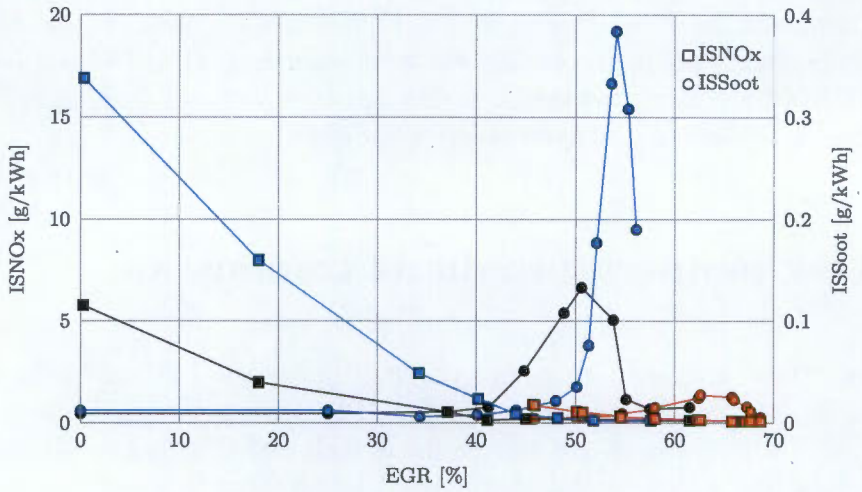

Figure 2.1: *ISNOx and ISSoot as a function of EGR using data taken from tests performed by Yao. et al. and Asad et al. [1, 2].*

Akihama et al. developed a map to show how soot and NOx formation varies with local equivalence ratio and temperature ($\phi - T$ map) [3]. A detailed chemical kinetic model was used which accounted for most of the processes involved in soot formation as discussed in Section 2.1.2. Very coarse combustion regions within this map were defined for HCCI, smokeless rich diesel combustion (LTC) and an ideal high temperature combustion (CDC) region. It was realised that increased EGR rate shifts combustion to lower temperatures and that if these temperatures are low enough to inhibit soot formation, fuel-air mixing has no effect on soot formation. Neely et al. used a similar map and refined the regions in which smokeless rich diesel combustion, HCCI, PCCI and conventional diesel combustion occur [4]. Adomeit et al. showed soot oxidation's dependency on local equivalence ratio and temperature [5]. For the reader's ease of comparison, these three maps in the cited

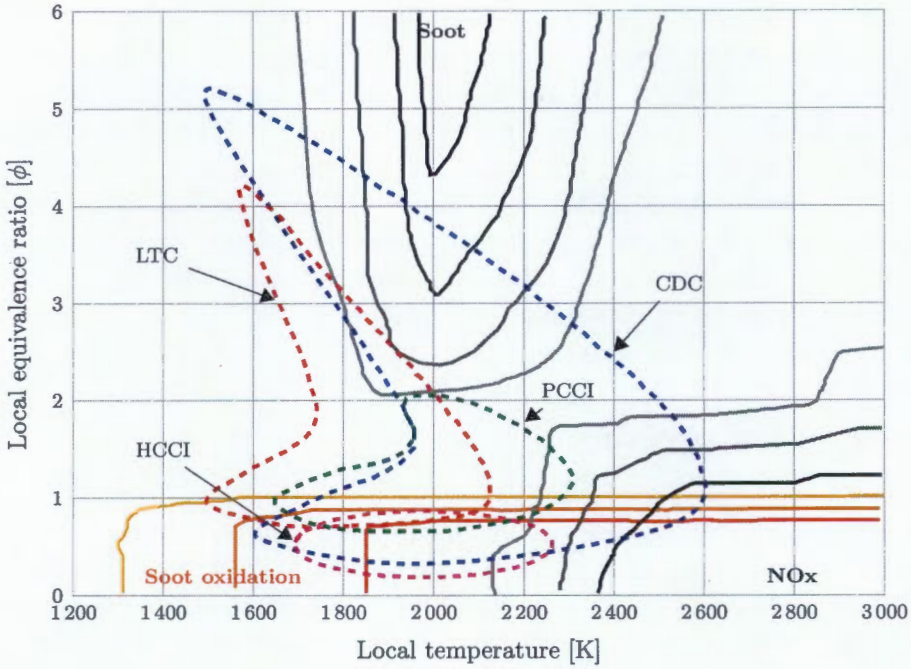

Figure 2.2: *Local equivalence ratio and temperature map compiled from data taken from studies performed by Akihama et al.,Neely et al. and Adomeit et al. ($\phi - T$), [3–5].*

literature have been combined to produce Figure 2.2 showing soot formation (ranging from approximately 1 % soot in the outer ring to 25 % in the inner), soot oxidation (increasing in rate towards the inner contour) and NOx formation (roughly 500 ppm in the outer ring and 5000 ppm in the inner), as well as the various combustion regions. From this map it is clear that soot and NOx formation and soot oxidation are very dependent on local equivalence ratio and temperature. The different combustion mechanisms on the map indicate that by using different operating parameters, such as EGR, multiple injections and strategic SoI strategies, one is able to control the combustion process to within favourable $\phi - T$ conditions. Relative to PCCI and HCCI, LTC has a much wider local equivalence ratio range and lower temperatures, primarily because PCCI and HCCI have greater premixing and use less EGR, resulting in leaner mixtures and generally higher peak temperatures. However, controlling combustion in terms of phasing and stability, when lean homogeneous mixtures are present, is a great challenge. The shape of the LTC and CDC regions are similar; however, the LTC area is at lower temperatures. As in the case of CDC where combustion control is easier due to the wide equivalence ratio range, according to Figure 2.2 LTC has a similar combustion control advantage over the other combustion strategies. However, LTC is not without its limits, such as, load (50 % [31]) and speed, generally increased CO and THC emissions due to incomplete combustion, poor combustion stability and various challenges associated with transient operation [44].

Ogawa et al. performed steady-state experiments on a single-cylinder, naturally aspirated, four-stroke, $1l$ direct injection (DI) engine with a common rail injection system, with the aim to characterise the effects of various operating parameters on LTC. SoI was controlled such that the start of combustion (SoC) occurred at TDC. Rail pressure, injection quantity, SoI and compression ratio were considered. Other researchers have done similar experiments which involved changing the same parameters, as well as boosting pressure and intake temperature. The effects of changing some of the aforementioned operating parameters on LTC and emissions within the LTC regime are discussed below, with respect to the different researcher's or research group's results.

2.3.1 Injection pressure

Increasing the injection pressure results in improved fuel atomisation and more energy being added to the mixing process. Consequently, fuel penetration and air utilisation is enhanced, which typically results in an increased premixed portion of combustion, in terms of quantity of fuel being burnt. Soot is typically understood to be formed during diffusion-controlled combustion [2], since this is reduced at higher rail pressures, soot formation is too.

The results from the experiments performed by Ogawa et al. [45] show that within the LTC regime, NOx emissions were all very similar and thus were not influenced by rail pressure. Higher injection pressures resulted in lower peak soot levels and also significantly delayed the point (in terms of EGR rate) at which soot levels increased noticeably. Peak smoke levels were all experienced at roughly the same EGR rate for the different rail pressures. Yun and Reitz [46] performed similar tests with NOx and soot results that were in line with Ogawa et al. The reduction in soot formation was hypothesized to be due to improved mixture preparation for the early heat release, inhibiting the soot formation processes. In addition to these findings, Asad et al. [2] found that the effectiveness of rail pressure in reducing soot out is not linear and decreases with increasing rail pressure. It was also noticed that HC emissions are reduced at higher rail pressures (improved combustion efficiency). This was most commonly noticed at high EGR rates. The benefit of this reduction was that increased EGR rates can then be achieved, thus further reducing soot and NOx emissions.

2.3.2 Boost pressure

Increasing the boost pressure increases the O_2 mass that enters the cylinder for a constant EGR % and fuelling, increasing lambda and thus reducing the effectiveness of the EGR. For this reason it is often advisable to compare the LTC emissions against O_2 % intake as

oppose to EGR [35]. In order to keep the O_2 % intake constant whilst raising the boost pressure, the EGR rate would need to be increased accordingly.

Asad and Zheng [35] found boost pressure had indistinguishable effects on NOx emissions at LTC. However, peak soot levels were noticed to be lower for the cases of higher boost pressure.. It was concluded that higher boost pressures could make a significant improvement to engine-out soot emissions at high EGR (low intake O_2 %) rates without affecting NOx. For a fixed oxygen concentration, the EGR rate at which CO and THC's significantly increase, is increased at higher boost pressures. This can be attributed to the leaner cylinder charge formed, on a mass basis, at higher boost and the same intake oxygen [2]. The occurrence of these emissions was stipulated to be as a result of the reduced flame temperatures and O_2 availability.

Conversely, Yao et al. [1] found that for an increase in boost pressure, there was an increase in peak soot levels. However, the EGR rate at which they began to increase was also retarded. It was hypothesised that the increased boost pressure resulted in a charge which was more prone to ignite, consequently shortening the ignition delay. The shortened ignition delay allows for less air-fuel mixing and thus higher local equivalence ratios, therefore higher peak soot.

2.3.3 Intake temperature

Higher intake temperatures result in hotter initial mixtures, therefore reducing ignition delay. The reduced ignition delay shortens mixing time and thus causes increased soot formation. Asad et al. [2] found that it was possible to keep the peak soot emissions, experienced during transition between CDC and LTC, below their target value of 0.01 g/kWh, if the EGR was cooled such that the intake temperature was 28 °C.

2.3.4 Start of injection (SoI)

Ogawa's LTC test [45] included an SoI sweep from -28 °ATDC to 5 °ATDC and results showed that for 11 % intake O_2 concentration, soot emissions varied significantly with SoI, reaching a maximum at -10 °ATDC and approached zero as SoI was both advanced and retarded. As intake oxygen was further reduced to 9 % by higher EGR rates, soot was no longer formed and thus SoI had no effect, but CO and THC levels increased with lower oxygen and increased further as SoI was retarded. At high levels of EGR, where the O_2 intake concentration was below 11 %, NOx was not affected by SoI.

Chapter 3

Defining the requirements of the test facility

The primary aim of this project was to build a test facility capable of operating under conventional diesel combustion (CDC) and low temperature combustion (LTC) using a state-of-the-art single-cylinder research engine and modern combustion testing instrumentation. This chapter details a summary of the desired operation of the test facility as seen in literature and from exposure to some of Sasol's other test facilities. A list of requirements are then derived and briefly discussed.

3.1 Summary of the test facility's desired operation

A summary of the intended system operation is presented here. Figure 3.1 shows a block-diagram of the test facility and the various important systems that were necessary for the construction of this test apparatus. The different systems in the figure are numbered and are referred to within the summary of the test apparatus operation. Similar apparatus layouts were used for LTC test work performed by Asad et al. [2] and Yao et al. [1].

The standard configuration for diesel research test facilities utilising a research engine is generally accepted as per the following [47, 48]: A boost conditioning system (1) supplies pressure and temperature controlled air to the engine, simultaneously measuring the mass flow rate. Fuel is supplied to the engine's (2) high pressure fuel pump by a fuel conditioning and metering system (3) at a regulated pressure. The high pressure fuel pump pressurises the fuel to a user-specified injection pressure. The injection quantity, injection timing, injection pressure, boost pressure and temperature, EBP and EGR valve position are pro-

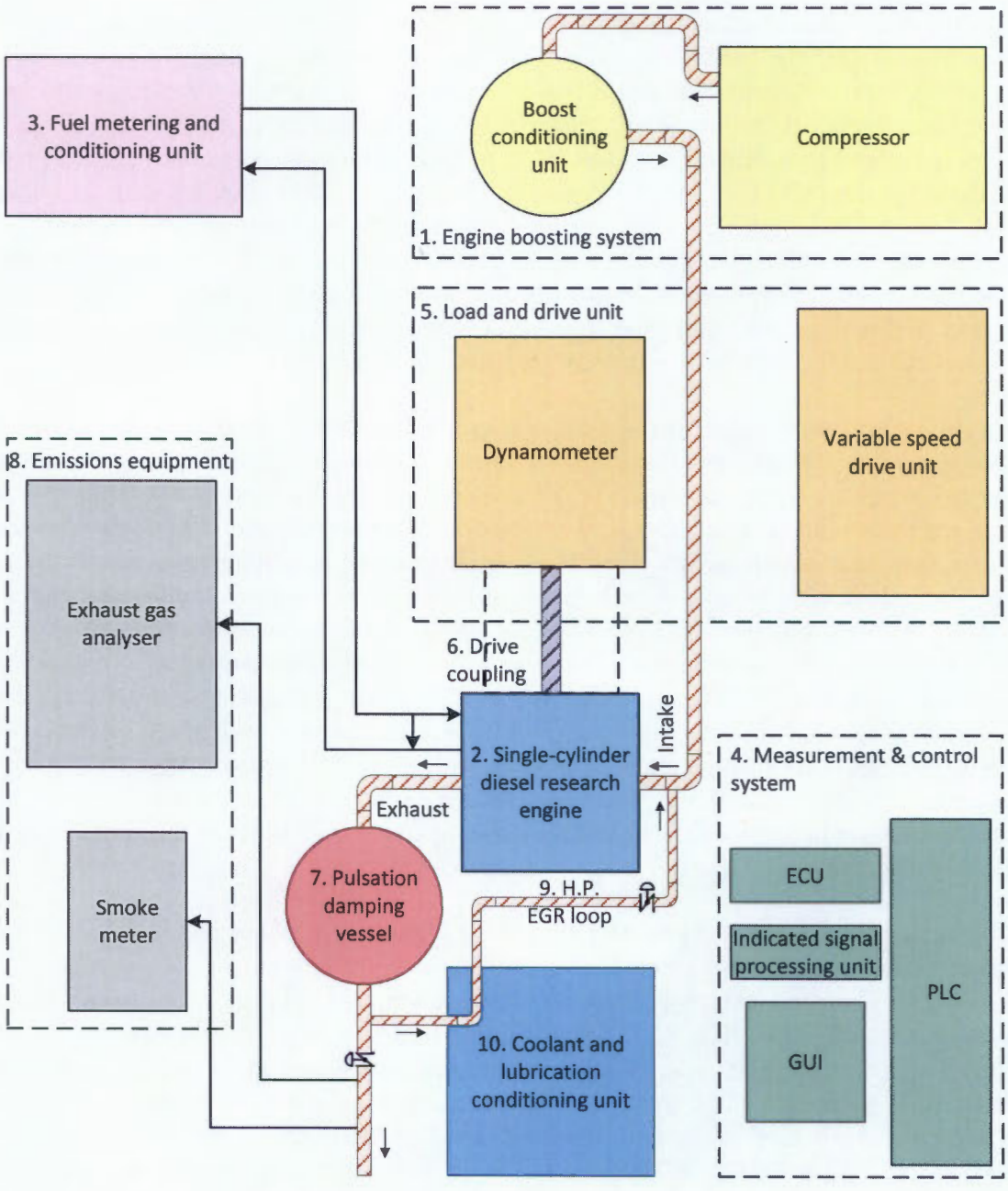

Figure 3.1: *Typical diesel research test facility subsystems and integration.*

vided to the engine control unit (ECU) user interface (UI) (4) by the test facility operator. The in-cylinder pressure is measured and typically processed in real-time to determine operating parameters such as indicated mean effective pressure (IMEP), heat release rate (HRR), integrated heat release rate and combustion phasing in terms of fuel mass fraction burned (MFB). In-cylinder pressure, HRR and the integrated heat release rate are generally plotted in real-time against °CA and monitored during testing to ensure system operation limits are not exceeded. Some of these parameters can be used by the ECU to perform closed-loop control, i.e. the 50 % mass fraction burned signal (MFB50) can be utilised by the ECU to perform closed-loop control on combustion phasing by adjusting SoI. The measurement, determination and real-time display of the aforementioned operating parameters has previously been achieved using a shaft encoder (crank-angle position determination), relative piezoelectric pressure transducer (in-cylinder pressure measurement), and a high-speed indicated signal processing unit (4) connected up to and operated from a computer. This data is usually captured up to a resolution of 0.05 °CA.

Controlled engine speed or brake torque is typically achieved using a controller, variable frequency drive (VFD) and dynamometer system (5) integrated with a load cell (or torque flange), which measures the engine brake torque. Complex drive cycles can be programmed into the dynamometer controller to simulate conditions representative of those experienced by engines in commercial vehicles. The engine flywheel is coupled with the dynamometer via a shaft with flexible couplings (6) to help absorb torsional oscillations and shock loading between the two units. Due to the increased temporal separation of the exhaust stroke (and intake stroke) intrinsic in a single cylinder engine (relative to a multi-cylinder engine), pressure pulsations are inherently present in the exhaust system (and the intake manifold). These pulsations cause fluctuations in pressure measurement, inconsistent sample quantities, and make exhaust gas flow control challenging, for example, EGR rate control. Therefore, the design and construction of large-volume vessels (7) are required and installed inline with the exhaust and inlet system, with the sole purpose of damping these pulsations.

The exhaust gas is analysed by two systems (8); namely, a smoke meter for soot concentration measurement, and an exhaust gas analyser multi-system (i.e. the Horiba MEXA-7200D) for the determination of the remaining important exhaust gas species concentrations (CO, CO_2, NO_2, NO, HC, O_2 and EGR %). The EGR % is a measurement derived from CO_2 concentrations in both the exhaust and inlet manifold. The high pressure loop EGR rate (9) is controlled using two valves; namely, an EBP valve and an EGR valve. The EBP valve is used to simulate the EBP that a turbocharger would otherwise generate. Exhaust gas in the EGR loop is driven to the intake manifold due to a pressure differential set up by the two valves and the specified boost pressure. The EGR valve is also used to control the flowrate of the exhaust gas whilst an inline dedicated EGR cooler is utilised for EGR temperature control. Typically a conditioning unit is used to supply coolant and lubrication to the engine at a controlled temperature (10). The oil supply is also generally pressure regulated to ensure a constant supply of lubrication.

A crucial element of the remote workings of the engine and its ancillary systems is the control system (4). This is achieved by using a high-speed controller that is programmed to operate as an ECU for engine parameter control, such as injection pressure, and a programmable logic controller (PLC) for the operation and control of ancillary systems. A more detailed requirement specification for the test apparatus control system is presented in Section 3.2.3. Finally, a multitude of software types with the ability to capture user-specified test data, as well as act as the user's control user-interface, exist. Some of theses programs include Horiba's STARS, LabVIEW and AVL's Puma and Indicom. Each of these software packages is merited; however, constraints such as functionality and cost generally result in the number of these packages used being limited to 2 or 3.

3.2 Requirement specification of the test facility

After the intended system operation had been established a detailed list of requirements for the LTC test apparatus construction was produced and divided up as follows:

i. Requirements of the test facility venue

ii. Required ancillary systems

iii. Sensor, control and data acquisition system requirements

The specification process for the test cell systems involved numerous decisions regarding numerical specifications of size, power, flow rate, measurement range, sensitivity etc. The full decision making process and justification of chosen values based on literature sources of best practice is too onerous to contain in this report and only the most important specifications are detailed in the following sections.

3.2.1 Requirements of the test facility venue

The test facility venue must be configured to provide all the basic requirements of the test apparatus, as well as to isolate the system from the operator in case of dangerous leaks or catastrophic failure. Based on a review of literature and the suite of components that were to be included in the test facility, a performance requirement specification was drawn up. The following requirements must be provided:

i. A means of controlling the ambient room temperature to a variety of setpoints between 15 °C and 35 °C

ii. A means of isolating the noise of combustion

iii. Test facility cooling water supply at 2 bar and approximately 20 °C

iv. Test facility ventilation flow rate of at least 2 m^3/s (determined in accordance with the methodology presented in [48])

v. Electrical power (single-phase and three-phase)

vi. Engine and dynamometer test bed with anti-vibration mountings

vii. High-pressure (7 bar) pneumatic lines with assorted pressure regulators between 3 and 6 bar

Discussion of requirements

The research testing was to be conducted at an educational facility with noise constraint requirements. Therefore, due to the obtrusive noise levels inherent in diesel engine combustion as a result of high peak pressure rise rates, the venue should employ noise isolating techniques. In addition, the engine ancillaries have a range of different requirements which also must be met by the test venue.

The performance of an engine is affected by the condition, temperature, pressure and humidity of the air entering and surrounding the engine. The engine and exhaust system (as well as other ancillaries) consistently radiate heat in varying quantities, which is changing the condition of this air. Therefore, not only do the exhaust gasses need to be extracted but also the excess heat within the test facility, in order to maintain a constant and repeatable environment.

3.2.2 Fundamental mechanical systems

The research engine requires ancillaries responsible for critical measurement and control of fluids to and from the engine as well as detection of combustion product species. Based on the information from literature and standard practice for engine test facility building, the following requirement specification was distilled:

i. Dynamometer and variable frequency drive controller system

ii. Temperature and pressure controlled air supply system with air mass flow measurement capabilities

iii. Fuel mass flow measurement system

iv. Fuel temperature conditioning system

v. Coolant and lubrication conditioning system

vi. Intake and exhaust system

vii. High pressure EGR loop

viii. Intake charge and exhaust gas pulsation damping systems

ix. Artificial EBP generation system capable of generating up to 1300 mbar (mechanical engine limit)

x. Exhaust gas analysing systems for measurement of particulate matter, CO, CO_2, NO_2, NO, HC

xi. Physical layout of the components of the test facility must provide sufficient space for the operator to move safely

Discussion of requirements

The critical system required for achieving LTC is the high pressure EGR loop. This EGR loop requires an EBP valve for generating a pressure differential between the exhaust and intake manifold (the driving force for the exhaust gas flow to the intake manifold), and an EGR valve with inline dedicated EGR cooler for EGR flow and temperature control. In addition, the EBP valve can be used to simulate the EBP that in the case of commercial vehicles, would otherwise be generated by the turbocharger.

3.2.3 Sensing, control and data acquisition system requirements

Based on literature and exposure to Sasol's test facility sensor, control and data acquisition systems the following requirement specification was arrived at:

i. Automated and manually actuated safety shutdown procedures must be implemented

ii. Precise control of EGR rate (accuracy to within ±1 % EGR about the setpoint) and recirculated exhaust gas temperature (accuracy to within ±1 °C about the setpoint) must be achieved

iii. Manual injection timing, injection mass and injection duration control must be implemented

iv. Engine fuel consumption (mass flow rate) must be measured with measurement accuracy of 0.01 kg/h

v. Fuel supply temperature to the high pressure fuel pump must have a setpoint control accuracy of ±1 °C

vi. Manual intake air temperature and pressure adjustability as well as control accuracy of ±5 °C and 10 mbar [49] respectively, must be provided

vii. Intake air mass flow rate must be measured

viii. Different exhaust gas species must be measured as a concentration and the necessary data must be recorded for conversion of these species concentrations to an indicated specific format

ix. Closed loop rail pressure control with the capability for manual and mapped rail pressure selection must be implemented

x. User must be able to set engine speed and accurate setpoint speed control must be achieved

xi. Implementation of closed-loop lubrication and coolant temperature control with the addition of lubrication pressure control must be achieved. A temperature control accuracy of engine outlet coolant and engine inlet oil of ±1 °C

xii. Must be able to measure indicated data at a resolution of at least 0.05 °CA (crank angle degrees)

xiii. Must be able to measure and capture assorted temperatures, pressures, flow rates and emissions accurately

xiv. Simultaneous capturing and real-time processing of data must be achieved

Discussion of requirements

The engine runs at speeds up to 4300 rpm with maximum combustion temperatures that typically exceed 2000 K and a peak cylinder pressure of 170 bar [6]. Therefore, it is critical that the engine's control system is extremely accurate and operates at a high frequency. If catastrophic failure occurs safety control features such as automated shutdown procedures need to be in place to minimise collateral damage and risk of harm to operator health. Temperatures, pressures, emissions and flow-rates are changing all the time in response to various anomalies. If proper analysis of tests is to be carried out, this data must be recorded, collated and output into a usable format.

Measurement and control accuracy of the rail pressure is considered to be critical. This is because during steady-state testing it is important that injection quantity per cycle is 'constant'. Conventional means of specifying the injection quantity (mg/cycle or ms/cycle) result in an injection duration setpoint, and in the case of setting the mass per cycle, the injection duration is a function of the rail pressure. However, the high frequency at which the rail pressure fluctuations typically occur, make it difficult for the duration corresponding to the instantaneous pressure in the rail to be implemented. Therefore, it is acceptable for the duration to be a function of the setpoint rail pressure and not the actual rail pressure. Since injection duration is therefore a constant for both setpoint methods, if rail pressure control is not precise the injected mass will oscillate with the changing rail pressure, producing an operating condition which is not steady-state. Therefore it is critical that rail pressure fluctuations be minimised.

In order to be able to compare the recorded emissions with data in literature, which may include tests performed on engines of different sizes operating under different conditions, it is common practice to present emissions data as a ratio of species mass flow rate to indicated power (indicated specific emissions format). This ratio is not dependent on engine size or friction and can therefore be directly compared with data in literature of the same format. For calculating the indicated specific emissions the critical measurements needed are exhaust species concentrations, exhaust mass flow rate, intake air humidity and indicated power. A detailed break-down of the calculations involved in this process is presented in Appendix B.3. A more in-depth discussion of the justification for using indicated data as opposed to brake data in this project, is presented in Section 5.2.

For successful LTC achievement, EGR rate control is critical. The engine needs to be able to transition between CDC operation (from 0 % EGR) to LTC (EGR rates upwards of approximately 55 %). In addition, it must be noted that at EGR rates in and around the LTC regime, combustion stability becomes increasingly sensitive to EGR rate (shown by the increased coefficient of variation in indicated mean effective pressure (COV_{IMEP}) in literature [50]), therefore minimising the variation in EGR rate becomes key.

Chapter 4

Design solution for the test facility

In Chapter 3 the requirements and intended layout of the test apparatus were presented, and ancillary system-types were identified. This chapter presents the final design solution which includes the:

i. selection of fundamental mechanical systems,

ii. design of control and data acquisition systems,

iii. integration of mechanical and electrical system, and

iv. design of system control methods

4.1 Selection of fundamental mechanical systems

Various testing instrumentation was procured and custom designed to be used in this project. These systems are briefly discussed here.

4.1.1 Boosting system

Within the constraints of the project the only boosting system available was the AVL *515X supercharger unit.* This unit comprised of a screw-feed Atlas Copco compressor which supplied pressurised air to a boost air conditioning unit. The boost air conditioning unit controlled the temperature and pressure of the air being supplied to the inlet manifold. It is a requirement of this conditioning unit to be positioned inside the test facility room

and as close to the inlet manifold as possible, in order to reduce heat loss between the conditioning unit and the engine. The compressor has a rotary piston gas meter which measures the inlet volume flow rate to it. An ambient relative humidity sensor was used in conjunction with the meter to determine the intake air mass flow rate.

Furthermore, the compressor makes use of two water separators, which remove moisture from the compressed air, essentially reducing the mass of air being supplied to the conditioning unit relative to what was originally measured. The system was therefore, inadequate in its original form and thus had to be modified. A high-pressure relative humidity sensor had to be installed downstream of the water separators. This sensor was used to correct the intake mass flow for the moisture removed by the water separators. A detailed analysis of this process, as well as the calculations used is presented in Appendix B.1. Table 4.1 summarises the unit requirements and the functional performance specification of the boosting equipment.

Table 4.1: *AVL 515X supercharger unit requirements and performance specifications.*

Parameter	Value
Power	17 kW
Electrical power supply	3×400 V / 50 Hz
Compressed air supply	3 − 6 bar
Pressure control range	800 − 4000 mbar (absolute)
Accuracy	±10 mbar
Temperature control range	30 − 130 °C
Temperature accuracy	±1 °C
Boost conditioning unit location	Close as possible to the inlet manifold
Pressure setpoint control	0...10 V = −800...3000 mbar (gauge)
Temperature setpoint control	0...10 V = 30...130 °C

4.1.2 Fuel conditioning and mass flow metering system

A fuel conditioning and metering system was available from Sasol. It comprised of two units, namely the AVL fuel mass flow meter unit (AVL 735S) and the AVL fuel temperature control unit (AVL 753C). The AVL mass flow system operates in series with the temperature control system. The mass flow system makes use of a coriolis mass flow sensor for fuel consumption determination. A controlled constant volume and pressure *measurement circuit* is used to transport conditioned fuel to the engine and return fuel from it. As fuel is used by the engine there is a corresponding pressure drop in the circuit. To maintain pressure, additional fuel is passed through the coriolis mass flow sensor into the circuit. The addition of fuel to the circuit is measured as the engine's fuel consumption in kg/h. Table 4.2 summarises the fuel conditioning unit's specifications, requirements and control.

Table 4.2: *AVL fuel conditioning unit requirements and performance specifications.*

Parameter	Value
Power	2.25 kW
Electrical supply	220 V / 50 Hz
Compressed air supply	3 – 6 bar
Mass flow range	0...125 kg/h
Fuel supply pressure	±4 bar
Temperature control range	10 ... 80 °C
Temperature accuracy	±1 °C
Fuel return temperature from engine, at system inlet	max. 110 °C
Unit Location	Inside the test facility
Fuel supply pressure setpoint control	Manual adjustment of pressure control valve

4.1.3 Single-cylinder research engine

AVL's 5402 single-cylinder light-duty diesel engine was available from Sasol and met the requirements of the apparatus. It is representative of a commercial four-cylinder high-speed direct-injection engine. By using a single-cylinder engine the interactions among the cylinders are avoided. In addition, there is the advantage of advanced operational flexibility, especially noticeable when operating at the engine's combustion limits. The engine came fitted with balancer shafts designed to counter 1^{st} order reciprocating engine vibrations. Table 4.3 shows the engine design specifications.

Table 4.3: *AVL 5402 single-cylinder research engine specifications.*

Parameter	Value
Engine	Single-cylinder four-stroke
Fuelling	Diesel, direct-injection
Compression ratio	17.0 : 1
Bore/stroke	85.0 mm / 90.0 mm
Swept volume	511 cm^2
Valves per cylinder	2 × intake, 2 × exhaust
Inlet ports	Tangential, helical, neutral
Fuel injection system	Common rail CP4.1
Inlet valves open (IVO)	8 °BGTDC
Inlet valves close (IVC)	226 °AGTDC (after gas TDC)
Exhaust valve open (EVO)	128 °ATDC (after TDC)
Exhaust valve close (EVC)	18 °AGTDC
Installation and control	AVL engine manual [6]

The engine also came complete with a common rail fuelling system capable of operating at a range of pressures up to a maximum of 1800 bar. The standard injector used was a piezoelectric injector. The specifications of the fuel system are summarised in Table 4.4.

Table 4.4: *Fuel injection system specifications.*

Parameter	Value
Injector type	Piezoelectric
Maximum injection pressure	1800 bar
Nozzle type	DLLA 162 P 2160
Number of nozzle holes	8
Hole diameter	0.12 mm
Spray angle	162 °
Flow	370 ml / 30 s
Needle lift	0.20 mm
Minimum energisation duration	100 μs

The combustion chamber geometry is typical of what is found in passenger vehicles. Figure 4.1 shows a technical drawing of the piston and bowl geometry.

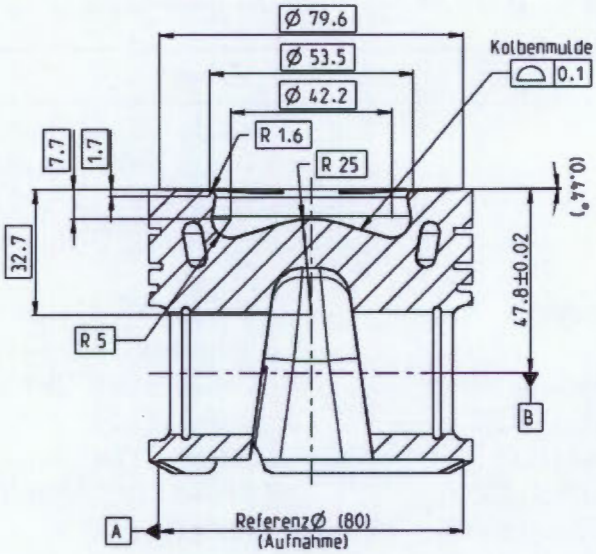

Figure 4.1: *Piston and bowl geometry [6].*

4.1.4 Dynamometer equipment

The dynamometer equipment chosen for this project was available from Sasol, and consisted of three integrated sub-systems supplied by Horiba:

i. *$Dynas_3$ LI 145* AC induction motor with torque and speed acquisition

ii. *Variable frequency drive* (VFD) for the $Dynas_3$ LI 145

iii. *$SPARC^E$* test stand controller

The asynchronous dynamometer used is able to accurately perform load and speed control individually. The VFD comprises of one mains converter and one machine inverter. These are used to convert the constant amplitude and frequency mains voltage into a system with a variable voltage and frequency. Both the converter and inverter made use of insulated gate bipolar transistors to allow for dynamometer load absorption and driving operation. The test stand controller is used for the accurate speed and load control. It also has the facility for performing road load simulations, both customised and standard.

Table 4.5: *Horiba dynamometer equipment requirements and performance specifications.*

Parameter	Value
Rated power (absorbing)	145 kW
Rated current	245 A
Rated speed (absorbing)	4500 rpm
Rated torque (absorbing), continuous operation	308 Nm
Rated power (driving)	135 kW
Rated speed (driving)	4380 rpm
Rated torque (driving), continuous operation	294 Nm
Max. speed gradient up to rated speed	13.60 rpm/s
Speed measurement accuracy	1 rpm
Torque control accuracy	$< \pm 0.17$ %
Torque measurement error	$\leqslant \pm 0.05$ %
Electrical requirements	3 AC 400 V / 50 Hz

4.1.5 Exhaust gas analysis system

Two systems were provided by Sasol for the exhaust gas analysis, namely the AVL 415S variable sampling smoke meter and the Horiba MEXA-7200D exhaust gas analyser. The AVL 415S makes use of the filter paper method to measure the soot concentration in the exhaust. The mass of exhaust gas sampled is measured using an orifice flow meter. As the exhaust gas is directed over the filter paper, it blackens. The amount by which it blackens for a measured exhaust gas quantity (the soot measurement) is detected using an optical reflectometer head. The soot content is reported as a filter smoke number (FSN) or soot concentration (mg/m^3). Integration of the smoke meter with the automation system is achieved over RS232 interfaces. The smoke meter's specifications and requirements are highlighted in Table 4.6.

Table 4.6: *AVL 415S variable sampling smoke meter requirements and performance specifications.*

Parameter	Value
Electrical requirements	230 V / 50 Hz
Smoke value measurement range	0...10 FSN
Soot concentration measurement range	0...32000 mg/m^3
Resolution	0.001 FSN / 0.01 mg/m^3
Repeatability	$\omega \leq \pm$(0.005 FSN + 3 % of meas. val.)

The Horiba MEXA analyser equipment is capable of measuring all the essential exhaust gases such as CO, CO_2, O_2, HCs, NO, and NO_2, using best practice methodology. The

unit facilitates three sample lines; namely, two heated and one at ambient temperature. The heated lines prevent the condensation of high-boiling-point HC or water vapour and consequent absorption of water soluble exhaust gas species. The singular purpose of the ambient line is for the measurement of CO_2 in the intake manifold for EGR rate determination, as discussed in Section 5.5. Table 4.7 highlights the MEXA's analysers used for the determination of different exhaust gas species concentrations. In addition, a series of analyser calibration and operation gases are required for the system and were procured in accordance with the MEXA-7200D user manual.

Table 4.7: *MEXA-7200D exhaust gas analysers used for exhaust species concentration determination.*

Analyser	Emission(s)
Non-dispersive infrared (NDIR) absorption detection	CO, CO_2
Flame ionisation detection (FID)	THC
Chemiluminescene detection (CLD)	NO, NO_2
Paramagnetic analyser	O_2

4.1.6 Coolant and lubrication conditioning unit design

Whereas the previously mentioned systems were available off-the-shelf, for reasons such as financial constraints, the coolant and lubrication conditioning unit was custom designed for this engine. A summary of the final design solution is presented here. For the detailed design description, the interested reader can refer to Appendix C. In addition, some of the conditioning unit computer-aided design (CAD) drawings are presented in Appendix F.7.

The final design of the conditioning unit housing had top and side perforated plates to allow for air cooling of the electric motors (seen in Figure 4.2). The back, front and floor panels were laser cut from 3 mm stainless-steel to support the load of the heat exchangers, pumps, fittings, pipes and the smaller components that also made up the conditioning unit. The wet sump was suspended from the floor panel of the housing such that the oil level in the sump was always at lease 100 mm lower than the oil drainage point of the engine.

Figure 4.3 shows the schematic layout of the conditioning unit. The four different circuits that were necessary for the final design are encapsulated and labelled within numbered boxes.

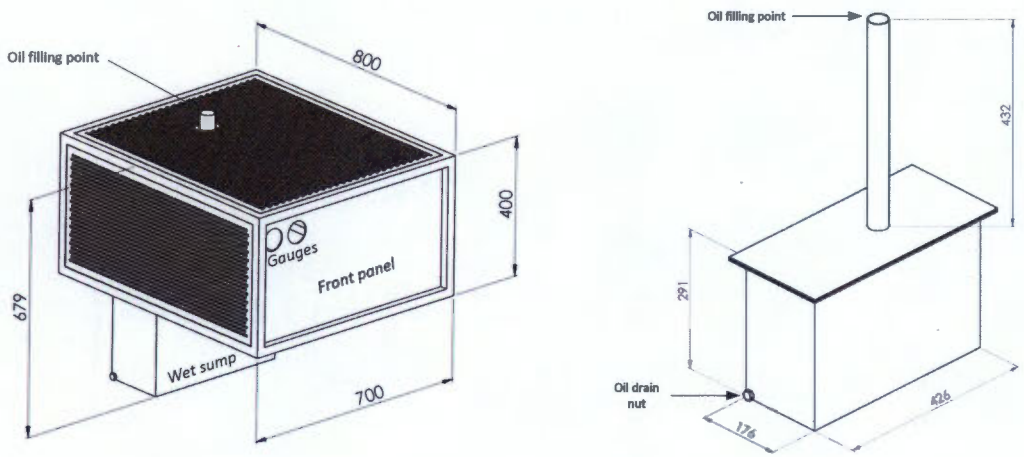

(a) *Housing*

(b) *Wet sump*

Figure 4.2: *Three-dimensional representation of the conditioning unit housing (a) and wet sump (b) assembly.*

The four functional circuits are as follows:

i. *Oil conditioning circuit:* This circuit performed accurate control of the oil temperature and pressure inlet to the engine.

ii. *Coolant conditioning circuit:* This circuit performed accurate temperature control of the coolant outlet from the engine.

iii. *Distilled water circuit:* This circuit was used for maintaining a constant temperature within the piezo-resistive inlet manifold pressure sensor. Distilled water was used because deposits can form in the transducer cooling jackets if water contains calcium. This has the potential to result in cooling channel blockages.

iv. *EGR cooler circuit:* This circuit controlled the temperature of the high-pressure EGR loop gas by controlling the cooling water flow rate through the dedicated EGR loop cooler.

All the heat exchangers utilised the test facility chiller water as the active coolant cooling fluid. The performance specifications and system requirements of the coolant and lubrication conditioning unit final design are presented in Table 4.8.

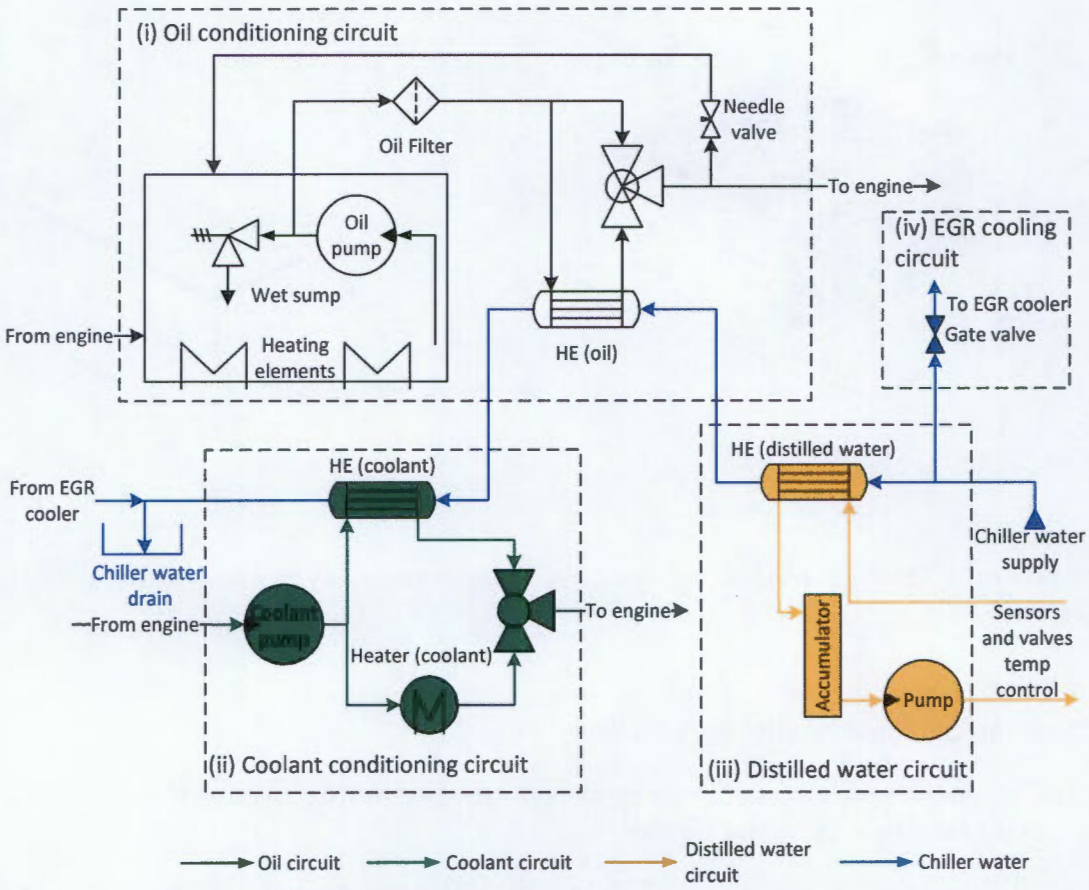

Figure 4.3: *Layout of the lubrication and coolant conditioning unit.*

Table 4.8: *Coolant and lubrication requirements and performance specifications.*

Parameter	Oil circuit	Coolant circuit
Nominal circuit temperature	85 °C	90 °C
Maximum circuit temperature	130 °C	120 °C
Conditioning unit circulation flow	10 l/min	–
Engine circulation flow	5...6 l/min	20 l/min
Heat exchanger cooling capacity	5 kW	20 kW
Heating element heating capacity	4 kW	3.5 kW
Working fluid	Castrol Magnatec 10W-40	25 % ethylene glycol
Circuit pressure	3.5 bar	1.5 bar
Control accuracy	±2 °C	±2 °C
Electrical power requirements	220 V / 50 Hz	3×220 V / 50 Hz

4.2 Control and data acquisition instrumentation

The test facility was fully instrumented with pressure, temperature, flow rate and humidity measurement equipment, some of which has already been presented in Section 4.1. The following section highlights the critical hardware and components used for the test facility control system and for the acquisition of indicated data as well as temperature and pressure measurements.

The test facility control system was separated into two integrated subsystems as follows:

i. Peripheral system controller (PSC)

ii. Engine control unit (ECU)

The *PSC* comprised of a fully functional Allen-Bradley programmable logic controller (PLC) with a selection of signal processing modules. These included digital, analog input and output, thermocouple, and frequency counter modules. This system was required to control the engine's ancillary systems as well as act as a channel through which relevant pressure, temperature and flow rate data could be measured by external devices.

The *ECU* comprised of a National Instruments CompactRIO containing an eight-module-slot chassis. Modules for the CompactRIO were chosen based on the components that needed to be controlled or sensors that were used for feedback control. The ECU's primary functions were to control the engine systems which required high-frequency closed-loop control such as rail pressure, and ensuring that the ECU's clock (measured crank angle position) was in phase with the engine's actual crank angle position.

Temperatures in the exhaust and EGR loop streams, and engine ancillary systems were measured using standard accuracy Wika Instruments K-type thermocouples. The temperature of the air entering the cylinder was measured using a standard accuracy WIKA J-type thermocouple. Both of these thermocouple types have a measurement resolution of 0.1 °C. The pressures in the intake, exhaust and EGR loop air streams were measured with WIKA A-10 pressure transducers. The exhaust pressure measurement was used as the feedback signal for manual EBP control.

The inlet manifold pressure was also measured with an absolute piezo-resistive transducer (Kistler 4075A10). This transducer was fitted with a coolant adapter which utilised the distilled water cooling circuit of the coolant and lubrication conditioning unit to minimise error due to variable intake temperature. The in-cylinder pressure was measured using a flush-mounted AVL piezoelectric relative pressure transducer (AVL GU22C). For in-cylinder pressure signal amplification and real-time in-cylinder performance data determination AVL IndiSmart Gigabit^{TM} system was available. The IndiSmart unit has

a variety of inputs for processing and recording different signal types; for example, the injector current analogue signal, and plotting them against °CA in real-time. The crank angle position was measured using a crank-shaft encoder (AVL 365C angle encoder) in conjunction with the IndiSmart system.

The computers and software packages available for the interfacing with the different systems were as follows:

- LabView 2012 SP1, CalVIEW V2.90, IndiCom Mobil^{TM}, RSlogix, STARS and the Horiba MEXA-7200D software packages were provided with their respective licenses.
- Three desktop computers and one laptop computer were provided, three of which were running Windows operating systems and the other, Linux.

The integration of these computers and software packages with the various systems in the test facility is discussed in Section 4.3.3.

The ECU and IndiSmart unit had to be positioned in the test facility room and as close to the engine as possible. To achieve this a custom-built stand was designed and manufactured for the test facility that would position this hardware and allow for the mounting of additional instrumentation where necessary. CAD drawings for the instrumentation stand are presented in Appendix F.3.

4.3 Mechanical and electrical system integration

4.3.1 Air-exchange system design

A custom-built air-exchange system was implemented to achieve the requirements presented in Chapter 3. Figure 4.4 shows the layout of the air exchange system which can be broken down into the intake, exhaust and EGR systems.

The intake system comprised of AVL's 515X supercharging equipment. This system was used to determine the intake mass flow rate and control the air supply pressure and temperature to the engine. The boost conditioning unit also acted as a pulsation steadying vessel to improve measurement accuracy and control in the intake manifold. The unit was connected to the engine via a 6 m long, 70 mm diameter, spring-steel reinforced hose which was insulated to reduce heat loss. The inlet manifold comprised of a 5 l plenum chamber to improve the mixture homogeneity of the charge air entering the cylinder in the case when EGR was used.

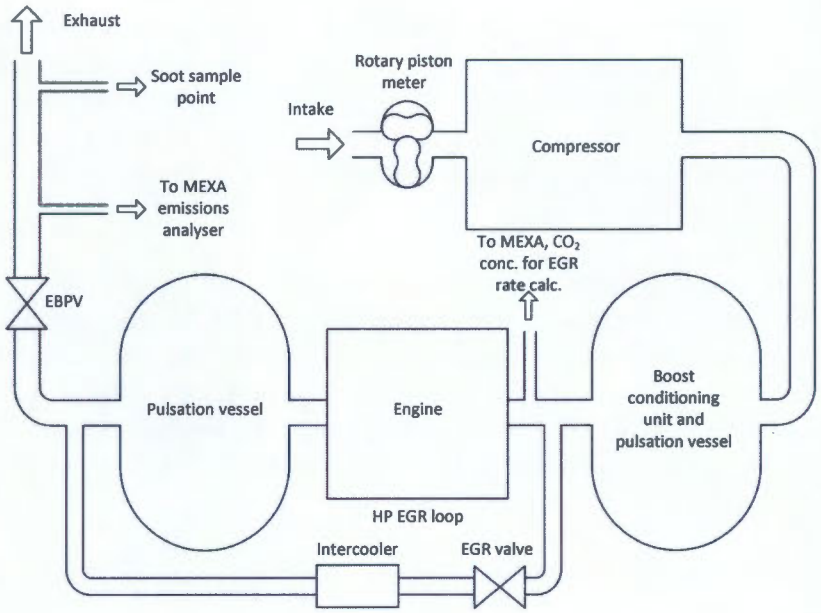

Figure 4.4: *Layout of the gas flow paths through the air-exchange system.*

The low frequency and large amplitude vibrations characteristic of single-cylinder research engines when experienced in combination with a rigid coupling between the exhaust manifold and exhaust system, can result in fatigue failure, typically occurring where the manifold is welded to the flange, which mounts to the engine block (this is typically where the bending stresses are maximum). This issue is combated by inserting a section of flexible exhaust between the engine's exhaust manifold and the custom-built exhaust system. This allows the engine and exhaust system to vibrate freely relative to each other.

The exhaust system was fitted with 1/4" NPT bosses along its length to allow for pressure and temperature sensor installation. Additionally, fittings for the sample lines were positioned in accordance with the AVL 415S smoke meter and MEXA-7200D exhaust gas analyser manuals. An EBP valve was installed for turbocharger EBP simulation, which simultaneously acted as the driving force for EGR flow. Custom designed stands were built for the exhaust and EBP valve. CAD drawings for these stands are presented in Appendix F.5.

A custom-built, 63 l pressure vessel was designed to act as an exhaust gas pulsation damping unit. Preliminary *thin-wall analysis theory* [51, 52] wall-thickness calculations were performed using the worst-case material yield stress at 500 °C for stainless steel grade 304. Based on the calculations, space, and geometric limitations and volume requirements, a preliminary design was developed. The preliminary design was then taken over and completed and manufactured by VBV Holdings. Due to capital constraints the resulting vessel was made from boiler carbon steel. With the inherent wet conditions of the exhaust

stream, a 2 mm stress corrosion layer was added, resulting in a 6 mm vessel wall thickness. The vessel was designed for a peak pressure of 3.5 bar (g) and tested up to 9 bar (g). A peak allowable vessel temperature of 500 °C at high pressures was designed for. The final product was sent to Intertek industry services for AIA approval. CAD drawings for the pulsation vessel and corresponding stands are presented in Appendix F.4 and F.6 respectively.

A high pressure EGR loop was designed to channel and control the temperature of a variable portion of exhaust gas to the plenum chamber of the inlet manifold. A standard EGR valve from a VW Polo 1.4 TDI engine was used. The valve came equipped with a cooling unit for EGR temperature control. Section 4.4.4 explains in more detail the operation and control of the EGR system. To protect the welded joint between the plenum chamber and the EGR line from fatigue, another flexible exhaust section was custom-designed and inserted.

4.3.2 Drive-shaft system

Coupling the engine to the dynamometer and guarding it was achieved as follows: A shaft was supplied by Sasol with a radial bearing on each end for locating the shaft. Adaptive plates were designed in accordance with the shaft flanges and the coupling surfaces of the dynamometer drive and engine flywheel as was detailed in the relevant system manuals. The engine and dynamometer combination is susceptible to torsional oscillations which are easily excited by the powerful forces generated by the engine [53]. The magnitude of these oscillations is a function of the relative damping of each element in the drive train between (and including) the engine and the dynamometer. To minimise these undesirable oscillations, two flexible rubber couplings were integrated into the design. A cross-sectional view through the final design is shown in Figure 4.5. CAD drawings for the shaft assembly are presented in Appendix F.1.

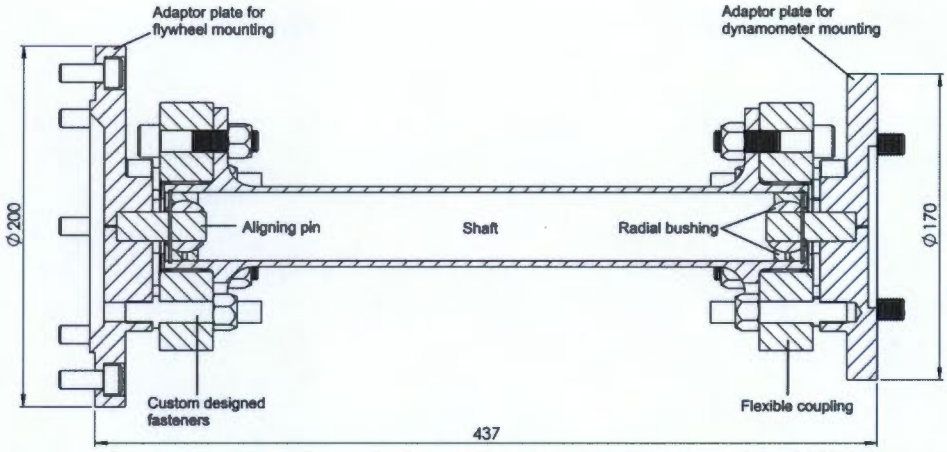

Figure 4.5: *Final design of drive-shaft assembly.*

A custom-built shaft guard (see Figure 4.6) was developed for the apparatus based on an existing Horiba guard design. The guard was made from 4 mm laser-cut and CNC bent mild steel welded together and powder-coated. The top surface of the guard was hinged to the bottom surface and fastened closed by means of an eye-bolt and nut assembly. The shaft guard was bolted to one of the cross-members of the ladder frame. CAD drawings for the custom designed shaft guard are presented in Appendix F.2.

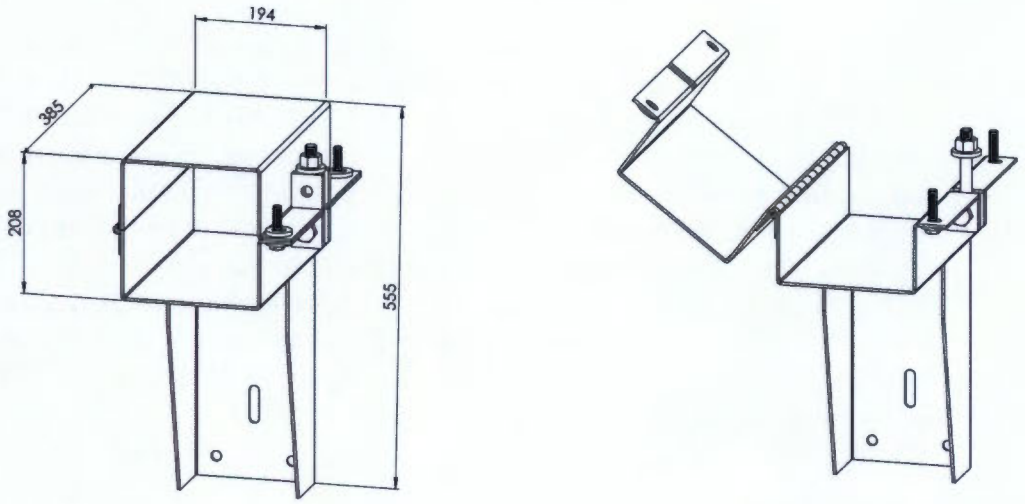

(a) *Dimensioned and closed isometric view*

(b) *Open isometric view*

Figure 4.6: *Three-dimensional representation of the shaft guard dimensioned and closed (a) and in the open position (b).*

4.3.3 Electrical integration of the apparatus

The electrical and mechanical integration of the test facility is displayed in Figure 4.7. It demonstrates how the main components are connected in terms of hard wiring to the PLC, ECU, and computers. In addition the different communication methods such as local area network (LAN), controller area network (CAN) bus and RS232, are depicted. It also details a full breakdown of the two controllers and the modules used as well as the positioning of the various thermocouples and pressure transducers depicted by red and blue x's respectively. Unless specifically shown on the diagram, all of these signals were appropriately wired to the thermocouple and analogue input modules of the PLC.

The system controller user-interface (UI) was spread over four computers within the control room as follows:

Computer 1 : The ECU had its own dedicated computer running LabView 2012 SP1 in conjunction with CalVIEW V2.90 for user-defined engine parameter control and system feedback. Communication between the ECU and LabVIEW was achieved using a LAN connection.

Computer 2 : The AVL IndiSmart was set up and controlled by a separate laptop computer using AVL's Indicom software. Communication with the IndiSmart was set up over a LAN connection.

Computer 3 : The MEXA was controlled over a LAN connection by a computer running the Horiba control software on a Linux operating system.

Computer 4 : The fourth computer was dedicated to the operation of the PLC, X-act dynamometer controller, AVL 415S, AVL 735S and the AVL 753C using the STARS software package. In addition, this computer was networked with the three other computers over a LAN connection, in order to receive and capture relevant data. A CAN bus was used to communicate with the X-act dynamometer controller and from the controller to the VFD and dynamometer. The setup of the PLC, such as system mapping and PID tuning was performed using RSlogix over a LAN connection; however, once setup was complete, operation of setpoint inputs was typically achieved using the STARS UI. The aforementioned AVL instrumentation required RS232 for communication with STARS.

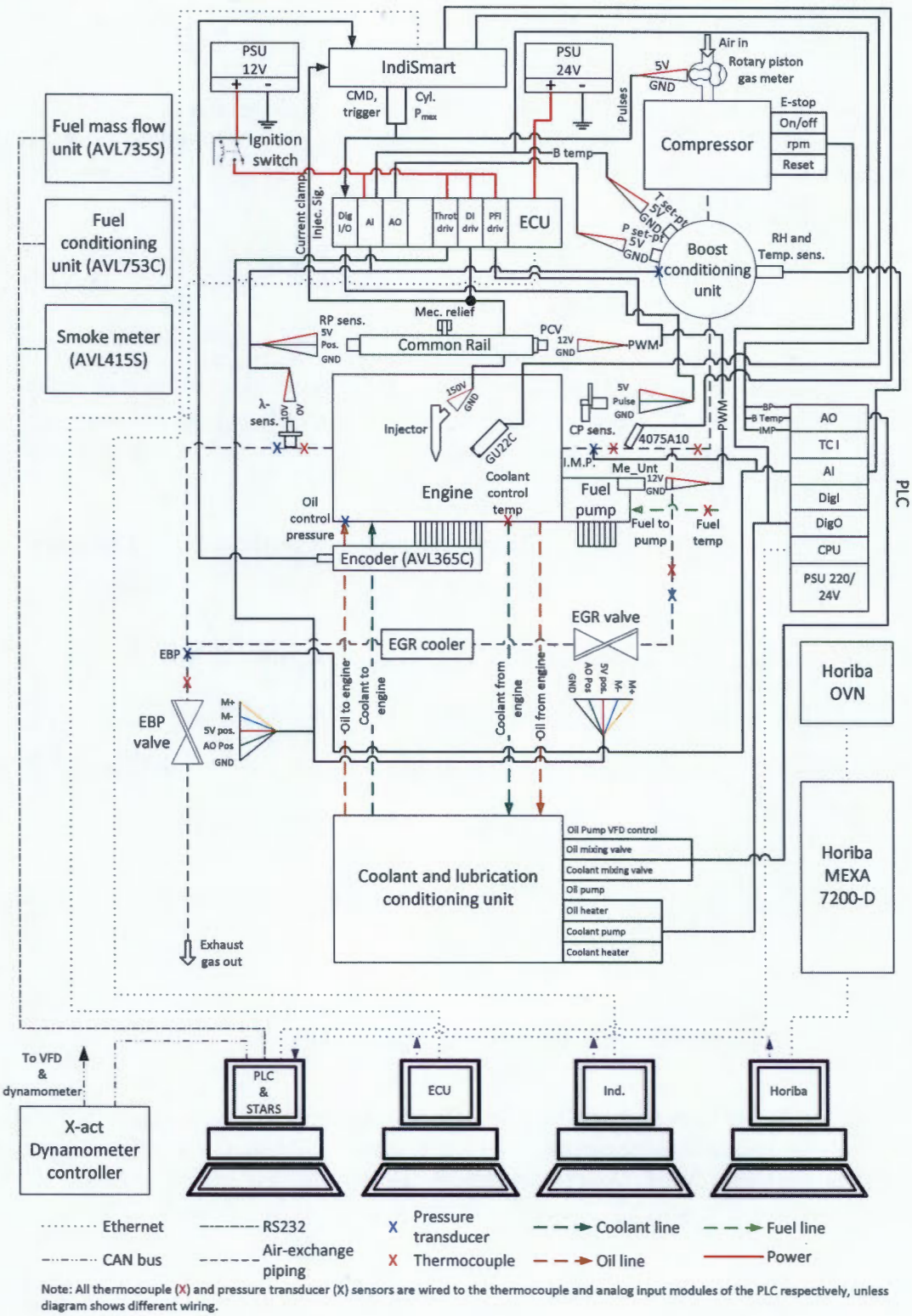

Figure 4.7: *Mechanical and electrical integration of the test apparatus.*

4.4 System control methods

This section highlights some of the control techniques implemented into the ECU. A brief summary of the injection calibration and corresponding injector lookup table as well as the boost and EBP lookup table development is also covered here. In this study, the term 'lookup table' is also referred to as a map.

4.4.1 ECU development scope

The original development of the LabVIEW programming code which was implemented into the Drivven and National Instruments custom ECU was not part of the scope of this project, and was completed as part of previous works [54]. Refinement of this code has occurred in successive projects undertaken at the SAFL [55].

This project resulted in further ECU development and modification. This included the implementation of:

i new strategies for achieving accurate rail pressure control,

ii intake boost and EBP maps custom designed for the AVL5402,

iii a full injector calibration map for the piezoelectric injector used in this project, and

iv a rail pressure map.

These modifications as well as their respective implementations are discussed throughout Section 4.4.

4.4.2 High pressure injection system control

This section starts by reporting the two methods used for rail pressure control throughout the project. A summary of the piezoelectric injector calibration and injection parameter lookup tables then follows. A detailed look at the development of said injector calibration and map integration with the control unit is presented in Appendix A.1.

Rail pressure control

Typically, for common-rail systems, rail pressure is controlled using two valves and a feedback pressure sensor on the rail. The first valve (metering unit) is used on the inlet to the high pressure pump. It has optimised control to ensure that the minimum required volume of fuel to maintain pressure is pumped per stroke at all operating conditions [30]. The rail is equipped with a pressure control valve (PCV) such that the additional fuel pumped into the rail can be relieved to maintain rapid and precise pressure control. That is to say, typically the metering unit and PCV have integrated controllers that are optimised to minimise the brake power losses and maximise the control accuracy. However, the time involved in optimising the rail pressure control for minimum brake losses is lengthy and unnecessary as this project is only concerned with indicated data (discussed further in Section 5.2). Two modes of rail pressure control were implemented, namely *metering unit mode* and *PCV mode.*

i. *Metering unit mode:* When operating in this mode the PCV's duty cycle is set to 100 % (fully closed). The metering unit is used in isolation to control the rail pressure. To put it simply, whatever fuel is pressurised by the pump is either injected into the engine or returned from the injector. The only time the PCV will activate is in the case of extreme rail pressure as a matter of safety, or if injection is disabled, in which case the mode will change automatically to PCV.

ii. *PCV mode:* This control mode uses the PCV to regulate rail pressure. The metering unit duty cycle (the amount of fuel pressurised and bypassed) for this control mode is defined by the specified fuel injection mass, engine speed and an additional percentage of fuel (varying between 20 % and 70 %) to ensure there is always sufficient fuel in the rail to maintain pressure. The additional fuel pumped into the rail is relieved by the PCV and in that way the rail pressure is maintained. However, the quantity of fuel being pumped into the rail is not optimal in terms of minimising brake losses.

Injector calibration

The piezoelectric injector used in the AVL5402 was calibrated using the LR Diesel Injector Service Unit 8000. It uses a diesel substitute with similar flow characteristics but a much higher flash point (for safety) as the calibration fluid. The unit takes an injection duration and rail pressure input and outputs the mass per injection measured using the unit's built-in coriolis flow meter.

Fuelling parameter lookup tables

Two lookup tables were used:

i. *Rail pressure table:* To determine the recommended rail pressure for a specified fuel quantity and engine speed.

ii. *Injection calibration table:* To determine the required injection duration to achieve a user-specified injection mass per cycle (mg/cycle) at a certain rail pressure.

The rail pressure map was taken from a Mercedes-Benz passenger vehicle with a similar cylinder size (approximately 500 cm^3). The injector calibration map was constructed using a template which is used by Sasol's fuels research team. More detail on the injector calibration and map design and construction is presented in Appendix A.1. The maps were integrated with the control system as indicated in Figure 4.8.

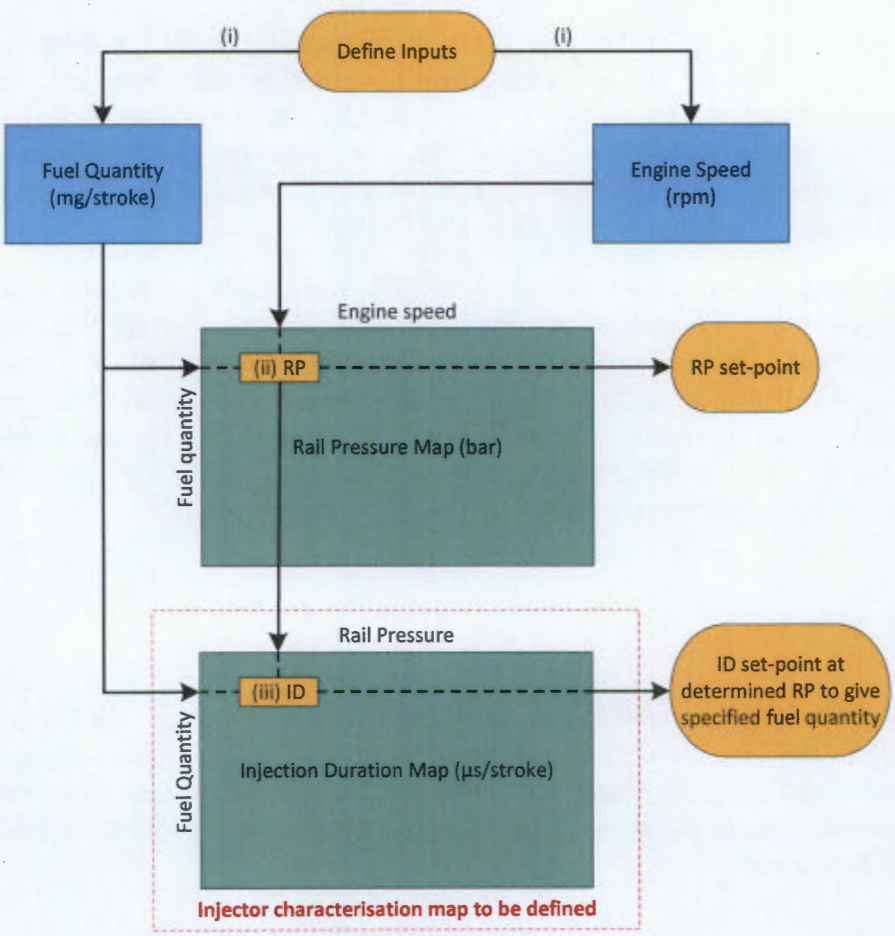

Figure 4.8: *Engine fuelling map integration.*

This diagram has three distinct steps:

i. Engine speed and mass of fuel is defined and input by the operator.

ii. Corresponding rail pressure (function of engine speed and fuel quantity) is output from the rail pressure map and input to the rail pressure setpoint input and injection duration map input.

iii. Injection duration (function of rail pressure and fuel quantity) is output from the injector calibration map and input to the duration setpoint input. The rail pressure input can be overridden if it is desired.

Fuelling parameter user operability

The injection control system was designed with customisable user operation. The operator was able to choose:

i. whether or not the rail pressure setpoint was controlled by the map or manually,

ii. to specify the fuel quantity as an injection duration or a mass per stroke (using mass per stroke makes use of the injector calibration map to determine the injection duration automatically),

iii. which mode of rail pressure control to use, namely metering unit control or PCV control, and

iv. to use up to 5 injections (two pilot, one main and 2 post injections) per cycle.

4.4.3 Boosting and EBP control

Control of the boosting pressure was performed in isolation by AVL's supercharging equipment; however, desired pressure setpoints were defined by the user and relayed to the boost control unit as a voltage signal. EBP typically generated by a turbocharger was simulated using a butterfly valve inline with the exhaust system. Generating a theoretical model to determine the exact EBP expected as a function of exhaust gas enthalpy and mass flow rate for a certain turbocharger is a complex task and is outside of the scope of this project. However, building a map based on existing engine test data and then calibrating it to the AVL5402 was achievable and acceptable for the purposes of the project.

Boost and EBP map

A boost and corresponding EBP map was developed based on the performance of an existing turbocharged production engine. Test data from a multi-cylinder turbocharged engine was supplied from AVL. It included boost and EBP across the load and speed range. The data showed greater load and boosting conditions than achievable with the current research engine setup. The soft valve springs on the AVL5402 puts a limit on the allowable boosting pressure of 1300 mbar gauge (g). Exceeding this limit could result in unwanted valve and piston contact and consequent catastrophic failure. Since the work done by a turbocharger is primarily dependent on exhaust mass flow rate and exhaust enthalpy which are directly related to engine speed and load respectively, the boost and EBP maps were constructed as a function of load and speed. Maps from AVL's data were constructed to characterise the turbocharger (that was used in these tests) as a function of BMEP and engine speed. The boost pressure was then scaled to meet the research engine's (AVL5402) boost pressure limits, and the EBP was scaled such that the pressure ratio (ratio between boosting and EBP) of the turbocharger remained unchanged. The maps were then calibrated according to the engine's (AVL5402) peak BMEP at each speed. An in-depth look at how the maps were constructed and calibrated for the research engine is shown in Appendix A.2.

Boost, EBP control and user operability

Figure 4.9 shows a schematic of how the maps were integrated with the control system. The user operation and back-end control of these parameters can be summarised as follows:

i. Engine speed and fuelling was defined by the user and input into the GUI.

ii. The control system calculated BMEP from the measured brake torque and speed. The BMEP and speed variables were then input into the boost and EBP maps to give the corresponding outputs.

iii. The boost pressure map output was converted to a voltage between 0 and 10 V and sent to the boosting unit's control system input. This input can be manually overridden and set to any other setpoint if the user wishes to disable the map.

iv. The recommended EBP output is displayed on the GUI.

v. The EBP valve position can then be appropriately adjusted by the operator according to the recommended EBP displayed on the GUI.

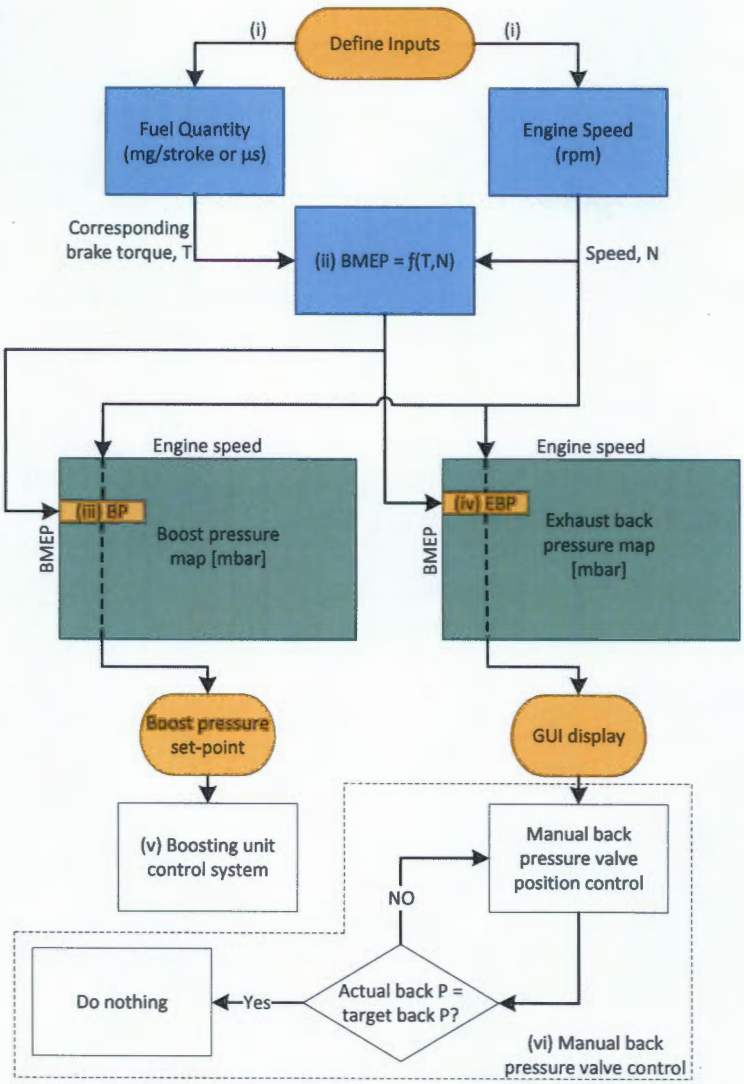

Figure 4.9: *Boosting and EBP determination process.*

4.4.4 Intake charge temperature and EGR % control

This section discusses the means of controlling the intake charge temperature and how it differed depending on whether or not the test involved EGR. A summary of the EGR % control is also presented in this section. Figure 4.10 illustrates the mechanical layout of the air exchange system relative to some of the signal wiring for the control of the EBP valve, EGR valve and EGR coolant valve, as well as the important temperature signals and sensor positions.

Intake temperature control

Intake air temperature control is important for maintaining constant intake mass flow rates. The boosting unit controls the intake air temperature according to a temperature feedback signal measured by a resistance temperature detector (RTD) Pt100 sensor located on the boosting unit, 6 m from the intake manifold. This is not ideal due to excessive heat loss between the boosting unit and the engine. Fixing the problem was attempted by moving the Pt100 to the inlet manifold. However, this was unsuccessful due to significant control delay in the boost conditioning unit.

There are two operating scenarios with this system that need to be understood when controlling the intake charge temperature. These are testing:

i. **without** EGR, and

ii. **with** EGR.

When testing without EGR the intake temperature was achieved by merely setting the boosting unit temperature higher than that required at the inlet manifold. When performing tests which include EGR, exhaust gas is introduced into the inlet manifold downstream of the Pt100 feedback sensor. Therefore, the boost conditioning unit does not automatically compensate for the potential change in intake air temperature. The intake air temperature becomes a function of the boosting air temperature and the recirculated exhaust gas temperature. Therefore, when testing with EGR, the intake temperature was manually controlled by controlling the temperatures of both gas streams to achieve the desired mixture temperature (intake charge temperature). The EGR temperature was controlled by an electrically actuated mechanical proportional valve which appropriately controlled the coolant flow through the EGR cooler, according to the EGR temperature feedback signal located downstream of the cooler (illustrated in Figure 4.10). Using the PLC, a PID controller was set up to generate an analogue signal for the proportional valve position setpoint, based on the EGR temperature.

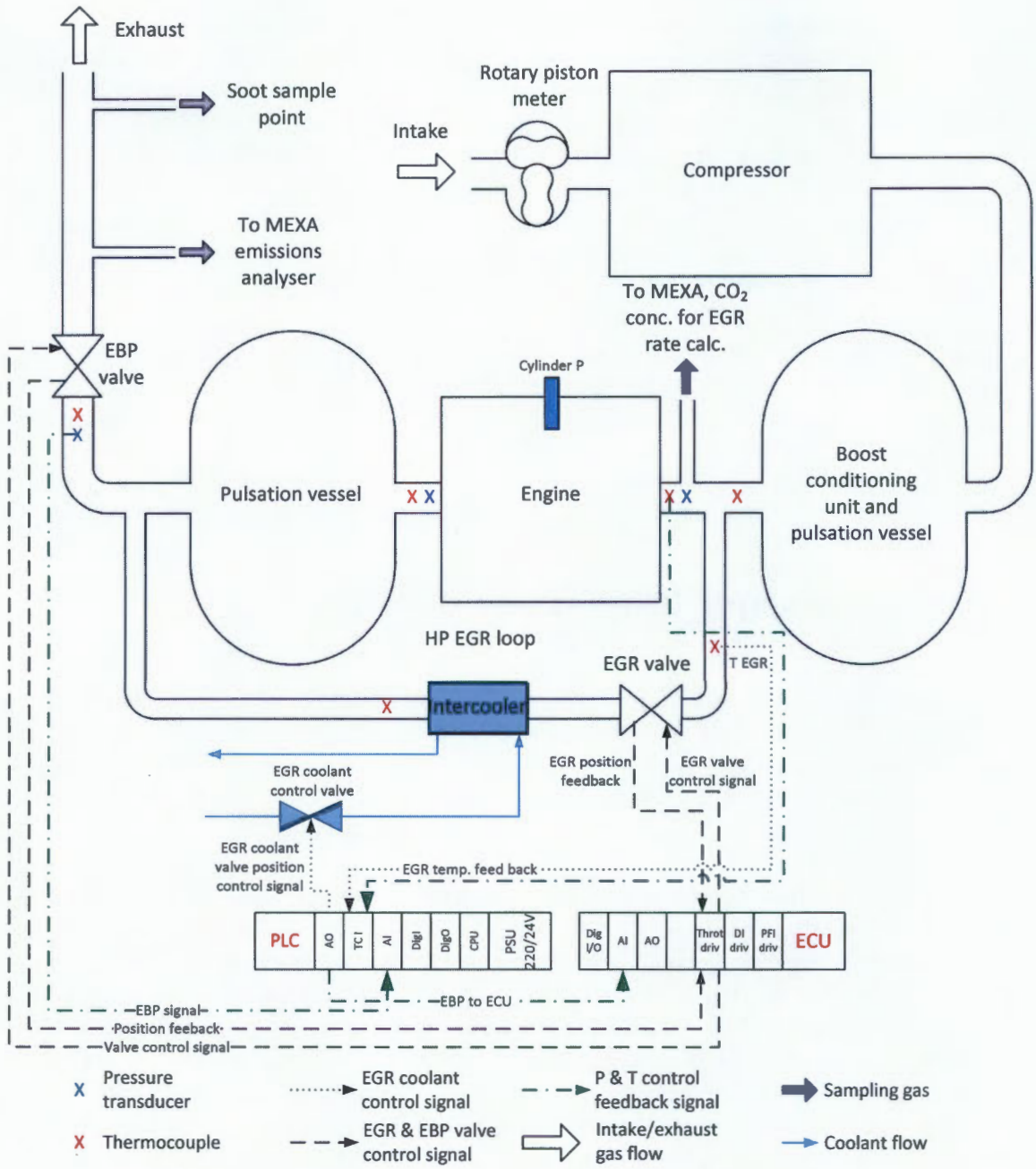

Figure 4.10: *Mechanical layout of the air exchange system relative to the EGR rate and temperature control systems.*

EGR rate control

The EGR % was a measurement derived from the CO_2 concentrations in both the exhaust and inlet manifold using the MEXA exhaust gas analysis equipment. The details of this measurement are discussed in Section 5.5. The EGR system as displayed in Figure 4.10 was designed for full manual control of the exhaust gas flow through the EGR loop using two manually set valves; namely, an EBP valve and an EGR valve. The valve positions were set by manually adjusting the voltage setpoints in the controller UI which corresponded to specific valve positions. These valve setpoint positions were achieved with closed-loop control of the individual valve positions using the ECU throttle driver module. For the purposes of this project, 'EGR' will refer to the gas flowing through the EGR loop and into the inlet manifold. The EGR rate is dependent on the pressure difference between the exhaust and the intake manifold, as well as the EGR valve position. Therefore, the EGR was driven by manually setting the EBP higher than the intake manifold pressure (by adjusting the EBP valve accordingly) and opening the EGR valve to facilitate flow. The electrical diagram in Section 4.3.3 (Figure 4.7) shows a detailed breakdown of the EBP valve and EGR valve actuator pins and hard wiring to the ECU throttle driver card.

4.5 Data acquisition system design

The data acquisition system was set up such that the raw data being measured by the various instrumentation could be processed and captured simultaneously. The user-interfaces across the four computers, the software, the purpose of each computer, and how they were networked was discussed in Section 4.3.3. This following section highlights how the data was captured.

The instrumentation used for measuring some of the important experimental parameters and results was discussed in Section 4.1 and 4.2. As was previously shown in Figure 4.7 all four computers were networked. The STARS computer had Indicom, ECU, MEXA, AVL 753C, AVL 735S and AVL 415S drivers, such that all relevant data could be captured in a single location (in STARS). STARS was set up to process some of the data before recording, therefore minimising post processing time. The averaged data captured in STARS was recorded at a frequency of 1 Hz and output as a *.xls* file. High speed real-time in-cylinder pressure data was also captured separately in Indicom at a high frequency and at 0.05 °CA intervals. This data was collected and averaged over 100 cycles per test point and output in AVL's *.iFile* format. Some of the critical experimental parameters and the equations used to define them in this project are presented in Section 5.5.

4.6 Final design layout

The individual sub-system designs that comprise the test facility were integrated and the layout of the contents was optimised for safety and ease of operation. Before the commencement of the test facility build, the key components of the apparatus were CAD modelled to ensure that all spatial constraints were taken into account. Figure 4.11 shows a CAD drawing of the test apparatus mechanical design layout with single-cylinder research engine. The drawing is colour-coded for identification of the previously discussed components. A photo of the final installation is shown in Figure 4.12.

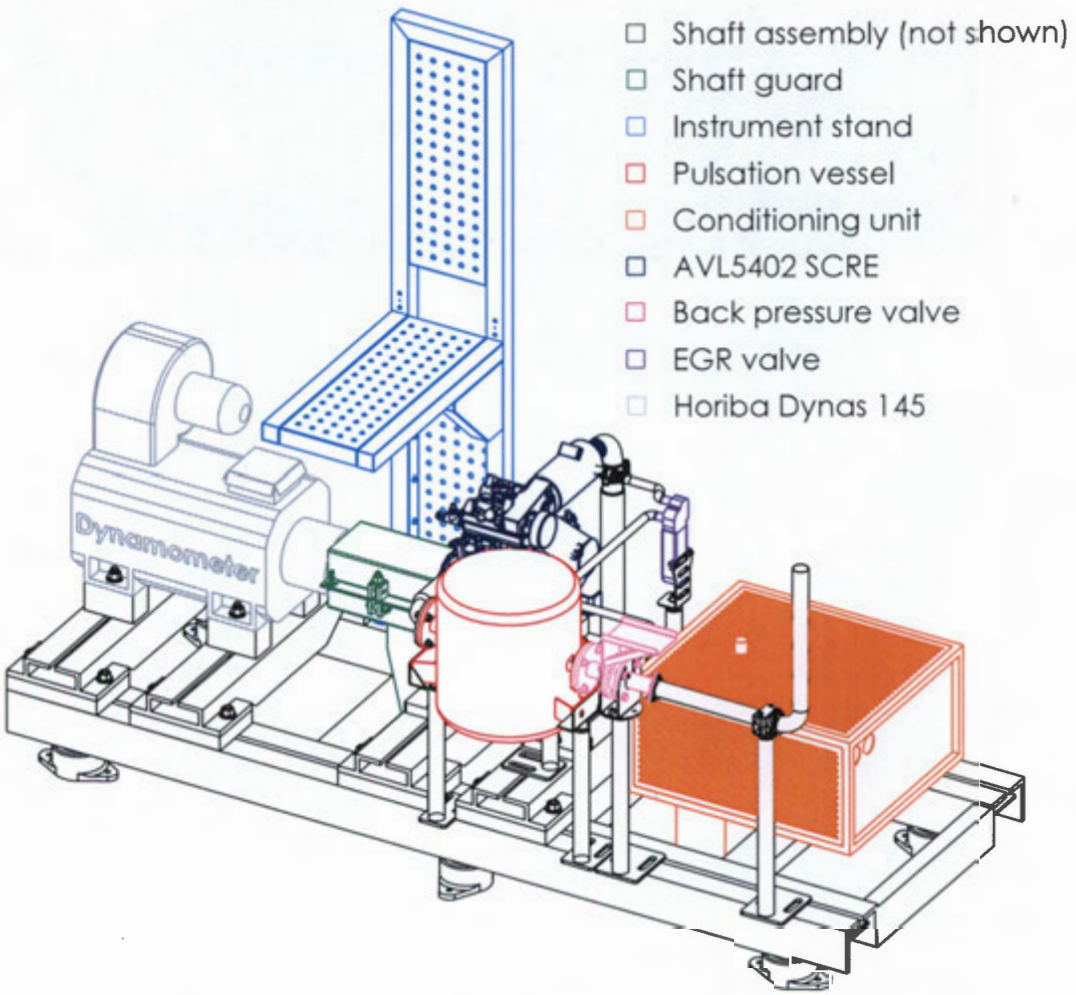

Figure 4.11: *CAD drawing of the test apparatus design layout.*

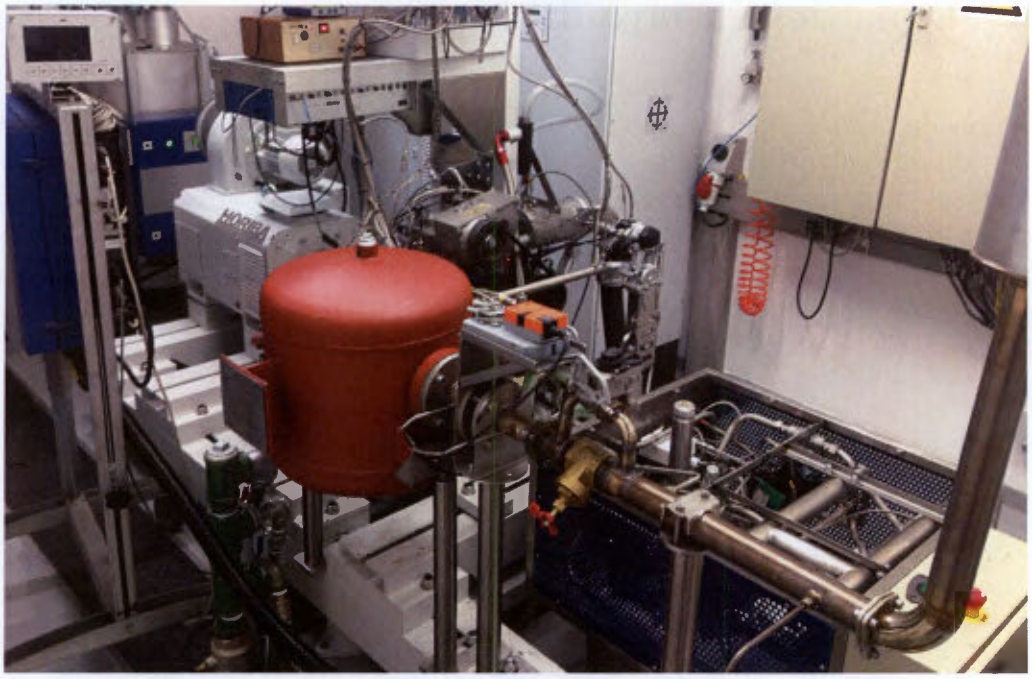

Figure 4.12: *Photograph of the test facility installation.*

Chapter 5

Determination of best testing practice

Over the course of this project the best methods of measuring certain parameters, in terms of repeatability and accuracy, were investigated. This section highlights the various methods and equations used for ensuring accurate and consistent data capturing, giving the reader a reference for comparing the data presented in following chapters.

5.1 LTC emissions target

The onset of LTC is not a sudden and precisely exhibited phenomenon, but rather a progressive change in combustion mode with conducive operational conditions for reducing engine out emissions of soot and NOx. However, for the purposes of this study a very specific working definition (effectively arbitrarily defined) for the "point of LTC operation" (which does not actually exist) was therefore needed in order to compare operational conditions which resulted in similar LTC operational characteristics. This definition for LTC is often defined by target ISNOx and ISSoot values, which to some extent are arbitrary. Passenger vehicle emissions data would be ideal to use for these emissions targets; however, they are reported in g/km, deeming them unusable for the purposes of this study. The next logical choice was to use heavy-duty emissions standards which are reported in grams per brake horsepower (g/bhph) and can be converted to grams per kilowatt-hour g/kWh. The US 2010 EPA heavy-duty emissions restrictions are the strictest in the world and were therefore chosen as the target ISNOx and ISSoot values. As a result, for this study, LTC was only considered to be achieved when ISNOx and ISSoot values were less than or equal to the US 2010 limits of 0.268 g/kWh and 0.0134 g/kWh respectively. To clarify, these

target emission values had to be achieved without the use of exhaust gas after-treatment systems. Furthermore, using similar target values was found to be fairly common practice in literature [56].

5.2 Justification for use of indicated performance data

Brake performance parameters are determined from the engine's output shaft. That is to say, it takes into account frictional and parasitic losses, such as those incurred by the high pressure fuel pump, and in the case of this engine the balancer shafts. These frictional losses vary among engines, especially when comparing single-cylinder engine data with multi-cylinder engine data, and therefore, result in differing brake data. In addition, the brake load is measured by the torque flange on the dynamometer. This is problematic in the case of a single cylinder research engine for two reasons:

i. Most of the ancillary systems that are normally driven by the engine are powered separately, and therefore the load is no longer representative of a commercial vehicle's operation. The most significant difference is the turbocharged air being supplied separately. Although a map was constructed to help simulate the EBP generated by a turbocharger, it is not perfectly representative.

ii. The test engine to be used is a small single-cylinder engine with a relatively low load capacity. In addition, the LTC tests will be conducted at low load conditions. The dynamometer used in this project is designed to be used with larger multi-cylinder engines. Therefore, at these low LTC load conditions, the accuracy of the torque flange becomes questionable.

Indicated load is the load calculated as a function of cylinder pressure and is not affected by engine friction. Thus, comparing indicated data among engines is simpler (in terms of being able to directly compare the indicated data of one engine with that of another) than comparing brake data which would require the difference in brake losses to be known accounted for. Therefore, based on the aforementioned, indicated data was the suitable choice for this project.

5.3 Fuel mass flow rate measurement technique

Three methods of measuring the fuel mass flow rate were available in this project. These were using:

i. the coriolis mass flow meter of the AVL 735S,

ii. the wide-band ETAS lambda sensor measurement and the intake air mass flow rate to calculate the fuel consumption, and

iii. lambda calculated from the Spindt method which uses the fuel composition and exhaust gas composition to calculate the air-fuel ratio. Fuel consumption can then be calculated from lambda and the intake air mass flow rate.

Due to the engine size and the low loads which were operated at for the most part, the fuel consumption during the EGR sweep tests was approximately 0.6 kg/h. The operating range of the coriolis meter is between 0 and 125 kg/h. Therefore, these tests required the flow meter to operate at its lower limit, resulting in questionable accuracy. Furthermore, it was found that the lambda readings for repeat tests using the ETAS equipment were inconsistent. The lambda calculated using the Spindt method was found to be most repeatable. Therefore, fuel mass flow rate and thus exhaust gas mass flow rate were calculated as a function of lambda determined using the Spindt method. A detailed comparison and analysis of the determination of the best fuel mass flow rate measurement method, including the relevant repeat data, is presented in Appendix B.2.

5.4 Injection parameter detection

Up until this point SoI has been referred to throughout the document. SoI is defined as the exact point at which the fuel starts to pass through the injector tip into the cylinder. Since a needle lift sensor was not available for this project, it was impossible to determine the exact SoI. As a result, throughout the rest of the document SoI will be more accurately referred to as the start of energisation (SoE). To clarify, SoE corresponds to the crank angle position at which the piezoelectric crystals started being energised.

The injector current signal was used to determine injection parameters such as SoE, start of de-energisation (SoD), injection duration and ignition delay. The current in the injector was measured using a current clamp which was wired to the IndiSmart unit, where it could be processed against crank position (°CA). An injector current signal noise up to 0.8 A in magnitude existed. Therefore, a threshold current of $\pm$ 1 A for SoE and SoD detection was set. Therefore, SoE was defined as the crank position at which the injector current exceeded 1 A. Similarly, the start of de-energisation was defined as the crank position at which the current dropped below - 1 A, as illustrated in Figure 5.1. The injection duration was defined as the difference between SoE and SoD (°CA), which could then be converted into a time using the engine speed.

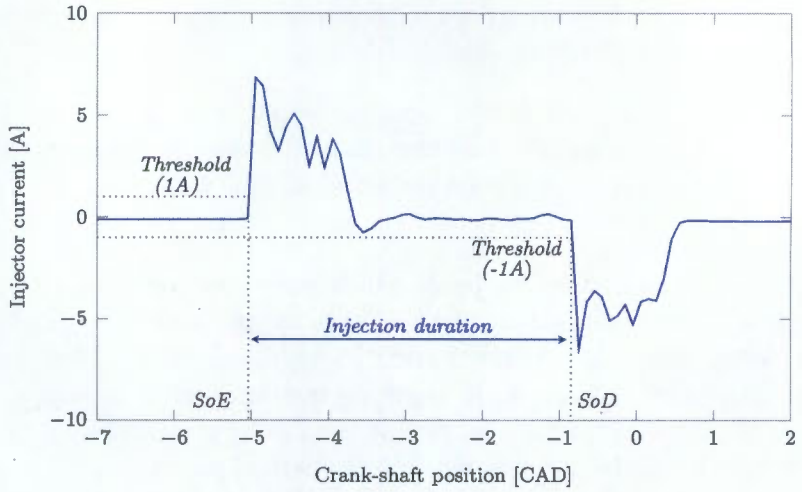

Figure 5.1: *Injector current signal illustrating how SoE, SoD and injection duration were measured.*

5.5 Experimental parameter processing

During the testing phase of this project different operating parameters were adjusted and the results studied, to see the different effects on emissions and combustion. In this study parameters such as injection pressure, SoE, boost pressure, EBP and intake manifold pressure were varied. The results of these studies will be presented and discussed in Chapters 7 and 8. This section details some of the experimental parameters that this project incorporated.

The relative in-cylinder pressure measurement was referenced to the absolute pressure transducer in the inlet manifold at the end of the intake stroke (intake bottom dead centre or IBDC). In an attempt to minimise pressure measurement noise, the inlet manifold pressure and in-cylinder pressure was averaged over 20 °CA from IBDC to 20 °CA after IBDC. The in-cylinder pressure was then adjusted to equal the intake manifold pressure and was achieved using the IndiSmart system. This process can be referred to as in-cylinder pressure 'pegging'.

As previously discussed in this chapter the engine load in this work will be represented using the in-cylinder performance data. The gross indicated mean effective pressure (IMEP) is representative of this. It is a measure of the work done on and by the piston and neglects all frictional losses experienced by the engine, which can vary significantly between engines.

The gross IMEP is defined as

$$\text{IMEP} = \frac{\oint pdV}{V_d}, \text{ [17]} \tag{5.5.1}$$

where IMEP is in bar, p is the cylinder pressure at a specific crank angle, V is the corresponding cylinder volume at the same crank angle, V_d is the cylinder displacement volume and the limits of the cyclic integral are from -360 °CA to 360 °CA. The nett heat release rate (HRR_{nett}) in Joules per degree crank angle (J/°CA)was calculated post testing by using the rate of change of in-cylinder pressure and volume data,

$$\text{HRR}_{\text{nett}} = \frac{\gamma}{\gamma - 1} p \frac{dV}{d\theta} + \frac{1}{\gamma - 1} V \frac{dp}{d\theta}, \text{ [17]} \tag{5.5.2}$$

where γ is the specific heat ratio (c_p/c_v) which was treated as a constant and θ is the crank angle position. Integrating the heat release rate from before SoI to 50 °CA after top dead centre (°ATDC) gave the approximate total heat released (THR) in Joules (J) during the combustion process.

$$\text{THR} = \int \text{HRR}_{\text{nett}} d\theta \tag{5.5.3}$$

A number of points along the integrated HRR_{nett} profile were of importance and used in various calculations. The crank angle values at 5 %, 10 %, 50 % and 90 % of the THR were used. The start of combustion (SoC) was defined at the crank angle for 5 % THR, this is also referred to as 5 % mass fraction burned or MFB5. Therefore, ignition delay in °CA (degrees crank angle) was defined as the difference between SoE and 5 % THR. Combustion phasing was controlled by adjusting 50 % THR °CA (or MFB50), the midpoint of the total heat release curve. The combustion burn duration was calculated as the difference in CA position between 10 % and 90 % THR (MFB90 - MFB10).

Cyclic variability in parameters such as IMEP, peak cylinder pressure and corresponding CA position at which such peak cylinder pressure occurs, are good indicators of combustion stability. Changes in any of these resulted in a change in the coefficient of variation for IMEP (CoV_{IMEP}). This was particularly useful when operating within the LTC regime where combustion stability is very poor, thus CoV_{IMEP} was a way of comparing combustion across tests. The equation for CoV_{IMEP} is defined as

$$\text{CoV}_{\text{IMEP}} = \frac{\sigma_{\text{IMEP}}}{\mu_{\text{IMEP}}} \tag{5.5.4}$$

where σ_{IMEP} is standard deviation of IMEP and μ_{IMEP} is the average IMEP over 100 cycles. Equations 5.5.1, 5.5.3 and 5.5.4 were calculated in Indicom in real time. The indicated data was continuously averaged in real time in Indicom and then recorded in STARS at a frequency of 1 hz during tests. Typically, 100 seconds of data (100 data points per parameter) in STARS was recorded and averaged to give a data point.

The majority of the testing in this project involved diluting the intake charge with exhaust gas (EGR). As a means of measuring the amount of exhaust gas dilution, the EGR rate

was calculated on a volumetric basis. The volume fraction of both the intake and exhaust CO_2 ($CO_{2,int}$ and $CO_{2,exh}$ respectively) were measured. The ambient CO_2 ($CO_{2,amb}$) was assumed to be 0 %. These values were combined to give the equation for the EGR rate.

$$EGR\% = \frac{CO_{2,int} - CO_{2,amb}}{CO_{2,exh} - CO_{2,amb}} \times 100 = \frac{CO_{2,int}}{CO_{2,exh}} \times 100 \tag{5.5.5}$$

The dilution effect (or effectiveness of the dilution in reducing peak combustion temperatures) at nominally constant EGR % but at different operating conditions can vary. Therefore, comparing results of tests conducted at high levels of EGR with respect to the intake oxygen concentration ($O_{2,int}$) as opposed EGR % can be more representative of the dilution effect. Rottger et al. proposed that the burnt mass fraction (FMAN) drawn into the engine is directly related to the intake oxygen concentration [57],

$$FMAN = \frac{EGR}{100} \times \left(1 - \frac{O_{2,exh}}{20.95}\right) = 1 - \frac{O_{2,int}}{20.95} \tag{5.5.6}$$

where $O_{2,exh}$ is the oxygen concentration in the exhaust. By rearranging Equation 5.5.6, the intake oxygen was calculated.

$$O_{2,int} = \frac{1 - FMAN}{20.95} \tag{5.5.7}$$

The exhaust emissions were converted from measured concentrations (ppm or %) to a mass flow rate basis (g/h) and then to an indicated specific form (g/kWh). This process was repeated for each data point recorded in 100 seconds (approximately 100 data points) and then averaged to give the indicated specific emission which could then plotted. The detailed conversion process can been seen in Appendix B.3.

Chapter 6

Commissioning, verification and characterisation testing

Before the complex-control LTC testing could commence, system testing was carried out to ensure the test apparatus performed according to its complete set of functional requirements. The tests in this project were conducted using diesel fuel complying with the *EN590:2009* specification. The interested reader can refer to Appendix D for a comprehensive fuel analysis. The purpose of this chapter is to detail these preliminary tests and results. This testing was divided into four main sections which were necessary for the commissioning of the test apparatus. These were:

i. Run-in of the single-cylinder diesel test engine.

ii. Performance and control accuracy of the test facility sub-systems.

iii. Characterisation of the engine under conventional boosted and naturally aspirated combustion.

iv. Assessing the attainability of LTC using the designed test apparatus.

6.1 Engine run-in

The most important factor that deems an engine run-in necessary is friction inherent in a new engine. Most of this friction is present in the cylinder liner. The research engine was run in according to AVL's five hour procedure. This included three 'motored tests' staggered by two 'fired tests' and is summarised as follows:

i. The *motored test* involved motoring the engine at 7 different speeds from 1000 rpm to 4000 rpm (500 rpm intervals). The engine was run at each speed for 15 minutes. After each motored test was complete, a fired test was carried out.

ii. The *fired test* comprised of four engine speeds (1000 to 4000 rpm and 1000 rpm intervals) and three loads per speed (3 bar, 6 bar and maximum IMEP). Each operating mode was run at for 10 minutes. Following each fired test, a motored test was run.

The test run-in was only considered to be complete once both the engine friction had stabilised and the five hour run-in procedure was complete. Engine friction was assessed by measuring the negative torque produced by the engine during the motored tests. When the difference in measured torque between motored tests was approximately zero, the engine friction had stabilised.

6.2 System control performance

This section highlights some of the critical control areas and how they perform during standard engine operation. Table 6.1 shows the system requirements and desired control accuracy.

Table 6.1: *Operating parameters and their respective range and accuracy.*

System Variable	Range	Accuracy
intake temperature	30 – 75 °C	±1 °C
intake pressure	0 – 1200 mbar(g)	±20 mbar
oil temperature	85 °C	±1 °C
coolant temperature	85 °C	±1 °C
EGR rate	0 % – ±70 %	±1 %
rail pressure	200 – 1800 bar(g)	±15 bar

Tests were performed to assess and verify the system's performance relative to the design requirements. The engine was run at 1500 rpm (the speed at which the LTC testing would be performed). Parameters such as boost pressure, injection pressure, intake temperature and EGR rate were adjusted individually. The measured parameters were compared to their setpoints and design accuracy as illustrated in Figure 6.1. Multiple setpoints for each parameter were tested; however, it was most appropriate to demonstrate the system's performance for operating conditions that were to be used for testing in the project. The tests were conducted over a 100 second time period, as typical 100 seconds of data was recorded at 1 Hz per test point during the CDC and LTC test work.

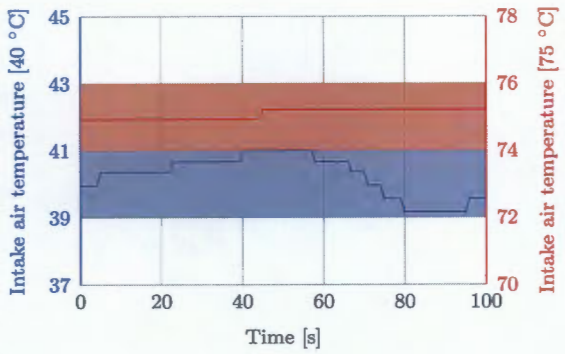

(a) *Intake air temperature control at 40 °C and 75 °C.*

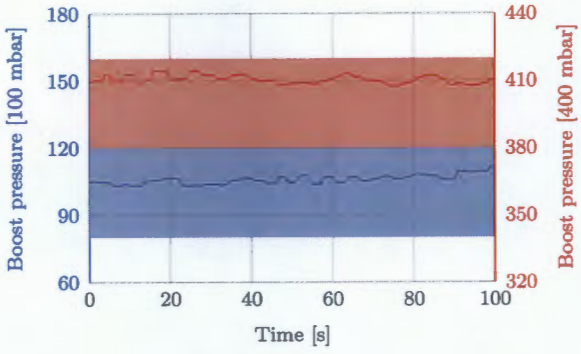

(b) *Boost pressure control at 100 mbar and 400 mbar (gauge).*

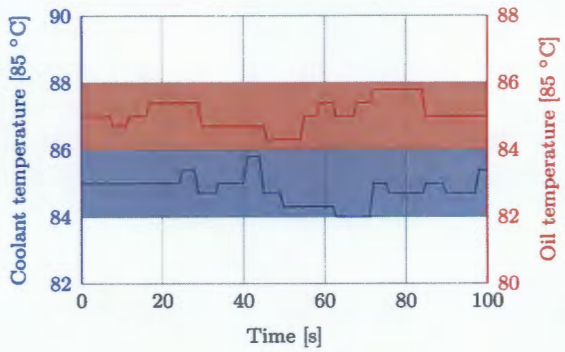

(c) *Coolant and oil temperature control at 85 °C.*

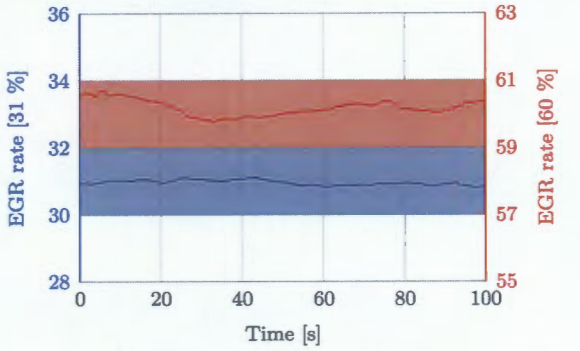

(d) *EGR rate control at 31 % and 60 %.*

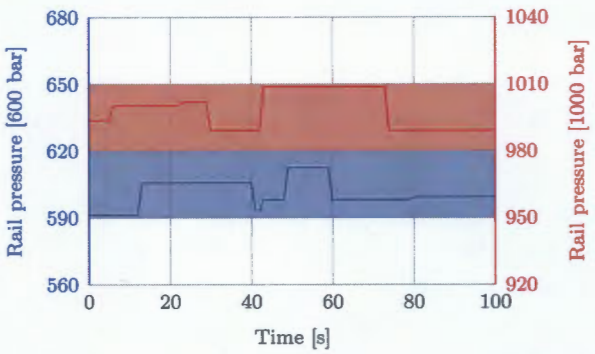

(e) *Rail pressure control at 600 mbar and 1000 mbar.*

Figure 6.1: *Control accuracy achieved by some of the systems, and how they performed relative to the design requirements over a 100 second time period.*

The plots in Figure 6.1 show a low setpoint on the left axis and a high setpoint on the right axis. The y-axes and plots are colour-coded. For each plot, design accuracy required is indicated by the shaded area. If the measured parameter moved outside of the shaded area, the design accuracy requirement was not being met and further work had to be done on the control or mechanical systems (sometimes both). The plots illustrate the operational

control of the final design and demonstrate that both setpoint and control accuracy criteria were met. Real-time rail pressure control was performed at a high frequency and in a closed-loop manner; however, the rail pressure data could not be recorded in the same fashion, hence the plot updates at inconsistent and extended time intervals. The chance of detecting inaccurate rail pressure using this pressure measurement is unlikely, due to its low update frequency. The rail pressure data was cross referenced with IMEP and CoV_{IMEP}, as fluctuations in these parameters are indicative of poor rail pressure control.

6.3 Engine characterisation

This section highlights how the engine's optimum performance, in terms of maximum IMEP at optimised SoE for best indicated specific fuel consumption (ISFC), was experimentally established across the speed and load range. In addition, the engine operating limits which shaped its performance, and which limit took effect at what speed are presented here.

The testing was carried out as follows:

i. *Naturally aspirated, full load test*: to determine the peak torque the engine can produce under naturally aspirated conditions subject to the engine's mechanical limits.

ii. *Boosted, full load test*: to determine the maximum torque the engine can achieve across the speed range, based on the engine's mechanical limits.

iii. *Boosted, engine performance test*: to determine the engine's performance in terms of best ISFC with respect to load and speed across its operating range.

It must be noted that for all tests SoE was optimised for best ISFC. Additionally, all tests made use of a single injection strategy, with rail pressure determination handled by the designed lookup table programmed into the ECU. The full engine speed range for the tests was from 1000 rpm to 4000 rpm at 500 rpm intervals. For the boosted tests, the compressed air source was treated as a turbocharger based on the boost and EBP lookup tables developed in this study. At each boost pressure and load condition, the model output a corresponding EBP, which was achieved via manual adjustment of the EBP valve.

Characterising the engine was also a means to establish reference data that is comparable to future test results generated within this study, or throughout external studies. Simultaneously, a better understanding and feel for the engine's limitations, capabilities and operation was gained. This section presents and discusses the results of this test work. In addition, unless explicitly stated by the use of 'brake' before the performance parameter, the results reported are on an indicated basis.

6.3.1 Results from the full load naturally aspirated and boosted testing

As an initial test, the full load capacity of the engine, both naturally aspirated and boosted, was determined. The hard test parameter limits responsible for shaping the engines load capacity were based on engine mechanical limits provided by AVL [6] and presented in Table 6.2. As expected, Figure 6.2 indicates that by boosting the engine and increasing the charge density, a greater peak IMEP results, due to the increased in-cylinder oxygen mass, and therefore, the ability to add more fuel. On average the IMEP values for the boosted curve were approximately 68 % greater than for the naturally aspirated test.

Table 6.2: *Mechanical engine limits.*

Variable	Limit	Reason
Max Exhaust Gas Temperature	650 °C	material limits of exhaust manifold
Max allowable Rmax	15 bar/°CA	engine noise and wear
Max allowable cylinder pressure	155 bar	engine component failure at 170 bar
Max allowable boost pressure	1200 mbar	valve springs too soft, valve piston contact

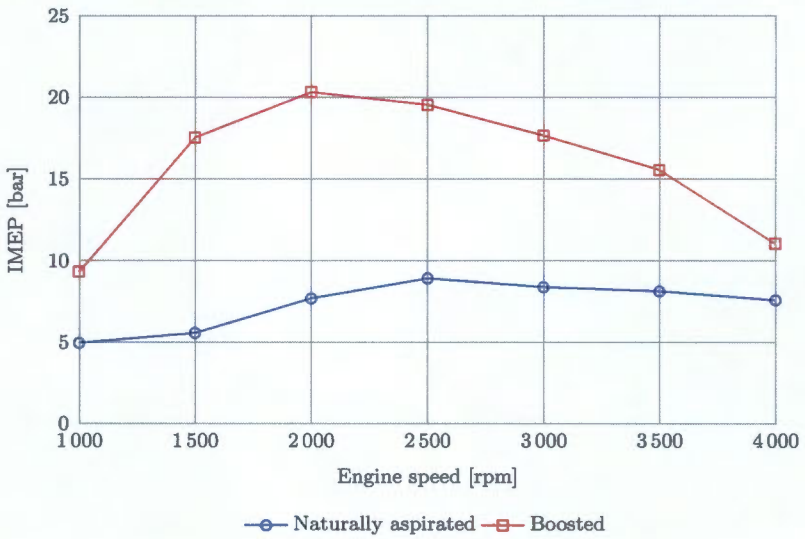

Figure 6.2: *Peak IMEP data for naturally aspirated and boosted tests.*

The engine mechanical limits, comprising the maximum allowable levels of engine exhaust gas temperature, cylinder pressure, and rate of in-cylinder pressure rise, typically limited the load capability of the engine at different speeds. Figure 6.3 (*a*) to (*d*) illustrates the indicated power and torqued results as well as the engine limiting operating parameters for both the naturally aspirated and boosted tests. Plots (*a*) and (*b*) correspond to the naturally aspirated test and (*c*) and (*d*) to the boosted test.

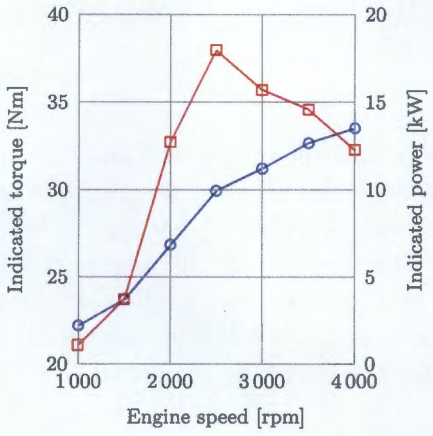

(a) *Indicated torque and indicated power results from the full load naturally aspirated test.*

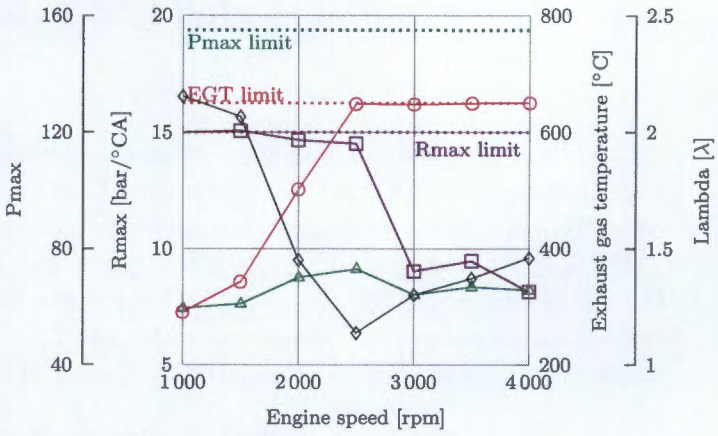

(b) *Maximum cylinder pressure, exhaust gas temperature, rate of cylinder pressure rise and lambda from full load naturally aspirated test.*

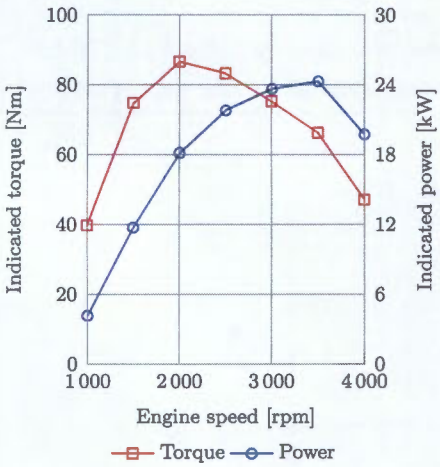

(c) *Indicated torque and indicated power results from the full load boosted test.*

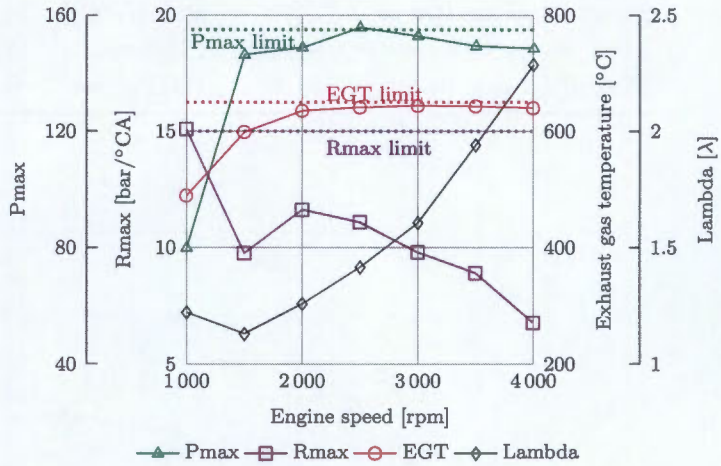

(d) *Maximum cylinder pressure, exhaust gas temperature, rate of cylinder pressure rise and lambda from full load boosted test.*

Figure 6.3: *Naturally aspirated and boosted test results, including the indicated torque and power accompanied by the engine operating parameters that limit the engine's load capacity.*

Figure 6.3 (a) demonstrates that the peak naturally aspirated indicated power of 13.5 kW occurred at 4000 rpm and a peak indicated torque of 37 Nm, at 2500 rpm. Figure 6.3 (b) indicates that the maximum rate of in-cylinder pressure rise (Rmax) limits the engine's load capacity at speeds below 2500 rpm. However, from 2500 rpm the exhaust gas temperature at the manifold becomes the dominant limiting factor, therefore inhibiting the use of any additional fuel as a means of increasing the engine's load capabilities.

Peak in-cylinder pressures were far from the engine's mechanical limit throughout the naturally aspirated test. For the boosted full load test, a peak power of 24.3 kW occurred at 3500 rpm and a peak torque of 86.6 Nm, at 2000 rpm (see Figure 6.3 (c)). The maximum rate of pressure rise only limited the boosted test at 1000 rpm. From 1500 rpm, peak in-cylinder pressures and exhaust gas temperatures were both approximately at their respective limits, and therefore, no additional fuel could be injected.

The naturally aspirated test reached a peak IMEP of 8.9 bar at 2500 rpm, whereas for the boosted test, a peak IMEP of 20.3 bar was reached at 2000 rpm. The difference can be attributed to the fact that the injection pressure map was developed based on a boosted engine, where higher average injection pressures are typically used without significantly increasing the HRR [17]. However, had other strategies been used for the naturally aspirated test; such as, the addition of a pilot injection, lower injection pressure, and reduced swirl, Rmax would have decreased [17]. Furthermore, since the exhaust gas temperature for the naturally aspirated test at 2000 rpm is still approximately 150 °C below the upper limit, additional fuel could have been injected into the cylinder, possibly shifting the maximum load of the naturally aspirated test to 2000 rpm.

Comparing lambda for the two tests indicates that fuelling at low speeds is far more limited, in terms of quantity injected, for the naturally aspirated test. Conversely, for the boosted test, lambda indicates that fuelling is far more limited at higher engine speeds. However, since peak in-cylinder pressure and the exhaust gas temperature are at their thresholds from 2000 rpm in the boosted test, increasing the applied engine load any more by running richer (by the addition of fuel) would typically have resulted in an engine limit being exceeded, and therefore possible engine component failure.

6.3.2 Results from engine performance testing

The final characterisation test included optimised SoE for best ISFC across the speed and load range. The maximum load was defined by the full load boosted curve determined in the previous test. The result of this test was a performance map for the single cylinder research engine. Contours of best ISFC in grams per kilowatt-hour (g/kWh) were plotted on a graph of IMEP and speed in Figure 6.4. The speed and load points at which the engine was tested are indicated by the blue asterisks. As previously mentioned, the engine intake boost, corresponding EBP, and rail pressure were controlled using the maps developed in this study. The selection of the optimum ISFC point at each speed and load was performed manually, post testing.

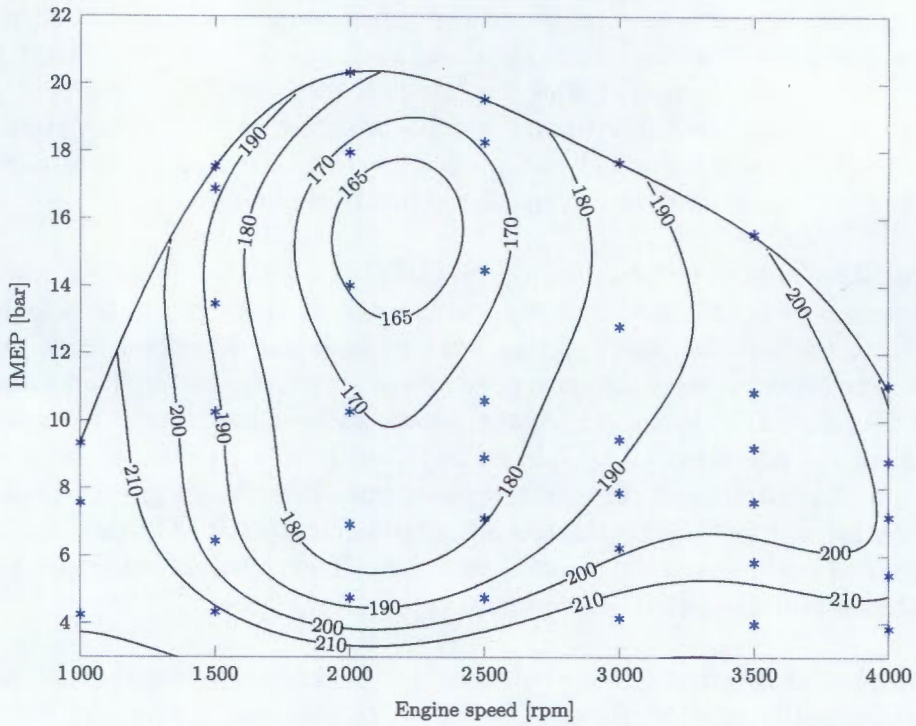

Figure 6.4: *Performance map illustrating contours of best ISFC (g/kWh) plotted on a graph of IMEP and engine speed.*

Figure 6.4 illustrates a maximum ISFC at low load conditions across the speed range. It further demonstrates that ISFC reduced with increased load, particularly at speeds between 1700 rpm and 2500 rpm. A global minimum ISFC was found to exist approximately at an IMEP between 13.5 bar and 17.5 bar at a corresponding speed between 2000 rpm and 2500 rpm; this is roughly 78 % load at the corresponding engine speed. Any further increase in load, from this minimum, resulted in increased ISFC until peak load was reached. The aforementioned trends highlighted in the performance map are in line with the trends seen in literature [17, 38].

6.4 Baseline EGR sweep and LTC investigation

In total, six tests were performed which involved transitioning the engine from CDC to LTC by adjusting the EGR rate. The first two tests were benchmark (or baseline) repeat tests and were required for the commissioning of the test facility, but also formed a part of the primary LTC tests (tests 3, 4, 5 and 6) presented in Chapter 7. Hereinafter these two tests will be referred to individually as *baseline 1* and *baseline 2*.

The baseline investigation (comprised of *baseline 1* and *baseline 2*) was defined to:

- determine if LTC could be achieved with the current test apparatus setup, and therefore achieve a range of EGR rates from 0 % to a maximum EGR rate (defined by the point at which the engine begins to misfire),
- assess the inherent challenges associated with LTC and transitioning to and from CDC,
- evaluate the test repeatability,
- assess combustion and emissions sensitivity to EGR rate and intake oxygen concentration, and
- establish a set of reference results to which the outcomes of the parametric test can be compared.

The EGR range for the tests can be divided into three sections, namely, CDC (from 0 % to 45 % EGR), soot hump (approximately between 45 % and 62 % EGR), and the LTC region (from approximately 62 % EGR upwards). The repeated test conditions used in this investigation are presented in Table 6.3. Combustion phasing in terms of MFB50, was controlled between 6 °ATDC and 7 °ATDC by manual adjustment of SoE. In addition, it must be noted that all tests were performed at nominally constant fuelling.

Table 6.3: *LTC parametric test conditions.*

Test no.	Speed [rpm]	Intake Temp. [°C]	Boost & back P. [mbar]	Rail P. [bar]	Inj. dur. [μs]	MFB50 [°ATDC]	SoE [°ATDC]	Parameter change
1 & 2	1500	40	400 & 800	600	484.0	$6 \sim 7$	Var.	–

6.4.1 Investigation of ISNOx-ISSoot relationship

The results of the first EGR sweep were positive as the typical ISNOx and ISSoot versus EGR rate curves, as well as the target emissions for the LTC operating regime, were both achieved; as commonly reported in literature. The first noted phenomenon discovered from this test was the fact that the relationship between the intake oxygen concentration and EGR rate was not linear (see Figure 6.5). The rate of reduction in intake oxygen with respect to increasing EGR rate, increased. This highlighted the importance of tightened EGR rate control at higher EGR rates.

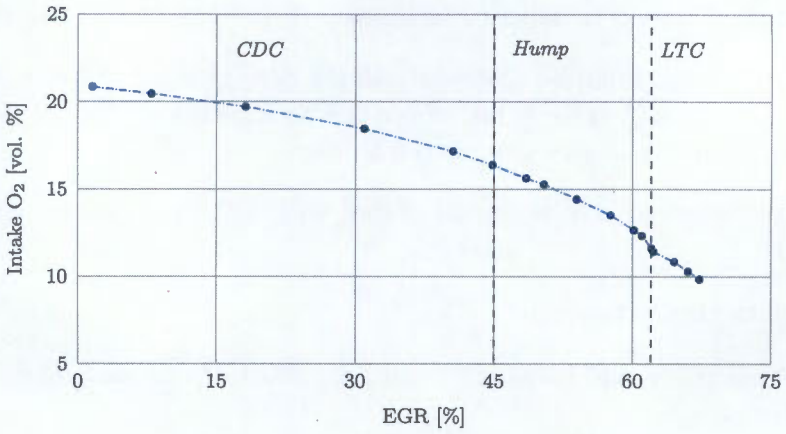

Figure 6.5: *Intake oxygen concentration against EGR rate for baseline 1.*

Figure 6.6 (a) and (b) demonstrates ISNOx and ISSoot as a function of EGR rate. Plot (b) is a magnified view of the LTC region on plot (a). The target ISNOx and ISSoot emissions are indicated by the red and blue dashed lines respectively. As expected, when the EGR rates were increased from zero, ISNOx immediately began to decrease from a maximum. At this point, ISSoot remained fairly constant, as peak combustion temperatures were assumedly still above that required for sufficient soot oxidation (> 1600 K as discussed in Section 2.1.2). Once EGR rates exceeded 40 %, the soot oxidation mechanism was quickly degraded, and soot formation became dominant, reaching a peak at about 58 % EGR. As EGR rates were further increased, causing the peak local combustion temperatures to drop to below those favourable for soot formation, soot emissions sharply declined. The ISNOx target was reached at approximately 50 % EGR. The soot emissions target, and thus LTC, was achieved at approximately 62.8 % EGR. It was expected that the ISNOx emissions target be reached first, whilst combustion was far more stable. The greater challenge was achieving the ISSoot emissions target due to the fact that combustion stability rapidly deteriorated as intake oxygen concentration was reduced below 12 %. This is indicated by the change in coefficient of variance for IMEP (CoV_{IMEP}) as depicted in Figure 6.7 and is briefly discussed in Section 6.4.2.

6.4.2 Investigation of combustion stability and sensitivity

From Figure 6.6 it is clear that engine-out soot was very sensitive to EGR rates greater than 40 %, especially between 58 % and 62 % EGR. The cylinder pressure and heat release rates for 0 % (CDC), 53.6 % (soot hump) and 62.8 % (LTC) EGR are plotted in Figure 6.7. LTC is known to require a much longer ignition delay, which helps to improve the air-fuel mixing, reducing the tendency for rich mixture regions in the combustion chamber. Additionally, the high dilution (11.3 % intake O_2) helps to reduce the maximum rate of

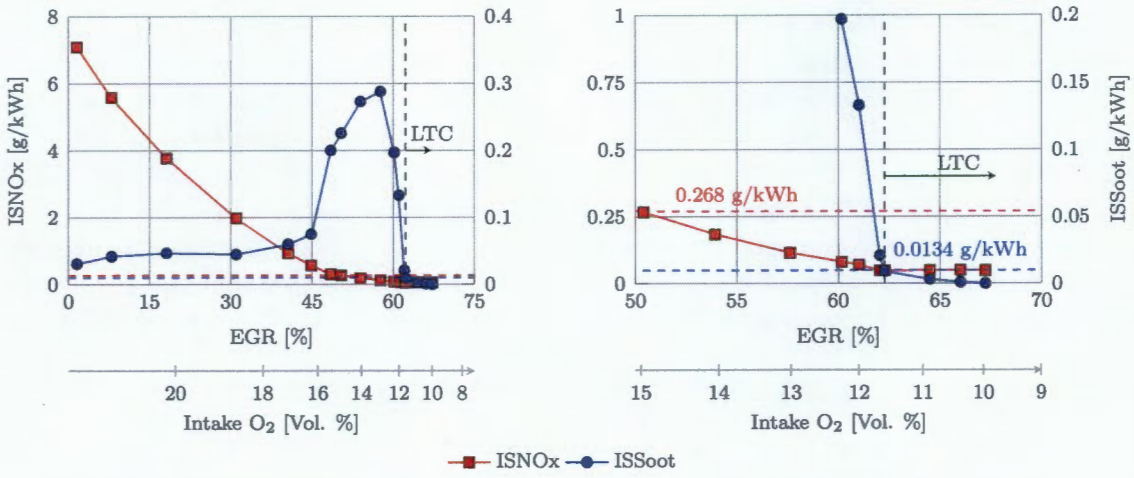

(a) *ISNOx and ISSoot as a function of EGR rate.* (b) *Magnification of the LTC region in plot (a).*

Figure 6.6: *ISNOx and ISSoot as a function of EGR for the full EGR range (a) and a magnified view focussing on the LTC region (b).*

heat release and lower the flame temperatures. The decreasing peak HRR, with increasing EGR, is clearly visible in the plot, as is the decreasing slope of the cylinder pressure during premixed combustion. A secondary consequence of the lowered peak HRRs in LTC was the audible reduction in engine combustion noise.

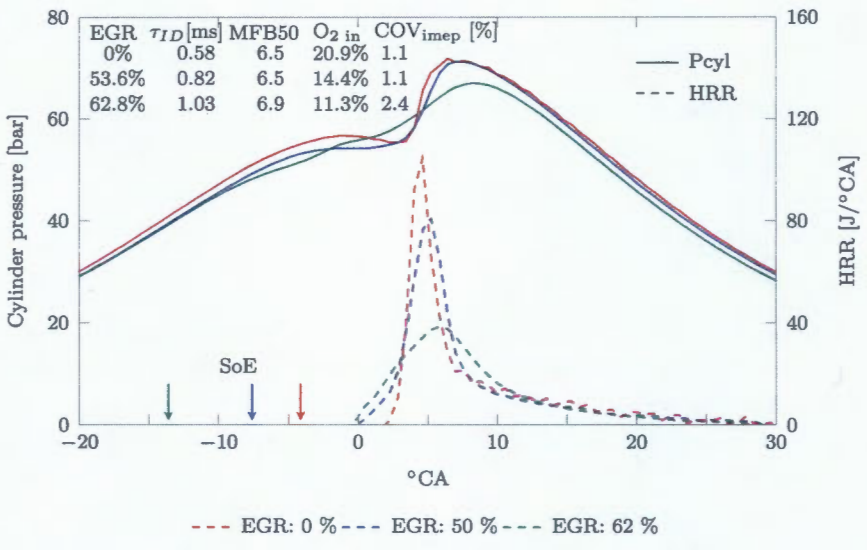

Figure 6.7: *Cylinder pressure and heat release rates for baseline 1.*

A consequence of high EGR rates is heightened sensitivity to slight changes in EGR %, as indicated by the cylinder pressure and HRR curves in Figure 6.8 from *baseline 1.* The low combustion temperatures, as well as the high charge dilution, generally result in incomplete combustion as the available oxygen is consumed during the combustion process [50]. It was found that EGR rate changes of as little as 1 % had a large effect on ISSoot and ISHC emissions, as well as IMEP, even with SoE controlled combustion phasing (MFB50 controlled between 6 °CA and 7 °CA). The ISHC emissions can drain a significant amount of fuel energy away from the combustion event, therefore promoting the reduction in IMEP. The typical high ISHC and ISCO emissions generally present within the LTC regime result in the poor fuel efficiency currently associated with this type of LTC combustion strategy.

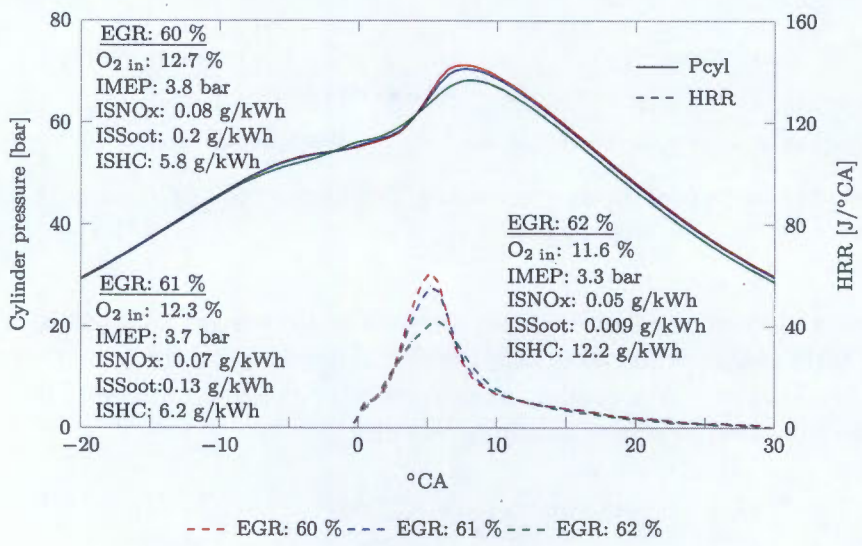

Figure 6.8: *Sensitivity of LTC to EGR rate for baseline 1.*

6.4.3 Test repeatability

Figure 6.9 demonstrates the ISSoot, ISNOx, ISHC and maximum in-cylinder pressure respectively, with regard to EGR rate. Where appropriate, error bars were plotted indicating one standard deviation, calculated from the data captured per test point, above and below said test point. The magnitude of the error bar is referred to as the standard error. The maximum standard deviation for EGR rate (on a volume basis) for the two baseline tests were both similar at approximately 0.50 % EGR; furthermore, they were not EGR rate dependant. The discrepancy in the emissions, possible causes for these differences, and repeatability within these regions are discussed now.

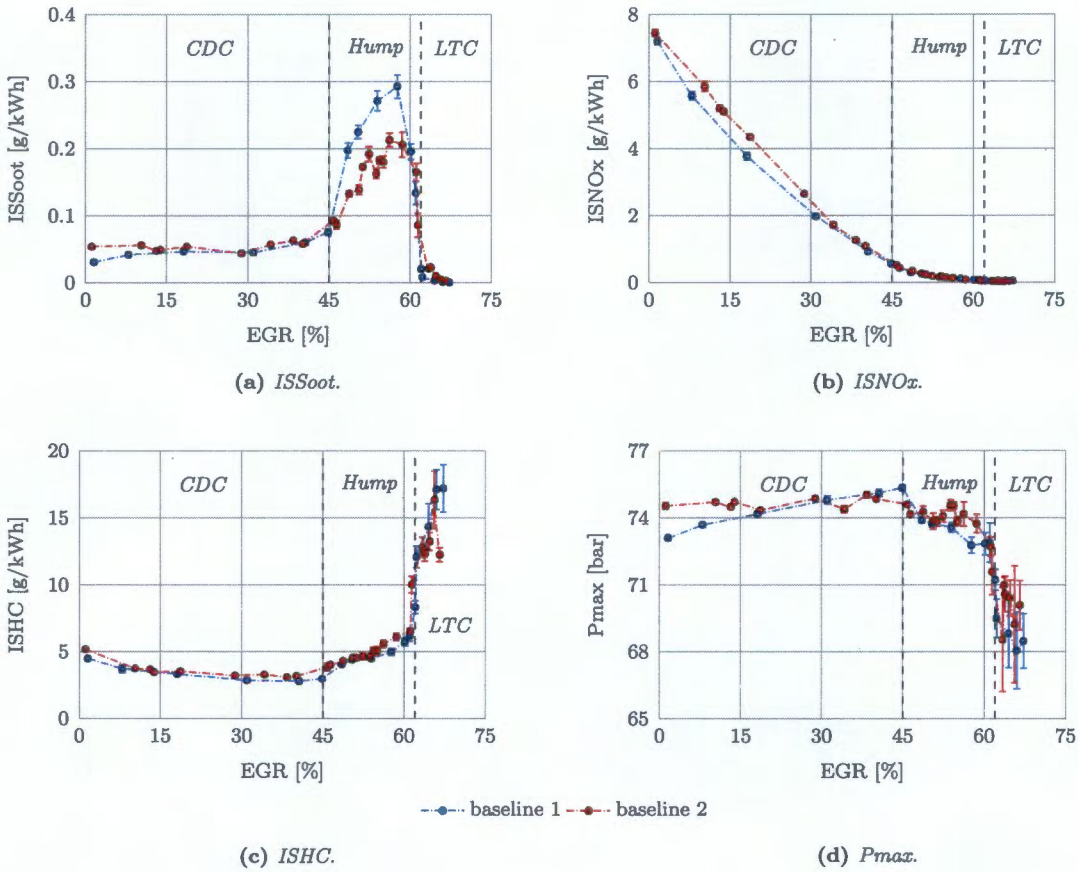

(a) *ISSoot.* (b) *ISNOx.*

(c) *ISHC.* (d) *Pmax.*

Figure 6.9: *Baseline test results demonstrating the variation in ISSoot (a), ISNOx (b), ISHC (c) and maximum in-cylinder pressure (d) with respect to EGR rate. Where applicable, the error bars indicating one standard deviation above and below the test point were included.*

CDC region

ISSoot was consistently higher for *baseline 2* within the CDC region (Figure 6.9 (a)). However, the difference in ISSoot between the two tests was noticeably larger at lower EGR rates (0 % – 13 % EGR) within this region. The ignition delay recorded in *baseline 2* was marginally longer than that of *baseline 1.* Although the difference in ignition delay was small, this difference could have potentially resulted in reduced peak local equivalence ratios at the SoC, thereby reducing soot formation. The combustion duration in *baseline 2* was measurably shorter than that of *baseline 1* (Figure 6.10), therefore indicating an increased rate of combustion. It was speculated that improved air fuel mixing caused a faster combustion rate, and therefore an enhanced rate of oxidation in the diffusion flame. As is already known, engine-out soot is the nett result of the competing soot

formation and soot oxidation reactions. Both of the aforementioned hypotheses would have resulted in reduced engine-out soot for *baseline 2* relative to *baseline 1*; however this is contrary to the ISSoot levels presented in Figure 6.9 (a). Tree and Svensson found that an increase in combustion pressure increases soot formation at a rate which could be as high as the square of the pressure [27]. It was therefore speculated that the peak cylinder pressure difference between the baseline tests (see Figure 6.9 (d)) counteracted the assumed effects of lengthened ignition delay and shortened combustion duration, and was the main contributing factor to the discrepancy in ISSoot emissions.

Additionally it was found that there was an expected correlation between ignition delay and ISNOx between *baseline 1* and *baseline 2* (Figure 6.9 (b)), i.e. longer ignition delays typically result in mixtures which are closer to stoichiometric, which are favourable for NOx formation reactions, therefore greater ISNOx. Additionally, as the intake charge was diluted with exhaust gas, the ISNOx steadily decreased at a declining rate. As discussed in Section 2.3 and 2.2.3, this is typically attributed to the reduction in peak combustion temperatures, predominantly due to the dilution effect. As expected with stable combustion within the CDC region, ISHC was fairly repeatable (see Figure 6.9 (c)).

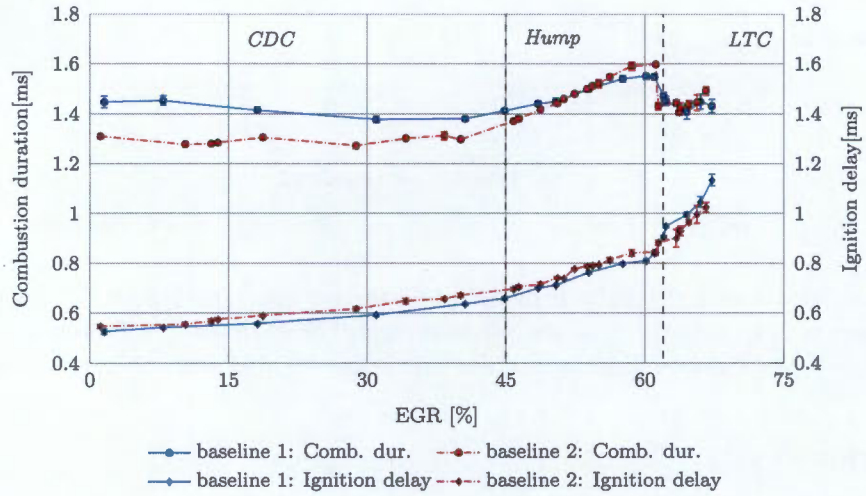

Figure 6.10: *Combustion duration and ignition delay against EGR rate with standard deviation error bars.*

Figure 6.11 and 6.12 illustrate the in-cylinder pressure, heat release rate (HRR), and injection current profile at 40 % EGR, as well as relevant test data for the two baseline tests at nominally the same operating conditions. SoE required for each baseline test at 40 % EGR, in order to maintain combustion phasing is indicated in the plots; SoC was also displayed for the two tests.

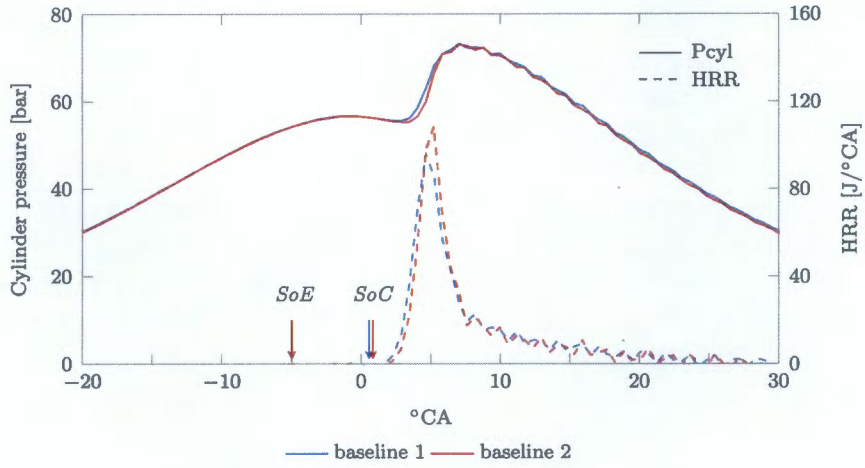

Figure 6.11: *In-cylinder pressure and HRR at 40 % EGR for the two baseline tests.*

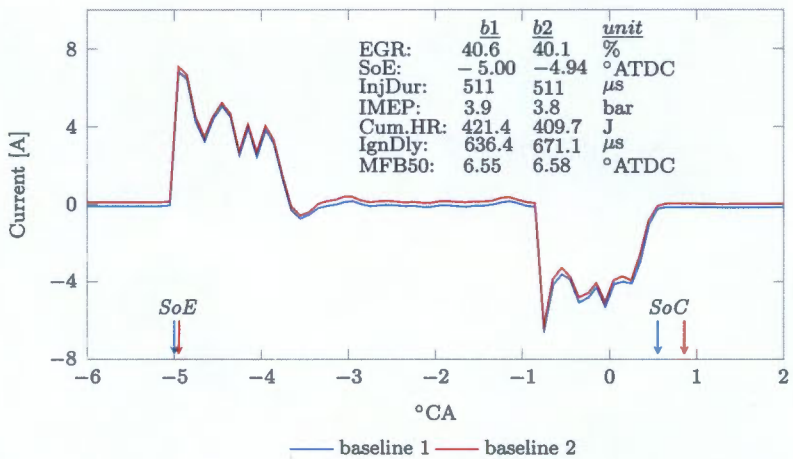

Figure 6.12: *Injection signal at 40 % EGR for the two baseline tests.*

The in-cylinder pressure profile and peak pressure were similar. There was; however, a noticeable difference in SoC and ignition delay. A longer ignition delay typically results in a greater premixed combustion portion and a corresponding increased peak HRR, as seen for *baseline 2* (Figure 6.11). Additionally, ISNOx for *baseline 2* at 40 % EGR was approximately 9 % greater due to the suspected improved conditions for NOx formation (Figure 6.9 (b)), as illustrated by the longer ignition delay and increased HRR in Figure 6.11. It was noticed that although the SoC phasing was different, the combustion phasing, in terms of MFB50, was essentially the same (see data presented in Figure 6.12), again indicating that the rate of heat release for *baseline 2* was greater than *baseline 1*. The actual injector current signal for the two tests (demonstrated in Figure 6.12) indicates

that, provided the rail pressure control was accurate, a similar quantity of fuel would have been injected, and at approximately the same SoE. The cumulative heat release for the two baseline tests (421.4 J and 409.7 J) presented on Figure 6.12 are similar, again implying a nearly constant injection quantity.

Ignition delay is heavily dependent on the rate of mixture formation and therefore, hinges on injection pressure, boost pressure, swirl rate and intake temperature. However, these operating parameters did not fluctuate significantly during testing, indicating no obvious cause of change in the mixture formation rate. Figure 6.13 illustrates the control of these operating parameters during the baseline tests.

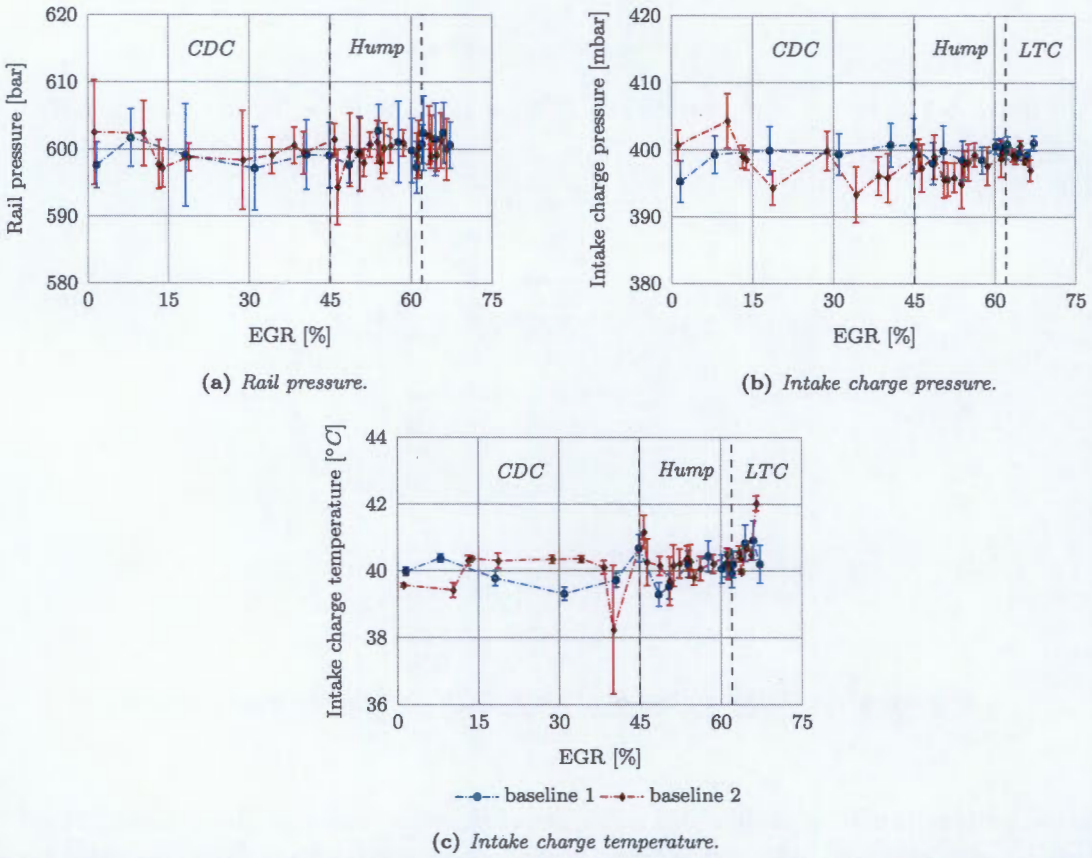

(a) *Rail pressure.*

(b) *Intake charge pressure.*

(c) *Intake charge temperature.*

Figure 6.13: *Rail pressure (a), boost pressure (b) and intake manifold temperature (c) repeatability with standard deviation error bars for baseline 1 and baseline 2.*

Soot hump region

To reiterate, the engine-out soot is the nett result of the competing soot formation and soot oxidation processes. As EGR rate was increased, the peak in-cylinder temperatures were reduced, predominantly due to the dilution effect (lowered oxygen concentration). Because the rate of reduction in soot oxidation with lowered temperature is greater than that of soot formation, the result is increased engine-out soot. With the aforementioned in mind, as well as the effect of mixing on soot formation, it was speculated that the discrepancy in peak ISSoot levels could be attributed to varying mixing rates. Better mixing, in terms of lower local equivalence ratios, generally results in less soot formation. Therefore, the better mixing for this region was probably achieved in *baseline 2*. The longer ignition delay of *baseline 2*, although small, across the soot hump (Figure 6.10) could have caused less soot formation by comparison with *baseline 1*, and thus lower ISSoot. The results of this hypothesis are in line with the ISSoot demonstrated in Figure 6.9 (a). Furthermore, the phasing of the peak ISSoot, with respect to EGR rate, was similar as expected. The ISNOx results were fairly consistent and did not demonstrate any strong dependence on ignition delay or combustion duration at EGR rates within this region.

As has already been discovered, ISSoot is very sensitive to EGR rates within the soot hump region. Therefore, the small control fluctuations in EGR rate have a significant influence on the measured engine-out soot. For this reason, there is a noticeable increase in the standard error of ISSoot across the soot hump, as demonstrated in Figure 6.9 (a).

LTC region

As expected, once EGR levels were sufficiently high, such that LTC was achieved, oxygen levels were low (from approximately 11.8 % oxygen concentration in the intake air as seen in Figure 6.15). The lower the oxygen concentration entering the cylinder for a nominally constant intake boost pressure, the more the fuel and air need to mix before auto-ignition can occur, resulting in longer ignition delays. However, as commonly understood in the case of HCCI combustion, the more homogeneous the fuel and charge mixture is, the harder it is to control SoC. It was postulated that this phenomenon contributed to the significantly increased CoV_{IMEP} (see Figure 6.15) and CoV_{MFB}. It was further hypothesised that the significant combustion instability, also demonstrated by increased peak in-cylinder pressure and ignition delay standard error (indicated in figures 6.9 (d) and 6.10 respectively) resulted in the inconsistent emissions (see increased ISHC standard error in Figure 6.9 (c)) and therefore varying proportions of intake charge mixture species. This varying intake charge mixture affects peak combustion temperatures, ignition delay, and thus mixture formation. It was speculated that this may have been part of the cause for the discrepancy in ISSoot between the two baseline tests within the LTC region (Figure 6.14 (a)).

ISNOx demonstrated little dependence on combustion variation at LTC EGR rates (Figure 6.14 (b)). This is to be expected, as peak combustion temperatures in this region are typically too low for thermal NO formation reactions. It is speculated that the measured NOx in this region is formed by the prompt NO mechanism, which favours rich flames and is suggested to be dominant over thermal NO formation rates at low combustion temperatures [26].

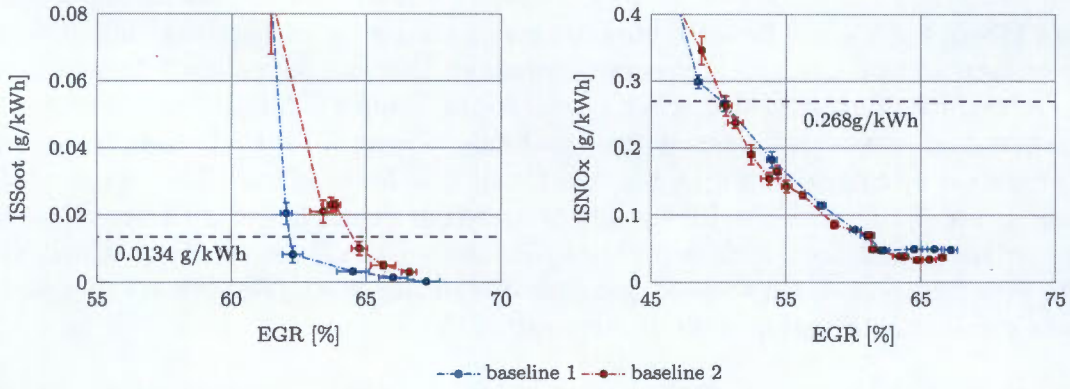

(a) *Magnification of ISSoot under LTC operation.*

(b) *Magnification of ISNOx under LTC operation.*

Figure 6.14: *ISNOx and ISSoot results with standard deviation error bars from baseline 1 and baseline 2.*

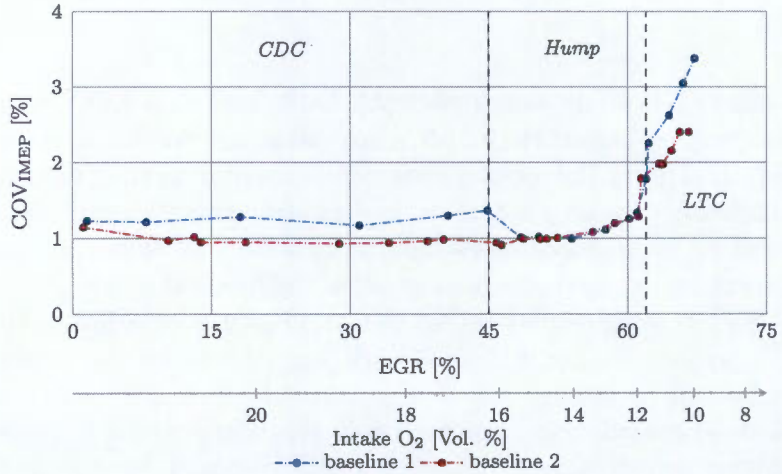

Figure 6.15: *Combustion stability in terms of CoV_{IMEP} against EGR and oxygen intake concentration.*

6.5 Discussion

The test results from this chapter demonstrated satisfactory control of the engine operating parameters. The results also indicated that the data acquisition system was capable of receiving, post processing, and storing significant test data such that further analysis of said data could be conducted. However, it must be mentioned that the transfer rate of data received by the ECU, such as injector rail pressure, to the computer running STARS, which ultimately stores the data, was slow and inconsistent. Recommended improvements to this setup are discussed in the project's recommendations chapter (Chapter 10).

The major achievement of this chapter was the realisation of the LTC operating regime, as defined by the stringent emissions target discussed in Chapter 5. This demonstrated the engines ability to supply controlled and varying quantities of EGR to the engine intake, such that LTC could be achieved. It was noticed that the repeatability could be improved, especially in the case of the ISSoot emissions, and should be investigated. In addition, combustion phasing control was challenging, especially within the LTC regime, but was achieved through manual adjustment of SoE. After analysis of the test data, it was concluded that the test apparatus operation was satisfactory for the purposes of the next phase of LTC testing, as presented in Chapter 7.

Chapter 7

Low temperature combustion testing

The purpose of this project, as far as the LTC testing was concerned, was to achieve a general understanding of the regime and gain a practical feel for the factors that influence the performance, combustion stability, and emissions, whilst operating under LTC and CDC-LTC transition conditions. It must be noted that the results from the two baseline tests are discussed in Chapter 6, as they were required as part of the test facility commissioning process. The test conditions are summarised for all six tests (including the two baseline tests) in Table 7.1 with bold text highlighting the parameters that were changed for each test within the parametric assessment. Tests 3 to 6 were defined as follows:

i. *SoE sweep within the LTC regime* (test 3) to assess the effects combustion phasing and ignition delay have on engine performance and emissions.

ii. *Parametric assessment* (tests 4, 5 and 6) to experimentally determine the effect that operating parameters, such as injection pressure, boost pressure and intake charge temperature have on engine performance and emissions in and around the LTC regime.

Table 7.1: *LTC parametric test conditions.*

Test no.	Speed [rpm]	Intake Temp. [°C]	Boost & back P. [mbar]	Rail P. [bar]	Inj. dur. [μs]	MFB50 [°ATDC]	SoE [°ATDC]	Parameter change
1 & 2	1500	40	400 & 800	600	484.0	6 ~ 7	Var.	–
3	1500	40	400 & 800	1000	402.8	Var.	-21 to -13	SoE
4	1500	40	400 & 800	**1000**	**402.8**	6 ~ 7	Var.	ΔRail P.
5	1500	40	**100 & 200**	600	484.0	6 ~ 7	Var.	ΔBoost P.
6	1500	**75**	400 & 800	600	484.0	6 ~ 7	Var.	ΔIntake T.

In addition to the tabulated test conditions, it must be noted that all tests were performed at nominally constant fuelling. To achieve this for the two tests conducted at an elevated rail pressure, the injection duration had to be shortened accordingly to ensure constant fuel mass flow into the cylinder.

7.1 The effect SoE has within the LTC regime

An experimental study was conducted to assess the sensitivity of various engine operation parameters and emissions to SoE whilst operating under LTC conditions. The engine was operated as per the test 3 specified conditions in Table 7.1 at a nominally constant EGR rate within the LTC region, of approximately 65.6 % (corresponding to an intake O_2 concentration of about 10.6 %). The SoE was adjusted from -13 °ATDC to -21 °ATDC. The results demonstrating significant dependence on SoE were plotted in the figures below. Figure 7.1 demonstrates the relationship between ignition delay and ISSoot and how they vary with SoE within the LTC region. Figure 7.2 indicates how SoE affected CoV_{IMEP}, ISFC, ISHC and ISCO under LTC conditions.

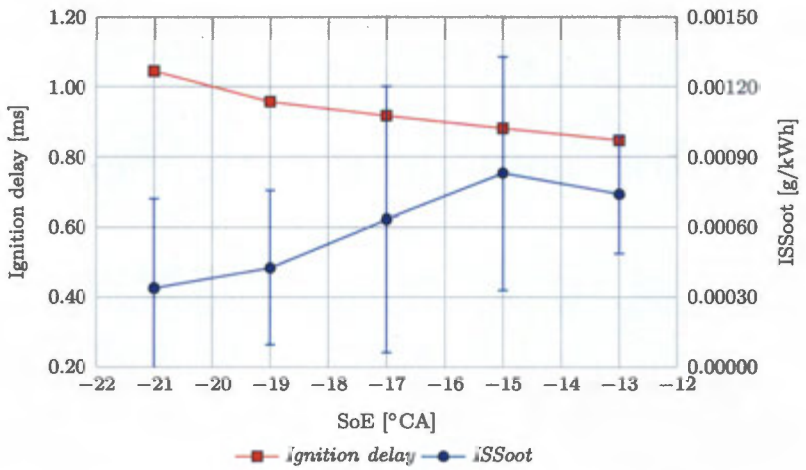

Figure 7.1: *The effect of SoE on ISSoot and ignition delay within the LTC region.*

As SoE was advanced, the ignition delay increased due to fuel being injected into a cooler and lower pressure environment. Additionally, as ignition delay was reduced, ISSoot typically increased. This can be attributed to less premixing and therefore greater inherent tendency for the formation of locally rich air-fuel regions in the cylinder. When the SoE was at -17 °ATDC, Figure 7.2 demonstrates that combustion stability, ISHC and ISFC were at a minimum, and ISCO was close to its minimum for the test. It was also noticed that the changes in ISHC and ISCO (approximately 26 % and 31 %) were significantly larger than for ISFC (approximately 2 %), indicating that the changes in ISCO and ISHC

are not only due to a change in indicated power. Further advancing or retarding SoE from -17 °ATDC, resulted in a deterioration in combustion efficiency, and corresponding increased unburned hydrocarbons. As expected, no significant change was noticed in the ISNOx.

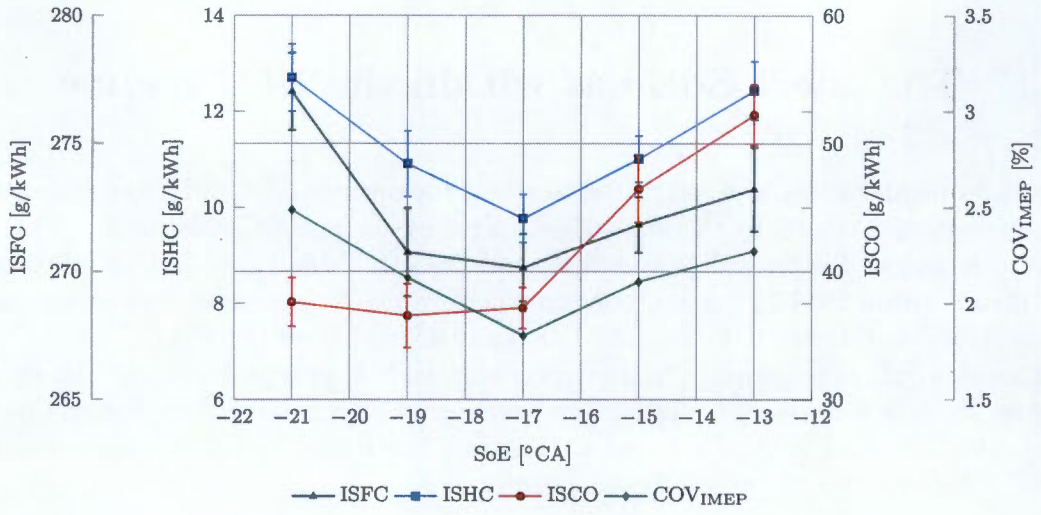

Figure 7.2: *The effect of SoE on ISFC, ISHC, ISCO and CoV_{IMEP} within the LTC region.*

7.2 Parametric sensitivity investigation

This study (test numbers 4, 5 and 6) involved looking at the effects of boost pressure, rail pressure and intake charge temperature relative to *baseline 1*'s results, for a range of EGR rates that corresponded to the turning point of the indicated specific soot hump and the LTC region. Hereinafter, the test conducted at increased rail pressure will be referred to as *RP 1000 bar*, the test conducted at increased intake charge pressure will be referred to as *boost 100 mbar*, and the test conducted at increased intake charge temperature will be referred to as *intake temp 75 °C*. Figure 7.3 illustrates the results of the three parametric investigations relative to *baseline 1*'s test outcomes. Each graph within the figure represents a different measurement, while each test is colour coded. The ISSoot and ISNOx prerequisites for LTC are indicated by dashed lines in Figure 7.4, (*a*) and (*b*) which illustrate a close-up view of ISSoot and ISNOx transitioning into the LTC region. The ignition delay, maximum rate of pressure rise and lambda for *baseline 1* and the three parametric tests are depicted across figures 7.5 and 7.6. The following sections will highlight some of the results for each test and how they compare with literature.

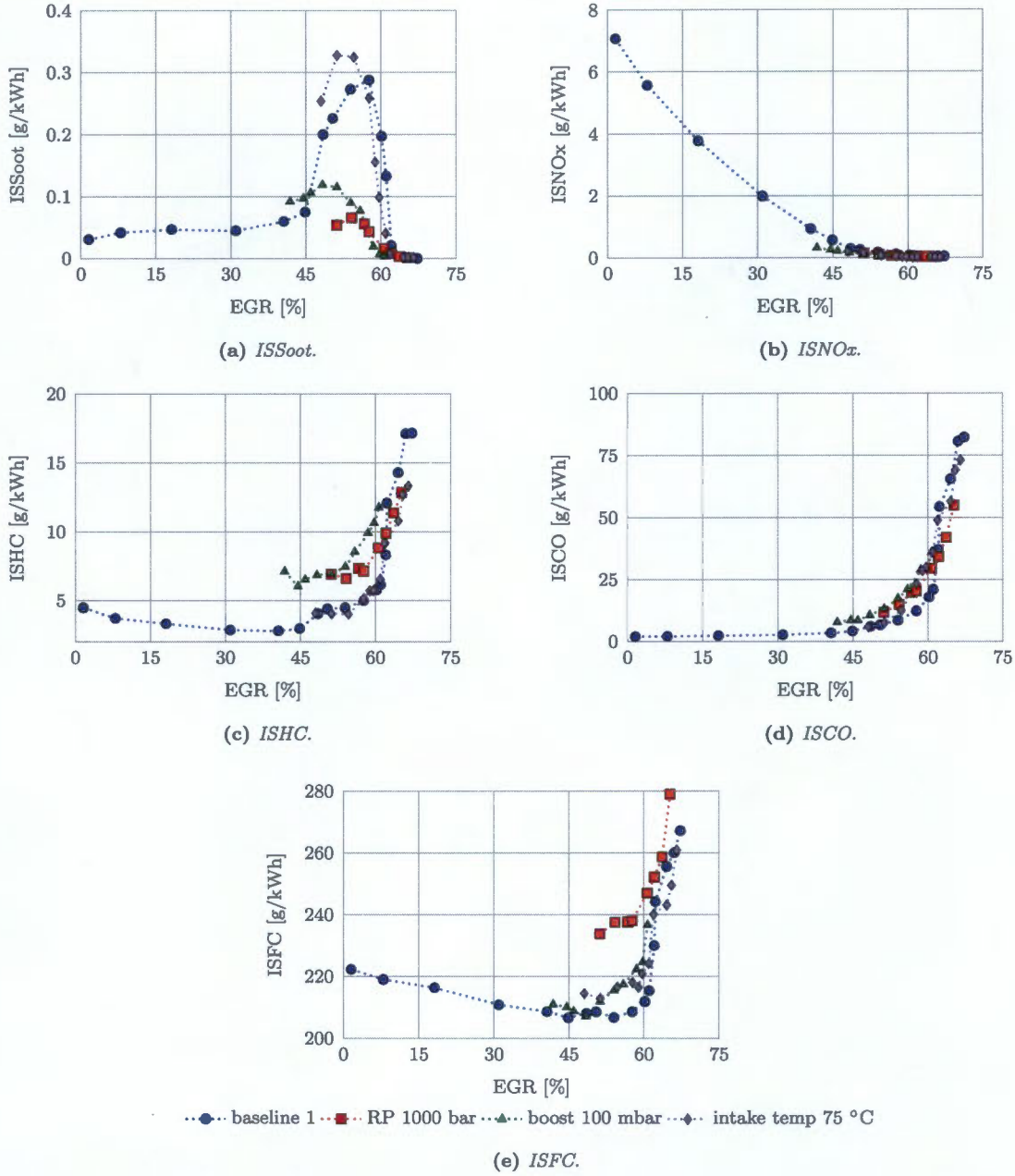

(a) *ISSoot.* (b) *ISNOx.* (c) *ISHC.* (d) *ISCO.* (e) *ISFC.*

Figure 7.3: *Effect of individual operating parameters on indicated specific emissions and ISFC.*

7.2.1 Rail pressure

Higher fuel injection pressure typically resulted in shortened ignition delays with intensified peak heat release rates as demonstrated in Figure 7.5, represented by the larger R_{max} values. These effects are thought to have been due to the improved air-fuel mixing achieved with

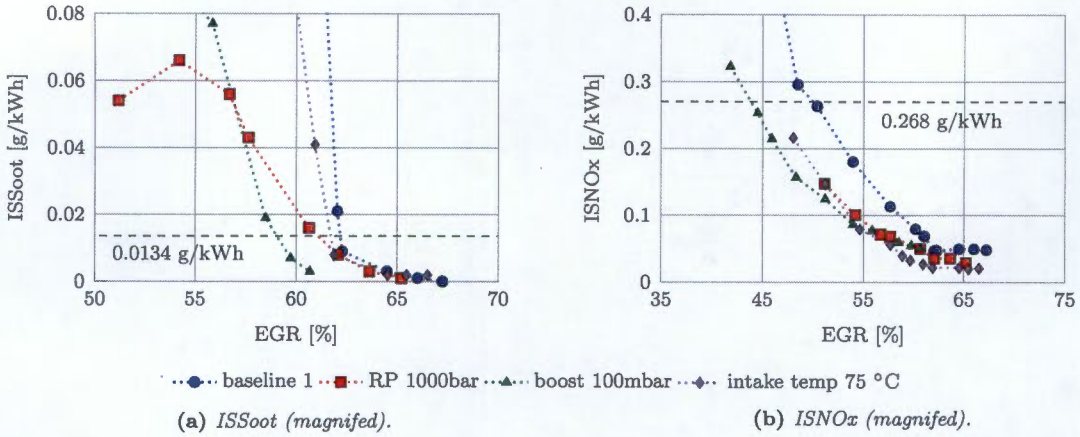

(a) *ISSoot (magnifed).* (b) *ISNOx (magnifed).*

Figure 7.4: *Close-up view demonstrating each parameter's effect on ISSoot (a) and ISNOx (b) emissions operating within the LTC regime.*

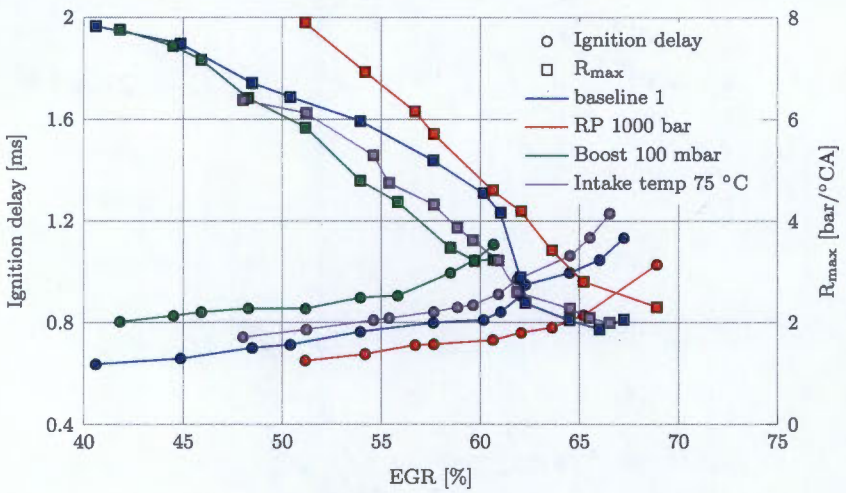

Figure 7.5: *Ignition delay and maximum rate of pressure rise against EGR for baseline 1 and the three parametric tests.*

higher injection pressures, generating a more homogeneous mixture before the SoC.

As discussed in Section 2.3.1, the nett effect of increased injection pressure is improved air fuel mixing before and during combustion. Consequently, leaner peak in-cylinder equivalence ratios ensue, and hence lowered peak ISSoot, as seen in Figure 7.3 (a). The effect of increased rail pressure on ISNOx at high EGR rates was negligible, and assumed to be due to its temperature dependence. At high EGR rates in and around the LTC region, temperatures are typically below that required for thermal NO formation; however, as the prompt NO mechanism favours rich flames and is said to dominate thermal NO formation

at temperatures lower than 2000 K [25], it is suspected that the NO being emitted from the engine was predominantly via this mechanism. However, no significant dependence on rail pressure was noticed. These results agreed with those seen by Asad et al. [2], Ogawa et al. [45] and Yun and Reitz [46].

For *RP 1000 bar*, ISFC indicated an approximate 7.5 % increase between 50 % and 60 % EGR relative to *baseline 1*. At high EGR rates, fuel had to be injected early in order to maintain constant combustion phasing. Injecting this early usually means injecting into a low density and temperature environment, which can result in greater fuel plume penetration and possible impingement of fuel on the cylinder wall. This can greatly increase the amount of unburned hydrocarbons in the exhaust.

7.2.2 Boost pressure

By decreasing the boost pressure, the mass of oxygen entering the engine for a nominally constant EGR rate is effectively reduced, therefore reducing the air-fuel ratio (seen in Figure 7.6 by the reduced lambda for the *boost 100 mbar* test relative to the *baseline 1* test). The effectiveness of the air-fuel dilution in reducing combustion temperatures for the same EGR rate was increased, relative to the other parametric tests, due to the reduced oxygen mass intake at lower intake boost pressures. This resulted in similar trends, but at reduced EGR rates. Consequently, LTC was achieved at approximately 58 % EGR for the *boost 100 mbar* test, as opposed to the *baseline 1* and other parametric tests, for which LTC occurred at approximately 62 % EGR. The increased effectiveness of the dilution in reducing peak combustion temperatures resulted in lowered ISNOx and increased ignition delay at the same EGR rates by comparison with the *baseline 1* test. In order to maintain constant MFB50 between tests, whilst at similar EGR rates of approximately 57 %, $SoE_{basline1}$ was set to -7.7 °ATDC, and $SoE_{boost100mbar}$ was set to -14.3 °ATDC.

ISCO and ISHC emissions were comparatively higher in the *boost 100 mbar* test for the same EGR rate. This can be attributed to the fact that, for a decreased boost pressure and a nominally constant EGR rate, a richer cylinder charge is formed on a mass basis. These results aligned with the findings of Asad et al. [35] and Yao et al. [1] under similar conditions.

A discrepancy was noticed in the reduced peak ISSoot values measured at 100 mbar boost pressure. As discussed in Section 2.3.2, Asad et al. [35] found that engine-out soot increased with decreasing boost pressure. However, Yao et al. [1] found that decreasing the boost pressure resulted in lowered peak soot values. He attributed his findings to the reduced propensity for auto-ignition at lower boost pressures, leading to increased ignition delay and thus a more uniform mixture during combustion. At the EGR rates corresponding to the peak ISSoot for the *baseline 1* test and the *boost 100 mbar* test, the ignition delay was

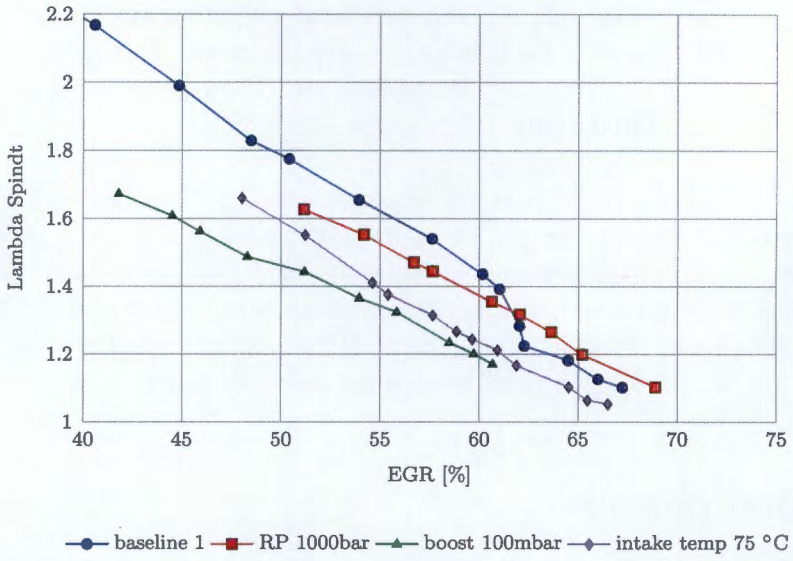

Figure 7.6: *Lambda calculated using the Spindt method against EGR for the baseline 1 and the three parametric tests.*

lengthened for the *boost 100 mbar*, corresponding with the findings of Yao et al.

At LTC conditions soot formation is suppressed due to low peak combustion temperatures. Therefore, the effect of oxygen concentration on ISSoot becomes negligible.

7.2.3 Intake charge temperature

Peak soot emissions were noticeably higher for increased intake temperatures (75 °C). This is consistent with the findings of Asad et al. [2], who reason that the increased intake temperature shortens ignition delay, thus increasing the propensity for locally rich regions which are favourable for soot formation, as discussed in Section 2.3.3.

However, Figure 7.7 demonstrates the relationship between combustion duration and ignition delay as a function of EGR for the *baseline 1* test, and the *intake temp 75 °C* parametric test. The data indicated in this graph reveals that the parametric test had a lengthened ignition delay and combustion duration. The longer ignition delay contradicts the reasoning given by Asad et al. and therefore cannot be used to explain why the peak indicated specific soot results in the parametric test are greater than those of the *baseline 1* test.

It is speculated that the lengthened ignition delay at elevated temperatures relative to

the *baseline 1* test was influenced by the lowered mass of oxygen entering the engine (indicated in Figure 7.6 by the *intake temp. 75 °C* test's reduced lambda at elevated intake temperatures relative to the *baseline 1* test). The effect of raising the intake temperature on intake oxygen mass, can result in lengthened mixture preparation times due to lowered oxygen availability and therefore also extended combustion duration (as demonstrated in Figure 7.7). A longer combustion duration can lead to longer residence times for soot formation reactions and therefore increase the engine-out soot. It is hypothesised that the effect of increased ignition delay on reducing soot formation was counteracted by the elevated intake temperature and consequently lowered oxygen mass.

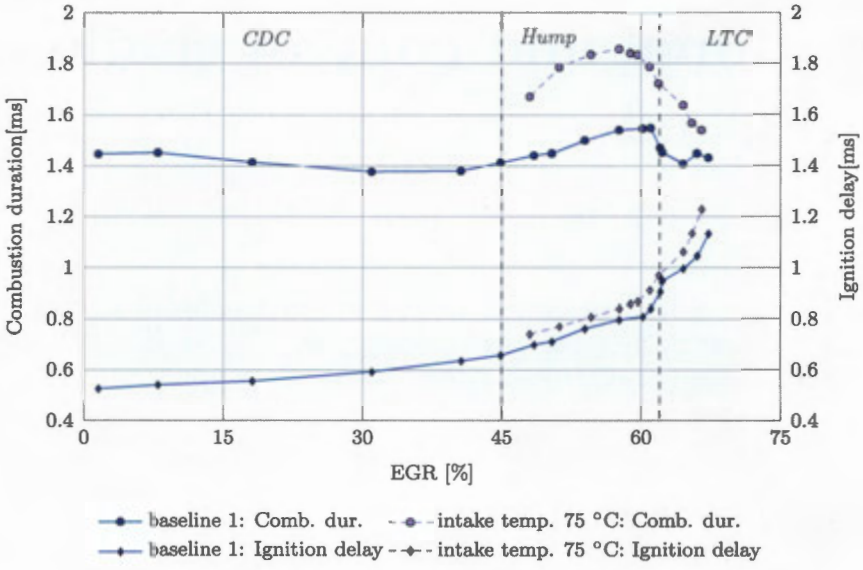

Figure 7.7: *Comparison between combustion duration and ignition delay against EGR for baseline 1 and the intake temp. 75 °C test.*

Chapter 8

Operational and control challenges experienced

Due to the prototype nature of the test facility setup a number of startup, commissioning and early research testing problems were encountered. This chapter deals with some of the more significant challenges experienced.

8.1 Rail pressure fluctuations

The quantity of fuel injected by the piezoelectric injector on a common rail system is a function of various parameters and fuel properties, including rail pressure, fuel viscosity and injection duration. The control system was set up such that the injection duration was determined by the user-specified injection mass and the setpoint rail pressure, not the actual rail pressure. Therefore, if the rail pressure fluctuated, the injected quantity would also, thereby causing a variation in the engine's operating conditions. It is for this reason that accurate rail pressure control was required. This section will allude to the modes of rail pressure control as discussed in Section 4.4.2 whilst discussing some of the rail pressure challenges faced, and how they were resolved.

8.1.1 Challenge description

Throughout the course of this project, there were various rail pressure control challenges faced, each one giving new understanding to what is required for each mode of control.

The following two operating conditions where poor rail pressure control was most prevalent were:

i. low load and low speed conditions using the metering unit control mode, and

ii. high load and high speed conditions using PCV control mode.

8.1.2 Solution and discussion

It was discovered that fluctuations in rail pressure, at low loads when using metering unit rail pressure control, is inherent; as the rail pressure cannot be relieved quickly enough with the small injection quantities in this mode. That is to say, this creates a situation where the fuel common rail can be quickly pressured by the metering unit valve, but very slowly depressurised by short fuel injections. It is common practice to switch to the PCV control mode during low loads and idle conditions. As the test data of interest was *indicated*, the increased brake losses associated with this approach would not have an effect on the results.

The AVL team achieves accurate rail pressure using PCV mode control. Furthermore, it was discovered that AVL's PCV mode involved fixing the metering unit duty cycle to 40 %, at a frequency of 400 Hz i.e. a constant volume of fuel is always being pressurised by the high pressure pump, regardless of the fuel quantity required by the engine. Therefore, the extra fuel present in the rail was relieved using accurate control of the PCV duty cycle at a fixed 600 Hz frequency. However, it was discovered that when operating the engine at high load and speed conditions the rail was effectively being starved of fuel, resulting in major rail pressure fluctuations. It was experimentally determined that at maximum fuel consumption a lower metering unit duty cycle was required (effectively reducing the quantity of fuel being diverted back to the measuring circuit without reaching the common rail) in order to maintain pressure. One would expect that the engine would experience large continuous parasitic losses if the metering unit were always set to a 60 % duty cycle. Additionally, this excessive pumping of fuel to the rail also increases the fuel temperature leaving the rail, which, if not controlled, will affect the fuel consumption measurement stability. For this reason, the control system was modified such that, when using PCV mode, the metering unit duty cycle was determined as a function of the specified injection mass and engine speed. Therefore, a close to optimum amount of fuel is pressurised at all times when in PCV mode.

After the rail pressure control issues were resolved it was noted that for all future testing, the rail pressure during low load conditions was most efficiently and accurately controlled using the PCV mode. Additionally, from medium to high loads and speeds, the metering unit control mode was the optimum means of controlling the rail pressure.

8.2 EGR valve servo motor burnout

The EGR valve used in this project was a standard original engine manufacturer (OEM) part from the Polo 1.4 *l* TDI. It was comprised of a sprung loaded poppet valve actuated by a geared servo-motor. When the valve was inactive, the spring held it in the closed position. The servo-motor operated off 5 V. The unit made use of a potentiometer for valve positional feedback. The analogue output signal from the potentiometer was a voltage between 0 V (valve in closed position) and 5 V (valve in fully open position), which was interpreted as the valve's position. The valve had two mechanical limits; namely, when the valve was fully open and when it was fully closed. In practice these correspond to a positional feedback voltage of approximately 0.8 V and 4.2 V.

8.2.1 Challenge description

Shortly after testing commenced, it was noticed that the EGR valve's servo-motor was operating at fairly high temperatures. The temperatures were not measured; however, the motor housing was too hot to touch at times. It was initially thought to be due to heat conduction from the hot exhaust gas being passed through the valve, this was until motor failure occurred. It was found that when the valve was set to the closed position (originally thought to be at 0 V feedback), the valve reached the end-stop before the feedback signal displayed 0 V. Since the controller instructed the motor to hold its position at 0 V the motor continued to close the valve up against the end-stop. It was speculated that the inherent high current through the stalled motor and consequent temperature rise resulted in motor burnout.

8.2.2 Protection measures

The National Instruments throttle driver module that was used to control the EGR valve has a 10 A and a 140 °C module temperature shutdown limit. Before motor failure, this was assumed to be sufficient to protect the servo-motor. After the motor burnout, additional motor protective precautions were installed. These are briefly summarised and explained as follows:

i. The throttle controller was set up such the mechanical end-stops couldn't be reached by the user. To achieve the EGR levels required in this project, the maximum extent to which the valve had to be opened was approximately 75 %. To achieve the fully closed valve position the unit was deactivated and the spring loaded poppet valve closed automatically.

ii. The motor was tested and it was noted that the typical current drawn by the motor was less than 1 A. It was observed that the only time the current exceeded 1 A was when the valve reached an end-stop. Since the valve was not to be activated at its end stops, a 2 A fuse was put in series with the electric motor. Therefore, if the program failed and the valve was driven against an end-stop, the fuse would burn out before motor failure. Additionally, the throttle driver module was set to shut down if it reached 85 °C or the motor current exceeded 6 A.

After these fixes were made the servo-motor no longer experienced high temperatures, not even at high EGR rates.

8.3 Fuel mass flow rate measurement challenges

8.3.1 Challenge description

On various occasions, at nominally constant fuel flow rates of approximately 0.55 kg/h, fluctuations in fuel mass flow rate exceeding 0.1 kg/h (or 18 %) were measured. The uncertainty of the coriolis fuel mass flow meter at 0.55 kg/h was calculated in accordance with the AVL 735S manual [58] to be approximately 0.63 %. This corresponds to a measurement accuracy of 0.55 kg/h $\pm$ 0.003 kg/h. Initially it was assumed that the fuel mass flow meter was operating on the lower edge of its range (0 to 125 kg/h), and thus could not expect stable measurements. However, repeat tests showed that sometimes the unit would yield stable measurements. As a result, further investigations were performed in an attempt to find the root cause.

8.3.2 Challenge discussion and solution

The fuel is returned from the engine at three points, namely, fuel bypassed from the high pressure fuel pump, fuel relieved from the high pressure rail, and fuel returned from the injector. These three streams mix in the fuel return manifold before being reintroduced into the fuel measurement circuit. The temperature of the fuel was measured in the fuel return manifold.

It was discovered that the high pressure fuel pump fuel supply pressure was not constant. This had a knock-on effect on the quantity of fuel being pressurised, and therefore, the quantity of fuel being relieved from the rail in order to maintain constant pressure. There was an inherent temperature rise associated with pressurising the fuel from the supply

pressure (nominally 5 bar), to the desired rail pressure of (approximately 800 bar). A corresponding temperature fluctuation was measured in the fuel return manifold which was in phase with the duty cycle of the PCV on the common rail.

The two common causes of measurement error when using the AVL 735S are the [58]:

i. mean fuel temperature change in the measurement circuit, and

ii. formation of vapour bubbles in the measurement circuit.

It is speculated that the change in temperature in the fuel return manifold resulted in temperature (and density) inhomogeneity as well as a change in the fuel measurement circuit's mean temperature. As previously stated, this can cause measurement error.

The following system changes were made:

i. Increased fuel pump throttling in an attempt to achieve an enhanced balance between fuel being pumped and fuel being consumed, such that less hot fuel needed to be relieved from the rail, and therefore reduced amplitude in fuel return temperature fluctuations.

ii. Installation of a pressure regulator as a means of steadying the high pressure pump fuel supply pressure.

These changes resulted in stabilised fuel return temperature. Consequently, the cyclic variations in the measured fuel flow rate ceased. However, it was later discovered that the repeatability of the AVL 735S was poor. Additional means of determining the fuel mass flow rate had to be investigated, the results and discussion of which are presented in Appendix B.2.

8.4 Dynamometer cooling fan failure

The dynamometer has a squirrel-cage cooling fan which is powered by an electric motor. This assembly is mounted on top of the dynamometer housing. Air is sucked in through an air filter and channeled downwards into the dynamometer.

8.4.1 Challenge description

During operation the squirrel cage broke up and fell into the dynamometer housing. Some of the fan blades landed on the stator winding, creating a conductive path to the housing,

subsequently causing a short circuit. The damage included the complete destruction of the cooling fan and breakdown of a small portion of the stator winding insulation. It was discovered that the engine balancer shafts moved out of phase, causing the test bed to vibrate vigorously. These vibrations were transmitted to the squirrel cage impeller, consequently the fan failed.

8.4.2 Challenge solution

To resolve the issue of the excessive engine vibration, the balancer shafts were realigned. As a preventative measure in the case of future fan failure, a metal grid was installed in the opening between the impeller housing and the dynamometer. Hence, if the impeller were to fail again, the debris would be contained within the impeller housing, thus protecting the dynamometer from further damage.

8.5 Excessive pressurised oil flow out of the crank case breather

The single cylinder research engine made use of a dry sump and utilises the wet sump built into the coolant and lubrication conditioning unit. Oil was pumped from the wet sump to the engine. The oil drained from the engine back to the wet sump under gravity.

8.5.1 Challenge description

On numerous occasions during testing pressurised oil was forced out of the crankcase breather 2 m into the air. If the oil splurges were not noticed immediately, oil was forced out of the crank case breather until insufficient oil existed in the system to maintain oil pressure. At this point a the safety mechanism activated, bringing the engine to a standstill.

8.5.2 Challenge solution

An additional breather pipe was installed on the return line from the engine (at the oil outlet from the engine). This resulted in the continuous drainage of oil from the engine, indicating that an air lock in the oil return pipe was blocking the flow of oil. A clear pipe was connected to the bottom of the dry sump such that when the crank case began to fill

up with oil, it could be seen from the control room. It was speculated that the oil in the dry sump collected until a point when its level was higher than the breather port, causing the pressure in the crank case to build up (as a result of blow-by) until it was sufficient to force the oil out through the crank-case breather. The installation of the additional breather proved to be a useful solution and no further oil drainage problems were experienced.

8.6 Oil contaminated by excessive intake water

One of the by-products of combustion is water vapour. When using EGR, the water vapour in the exhaust gas forms part of the charge air, and is reintroduced into the engine. If this water vapour condenses before it enters the engine, it collects in the plenum chamber of the inlet manifold. This liquid collects until it overflows into the cylinder. Some of this liquid water gets into the oil circuit, and changes the oils characteristics by, for example, reducing its viscosity. This problem was detected in the research engine during an oil change. The white foam that forms in oil when coolant is mixed into the oil circuit was noticed.

A collection vessel was attached to the plenum via a ball valve. When operating the engine with EGR, the ball valve could be opened, such that water vapour that condensed in the intake manifold was able to drain out of the plenum chamber. It must be noted that this was a sealed unit and therefore air could not escape the system unless it was out of the exhaust.

Chapter 9

Conclusions

The two main objectives of this project were:

i. To construct and attain accurate control of a safe state-of-the-art diesel research test facility which utilises a single-cylinder diesel research engine. In addition, it was necessary to characterise the engine as part of the commissioning process. The characterisation was in terms of peak load capacity across the speed range, and minimum ISFC across the full speed and load range of the engine.

ii. To assess whether LTC could be achieved using the designed setup operated at part-load conditions. To clarify, the goal was to determine whether the 2010 EPA emissions standards for NOx and soot could be met using LTC without the use of exhaust after-treatment systems.

Based on the project activities and experience, the following conclusions could be drawn:

9.1 Test facility performance

Upon completion of the commissioning tests, both of the project objectives were successfully achieved. The following key conclusions were drawn:

i Operation across the engine's speed and load range at a variety of different parameter set-points was achievable.

ii LTC was successfully realised with the test apparatus by gradually increasing the EGR rate. A secondary conclusion to this, is that the EGR loop control methods used were sufficient to achieve controlled flow of exhaust gas to the inlet manifold.

iii During the testing involving the determination of the engine's naturally aspirated and boosted full load capacity, a single injection strategy was employed. It was discovered that increased peak engine-out torque could be realised using a multi-injection strategy in cases where the maximum rate of pressure rise limited the full load capacity of the engine. Therefore, the absolute maximum load capacity of the engine at certain speeds, was not in fact reached.

iv The rail pressure control at low load and speed tests should be realised using the PCV control mode. However, from mid-range to high load and speed conditions the rail pressure should be achieved using the metering unit control mode.

v The current state of the data capturing setup, in terms of data captured in STARS from the ECU and associated data transfer rates and apparent inconsistencies, is insufficient for the analysis of rail pressure stability as stochastic behaviour is seldom detected.

9.2 Soot hump and LTC testing

The conclusions drawn from the additional LTC investigations performed, were of secondary importance. However, the conclusions considered to be of interest are presented now:

i The effects of different operating parameters on combustion characteristics and corresponding emissions cannot be generalised for all conditions. Increasing the intake charge mixture (fresh air and exhaust gass mixture) temperature can potentially result in either an increase or decrease in ignition delay depending on the operating conditions. The increased charge temperature can result in higher in-cylinder charge temperatures earlier on in the compression stroke, such that combustion starts earlier. However, the increased mixture charge temperature will also result in less mass of oxygen entering the engine. If the the oxygen content in the cylinder, due to the EGR dilution, is already resulting in a close to stoichiometric mixture, the effect of increasing the intake temperature and corresponding reduction in mass of oxygen (for nominally constant fuelling) can lead to lengthened ignition delays.

ii The emissions demonstrated in this study (with the exception of NOx) appear to be very sensitive to operating parameters in the soot hump region. The emissions are less sensitive to variation in operating parameters within the LTC regime.

iii Increasing the injection pressure when transitioning from CDC to LTC was found to be the most effective means of reducing peak engine-out soot emissions.

iv Optimising for best ISFC by adjusting SoE appears to be a critical measure in minimising emissions of ISHC and ISCO within the LTC regime. The results of the SoE sweep indicated that by optimising SoE for best ISFC, ISHC and ISCO were simultaneously minimised (see Figure 7.2 in Chapter 7).

In conclusion, the results of the tests conducted in this project have aided in partially validating the original motivation for designing a test facility that could be used for subsequent LTC studies. Furthermore, the test apparatus, although subject to certain recommendations listed in Chapter 10, is now functional and available for further research into the effects of fuel formulation on LTC combustion and CDC-LTC transitions.

Chapter 10

Recommendations

During the commissioning and final testing phases of the project, a number of challenges associated with the testing apparatus and its control during certain operating conditions were experienced. Many of these were addressed and subsequently fixed; however, some of the modifications were not implemented and are addressed below:

i. Closed-loop EGR rate and EBP control should be implemented into the ECU. The manual control of EGR rate is a tedious process and in some instances it can take over an hour to record one test point. It is expected, based on the experience gained during the course of this project, that closed-loop control would result in reduced time and resources wasted in achieving specified EGR rates. In addition, this could enhance the control accuracy of the EGR rate, which is crucial in and around the LTC region. The control algorithm should include an EBP setpoint and an EGR rate setpoint. It is recommended that the EBP valve is controlled in response to the back pressure feedback signal, and the EGR valve be controlled in response to the EGR rate measurement.

ii. Butterfly valve actuators with enhanced positional accuracy should be installed, in order to further improve the EGR rate control accuracy. The EGR and EBP valves used in this project are from a commercial multi-cylinder vehicle, and therefore, are designed for transient operation. These valves have coarse gearing with significant backlash. This causes hunting about certain setpoints.

iii. Closed-loop intake air temperature control should be implemented. In order for this to be achieved, it is recommended that the boost air conditioning unit be relocated closer to the engine (as close as possible for enhanced transient response). It is further recommended that the RTD Pt100 temperature sensor which the unit uses for its temperature control feedback signal, be installed in the engine's inlet manifold.

The boosting unit's high-precision temperature control system could then be used to control the intake charge mixture temperature (accounting for the temperature effects of EGR). This would result in intake temperature control using two setpoints, namely, the EGR temperature and intake mixture temperature. These changes are likely to result in improved intake charge temperature control and reduced testing time.

iv. Closed-loop control on combustion phasing, in terms of MFB50 (or a user specified condition), by adjusting SoE should be implemented, especially for LTC testing. Improved combustion phasing control could significantly improve combustion stability, and consequently stabilise HC and CO emissions measurement errors, particularly noticed in the LTC regime.

v. The relative humidity sensor used for determining the drying effect of the compressor water-separators, should be relocated from the boost conditioning unit to the compressor exhaust where the environment temperatures are below 80 °C. The saturation pressure of the air at the point where the relative humidity sensor is positioned, is calculated in accordance with the SAE J177 [59] recommended equation. This equation becomes increasingly inaccurate at temperatures exceeding 80 °C. Therefore, exceeding this threshold intake temperature with the boosting unit, whilst the relative humidity sensor is installed in it, will result in the inaccurate determination of intake water vapour mass flow rate. This has a knock-on effect, and increases the error in the calculated exhaust mass flow rate and therefore the indicated specific emissions.

vi. The boost and EBP maps should be calibrated and made a function of IMEP across the speed range, as opposed to BMEP. The two modes of rail pressure control have differing resulting frictional effects on the engine, and consequently cause different BMEPs for similar fuel quantities. The differing BMEPs result in different boost pressures. Making the boost pressure and EBP a function of IMEP will result in boost and exhaust back pressure conditions which are independent of the mode of rail pressure control used. In addition, if changes are made to the rail pressure control or any other operating parameter that may result in a change in engine friction, it will not have an effect on the boost and EBP setpoints. It must be noted that this did not have an effect on the test results obtained in this project, as the mode of rail pressure control was constant during operation that included using the boost and EBP maps.

vii. A CAN bus communication platform should be set up to replace the Ethernet communication among the test computers and controllers. This communication protocol has been employed in some of Sasol's other engine test facilities. It has successfully demonstrated an increase in reliable measurement data transfer rates. In addition, the inconsistencies associated with the variable delay time periods present when receiving data in STARS over the LAN connection (sent from the LabVIEW or Indicom PC), have been reduced by the implementation of a CAN bus communication platform.

viii. EGR cooling and intake temperature should be controlled such that the dew point temperature of the mixture in the inlet manifold is not reached. Thereby, minimis-

ing the quantity of condensation collecting in the inlet plenum chamber, effectively resulting in a lowered exhaust mass flow rate which is not detected.

Chapter 6 highlighted that the system repeatability could be improved. Therefore in addition to the aforementioned modifications, it is recommended that the possible sources of repeatability error be investigated before further research is conducted on the test apparatus.

References

[1] M. Yao, Q. Zhang, H. Liu, Z. Zheng, P. Zhang, Z. Lin, T. Lin, and J. Shen, "Diesel Engine Combustion Control : Medium or Heavy EGR ?," *SAE International*, no. SAE 2010-01-1125, 2010. (Cited on pages xii, 12, 15, 16, 19, 20 & 85).

[2] U. Asad, P. Divekar, M. Zheng, and J. Tjong, "Low Temperature Combustion Strategies for Compression Ignition Engines: Operability limits and Challenges," *SAE International*, no. SAE 2013-01-0283, 2013. (Cited on pages xii, 16, 18, 19, 20, 85 & 86).

[3] K. Akihama, Y. Takatori, K. Inagaki, and A. M. Dean, "Mechanism of the Smokeless Rich Diesel Combustion by Reducing Temperature," *SAE International*, vol. 2001, no. SAE 2001-01-0655, 2001. (Cited on pages xii, 9, 15, 16 & 17).

[4] G. D. Neely, S. Sasaki, Y. Huang, J. A. Leet, and D. W. Stewart, "New Diesel Emission Control Strategy to Meet US Tier 2 Emissions Regulations," *SAE International*, no. SAE 2005-01-1091, 2005. (Cited on pages xii, 15, 16 & 17).

[5] P. Adomeit, S. Pischinger, M. Becker, H. Rohs, and A. Greis, "Laser optical diagnostics and numerical analysis of HSDI combustion systems.," in *Proceedings of conference on thermo-and fluid dynamic processes in diesel engines, Thiesel 2004*, p. 331, 2004. (Cited on pages xii, 16 & 17).

[6] AVL, "SASOL TECHNOLOGY LTD SINGLE CYLINDER RESEARCH ENGINE 5402," Tech. Rep. December, AVL, 2013. (Cited on pages xii, 26, 31, 32 & 65).

[7] Government of South Africa, "A NATIONAL STRATEGY FOR THE CONTROL OF EXHAUST EMISSIONS FROM ROAD-GOING VEHICLES IN SOUTH AFRICA," 2015. Available: http://www.mediaforjustice.net/TheAirThatWeBreath/HYPERLINKS/vehicleemissions.htm. (Cited on page 1).

[8] Department of Energy, "Discussion Document on the review of Fuel Specifications and Standards for South Africa," *Government Notice*, 2011. Available: http://www.gov.za/sites/www.gov.za/files/34089_gon204.pdf. (Cited on page 1).

[9] Engineering News, "Mid-2017 clean fuels compliance deadline off the table." Available: http://www.engineeringnews.co.za/article/mid-2017-clean-fuels-compliance-deadline-off-the-table-2014-05-06. (Cited on pages 1 & 2).

[10] M. K. Khair and H. Jaaskelainen, "Exhaust Gas Recirculation," 2014. Available: http://www.dieselnet.com/tech/engine_egr.php. (Cited on pages 1, 2, 13, 14 & 15).

[11] W. A. Majewski and H. Jaaskelainen, "Engine Design for Low Emissions," 2015. Available: http://www.dieselnet.com/tech/engine_design.php. (Cited on page 2).

[12] DieselNet, "Fuels: European Union: Automotive Diesel Fuel." Available: http://www.dieselnet.com/standards/eu/fuel_automotive.php. (Cited on page 2).

[13] E. Olivares, "Japan: Fuels: Diesel and Gasoline," 2013. (Cited on page 2).

[14] US EPA, "Diesel Fuel — Fuels and Fuel Additives — US EPA," *EPA.gov*, Nov. 2012. Available: http://www.epa.gov/OTAQ/fuels/dieselfuels/index.htm. (Cited on page 2).

[15] Delphi, "Worldwide Emissions Standards," 2015. Available: http://www.delphi.com/docs/default-source/catalogs/delphi-worldwide-emissions-standards-pc-ldv-15-16.pdf?sfvrsn=2. (Cited on page 2).

[16] G. Bression, D. Soleri, S. Savy, S. Dehoux, D. Azoulay, H. B.-H. Hamouda, L. Doradoux, N. Guerrassi, and N. Lawrence, "A Study of Methods to Lower HC and CO Emissions in Diesel HCCI," *SAE International*, no. SAE 2008-01-0034, 2008. (Cited on page 3).

[17] J. B. Heywood, *INTERNAL COMBUSTION ENGINE FUNDAMENTALS*, vol. 21. Singapore: McGraw-Hill Book Co, 1 ed., 1988. (Cited on pages 3, 8, 10, 59, 67 & 68).

[18] U. Asad and M. Zheng, "Efficiency & Stability Improvements of Diesel Low Temperature Combustion through Tightened Intake Oxygen Control," *SAE International*, vol. 3, no. SAE 2010-01-1118, pp. 788–800, 2010. (Cited on page 3).

[19] DieselNet, "How Emissions Are Regulated." Available: http://www.dieselnet.com/standards/intro.html. (Cited on page 5).

[20] T. Li, R. Moriwaki, H. Ogawa, R. Kakizaki, and M. Murase, "Dependence of premixed low-temperature diesel combustion on fuel ignitability and volatility," *International Journal of Engine Research*, vol. 13, pp. 14–27, Dec. 2011. (Cited on page 6).

[21] S. Cong, C. P. Garner, and G. P. McTaggart-Cowan, "The effects of exhaust back pressure on conventional and low-temperature diesel combustion," *Journal of Automobile Engineering*, vol. 225, pp. 222–235, Feb. 2011. (Cited on page 6).

[22] W. A. Majewski and H. Jaaskelainen, "Environmental Effects of Emissions," 2004. Available: http://www.dieselnet.com/tech/env_effect.php. (Cited on page 6).

[23] M. K. Khair and H. Jaaskelainen, "Emission Formation in Diesel Engines," 2015. Available: http://www.dieselnet.com/tech/diesel_emiform.php. (Cited on pages 6 & 10).

[24] K. Mollenhauer and H. Tschöke, *Handbook of diesel engines.* Springer, 1 ed., 2010. (Cited on pages 6, 7, 13 & 14).

[25] J. E. Dec, "A Conceptual Model of DI Diesel Combustion Based on Laser-Sheet Imaging*," *SAE International*, no. SAE 970873, 1997. (Cited on pages 7, 8, 11 & 85).

[26] K. K. Kuo, *Principles of combustion.* John Wiley, 2005. (Cited on pages 7 & 78).

[27] D. R. Tree and K. I. Svensson, "Soot processes in compression ignition engines," *Progress in Energy and Combustion Science*, vol. 33, pp. 272–309, June 2007. (Cited on pages 8, 9, 15 & 74).

[28] T. Aizawa and H. Kosaka, "Investigation of early soot formation process in a diesel spray flame via excitationemission matrix using a multiwavelength laser source," *International Journal of Engine Research*, vol. 9, pp. 79–97, Jan. 2008. (Cited on page 8).

[29] T. Kitamura, T. Ito, J. Senda, and H. Fujimoto, "Mechanism of smokeless diesel combustion with oxygenated fuels based on the dependence of the equivalence ratio and temperature on," *International Journal of Engine Research*, vol. 3, no. 4, pp. 223–248, 2002. (Cited on page 8).

[30] R. Baranescu and B. Challen, *Diesel engine reference book.* Bath: Society of Automotive Engineers Inc., 2 ed., 1999. (Cited on pages 10, 13 & 45).

[31] T. Li and H. Ogawa, "Regulated emissions and speciated hydrocarbons from smokeless low-temperature combustion diesel engines with ultra-high exhaust gas recirculation and exhaust oxidation catalyst," *Proceedings of the Institution of Mechanical Engineers, Part D: Journal of Automobile Engineering*, vol. 223, pp. 673–683, May 2009. (Cited on pages 11 & 17).

[32] Musculus, "Conceptual models for partially premixed low-temperature diesel combustion," *Progress in Energy and Combustion Science*, vol. 39, no. 2-9, pp. 246–283, 2013. (Cited on page 11).

[33] H. Jaaskelainen and M. K. Khair, "Common Rail Fuel Injection," 2015. Available: http://www.dieselnet.com/tech/diesel_fi_common-rail.php. (Cited on page 11).

[34] S. Han, E. Shim, J. Jang, J. Park, C. Bae, J. Park, and H. Kim, "Operating Range of Low Temperature Diesel Combustion with Supercharging," *SAE International*, no. SAE 2009-01-1440, 2009. (Cited on page 12).

[35] U. Asad and M. Zheng, "Efficacy of EGR and Boost in Single-Injection Enabled Low Temperature Combustion," *SAE International*, vol. 2, no. SAE 2009-01-1126, 2009. (Cited on pages 12, 19 & 85).

[36] H. Jaaskelainen and M. K. Khair, "Turbocharger Fundamentals," 2015. Available: http://www.dieselnet.com/tech/air_turbocharger.php. (Cited on page 12).

[37] C. F. Taylor, *The Internal-combustion Engine in Theory and Practice: Thermodynamics, fluid flow, performance*. MIT Press, 1985. (Cited on page 12).

[38] Q. Xin, *Diesel engine system design*. Woodhead Publishing Limited, 2011. (Cited on pages 13 & 68).

[39] N. Ladommatos, S. M. Abdelhalim, H. Zhao, and Z. Hu, "The Dilution, Chemical, and Thermal Effects of Exhaust Gas Recirculation on Diesel Engine Emissions - Part 1: Effect of Reducing Inlet Charge Oxygen," *SAE International*, no. SAE 961165, 1996. (Cited on page 14).

[40] N. Ladommatos, S. M. Abdelhalim, H. Zhao, and Z. Hu, "The Dilution, Chemical, and Thermal Effects of Exhaust Gas Recirculation on Diesel Engine Emissions - Part 2: Effects of Carbon Dioxide," *SAE International*, no. SAE 971660, 1996. (Cited on page 14).

[41] N. Ladommatos, S. M. Abdelhalim, H. Zhao, and Z. Hu, "The Dilution, Chemical, and Thermal Effects of Exhaust Gas Recirculation on Diesel Engine Emissions - Part 3: Effects of Water Vapour," *SAE International*, no. SAE 971659, 1997. (Cited on page 14).

[42] N. Ladommatos, S. M. Abdelhalim, H. Zhao, and Z. Hu, "The Dilution, Chemical, and Thermal Effects of Exhaust Gas Recirculation on Disesel Engine Emissions - Part 4: Effects of Carbon Dioxide and Water Vapour," *SAE International*, no. SAE 971660, 1997. (Cited on page 14).

[43] D. Tomazic and A. Pfeifer, "Cooled EGR A Must or an Option for 2002 / 04 Reprinted From : Compression Ignition Combustion and In-Cylinder Diesel Particulates and NOx Control," *SAE International*, no. SAE 2002-01-00962, 2002. (Cited on page 15).

[44] S. Han, C. Bae, and S. B. Choi, "Effects of operating parameters on mode transition between low-temperature combustion and conventional combustion in a light-duty diesel engine," *International Journal of Engine Research*, vol. 14, pp. 231–246, Aug. 2012. (Cited on page 17).

[45] H. Ogawa, T. Li, and N. Miyamoto, "Characteristics of low temperature and low oxygen diesel combustion with ultra-high exhaust gas recirculation," *International Journal of Engine Research*, vol. 8, pp. 365–378, Jan. 2007. (Cited on pages 18, 19 & 85).

[46] H. Yun and R. D. Reitz, "Combustion optimization in the low-temperature diesel combustion regime," *International Journal of Engine Research*, vol. 6, pp. 513–524, Jan. 2005. (Cited on pages 18 & 85).

[47] R. D. Atkins, *An Introduction to Engine Testing and Development.* SAE International, 2009. (Cited on page 20).

[48] A. J. Martyr and M. A. Plint, *Engine Testing.* London: Elsevier Ltd., 2007. (Cited on pages 20 & 24).

[49] AVL, "AVL SUPERCHARGER SYSTEM 515X," Tech. Rep. April, AVL, 2013. (Cited on page 26).

[50] U. Asad and M. Zheng, "Tightened intake oxygen control for improving diesel low-temperature combustion," *Journal of Automobile Engineering*, vol. 225, pp. 513–530, Apr. 2011. (Cited on pages 27 & 72).

[51] R. T. Fenner and J. Reddy, *Mechanics of Solids.* CRC Press, 1991. (Cited on page 39).

[52] S. Chattopadhyay, *Pressure Vessels: Design and Practice.* CRC Press, 2004. (Cited on page 39).

[53] G. Meurant, *Engine Testing: Theory and Practice.* Elsevier, 2013. (Cited on page 40).

[54] M. Wattrus, "Optimised combustion control for different diesel fuels," Tech. Rep. September, 2007. (Cited on page 44).

[55] T. Rockstroh, "Combustion Characteristics of Synthetic Gasoline in Modern Charge Boosted GDI Engines," tech. rep., 2015. (Cited on page 44).

[56] S. L. Kokjohn, R. M. Hanson, D. a. Splitter, and R. D. Reitz, "Fuel reactivity controlled compression ignition (RCCI): a pathway to controlled high-efficiency clean combustion," *International Journal of Engine Research*, vol. 12, pp. 209–226, June 2011. (Cited on page 56).

[57] E. M. Kurtz and D. G. Kuhel, "An evaluation of cetane sensitivity in low-temperature combustion and options to compensate for market cetane variation," *International Journal of Engine Research*, 2014. (Cited on page 60).

[58] AVL, "AVL Fuel Mass Flow Meter Product Guide," Tech. Rep. August, AVL, 2009. (Cited on pages 91 & 92).

[59] SAE, "J177: Measurement of Carbon Dioxide, Carbon Monoxide, and Oxides of Nitrogen in Diesel Exhaust - SAE International," 1995. (Cited on page 99).

[60] European Parliament, "EUROPEAN PARLIAMENT." Available: http://www.europarl.europa.eu/sides/getDoc.do?pubRef=-//EP//NONSGML+REPORT+A5-1999-0043+0+DOC+WORD+V0//EN. (Cited on page 121).

[61] L. G. Dodge, T. J. Callahan, and T. W. Ryan, "Humidity and temperature correction factors for NOx emissions from diesel engines. Prepared for: ENVIRON International Corporation," Tech. Rep. 03, 2003. (Cited on page 123).

[62] M. Adachi and H. Nakamura, *Engine Emissions Measurement Handbook*. SAE International, 2014. (Cited on page 125).

Appendix A

Control maps

A.1 Injector calibration for rail pressure determination map

In modern day vehicles, engine maps (also known as lookup tables) are used to define an optimal set of operating parameters that collectively result in improved combustion efficiency and output emissions. There are many variables to be considered when running an engine under LTC conditions, including injection timing, rail pressure, engine speed, injection mass, boost pressure etc. It is ideal if these parameters can be automated and optimised, such that they do not have to be physically adjusted between test points.

In commercial vehicles, rail pressure maps are used and defined as a function of engine speed and required injection mass per stroke. A map of this kind for an engine of similar cylinder capacity to the AVL5402 was used. However, since the flow characteristics through every injector nozzle are different, the mass of fuel injected at a certain pressure for a specified duration was unknown. Thus a full injector calibration was performed on the piezoelectric injector. This section details the development of said injector calibration map and how it was integrated into the control system.

A.1.1 Defining the problem

Figure A.1 shows a flowchart of how the lookup tables will be integrated within the control system. This gives a better idea of the format of injector characterisation table needed.

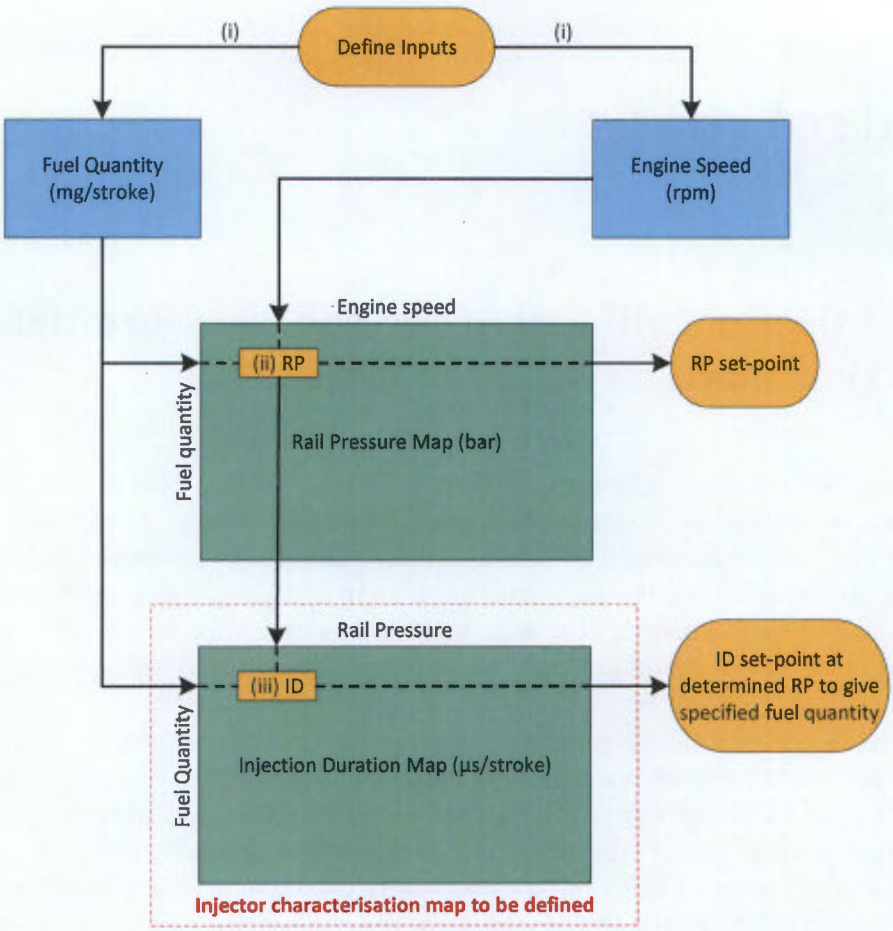

Figure A.1: *Integration of engine fuelling maps.*

The fuelling control is to operate as follows:

i. User inputs the mass of fuel to be injected per stroke and the desired engine speed.

ii. The optimum rail pressure is determined using these parameters in conjunction with the rail pressure map.

iii. The rail pressure output from the map as well as the user-set mass of fuel are sent to the injection duration map. Here the required duration is output to the injector.

Since an injection duration map needed to be generated and injection duration as a function of fuel quantity and rail pressure was unknown, the following was done:

i. Full injector characterisation to define the mass per injection as a function of rail pressure and injection duration.

ii. Use of characterisation data to populate injection duration map of the form shown in Figure A.1.

iii. Integration of the lookup table with the control system.

A.1.2 Apparatus

The LR Diesel Injector Service Unit 8000 (DISU 8000) was used for the injector calibration (Figure A.2). It uses a diesel substitute with similar flow characteristics and a much higher flash point (for safety) as the calibration fluid. The injection duration and rail pressure are input by the user and the mass per injection was measured using the units built-in coriolis flow meter.

A.1.3 Method

Injector characterisation

Firstly the injection mass as a function of rail pressure and injection duration was experimentally determined on the DISU 8000. Rail pressure and injection duration intervals and ranges were defined and laid out as shown in the Table A.1. The white blocks indicate all the test points that were run. The grey and yellow blocks were points to be determined by means of linear interpolation.

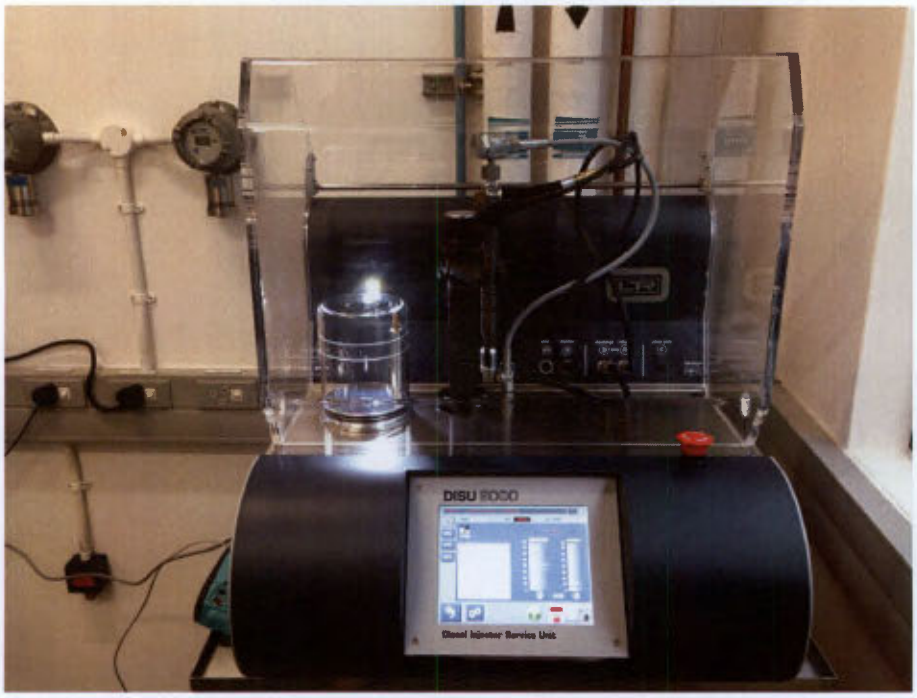

Figure A.2: *LR Diesel Injector Service Unit 8000.*

Table A.1: *Template used for calibrating the piezoelectric injector of the form injection mass as a function of rail pressure and injection duration.*

Rail Pressure [bar]

float y \ x	160	200	300	400	500	600	700	800	900	1000	1100	1200	1300	1450	1600	1800
0																
200																
250																
300																
350																
400																
450																
500																
600																
700																
800																
900																
1000																
1200																
1400																
1600																
1800																
2000																

Injection Duration [µs/strk]

Injection Mass [mg/strk]

Injection Mass [mg/strk]

Measured data | Interpolated 1st degree | Interpolated 2nd degree

Table A.2: *Template of injection duration map as a function of rail pressure and injection mass.*

Rail Pressure [bar]

float y \ x	160	200	300	400	500	600	700	800	900	1000	1100	1200	1300	1450	1600	1800
0																
0.5																
1																
1.5																
2																
2.5																
3																
3.5																
4																
4.5																
5																
7.5																
10																
20																
30																
40																
50																
60																
70																
85																

Injection Mass [mg/strk]

Injection Dur. [µs/strk]

Injection Duration [µs/strk]

Populating the injection duration map

The characterisation map then had to be converted to a usable format, i.e. a table that gives injection duration as a function of rail pressure and injection mass as indicated in Table A.2. This table shows the skeleton of the map that had to be populated in order to achieve this. Note the swap in position between injection mass and injection duration relative to Table A.1. The rail pressure and injection mass range and intervals were based on an existing lookup table used in modern motor vehicles.

The table conversion was carried out as follows:

i. The equation for the relationship between injection duration and injection mass at each rail pressure (rail pressures displayed in Table A.2) was determined. This was done by plotting each graph and manipulating the graph such that the injection mass was 0 g for injection durations less than 100 μs, as is typically the case for a piezoelectric injector. The graph below shows 1 of the 16 graphs plotted with a manipulated trendline and accompanying equation.

ii. Using the equation and the known injection masses (y), the corresponding injection durations (x) could be determined.

iii. This was repeated for each rail pressure, resulting in a complete injection duration map. The map was then implemented into the control system as shown in Figure A.1.

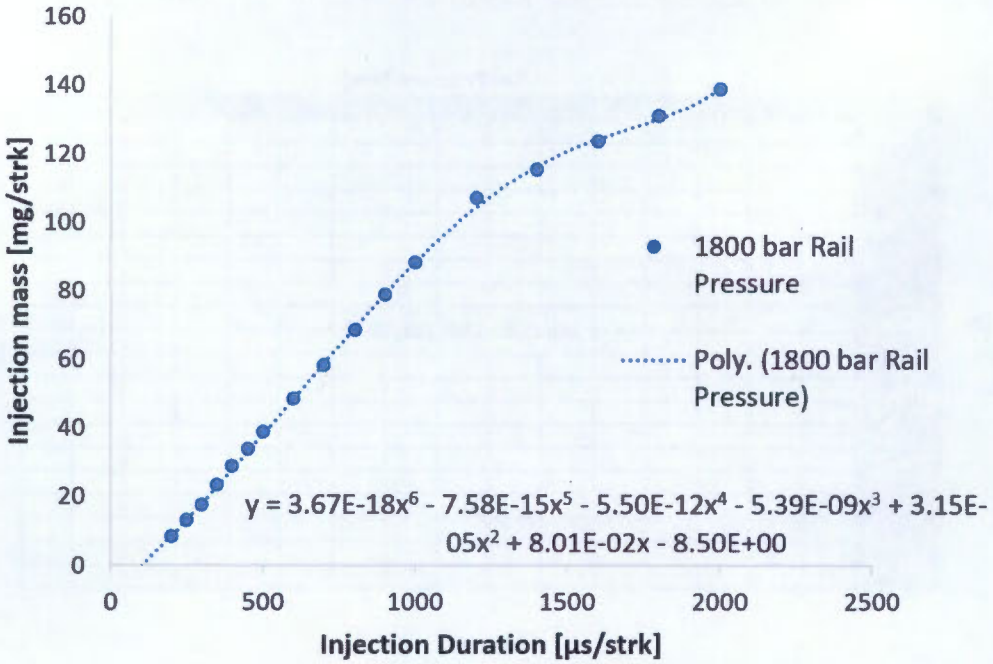

Figure A.3: *Relationship between injection mass and duration at 1800 bar rail pressure. The trend line and equation are also displayed.*

A.2 Boost and EBP maps

The test apparatus makes use of a EBP valve which was used to simulate the exhaust's back pressure typically generated by a turbocharger. Generating a model to determine the exact EBP expected as a function of exhaust gas enthalpy and mass flow rate for a certain turbocharger is a complex task which is outside the scope of this project. However, building a map based on existing engine test data and then calibrating it to the AVL5402 was achievable and acceptable for the purposes of the project.

Test data from a turbocharged multi-cylinder engine was supplied by AVL. It included boost and EBP across the load and speed range. Since the work done by a turbocharger is primarily dependent on exhaust mass flow rate and exhaust enthalpy, which are directly related to engine speed and load respectively, the boost and EBP maps were constructed as a function of load and speed.

The soft valve springs on the AVL5402 limited the intake boost pressure to 1300 mbar (gauge). Exceeding this limit could result in unwanted valve and piston contact and consequent catastrophic failure. Figure A.4 shows the relationship between the boost and EBP

(taken from AVL's data) at full load across the speed range. It was made clear by the peak boost and back pressure conditions that this turbocharger is too powerful in terms of pressures, for the AVL5402. Additionally, it was suspected that the peak BMEP achievable by Sasol's research engine would be significantly lower than the larger engine AVL used to produce the test data. This was attributed to the fact that Sasol's engine was limited by lower peak boosting pressures.

The following section details how the data was manipulated and calibrated to fit the AVL5402.

A.2.1 Method

The steps involved in the boost and EBP map construction were as follows:

i. The maximum boost pressure versus speed curve was scaled such that the curve shape remained the same but the peak boost pressure did not exceed 1200 mbar. Additionally, the EBP was scaled such that the pressure ratio (ratio between boost and EBP) was the same as the original data supplied by AVL. Figure A.4 illustrates the boost and EBP scaling process.

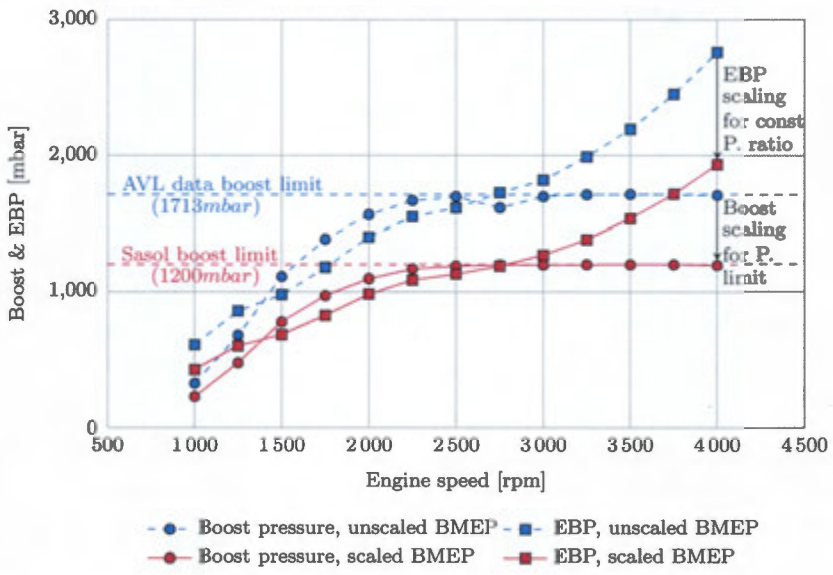

Figure A.4: *Graph showing how AVL's peak boost and EBP versus speed data was scaled to meet the research engine's maximum allowable boost pressure specification.*

ii. A full load test was performed using the peak scaled boost and EBP data as setpoints

for each engine speed (1000 rpm to 4000 rpm at 500 rpm intervals) to establish the maximum BMEP curve for the engine.

iii. AVL's data displayed load test points at each speed typically from 0 bar BMEP to maximum BMEP at 1 bar BMEP intervals. The boost and EBP at each speed was calibrated to the engine by using the percentage change between each load point in AVL's data (at a set speed) to scale the full load test results from maximum to 0 bar BMEP. That is to say, the BMEP data from the AVL test was proportionally replaced with the data obtained from the full load test. Figure A.5 illustrates how boost and EBP were scaled according to BMEP at 2500 rpm, in order to keep the curve shapes the same. This scaling was performed at each speed point.

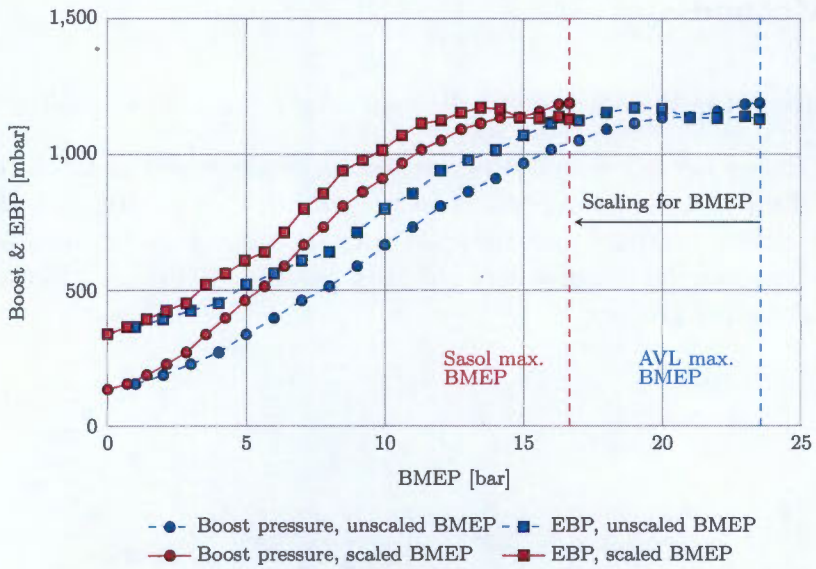

Figure A.5: *Graph showing how the boost and EBP at 2500 rpm (same method used at all other speed points) was scaled for BMEP such that the curve shapes remained the same but fit within the research engine's load range.*

iv. The equations for the trend lines of the boost and EBP as a function of BMEP at each speed was obtained. The coefficient of determination (or r^2 also known as R squared) for each fit was greater than 0.990. The equations were used to populate the boost and EBP maps as a function of BMEP and engine speed. Note that each equation corresponds to either the boost or the EBP as a function of load at a certain speed. That is to say, one equation for boosting pressure and one equation for EBP as a function of BMEP, per test speed point was defined and used to populate the map.

A three-dimensional representation of the resulting boost and exhaust back pressure maps using linear interpolation between adjacent points on the maps, is displayed in Figure A.6.

Each grid line intersection is representative of a data point in the populated maps. The grid lines in the BMEP-Boost pressure plain (and EBP plain) at each speed interval are representative of the equations that were defined and used to populate the maps.

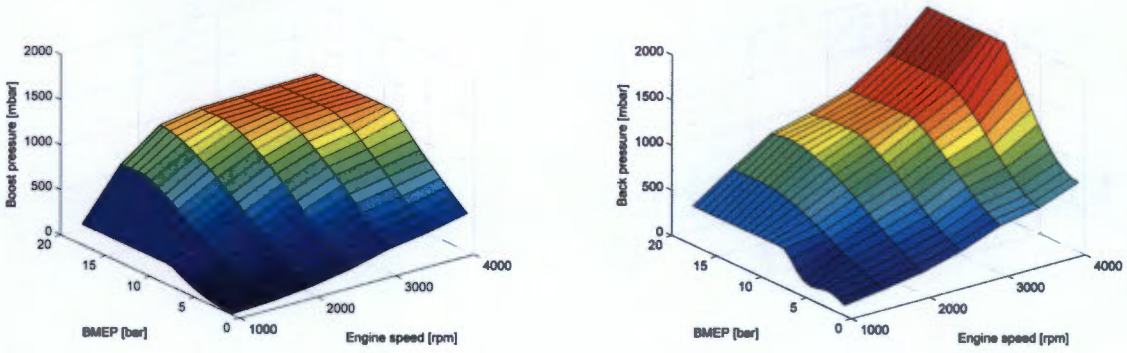

(a) *Boosting pressure.* (b) *EBP.*

Figure A.6: *Three-dimensional representation of boost (a) and EBP (b) maps.*

Appendix B

Data processing

This appendix details some of the more critical calculations that were performed in order to achieve the most accurate fuel and intake air mass flow rate as well as the indicated specific emissions.

B.1 Exhaust gas mass flow rate calculation

In order to accurately calculate the specific emissions, the exhaust mass flow rate had to be determined. This is defined as the sum of the intake air and injected fuel mass flow rates, as seen in Equation B.1.1. However, determining the intake air mass-flow rate was a complex task.

$$\dot{m}_{exh} = \dot{m}_{air} + \dot{m}_{fuel} \qquad \text{(kg/h)} \tag{B.1.1}$$

The air enters the compressor through a volume flow rate meter. It then passes through the compressor, and before it is sent to the engine, the compressed air is dried. Therefore, the change in mass flow rate had to be accounted for.

This section details how the change in moisture content is dealt with, with respect to its effects on the air mass flow rate.

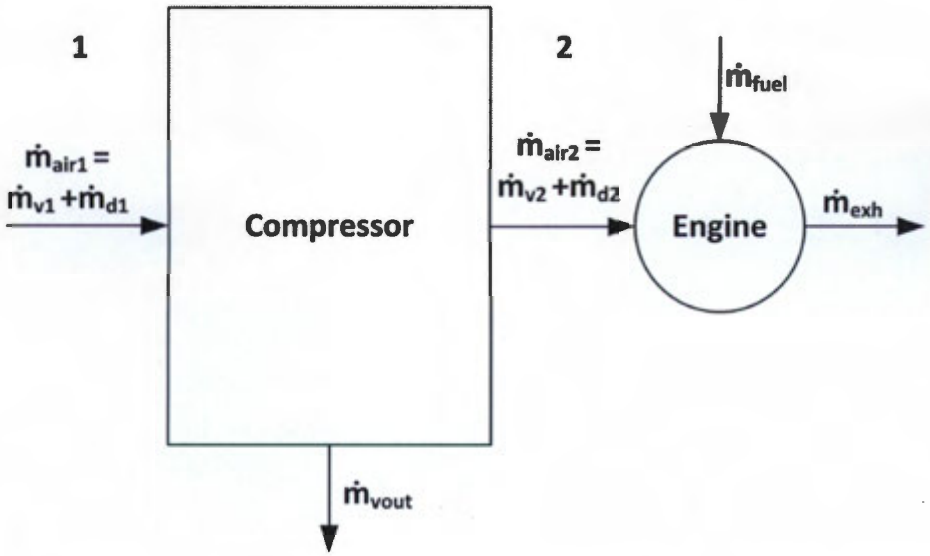

Figure B.1: *Air flow path from the atmosphere to the exhaust system.*

Figure B.1 displays a flow diagram of the water vapour and dry air from the ambient air, through the apparatus, to the exhaust of the engine. The subscript (1) denotes ambient conditions before entering the compressor and (2), the air to the engine. The assumptions made when tackling this problem were as follows:

i. There are no significant unintended leaks between the inlet to the compressor and the exhaust.

ii. When the compressed air enters the water separator, only water is removed and no dry air. Therefore, it follows that the mass flow rate of the dry air entering the compressor ($\dot{m}_{d1}$) is equal to the mass flow rate of the dry air entering the engine ($\dot{m}_{d2}$). Consequently, the mass flow rate of the dry air will be denoted by $\dot{m}_d$.

iii. The water vapour and dry air both behave like ideal gases.

iv. Dalton's law of additive partial pressures applies.

At the inlet to the compressor, the following variables were measured: the dry bulb temperature (T_1) in °C, barometric pressure (P_1) in kPa, relative humidity (ϕ_1) and volume flow rate ($\dot{V}_1$) in m^3/h.

Step 1: ***Determine the equation for the air mass flow rate to the engine***

From the assumptions stated above, it is clear that $\dot{m}_{air2}$ is the sum of the $\dot{m}_d$ and the mass flow rate of the water vapour after the air is dried ($\dot{m}_{v2}$).

$$\dot{m}_{air2} = \dot{m}_d + \dot{m}_{v2} \qquad \text{(kg/h)} \tag{B.1.2}$$

Step 2: ***Calculate $\dot{m}_d$***

Relative humidity is defined as the ratio of the actual pressure due to the water vapour (P_{V1}), to the saturated vapour pressure ($P_{sat@T_1}$) at a constant temperature. $P_{sat@T_1}$ is calculated using the Arden Buck equation at T_1,

$$P_{sat@T1} = 6.1121e^{\left(\left(18.678-\frac{T_1}{234.5}\right)\left(\frac{T_1}{257.14+T_1}\right)\right)} \qquad \text{(kPa)} \tag{B.1.3}$$

and thus, P_{V1} was calculated from the relative humidity,

$$\phi_1 = \frac{P_{V1}}{P_{sat@T_1}} \tag{B.1.4}$$
$$\therefore P_{V1} = \phi_1 P_{sat@T_1} \qquad \text{(kPa)}$$

From Dalton's Law, the partial pressure of the dry air at 1 (P_{d1}), was calculated,

$$P_{d1} = P_1 - P_{V1} \qquad \text{(kPa)} \tag{B.1.5}$$

Thus, from the ideal gas law, $\dot{m}_d$ was calculated,

$$P_{d1}\dot{V}_1 = \dot{m}_d R_d T_1 \tag{B.1.6}$$
$$\dot{m}_d = \frac{P_{d1}\dot{V}_1}{R_d T_1}$$

Where P_{d1} is the partial pressure of the dry air, $\dot{V}_1$ is the volume flow rate of the air and R_d is the gas constant for dry air ($0.2870\ kPa \cdot m^3/kg \cdot K$).

Step 3: ***Calculate $\dot{m}_{v2}$***

Again, using the Arden Buck equation (Equation B.1.3), $P_{sat@T2}$ was calculated. Since ϕ_2 is measured, the partial pressure, P_{v2}, could be calculated,

$$P_{v2} = \phi_2 P_{sat@T2} \tag{B.1.7}$$

The humidity ratio, ω, is defined as the mass of water vapour present in a unit mass of dry air and can be written as follows,

$$\omega = \frac{m_v}{m_d} \qquad \text{(kg water vapour/kg dry air)} \tag{B.1.8}$$
$$= \frac{\dot{m}_{v2}}{\dot{m}_{d2}}$$

Using the ideal gas relationship and substituting for the partial pressure of the dry air, the humidity ratio can be expressed in terms of the total pressure, P_2, and the vapour pressure P_{v2}.

$$\omega_2 = \frac{\dot{m}_{v2}}{\dot{m}_{d2}} = \frac{0.622 P_{v2}}{P_2 - P_{v2}} \tag{B.1.9}$$

Equation B.1.9 can then be rearranged to solve for $\dot{m}_{v2}$,

$$\dot{m}_{v2} = \dot{m}_{d2}\left(\frac{0.622 P_{v2}}{P_2 - P_{v2}}\right) \qquad \text{(kg/h)} \tag{B.1.10}$$

Step 4: *Calculate exhaust gas mass flow rate, $\dot{m}_{exh}$*

Equation B.1.2 was used in combination with the fuel flow rate ($\dot{m}_{fuel}$, determined in Appendix B.2), and Equation B.1.1, to determine the exhaust gas mass flow rate.

These equations were programmed into STARS, such that $\dot{m}_{exh}$ could be calculated and thus used to determine the specific emissions in real time.

B.2 Fuel mass flow rate determination

The AVL 735S was used to measure the fuel mass flow being injected into the engine per hour. During data analysis, post testing, it was noticed that the mean fuel flow rate fluctuated between tests, even though the tests were conducted at nominally constant fuelling. A carbon balance between the emissions and the fuel flow also showed a discrepancy of up to 22 % at specific test points where the fuel mass flow had a fluctuation amplitude of up to 16 %. Since emissions are typically reported on a mass basis, and thus are a function of exhaust gas flow rate, it was necessary to determine the actual fuel mass flow. Two additional options for determining the fuel mass flow rate were investigated:

i. using the intake air mass flow and lambda measured from the ETAS wide band lambda sensor (λ_{ETAS}), and

ii. using the intake air mass flow and lambda calculated from the emissions using the Spindt method (λ_{spindt}).

The mass flow rate of the fuel was calculated from both lambda values and compared with the measured fuel flow rate (illustrated in Figure B.2) for three repeat tests at nominally constant fuelling. For these tests, the exhaust lambda ranged from approximately 3.3, at 0 % EGR to 1.1 at approximately 68 % EGR. It was clear, for the higher lambda values, that there was a large discrepancy between the fuel flow rate calculated from the λ_{ETAS} relative to the other mechanisms. It is speculated that this is due to the sensor's poor sensitivity at higher lambda values (small mV change results in large measurement change). In extreme cases, it was found that the fuel flow variation between tests for the AVL measured fuel flow rate exceeded 16 %. However, the fuel flow rate calculated from λ_{spindt}, varied by approximately 6 % between tests. Although a variation of 5 % (or less) would be ideal, this was the most repeatable measurement that could be achieved using the current setup.

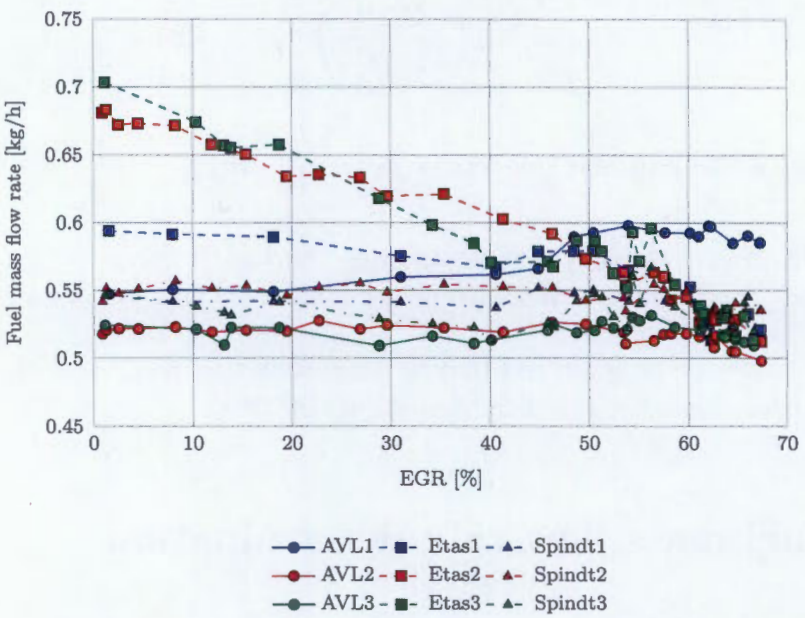

Figure B.2: *Fuel mass flow comparison between the measured and calculated quantities using the AVL 735S, ETAS wide band lambda sensor and the Spindt method, for three repeat tests.*

As a means of determining the relative accuracy of the fuel mass flow rate calculated using λ_{spindt}, it was cross-referenced with the mass of carbon measured in the exhaust. It was assumed that the exhaust carbon measurement was the most accurate measurement available for comparison. The percentage difference between the exhaust gas carbon mass and the carbon mass of the fuel mass flow determined by λ_{spindt} was plotted against EGR in Figure B.3. The results of the carbon balance demonstrated a maximum uncertainty of

approximately 6 %. This is a significant improvement on the 22 % uncertainty originally determined by means of a carbon balance between the fuel flow rate measured by the AVL 735S and the mass of carbon in the exhaust stream.

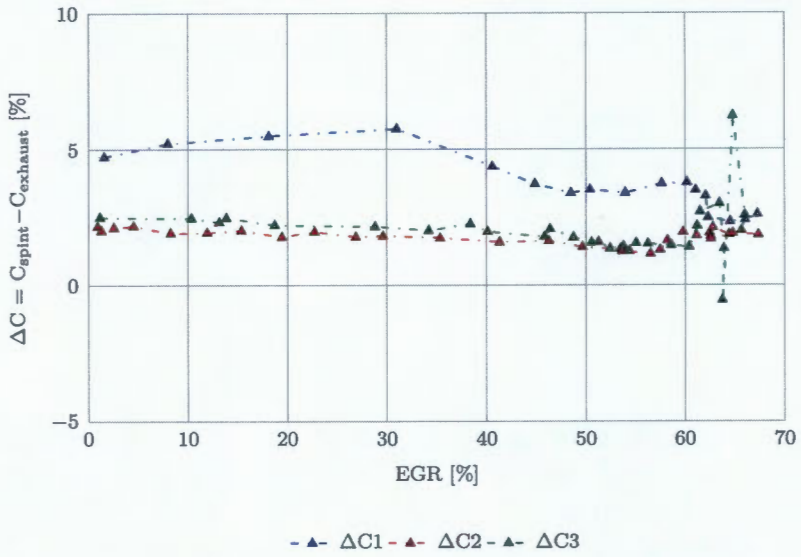

Figure B.3: *Carbon mass balance between measured exhaust gas carbon and carbon content from the fuel mass flow rate which was calculated using* λ_{spindt}.

Since the fuel mass flow measurement determined by the AVL 735S was speculated to be inaccurate, a recalculation was a necessity for all the emission's test data, using the fuel flow rate as determined by λ_{spindt}. The post processing methodology for the emissions data can be seen in the following section (Appendix B.3).

B.3 Indicated specific emissions

In order to directly compare the emissions of different engines and assess them within various combustion regimes, the exhaust gas emissions are normally reported on an indicated or brake specific basis [g/kWh]. The following section will explain the method used to determine the indicated specific emissions. This methodology is similar to that used by Horiba and in accordance with 88/77/EWG [60] and the *Directive 1999/96/EC of the European Parliament and the Council* [60]. Note that the numbers attached to the subscript in following equations pertain to Figure B.1, thus the subscript '2' refers to the conditions at the intake to the engine.

B.3.1 Conversion of emissions to a mass basis

The calculated mass of a specific exhaust gas species is dependent on the exhaust gas mass flow rate and the species' concentration. The MEXA reports the water soluble exhaust gas emissions as a concentration on a dry basis (i.e. CO, CO_2, O_2 and NOx), and the remaining (THC), on a wet basis. Since the dry basis concentrations are not representative of the actual concentrations, a factor (K_{wr}) needed to be determined to convert the concentrations from a dry to wet basis, which took into account the water content in the exhaust. There are sources of water vapour in the exhaust; these are the intake air humidity and the water vapour formed as a by-product of the oxidation of hydrocarbons (i.e. combustion).

Intake humidity ratio

The humidity ratio (ω_2) of the intake air defines the mass of water vapour entering the engine per equivalent mass of dry air. It was determined using the partial pressure of the water vapour (P_{v2}) and dry air (P_{d2}) entering the engine. These two variables were determined in appendix B.1 to calculate the intake air mass flow rate. The equation for humidity ratio follows:

$$\omega_2 = \frac{\dot{m}_{v2}}{\dot{m}_{d2}} = \frac{0.622 P_{v2}}{P_{d2}} \tag{B.3.1}$$

Dry to wet conversion factor

The dry to wet conversion factor ($K_{W,r}$) is calculated as follows,

$$K_{W,r} = \left(1 - F_{FH} \times \frac{\dot{m}_{fuel}}{\dot{m}_{dryair}}\right) - K_{W2} \tag{B.3.2}$$

Where

$$F_{FH} = \frac{y}{1 + \left(\frac{\dot{m}_{fuel}}{\dot{m}_{dryair}}\right)}, \tag{B.3.3}$$

and

$$K_{W2} = 1.608 \times \frac{\omega_2}{1 + (1.608 \times \omega_2)}, \tag{B.3.4}$$

NOx formation reactions are kinetically controlled during combustion and dependent on fuel composition and the time-temperature history of combustion [61]. Studies have shown that emissions are sensitive to intake temperature and absolute humidity. Since there are benefits to testing at different intake temperatures and humidities, correction factors are typically required when these emissions are reported, as a means of enforcing consistent intake air conditions.

Since intake air temperature was controlled to within 1.5 °C of the set point, and because as part of the parametric study it was desirable to see the effect intake temperature has on NOx emissions, NOx was not corrected for intake air temperature.

Conversion from dry to wet

All the dry emissions were converted to a wet basis,

$$conc_{wet} = conc_{dry} \times K_{W,r} \tag{B.3.5}$$

Water concentration

The water concentration in the exhaust was then determined by a carbon balance,

$$H_2O = \frac{(0.5 \times y \times (CO + CO_2 + 3THC) - 4THC)}{(1 + \frac{CO}{3.8CO_2})} \tag{B.3.6}$$

Where y is the fuel hydrogen to carbon ratio as determined by a $GC - by - GC$ fuel analysis, and CO and CO_2 are dry basis concentrations where as THC is wet.

N_2 concentration

Assuming that no other exhaust gas species exist, the only remaining gas is N_2 and is calculated as follows,

$$N_2 = 1 - (H_2O + CO_{2wet} + CO_{wet} + O_2 + NOx_{wet} + THC) \tag{B.3.7}$$

Exhaust molar flow determination

Using the known molar masses of the different exhaust gas species, as well their concentrations, the molar mass of the exhaust gas was determined,

$$mm_{exh} = CO_{2wet} \times CO_{mm} + CO_{wet} \times CO_{mm} + O_2 \times O_{2mm} + NOx_{wet} \times NO_{mm} + THC \times THC_{mm} + H_2O \times H_2O_{mm} \quad [kg/kmol], \tag{B.3.8}$$

where the subscript 'mm' denotes molar mass.

Using the calculated molar mass and the known exhaust mass flow rate, the exhaust molar flow was calculated,

$$\dot{m}_{exhmolar} = \frac{\dot{m}_{exh}}{mm_{exh}} \quad [kmol/h] \tag{B.3.9}$$

Conversion to mass basis

Finally, using the calculated wet concentrations, the known species molar masses, as well as the exhaust molar flow, the mass flow of each emissions could be calculated in this form,

$$\dot{m}_{species} = mm_{species} \times conc_{wet} \times \dot{m}_{exhmolar} \quad [kg/h] \tag{B.3.10}$$

B.3.2 Conversion of mass basis emissions to indicated specific

Since the research engine only has one cylinder, the friction mean effective pressure (FMEP) is not representative of a multi-cylinder engine. For this reason the emissions were converted on an indicated basis and not using brake power. The emissions were converted as follows:

$$IS_{species} = \frac{\dot{m}_{species}}{P_{ind}} \quad [g/kWh], \tag{B.3.11}$$

where the subscript 'species' refers to the gas molecule being determined, (i.e. if the indicated specific CO was being determined, $IS_{species}$ and $\dot{m}_{species}$ would be replaced with $ISCO$ and $\dot{m}_{CO}$ respectively), and P_{ind} is the indicated power.

B.3.3 Indicated specific soot

The conversion of the soot concentration to indicated specific soot (ISSoot) involved a different process. The specific gas constant (R_s) was determined from the *specific ideal*

gas law. Figure 1.3 in the SAE Engine Emissions Handbook [62] shows the relationship between exhaust gas density and the excess air ratio (λ) at standard conditions (T = 20 °C and P = 101.3 kPa). It was realised that the exhaust gas density ($\rho_{exh20°C}$) does not vary significantly for λ above λ equal to 1. The exhaust gas density at standard conditions was found to be approximately 1.205 kg/m^3.

$$\begin{aligned} PV &= MR_sT, \\ \frac{m}{v} &= \frac{P}{R_sT}, \\ \therefore R_s &= \frac{P}{\rho_{exh20°C}T} \\ &= 286.92\ J/kgK \end{aligned} \tag{B.3.12}$$

The AVL smoke meter reports the soot concentrations corrected to 1 bar and 25 °C. Therefore the exhaust gas density was recalculated for these conditions,

$$\begin{aligned} \rho_{exh25°C} &= \frac{P_{1bar}}{R_sT_{25°C}} \\ &= 1.17\ kg/m^3 \end{aligned}$$

Finally ISSoot is determined using the measured soot concentration ($soot_{conc}$ $[mg/m^3]$), the exhaust gas density at 25 °C, exhaust mass flow rate ($\dot{m}_{exh}$ $[kg/h]$), and the indicated power (P_{ind} $[kW]$) as shown in equation

$$ISSoot = \frac{\left(\frac{soot_{conc.}}{\rho_{exh25°C}}\right) \times \dot{m}_{exh}}{P_{ind}} \qquad [g/kWh] \tag{B.3.13}$$

B.4 Dealing with the elevated intake temperature test

The methodology carried out in Appendices B.1 and B.3, was successful in producing sound results for all the tests, except one. The LTC parametric test, involving an increased intake temperature of approximately 75 °C, required that the boosting unit be heated up to 130 $°C$ to compensate for the heat loss in the insulated pipe between the unit and the engine. The relative humidity sensor used to determine the water content in the intake, after the water separators within the compressor unit, was positioned in the AVL boost conditioning unit. The saturation pressure equation, defined within SAE J177, becomes increasingly inaccurate in temperatures exceeding 80 °C. It was noticed that if this equation

was used to determine the saturation pressure, it resulted in the ambient air having a humidity ratio 60 % lower than the air entering the engine. Based on the fact that the average nett drying efficiency of the water separators is approximately 30 % (however, sensitive to the ambient humidity ratio), this is very unlikely to be a true phenomenon.

The ambient humidity ratio for baseline test 1 (10.10 $g_{WaterVapour}/kg_{DryAir}$) and the elevated temperature parametric test (10.14 $g_{WaterVapour}/kg_{DryAir}$) varied by approximately 0.4 %. Since the ambient temperature, pressure and humidity ratio were similar, it was assumed that the drying efficiency experienced in the two tests was approximately constant. Since the ambient humidity ratio was measured and the drying efficiency was assumed, the engine intake air humidity ratio could be determined. The humidity ratio was then worked backwards to yield a more realistic intake air mass flow rate.

Appendix C

Coolant and lubrication conditioning unit design

The primary objective of this unit was to achieve fluid flow and temperature control of the oil and coolant, as well as pressure control for the oil circuit. A conditioning unit based on the performance specifications of the AVL-577 (AVL's coolant and lubrication conditioning unit) was designed in an attempt to reduce overall test apparatus costs. The AVL-577 is a standardised unit that can be used for a large variety of engine types and sizes. Since the AVL5402 is a relatively small engine in relation to the other engines this unit can be used for, the unit's design could be optimised by reducing the cooling and heating component capacities, as well as the pump sizes. The design solution could also eliminate all components that were not essential.

C.1 Requirement specifications

The requirement specifications for the conditioning unit are separated into two sections. These are the:

i. operation requirement specifications, and

ii. spatial and geometric requirement specifications.

C.1.1 Operation requirement specifications

The operation requirement specifications for the lubrication circuit and coolant circuit are presented in tables C.1 and C.2 respectively.

Table C.1: *Oil circuit requirement specifications.*

Oil pressure		
Relief valve setting	4 bar	engine inlet
Minimum	3 bar	
Temperature		
Normal working	85 °C	±2 °C
Maximum	130 °C	engine inlet
Oil flow rate through the engine	approx. 5–6 l/min	
Conditioning unit circulation flow rate	10 l/min	recommended
Heat exchanger cooling capacity	5 kW	
Heater heating capacity	4 kW	
Lubricant	Castrol Magnatec 10W-40	

Furthermore, the unit must incorporate two additional circuits with the following requirement specifications:

i. *EGR cooling circuit*: This circuit is to make use of the test facility cooling water (chiller water) to cool the gas in the high pressure EGR loop. The gas temperature control must be achieved by controlling the flow rate of the test facility water through the EGR intercooler. The EGR temperature control is to be automated using the PLC.

ii. *Distilled water circuit*: This circuit must supply constant-temperature distilled water to the cooling jacket of the inlet manifold piezo-resistive absolute pressure transducer. The measurement of these sensors is sensitive to varying environment temperatures and therefore require cooling in order to minimise pressure measurement error. In addition this circuit must also supply the EBP valve electronics with cooling water. The distilled water is necessary, as if calcium-containing water is used it can result in the formation of deposits and consequently may cause a blockage in the cooling jacket of the piezo-resistive absolute pressure transducer.

In addition, the unit must have two mechanical analogue temperature gauges, one for the

Table C.2: *Coolant circuit requirement specifications.*

Coolant pressure		
Pressure	approx. 1.5 bar	engine inlet
Temperature		
Normal working	90 °C	±2 °C
Maximum	120 °C	engine outlet
Coolant flow		
Standard	20 l/min	recommended
Heat exchanger cooling capacity	20 kW	
Heater heating capacity	3.5 kW	
Coolant		
Basic	demineralised water	
Anti-freeze	25 % ethylene glycole	

engine coolant and the other for the oil circuit. This is required as a safety precaution, so that the temperatures can be monitored by the operator from within the test facility room if necessary.

C.1.2 Spatial and geometric requirements

The conditioning unit was to be mounted on the test bed. After assessing the layout of the test apparatus, and determining the spatial limitations that had to be considered, the optimum outer dimensions (excluding the wet sump), in terms of minimising the units test facility foot-print and ease of installation were 800 mm × 700 mm × 400 mm ($l \times w \times h$). These dimensions also resulted in space for the mounting of the exhaust and pulsation vessel stands. All conditioning unit plumbing and sensors had to be contained within this housing.

The engine made use of a dry sump (no oil collection within the engine) and therefore the addition of a wet sump (oil storage tank) to the conditioning unit was essential. In order to keep the test facility foot-print of the conditioning unit to a minimum, the wet sump must be positioned within the unit itself. However, the vertical position of the oil level in the sump relative to the oil return from the engine is very important. This is because gravity is the main driving force behind the oil being drained from the engine to the sump. According to AVL (the research engine supplier) the difference in height between these two

levels must be at least 100 mm. Once the engine has been mounted to the test-bed, the oil return height will be approximately 440 mm from the test facility floor. Once the anti-vibration mountings have been attached to the conditioning unit and the unit positioned on the test bed, the base of the unit will be approximately 300 mm from the test facility floor. Therefore, the design has to ensure that the minimum required difference between oil return height and wet sump oil level is achieved. In addition, the wet sump must have a capacity of at least 10 l. Furthermore, the sump's dimensions must take into account the:

- size of the heating element fittings,
- low power-density of heating elements required to prevent oxidation of the oil and therefore, the realisation that longer element lengths are necessary to achieve the same heating capacity as water heating elements,
- positioning of conditioning unit components such that the sump can be easily fitted inside the conditioning unit and removed for maintenance, and
- minimum volume requirement of the sump is 10 l.

C.2 Design solution

The final design of the conditioning unit housing had top and side perforated plates to allow for air cooling of the electric motors (seen in Figure C.1). The back, front and floor panels were laser cut from 3 mm stainless steel to support the load of the heat-exchangers, pumps, fittings, pipes and the smaller components that also made up the conditioning unit. The housing had rubber feet mounted to it and was positioned on the ladder frame. The wet sump was suspended from the floor panel of the housing such that the oil level in the sump was always at lease 100 mm lower than the oil drainage point of the engine.

Figure C.2 shows the schematic layout of the conditioning unit. The four different circuits that were necessary for the final design are encapsulated and labelled within numbered boxes. These were:

i. *Oil conditioning circuit:* Comprised of a wet sump with a submersible gear pump as well as two low watt density heating elements. The pump outlet was fitted with a 4 bar mechanical relief valve as a safety precaution to prevent over-pressurisation of the circuit. A standard inline oil filter was integrated into the circuit. A three-way electrically actuated mixing valve was used to control the amount of hot oil from the wet sump being cooled by the 5 kW shell-in-tube heat exchanger. This was controlled according to the temperature of the oil entering the engine which was set to 85 °C. An oil circulation branch off the oil feed to the engine with an inline manually operated

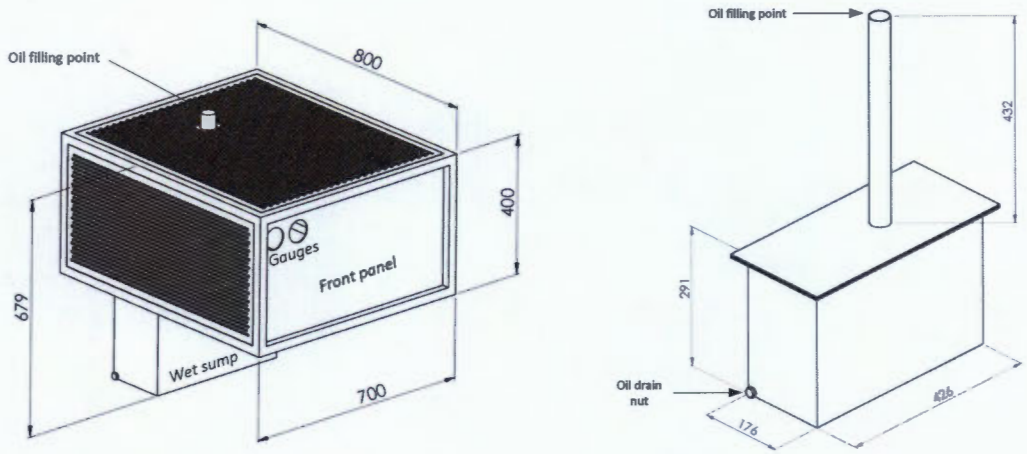

(a) *Housing*

(b) *Wet sump*

Figure C.1: *Three-dimensional representation of the conditioning unit housing (a) and wet sump (b) assembly.*

needle valve was included to promote oil circulation within the conditioning unit of approximately 10 l/min. The pump speed was controlled by a variable frequency drive (VFD) which adjusted the motor speed according to the oil pressure at the engine inlet (3.5 bar setpoint). If the oil pressure drops below 3 bar there is a hard-wired switch and a back-up program which will both result in complete engine shut-down, bringing the engine to a gradual stop.

ii. *Coolant conditioning circuit:* Comprised of a centrifugal pump capable of pumping 20 l/min, a 3.5 kW heater, a 20 kW heat-exchanger and a three-way electrically actuated mixing valve. The mixing valve controlled the proportional flow of coolant from the heater and heat-exchanger according to the coolant temperature leaving the engine. This was set to 85 °C.

iii. *Distilled water circuit:* Comprised of a 1 kW heat-exchanger, accumulator and a small, 5 l/min capacity pump. Distilled water was used in the circuit to minimise the risk of deposits in the cooling jacket of the piezo-resistive sensor, whilst simultaneously acting as the cooling fluid for the sensor and EBP valve.

iv. *EGR cooler circuit:* This circuit used the test facility chiller water and an electrically controlled gate valve to appropriately control the flow rate of water through the EGR cooler according to the EGR temperature sensor and setpoint.

All the heat exchangers utilised the test facility chiller water. The water was fed into the conditioning unit at one point and drained from one point to minimise clutter.

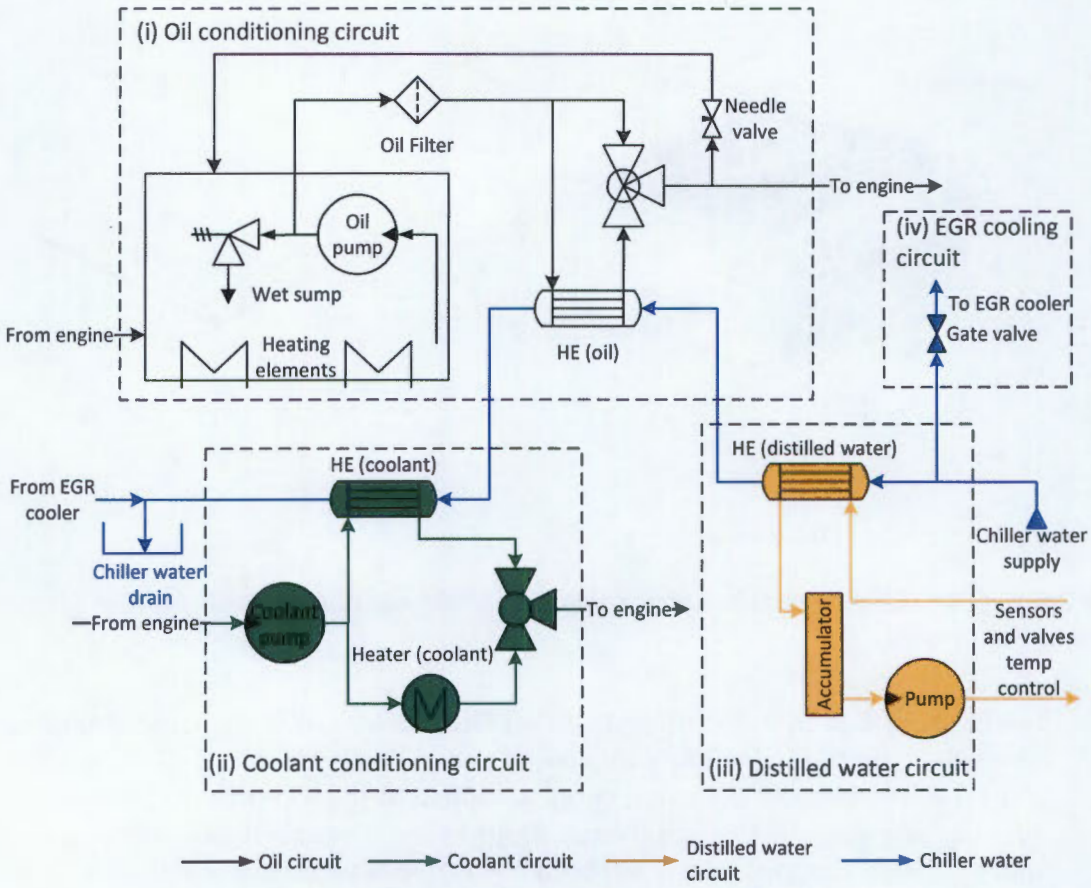

Figure C.2: *Layout of the lubrication and coolant conditioning unit.*

Appendix D

EN590 fuel analysis

Property	Units	Method	Result
Appearance	Rating	CALTEX CMM 76	1
Colour	Rating	ASTM D1500	<0.5
Density at 15 °C	kg/l	ASTM D4052	0.8358
Density at 20 °C	kg/l		0.8328
Distillation		ASTM D86	
IBP	°C		193.1
5%	°C		207.1
10%	°C		218.1
20%	°C		231.1
30%	°C		246.4
40%	°C		262.2
50%	°C		277.0
60%	°C		288.2
70%	°C		298.8
80%	°C		311.7
90%	°C		333.0
95%	°C		347.9
FBP	°C		355.6
Copper Corrosion		ASTM D130	1A
Total Sulphur	mg/kg	ASTM D5453	<1
Nitrogen Content	mg/kg	ASTM D 4629	<0.3
Water Content	mg/kg	IP438	44
Acid Number/Total Acids	mg KOH/g	ASTM D664	0.064
Bromine number	gBr/100g	ASTM D1159	<0.01
Kinematic Viscosity at 40°C	cSt	ASTM D445	2.79
Flash point	°C	ASTM D93	84
Derived Cetane Number	Rating	ASTM D6890 (Mod)	56.1
Cetane Number	Rating	ASTM D613	53.8
Cetane Index	Rating	ASTM D4737	54.3
Cloud point	°C	ASTM D2500	-21
CFPP	°C	IP309	-22
Pour point	°C	ASTM D97	-31
Carbon residue	mass %	ASTM D4530	0.02
Ash content	mass %	ASTM D482	<0.01
Lubricity (HFRR)	um	CEC F06-A-96	327
SL BOCLE	g	ASTM D6078	5100
Oxidation stability	mg/100 mL	ASTM D2274	0.3

Total contaminants	mg/kg	IP440	0.6
Mononuclear Aromatics	mass %	GC x GC	22.36
Polynuclear (2+3) Aromatics	mass %		6.85
Total Aromatics	mass %		29.21
Carbon Content	mass %		86.80
Hydrogen Content	mass %		13.20
Molar H/C ratio	mol/mol		1.81

Appendix E

Standard operating procedures

University of Cape Town
Sasol Advanced Fuels Laboratory

Operating Procedure:

BE AWARE OF RISKS PERTAINING TO TASK

Procedure number:	
Procedure Description:	**Operating procedure for AVL5402SCRE test facility**
Procedure compiled by:	Timothy Cole King
Procedure revision date:	20 February 2015
Procedure approved by:	
Nature of revision:	To include changes made in operating procedure ☐ To include instrument modifications ☐ Changes made to wording in procedure document ☐ Other: First Operating Procedure ✓
Re-training required:	**Yes** ☐ **No** ✓

STANDARD OPERATING PROCEDURE FOR AVL5402 SCRE TEST FACILITY

1. GENERAL

Before the engine is operated user must have undergone specific engine testing and general test practice training. This SOP document is NOT sufficient by itself.

Scope

The Operating procedure described herein details the following:

- Pre-start up inspections
- Start-up procedures for each of the test facility supporting sub-systems
- Start-up procedure of the AVL5402SCRE
- Procedure for setting fuelling parameters
- Shutdown procedure for the AVL5402 as well as supporting subsystems
- Operating limits for the AVL5402 SCRE (single-cylinder research engine)

Objectives

The aim of this SOP is to provide a comprehensive set of instructions that document the routine activity of starting and stopping the AVL5402SCRE test apparatus. This document will also cover a brief overview of the control system and data logging protocol.

References

Definitions

AVL5402SCRE: AVL's single cylinder diesel research engine
VFD: variable frequency drive
SOP: standard operating procedure
RT: real-time
°CA: degrees crank angle

2. PRINCIPLE HAZARDS

- Flammable liquids
- Oil, coolant and fuel spills resulting in slippery floors
- Pressurized equipment
- Temperatures up to 800K (hot equipment)
- Electrical equipment shock/fire hazard
- Toxic diesel exhaust gasses

3. PERSONAL PROTECTIVE EQUIPMENT

Closed shoes and long pants should always be warn in the laboratory, however, depending on area additional PPE should be worn.

Control room

- Ear protection during engine operation

Test cell

- Safety glasses
- Laboratory coat or overall jacket
- Ear protection

4. FIRST AID AND MEDICAL CARE WITH RESPECT TO DIESEL FUEL AND EXHAUST GAS MSDS AND BURNS

Eye contact
If eyes come in contact with exhaust gases check for and remove any contact lenses. Immediately flush eyes with plenty of water for at least 15 minutes, occasionally lifting the upper and lower eyelids. Get medical attention immediately

Skin contact
If skin comes in contact with hot exhaust pipe, the aim is to cool the burn area down. This can be done by running under cool water or a cool, damp and clean cloth. Do not apply ice directly to the burn. Cool burn until patient feels the burn and heat going away. Apply sterile dressing immediately after cool to avoid infection. Seek medical attention depending on the degree of burn. First degree burns may not require medical attention.

Inhalation
If exhaust gases are inhaled move exposed person to an area containing fresh air. If not breathing, breathing is irregular or if respiratory arrest occurs, provide artificial respiration or oxygen by trained personnel. Loosen tight clothing such as a collar, tie, belt or waistband. Get medical attention immediately.

Ingestion
If coolant, fuel, oil or any other harmful fluid is ingested, wash out mouth with water. Do not induce vomiting unless directed to do so by medical personnel. Never give anything by mouth to an unconscious person. Get medical attention immediately.

Protection of first-aiders
No action shall be taken involving any personal risk or without suitable training. It may be dangerous to the person providing aid to give mouth-to-mouth resuscitation

Notes to physician
No specific treatment. Treat symptomatically. Contact poison-treatment specialist immediately if large quantities have been ingested or inhaled

Lacerations
Stay Safe. If you are not the victim, practise first aid measures and wear personal protective equipment, latex gloves, safety spectacles and long sleeves.
Control the bleeding before anything else. Putting pressure directly on the laceration while holding it above the level of the heart for 15 minutes, should be enough to stop bleeding. Seek medical care; contact medical station immediately/dispatch ambulance.

5. GENERAL PROCEDURE

For human safety and the longevity of the research equipment, it is important that specific protocol be adhered to when starting up, running and shutting down the test apparatus.

5.1. Apparatus

The AVL5402 is a single cylinder diesel research engine that was installed at SAFL for diesel research purposes. This engine is accompanied by multiple supporting sub-systems that work in unison.

5.2. Preparation and preventative actions before start-up

Prior to starting up any of the engine ancillaries, there are a number of checks that need to be carried out. These include:

i. Check engine log book and ensure all maintenance is up to date

ii. If maintenance has been performed check all associated parts, and make sure all electrical connections have been secured/fastened sufficiently.
iii. Check the test cell floor for spillages that could result in engineer or technician slipping.
iv. Check shaft assembly bolts are firmly fastened
v. Check the shaft guard is securely closed
vi. Check sensing and electrical lines are all securely connecting and are out of reach of hot surfaces and rotating parts.
vii. Check air supply hose between the compressor and the boosting unit, as well as the hose between the engine and the boosting unit, and ensure that they are securely fixed to their corresponding hose tale fittings.

5.3. Turn on supporting sub-system power

i. Compressor circuit breaker
ii. Boost conditioning unit circuit breaker on control box
iii. Coolant and oil conditioning unit circuit breaker on control box
iv. Indismart power button

5.4. Switch on test facility water and ventilation

i. On the facility control panel switch on the two black nobs labelled "COOL WATERPUMP" and "HOT WATERPUMP" to turn on the test facility cooling water. This water is necessary for supplying cooling to the fuel, oil and coolant conditioning units. The compressor also requires test facility water for cooling.
ii. Turn on ventilation such that a vacuum is generated in the test cell. This will ensure that no exhaust gas enters the control room or any other unwanted areas.

Test facility sub-system setup and activation via GUIs

Once power has been physically turned on to all the subsystems and the test facility cooling water and ventilation are being sufficiently supplied, controlled activation of each sub-system can commence. This is done using four programs namely, STARS, CalVIEW, AVL Fuel Measuring System and Indicom software. The following systems are activated respectively:

5.5. Turn on the lubrication and coolant conditioning unit

i. In STARS turn on "Oil Pump" and "Coolant Pump". This will automatically turn on heating and gradually heat the oil and coolant up to the required temperature.
ii. Once the conditioning unit is on, wait until coolant temperature entering the engine exceeds 80°C and the oil temperature exceeds 75°C before turning the engine over (This could take up to 20minutes).

5.6. Fuel supply

i. In STARS, turn on the low pressure fuel pump from fuel drum by clicking "210L Fuel Pump"
ii. In the AVL Fuel Measuring System program ("AVL735-AVL753C 2.1") start up the AVL fuel conditioning unit by selecting the drop-down menu in the top left corner. The fuel flow meter and the temperature control meter that make up the unit must be started up individually. From the drop down menu select AVL735/online and click "stand by". Again from the drop down menu select AVL753C/online and click "conditioning mode".
iii. In STARS select "AVL Fuel solenoid" to allow for flow from the unit to the engine. Wait until fuel pressure reads 2bar abs, this may take up to 1 minute.

iv. In STARS select "Ignition On". Watch fuel pressure rise to ±6bar abs. If the fuel pressure does not rise above 4.5bar abs the engine should not be run until the problem is resolved and desired fuel pressure is reached. The diesel fuel is the high pressure fuel pump's only source of lubrication and thus insufficient pressure can result in pump failure.

5.7. Start-up supercharging system

i. On the "MAIN CONTROLS" tab in CalVIEW set the desired boost pressure to 0mmbar gauge (1atm).
ii. In STARS, select "Air Compressor" and "Compress RPM" so that the red dot next to each button turns green. This will result in a supply of air at 1atm to the engine.

5.8. Setting up and running dynamometer

Before starting this step, make sure:

- *Oil and coolant temperatures are above 75°C and 80°C* respectively, and
- *there is at least 4.5bar fuel pressure in the fuel supply line to the HP fuel pump*

i. In STARS on the "Main" controls tab, under "Functions" select "Enable" and under "Control Modes" select "Throttle: Speed".
ii. In STARS under "Ramp Mode" specify the time (typically five seconds) to reach speed setpoint ("Ramp Time") and specify first speed to be 1000rpm.
iii. Select "Apply Demands", dynamometer will start turning the engine, reaching the specified speed at the "Ramp Time" set point.

5.9. Real-time AVL Indicom software

This software is installed on a separate laptop as it needs to process and calculate a significant amount of data over very short instances of time. It is used for recording real time data such as in-cylinder pressure, heat release, injection timing and duration relative to °CA.

i. Start up the designated laptop and open the AVL Indicom software (connection between the laptop and the Indismart equipment should be established automatically).
ii. Select the "Start continuous acquisition" button in order for the Indismart to start sending data, and for Indicom to display it and perform necessary RT calculations.

Fault "SyncStopped": The ECU needs to synchronise the crank angle encoder with the cam phase sensor. It is synchronised when it measures one cam phase pulse for every 720 crank angle encoder pulses. If it does not measure the right amount of pulses it displays a fault indicated by a light that will either stay on or flash intermittently beneath "SyncStopped". In order to clear this fault select the EPT (Engine Position Tracker) tab and click "EPTFlagClear". This will clear the fault and retry synchronization. If the error persists, this will probably mean that the encoder or Indismart power is off.

5.10. Setting up fuelling parameters (CalView "MAIN CONTROLS" tab)

Before operating the engine under firing mode, correct injection timing and duration must be setup.

i. Setup the fuelling parameters in CalVIEW on the "MAIN CONTROLS" tab, under the "Fuelling" heading. Here you can set the injection duration and timing of two pilot, one main and two post ejections.
ii. Under the "Engine Controls" heading the desired fuel rail pressure can be set.

Once fuelling parameters have been set, select "MainEnable1" and select whichever pilot and post injections you setup and the injector will start injecting fuel accordingly.

The engine will now be running in fired mode.

5.11. General data logging

There are two important programs where data can be logged, namely STARS and Indicom. In STARS we log the subsystem data such as certain pressures, temperatures or flow rates of for example oil, coolant, fuel or air supply that when varied could have an impact on the repeatability of combustion properties or exhaust gas analysis. The results from the exhaust gas analyser and smoke meter are also recorded here. In Indicom, combustion data such as in-cylinder pressure, injection timing and rate of heat release is recorded as a function of °CA. The data logging procedure should typically be carried out as follows.

i. Reach desired operating mode and wait 1 minute in order to ensure combustion stabilisation.
ii. Take smoke sample. Typically using the auto sample duration mode is sufficient.
iii. Once the results of the smoke sample have been taken, 30seconds of STARS data logging can begin. It will input the same smoke value as recorded in when the smoke sample was taken into each line of data STARS logs.
iv. Once data logging for the specific operating mode is complete the file can be exported as a *.csv file.
v. Finally log approximately 10cycles on Indicom. These files are save as AVL's iFile format. In order to convert this iFile into a usable format run the iFile through the iFile to M file conversion script. This data can then be accessed, plotted into graphs and saved.

5.12. Engine shutdown procedure

The engine shutdown procedure is very similar to the reverse order of the start-up procedure and will be summarised here:-

i. In CalVIEW turn off "EngineRunEnable".
ii. Continue to motor the engine so as to pump out all residual gases and help remove particulate build up. This should be done for five minutes at a variety of speeds between 1000 and 4000rpm. During this process it is important that the heating elements in the boost conditioning unit are off such that the continued air flow through the unit causes cooling of the elements.
iii. Bring dynamometer speed down to 1000rpm and then, in STARS, under "Functions", select "Disable". This will stop the dynamometer and turn the ignition off.
iv. In the "AVL Fuel Measuring System" program turn the fuel conditioning unit off by selecting "Pause" on both the AVL735/online and AVL753C/online.
v. In STARS deactivate the "AVL Fuel Solenoid" valve and turn off the "210L Fuel Pump".
vi. In STARS turn off the "Oil Pump" and "Coolant Pump"
vii. Turn off power to supercharging unit, compressor and oil and coolant conditioning unit.
viii. Turn off test facility water
ix. Turn off Indismart
x. After approximately 30 minutes turn off the ventilation
xi. The ball valve on the pulsation vessel must be opened to drain any potential condensate that may have collected during the test. This will prevent corrosion and thus increase the life of the vessel.

5.13. Operating Limits for the AVL5402SCRE

Temperature Limits for the AVL5402SCRE

Measurement	Lower Limit [°C]	Upper Limit [°C]
Supercharger supply	30	130
Exhaust gas @ manifold	-	800
Exhaust gas in pulsation vessel	-	700
Coolant entering engine	80	120
Oil entering engine	75	130

Speed limits for the AVL5402SCRE

Measurement	Lower Limit [RPM]	Upper Limit [RPM]
Engine	800	4200 continuously (or 4500 instantaneously)
Oil pump	12500 (for min oil flow)	1375 (max motor speed)

Pressure limits for the AVL5402SCRE

Measurement	Lower Limit [mbar]	Upper Limit [mbar]
Supercharger supply	200abs	4000abs
Inlet manifold/boost	200abs	2300abs (valve springs)
In-cylinder	none	170bar abs
Oil	3000	4000
Coolant entering engine	1500 gauge	1500 gauge
Fuel to HP pump	4500abs	7500abs
Rail pressure	230bar gauge (120bar gauge @start-up)	1800bar gauge (300bar gauge @start up)

Torque limits for the AVL5402SCRE

Measurement	Lower Limit [NM]	Upper Limit [NM]
Dynas 145	-	**72**
Indicom	-	**87Nm**

6. EMERGENCY SHUTDOWN OF SYSTEM

The goal of an emergency stop is to bring the engine down to a safe mode of operation as quickly as possible in the event of part, sub-system or control failure. If oil or fuel pressure drop below minimum allowable pressure or failure of the drive shaft occurs, simply stopping injection will not be sufficient, the engine will need to be brought to a complete stop. If for example, maximum allowable in-cylinder pressure is passed then bringing the engine to a complete stop is not required, instead forcing the engine into a state of idle mode and monitoring the engines pressure trace for irregularities will be sufficient. If there is a noticeable peak pressure difference or increased cycle-to-cycle variation, the engine should be brought to a stop and assessed.

Engine conditions that can be monitored with senses have been integrated into the control system such that, should maximum or minimum conditions be reached (as specified in the tables above), the correct response will automatically and instantaneously be carried out.

Emergency engine shut-off

In the event where an emergency engine shutoff has to be carried out manually there are two main ways of doing this:-

i. In STARS, on the "Main" tab under "Functions", click "Stop Engine". This will automatically turn the ignition off (stop injection) and slow the engine down to 0rpm in as shorter period as possible.

ii. By physically hitting the red emergency stop button, power is completely cut-off to the test apparatus causing everything to shut down. This method of shutdown must be a last resort as the heating elements in the supercharging unit require the flow of air across them for cooling purposes before powering down. This method also puts a large amount of stress on the dynamometer, drive shaft assembly, engine and supporting subsystems.

Emergency Fuel shut-off

In the case where fuelling to the combustion chamber needs to be shut off in an emergency, the two most efficient ways of achieving this are as follows:-

i. In CalVIEW, on the "MAIN CONTROLS" tab, click "EngineRunEnable". This will stop all fuel injection and depressurise the common rail.

ii. In STARS, on the "Main" tab, select "Ignition off". This will disable the ECU and thus stop it from injecting fuel.

7. CRITICAL EQUIPMENT LIST

i. Fire extinguishers in case of a fire

ii. Spill kit in case of fluid spills

8. Cleaning procedure

After running fired tests the engine should be motored for 5minutes at a range of pressures between 0 and 1.3bar gauge (the intake air heaters should be off at this time). This will flush the engine of all residual gases, help remove soot particles and force cooling of the equipment comprising the air-exchange system. The ball valve on the pulsation vessel should then be opened to drain any potential condensate that may have collected during the test. This will prevent corrosion and thus increase the life of the vessel.

Procedure number:	*Procedure revision date:*

SAFETY OPERATING PROCEDURE BLOCK STRUCTURE:

Job	Job Step	Method	Hazard	Risk	Control Measure	Task observation	
						Task executed effectively	Deviations noticed
Sub-system start-up – **Electrical**	1.1	Check that all electrical wires between the engine, ECU and Indismart are out of reach of rotating parts.	Exposed/broken wiring	Electric shock	Wear rubber soled shoes		
	1.2	Check for spilled liquids in close proximity to electrical wiring.	Spilled liquids, exposed/broken wiring	Electric shock, slipping	Access to spill kit, wear rubber soled shoes, lab coat and protective eye-wear		
	1.3	Ensure that plugs/wiring on the common rail, high pressure pump, injector, throttle body, back pressure valve and EGR valve are secure.	Exposed wiring	Electric shock	Wear rubber soled shoes		
	1.4	Turn on power to all the subsystem units and make sure all the control box circuit breakers are closed.					
	1.5	Switch on the STARS computer, CalVIEW computer and the Indic laptop.					
Sub-system start-up – **test facility water**	2.1	Check all test facility drainage pipes are secured in the drain to avoid spillage	Spilled liquids	Slipping	Access to spill kit, wear lab coat, closed shoes and protective eye-wear		
	2.2	Turn on test facility water on the switch board by switching the two knobs labelled "Cool water pump" and "Hot water pump"					
	2.3	Check piping and joins in the test facility water supply for leaks.	Spilled liquids	Slipping	Access to spill kit, wear lab coat, closed shoes and protective eye-wear		
	2.4	Make sure the ball valve in the test cell is open to ensure water flow through the subsystems.					
	2.5	Check for water flow leaving all the pipes entering the drain to ensure flow through all the systems which require cooling.					

Sub-system start-up – **ventilation**	3.1	Check supply and suction orifices of the ventilation and make sure there are no obstructions.					
	3.2	Check exhaust pipe exit aligns with suction orifice of ventilation to ensure all exhaust gas is extracted.					
	3.3	When turning on the ventilation the aim is to generate a vacuum in the test cell such that no exhaust gas is able to enter the control room. This is achieved by having greater extraction than supply. This can be checked by opening the door leading into the test cell, you should experience a suction force.	Door	Catching fingers in door as it is sucked closed due to vacuum	Keep fingers clear of the door and warn surrounding colleagues before turning the ventilation on.		
Sub-system start-up – **Lubrication and coolant conditioning unit**	4.1	Adjust the oil bypass needle valve to fully open allowing for maximum oil flow rate.					
	4.2	Turn on coolant and oil pumps in STARS and then check unit and engine for leaks.	Oil and coolant leaks	Slipping, ingestion and eye penetration	Access to spill kit, wear lab coat, closed shoes and protective eye-wear		
	4.3	As oil heats up the motor speed increases until it reaches maximum speed (1375rpm), at this point the pressure will begin to drop as the oil continues to heat up and viscosity decrease. Oil pressure must be kept above 3 bar and the oil pump must rotate between 1000 and 1350rpm. This is achieved by adjusting the needle valve accordingly.					
	4.4	Engine may not be turned over until oil temperature exceeds 75°C and coolant temperature exceeds 85°C.					
Sub-system start-up – **Supercharging system**	5.1	Check for secure attachment of compressed air lines between compressor and supercharger unit as well as between the supercharger unit and the engine.	Compressed air line hoses bursting off whilst engineer or technician is in the test cell	Being struck by hose or hose clamp	Thoroughly check hose and hose clamp attachments. Wear protective shoes, eye protection and a lab coat (ideally a hard hat to).		
	5.2	Turn on supercharging equipment and check for leaks. Leaks will result in an inaccurate measurement of air through the engine.					
Sub-system start-up – **Dynamometer**	6.1	Check drive shaft assembly is securely fastened.	Drive shaft coming loose	Mild, moderate or fata wounds caused by drive shaft assembly			
	6.2	Check shaft guard is fastened closed tightly	Shaft guard not being able to contain the drive shaft assembly in the	Mild, moderate or fata wounds caused by drive shaft assembly			

			event of failure				
	6.3	Set dynamometer start-up conditions and apply demand.					
Sub-system start-up – **Indicom software**	7.1	Establish connection between engine and computer and start the real time sensing. This system is the engineer's only way of monitoring what is going on in the engine. If proper connection is not established, fired operation should not commence.					
		Check "SyncStopped" fault is not displaying. If it is, take appropriate action.					
Sub-system start-up – **Fuel supply**		Check fuel lines for damage and any potential sources of leaking.	Leaking fuel	Fire, slipping, ingestion and eye penetration	Thorough fuel line check, Wear protective shoes, eye protection and a lab coat		
		Turn on fuel supply to the engine and wait until pressure reaches 2bar. Then turn on low pressure pump to raise the fuel pressure to 6bar. Fuel pressure must be between 4.5 and 7.5 bar abs before the engine is turned over.					
		Setup correct fuelling parameters on CalVIEW for required initial operating conditions					

Deviations noticed:	Corrective action:

EQUIPMENT, METHODS AND PROCEDURES CAN NOT BE USED WITHOUT BEING DECLARED COMPETENT BY AN OBSERVER (QUALIFIED PERSON).

Procedure number:	Trainee:	Control Number:	Signature:	Observer:	Control Number:	Signature:	Date:

I HEREBY ACKNOWLEDGE RECEIPT OF THE ABOVE-MENTIONED DOCUMENT AND DECLARE THAT I HAVE READ AND UNDERSTAND THE CONTENTS AND THAT I WILL ADHERE TO THIS PROCEDURE/WORK INSTRUCTION DURING THE PERFORMANCE OF MY DUTIES.

Appendix F

Technical drawings

This appendix presents technical drawings for some of the components designed. These include the:

1. Flexible drive-shaft assembly
2. Shaft guard
3. Instrument stand
4. Pulsation vessel
5. Stands for back pressure valve and exhaust system
6. Stands for pulsation vessel
7. Conditioning unit

The test apparatus assembly drawing below highlights the aforementioned components.

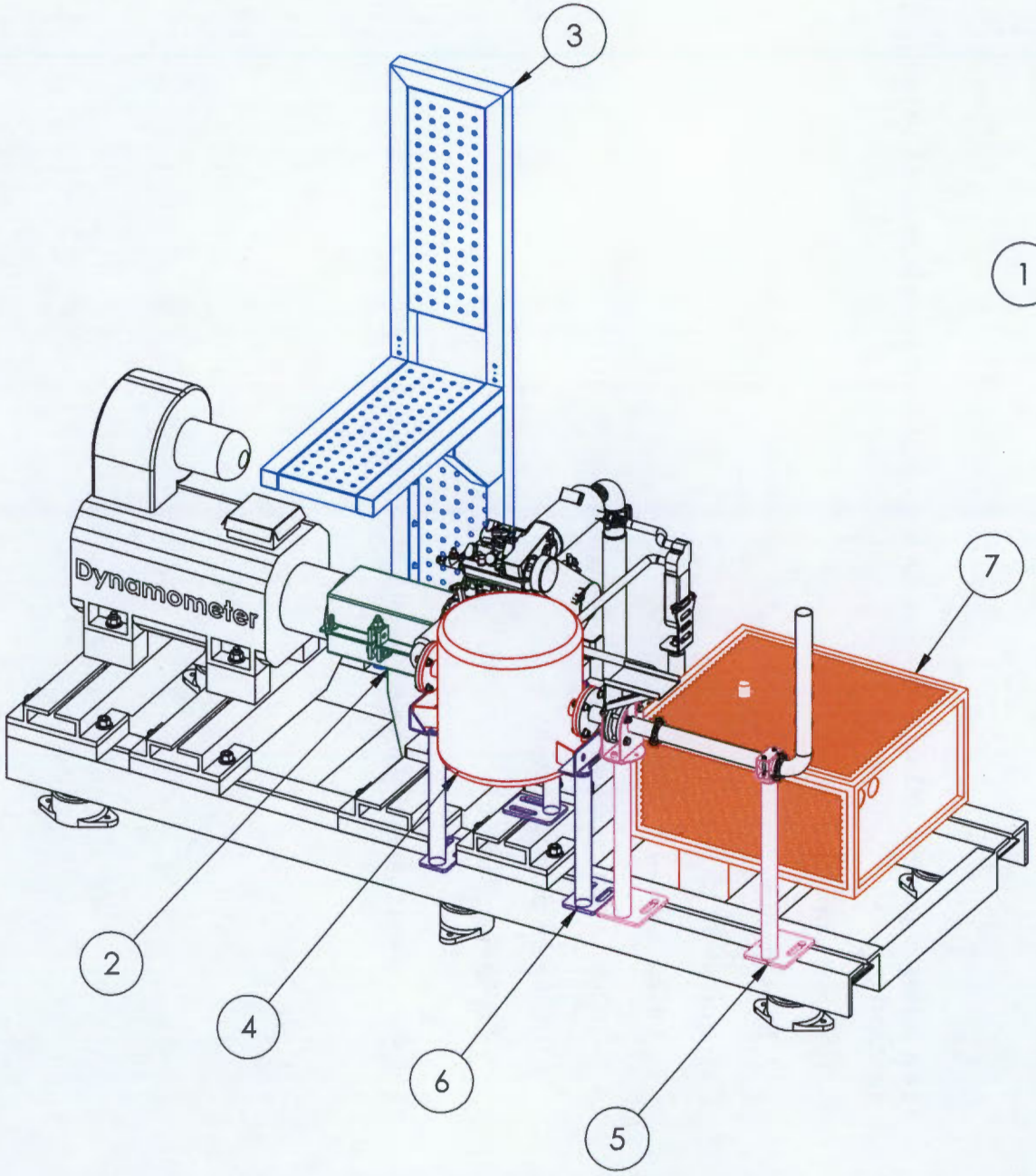

1 Shaft assembly is located within the confines of the shaft guard, part no. 2.

ITEM NO.	PART NUMBER	QTY.
1	Shaft and coupling assembly	1
2	Shaft guard	1
3	Instrument stand	1
4	Pulsation vessel	1
5	Exhaust stands	2
6	Stands for pulsation vessel	3
7	Conditioning Unit	1

A4 Landscape	University of Cape Town Department of Mechanical Engineering			
	Title: Test cell Assembly			
Assembly Drawing	Scale: 1:50	Date: 2015/07/11	Sheet	of
	Drawn By: Timothy Cole King		Drawing Number	

F.1 Shaft assembly

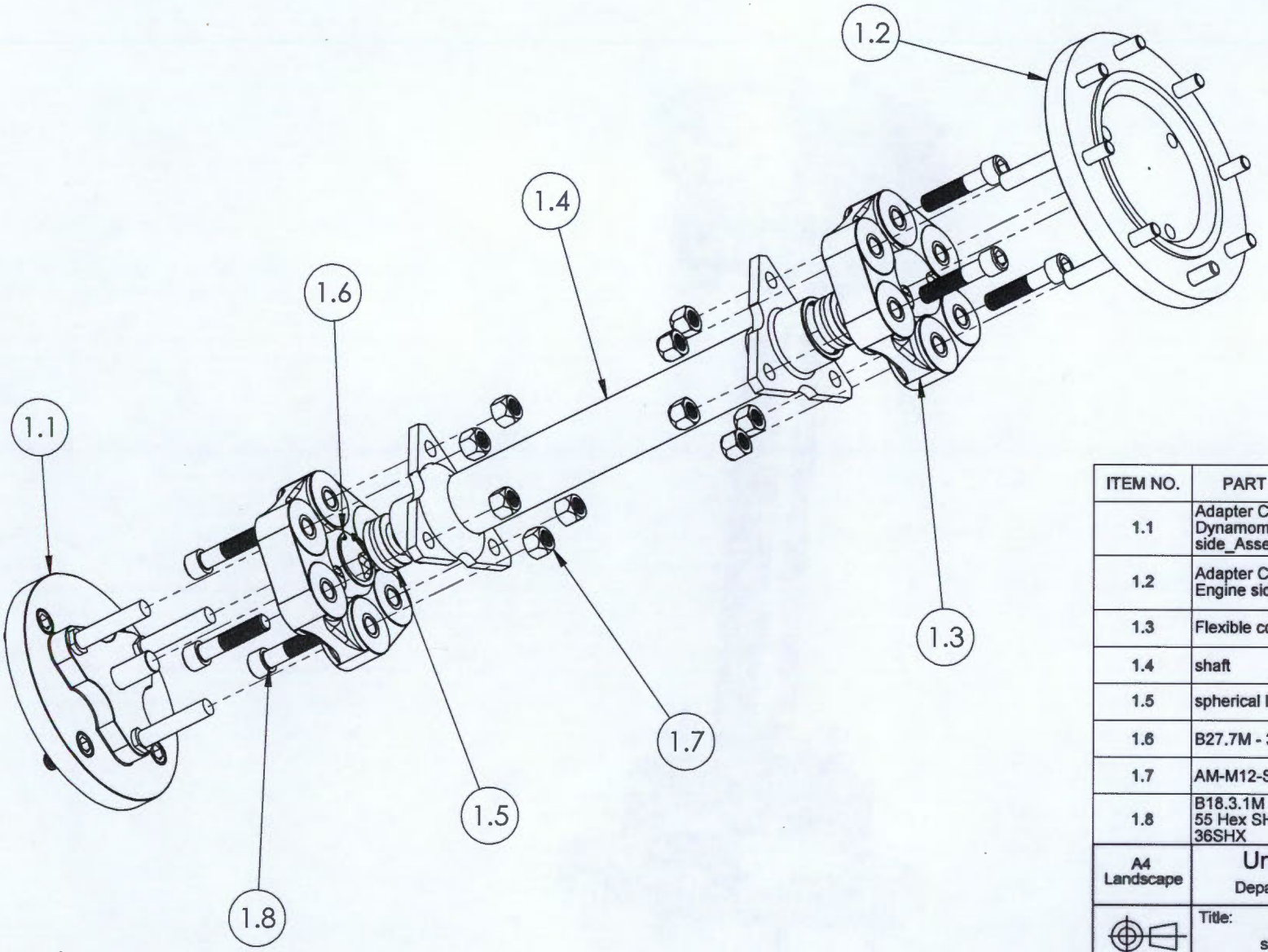

ITEM NO.	PART NUMBER	QTY.	Material
1.1	Adapter Coupling Dynamometer side_Assembly	1	
1.2	Adapter Coupling Engine side_ Assembly	1	
1.3	Flexible coupling	2	
1.4	shaft	1	En24(X)
1.5	spherical bushing PB16	2	
1.6	B27.7M - 3BM1-38	2	
1.7	AM-M12-S	12	
1.8	B18.3.1M - 12 x 1.75 x 55 Hex SHCS – 36SHX	6	

A4 Landscape	University of Cape Town Department of Mechanical Engineering			
	Title: shaft and couplings assembly BOM			
Assembly Drawing	Scale: 1:4	Date: 2015/07/08	Sheet1	of 8
	Drawn By: Timothy Cole King		Drawing Number 1(a)	

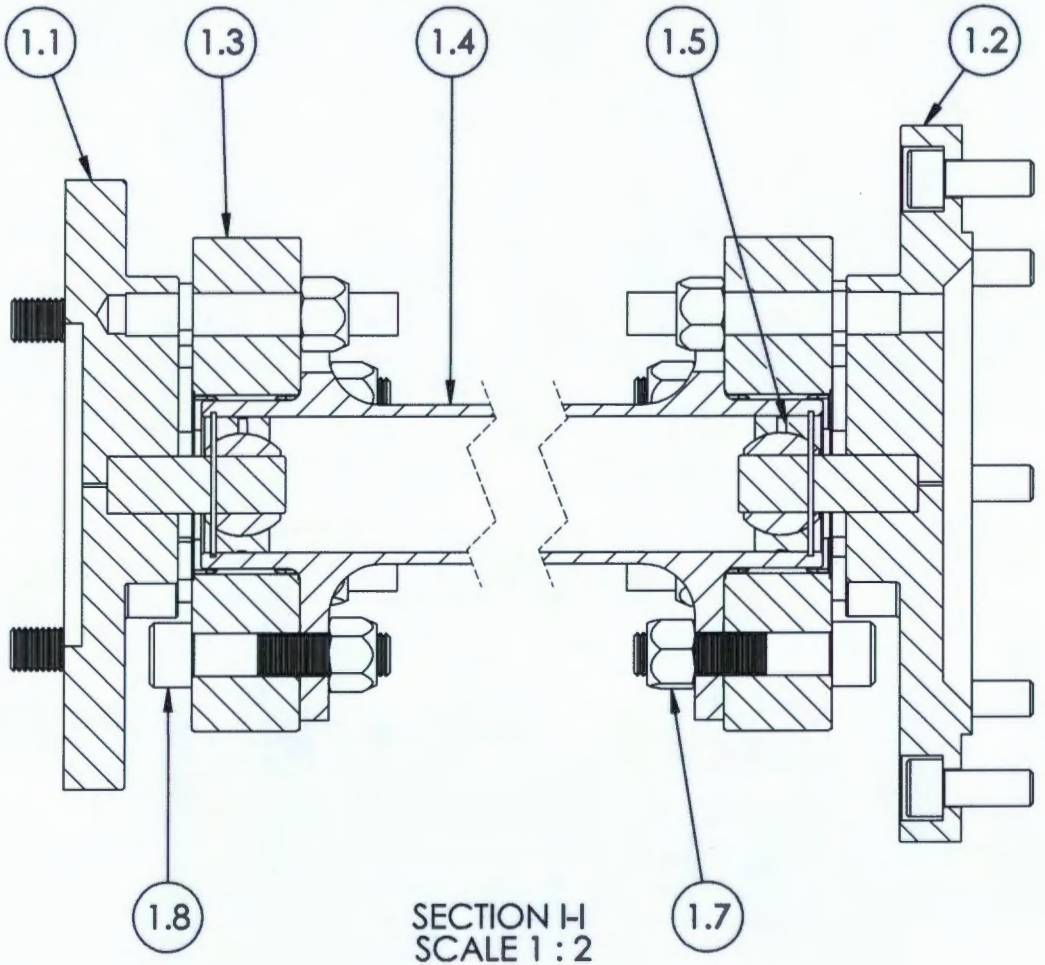

SECTION I-I
SCALE 1 : 2

ITEM NO.	PART NUMBER	Default /QTY.	Material
1.1	Adapter Coupling Dynamometer side_Assembly	1	
1.2	Adapter Coupling Engine side_ Assembly	1	
1.3	Flexible coupling	2	
1.4	shaft	1	En24(X)
1.5	spherical bushing PB16	2	
1.6	B27.7M - 3BM1-38	2	
1.7	AM-M12-S	12	
1.8	B18.3.1M - 12 x 1.75 x 55 Hex SHCS – 36SHX	6	

A4 Landscape	University of Cape Town Department of Mechanical Engineering			
	Title: shaft and couplings assembly_BOM			
QTY 1	Scale:	Date: 2015/07/08	sheet2	of 8
Material: 304 SS	Drawn By: Timothy Cole King		Drawing Number 1(b)	

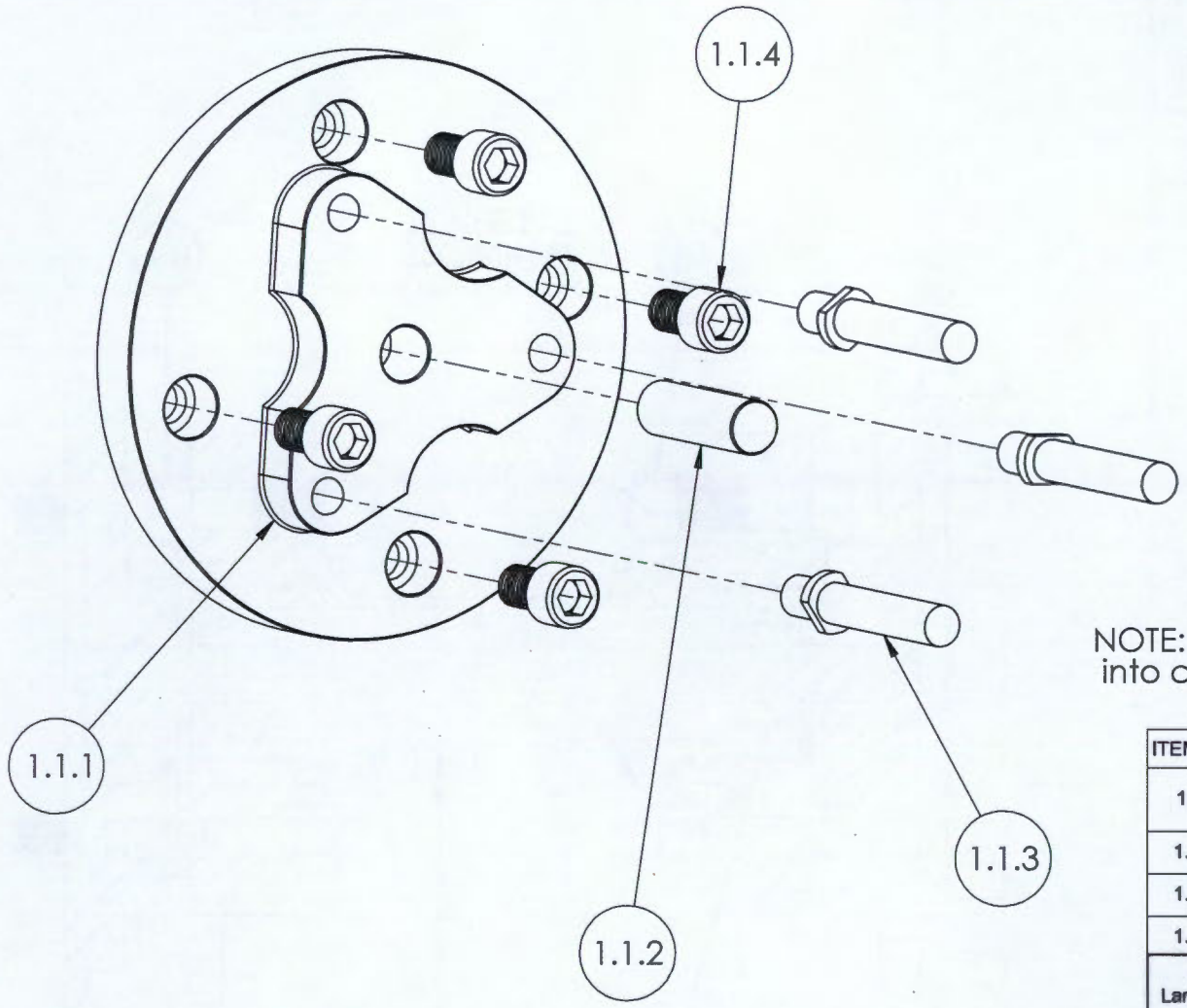

NOTE: Part number 4.1.2 to be press-fit into centre hole of part number 4.1.1

ITEM NO.	PART NUMBER	QTY.	Material
1.1.1	Adapter Coupling Dynamometer side AVL type	1	304_SS
1.1.2	Adaptor coupling locating pin	1	M300
1.1.3	bolt_ flexi-coupling to adaptive coupling	3	En 24 (T)
1.1.4	B18.3.1M - 12 x 1.75 x 20 Hex SHCS -- 20SHX	4	HT_Steel

A4 Landscape	University of Cape Town Department of Mechanical Engineering			
	Title: Adapter Coupling Dynamometer side_Assembly			
Assembly Drawing	Scale: 1:1	Date: 2015/07/08	Sheet3	of 8
	Drawn By: Timothy Cole King		Drawing Number 1.1	

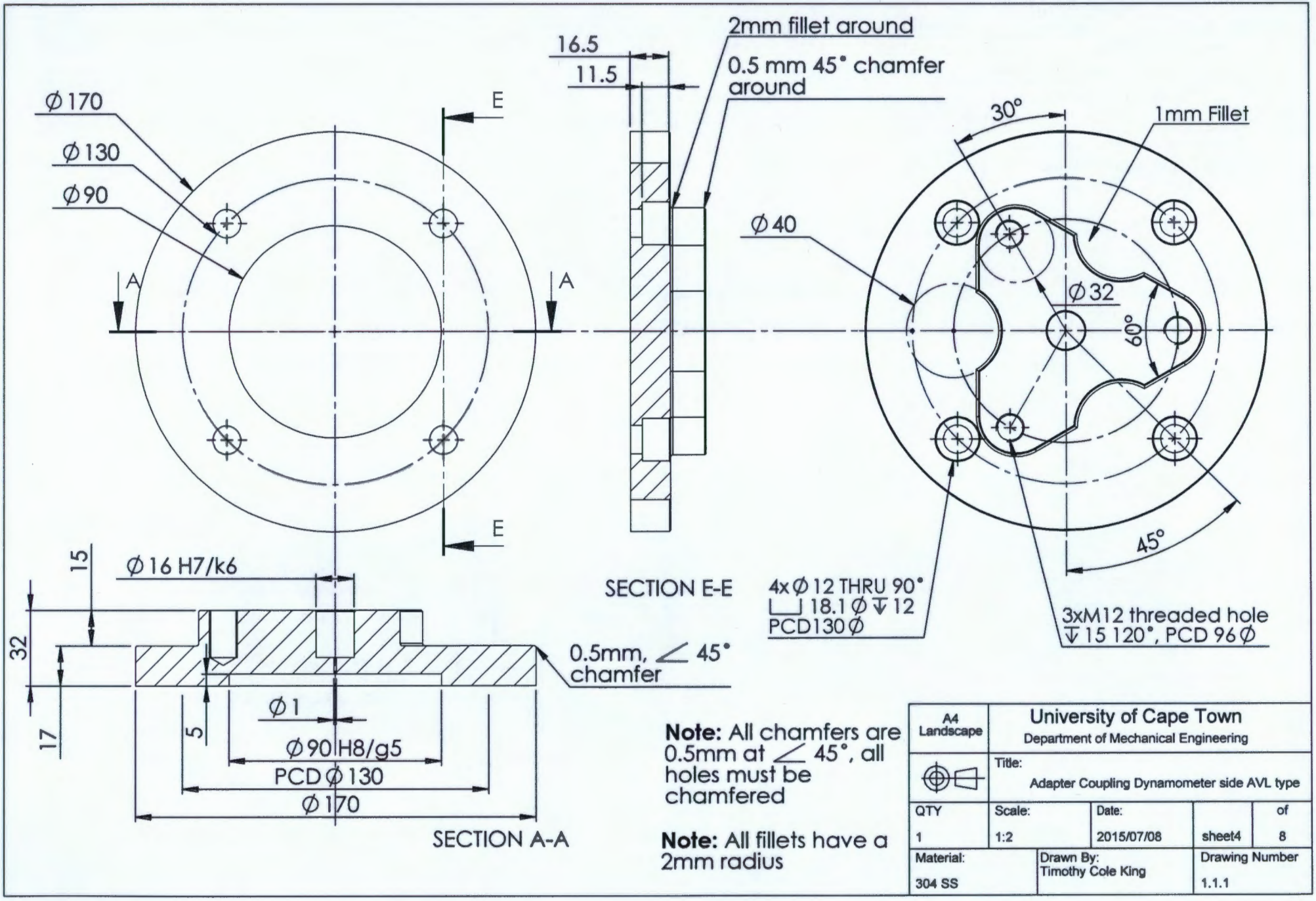
Ø170
Ø130
Ø90
E
A
A
E
16.5
11.5
2mm fillet around
0.5 mm 45° chamfer around
30°
1mm Fillet
Ø40
Ø32
60°
45°
SECTION E-E
4xØ12 THRU 90°
⌴ 18.1Ø↧12
PCD130Ø
3xM12 threaded hole
↧15 120°, PCD 96Ø
15
Ø16 H7/k6
32
17
5
Ø1
Ø90 H8/g5
PCD Ø130
Ø170
0.5mm, ∠ 45° chamfer
SECTION A-A
Note: All chamfers are 0.5mm at ∠ 45°, all holes must be chamfered
Note: All fillets have a 2mm radius
A4 Landscape
University of Cape Town
Department of Mechanical Engineering
Title:
Adapter Coupling Dynamometer side AVL type
QTY
1
Scale:
1:2
Date:
2015/07/08
sheet4
of
8
Material:
304 SS
Drawn By:
Timothy Cole King
Drawing Number
1.1.1

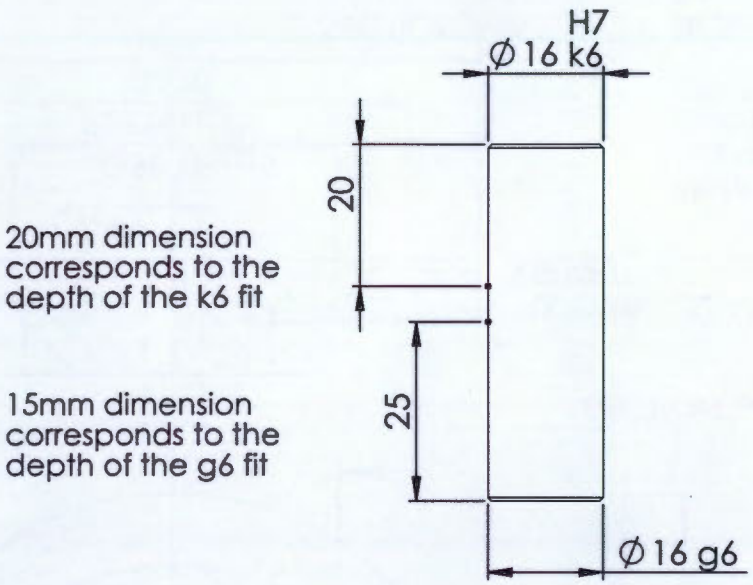

20mm dimension corresponds to the depth of the k6 fit

15mm dimension corresponds to the depth of the g6 fit

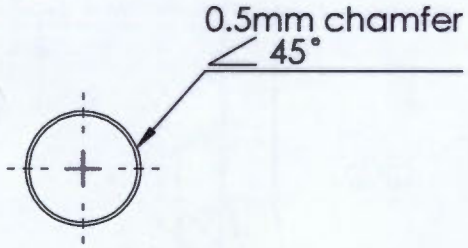

A4 Landscape	University of Cape Town Department of Mechanical Engineering			
	Title: Adaptor coupling locating pin			
QTY 1	Scale: 1:1	Date: 2015/07/08	sheet5	of 8
Material: M300	Drawn By: Timothy Cole King		Drawing Number 1.1.2	

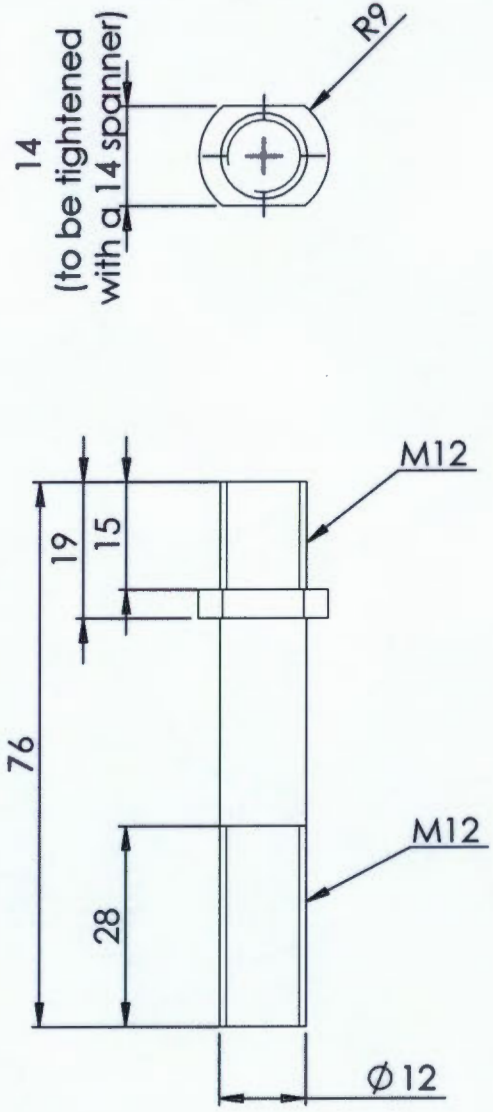

A4 Landscape	University of Cape Town Department of Mechanical Engineering			
	Title: bolt_ flexi-coupling to adaptive coupling			
QTY 1	Scale: 1:1	Date: 2015/07/08	sheet6	of 8
Material: 304 SS	Drawn By: Timothy Cole King		Drawing Number 1.1.3	

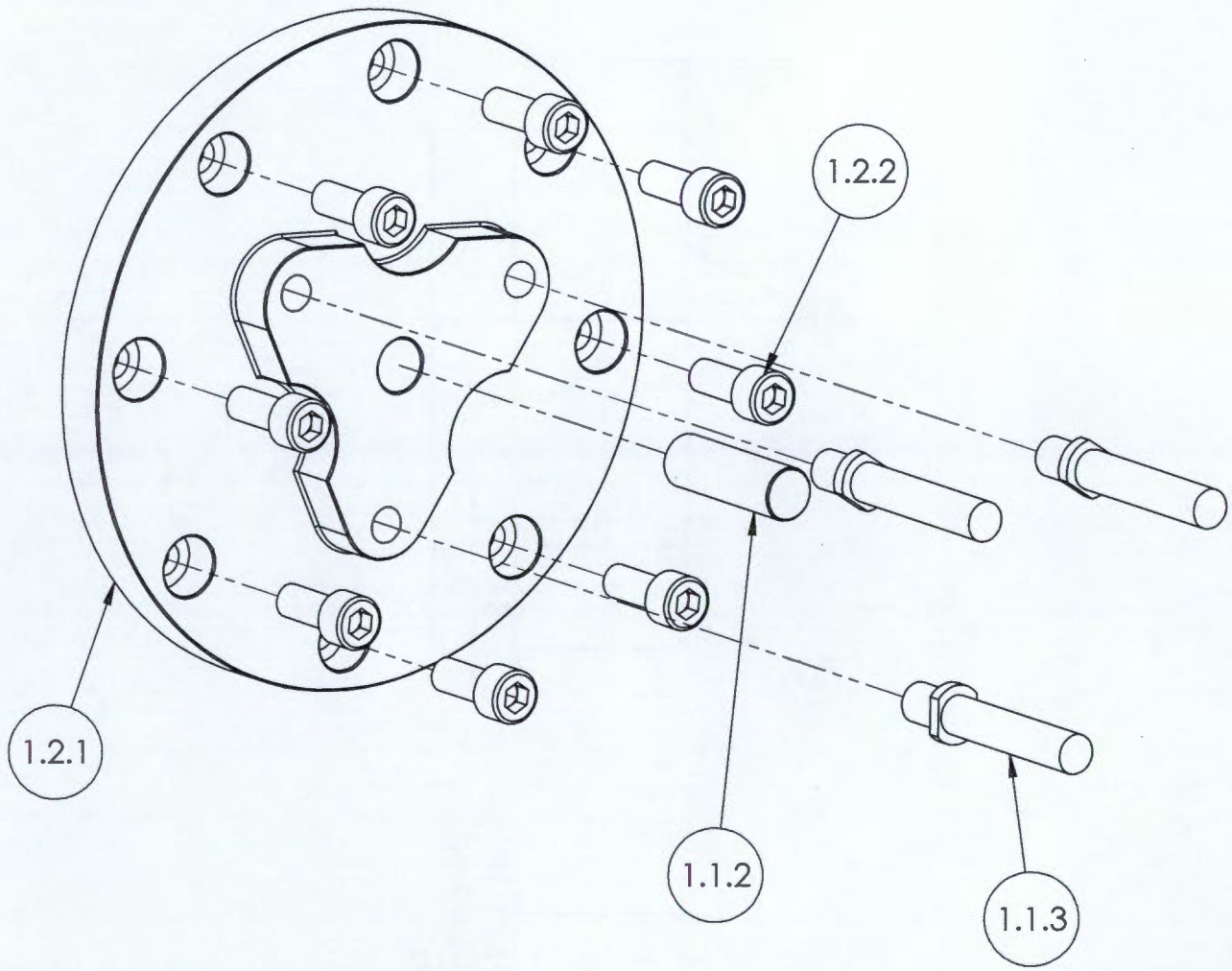

ITEM NO.	PART NUMBER	QTY.	Material
1.2.1	Adapter Coupling Engine side AVL type NEW	1	SS_304
1.2.2	DIN 912 M10 x 25 — 25N	8	
1.1.2	Adaptor coupling locating pin	1	M300
1.1.3	bolt_ flexi-coupling to adaptive coupling	3	En 24 (T)

A4 Landscape	University of Cape Town Department of Mechanical Engineering			
	Title: Adapter Coupling Engine side_ Assembly			
Assembly Drawing	Scale: 1:1	Date: 2015/07/08	Sheet7	of 8
	Drawn By: Timothy Cole King		Drawing Number 1.2	

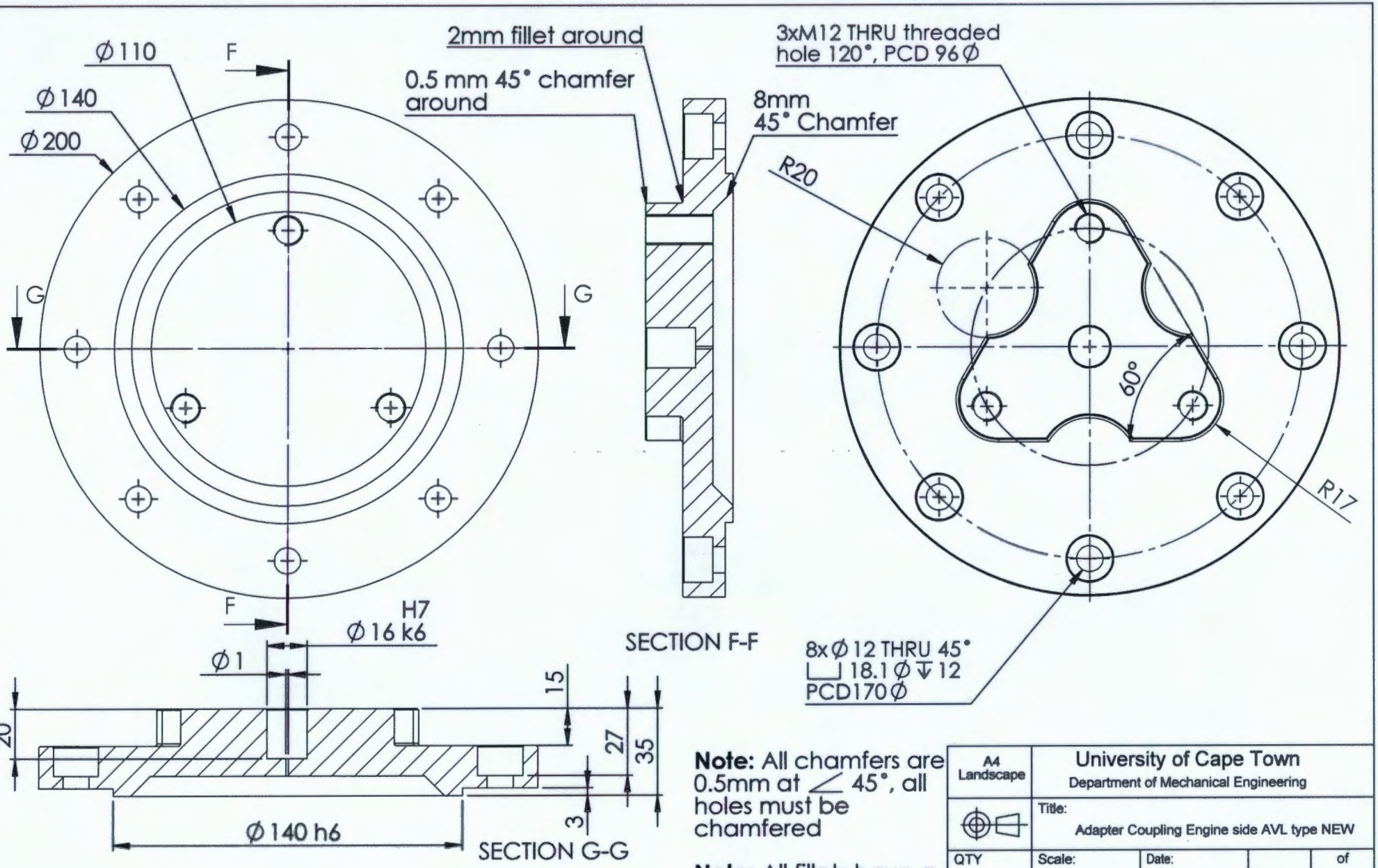

Note: All chamfers are 0.5mm at ∠ 45°, all holes must be chamfered

Note: All fillets have a 2mm radius

A4 Landscape	University of Cape Town Department of Mechanical Engineering			
	Title: Adapter Coupling Engine side AVL type NEW			
QTY 1	Scale: 1:2	Date: 2015/07/08	sheet8	of 8
Material: 304 SS	Drawn By: Timothy Cole King		Drawing Number 1.2.1	

F.2 Shaft guard

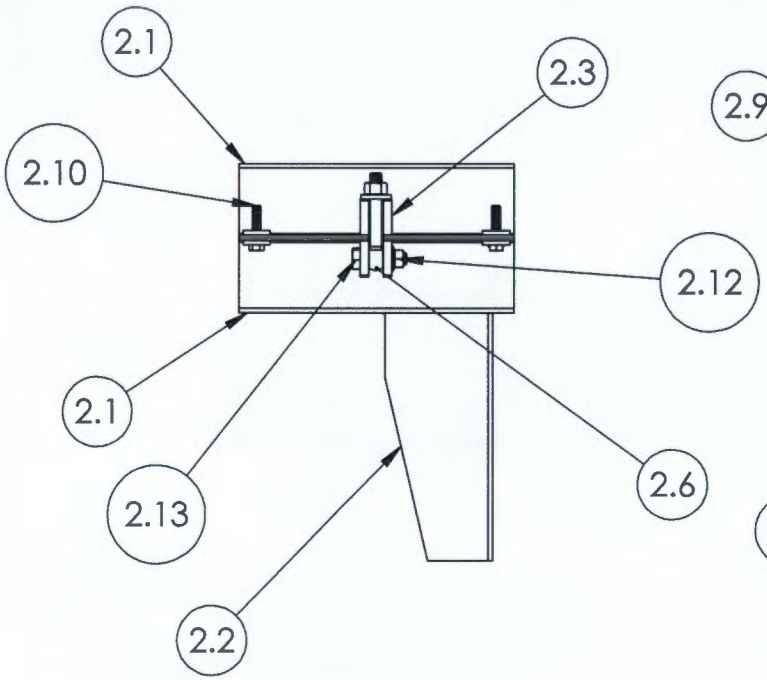

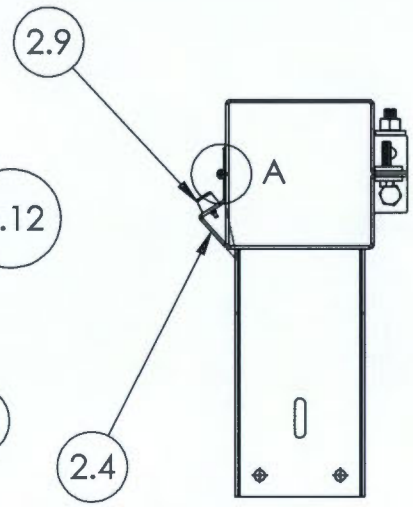

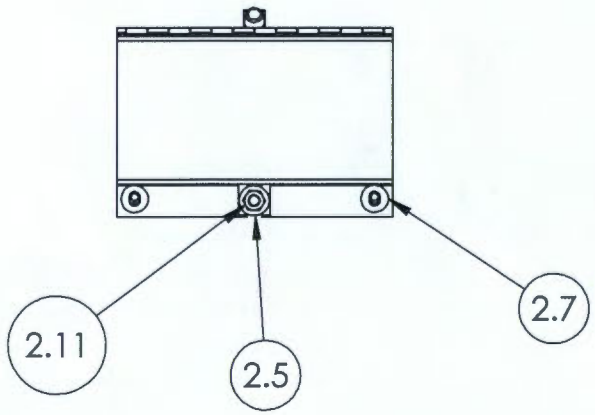

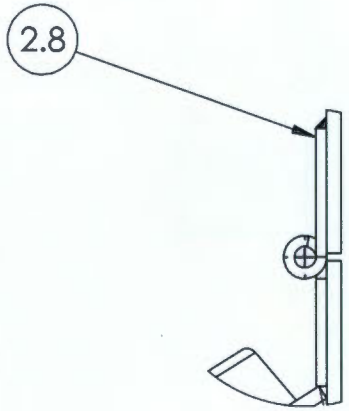

DETAIL A
SCALE 1 : 2

ITEM NO.	PART NUMBER	QTY.	Material
2.1	Cover Top with slot	2	LC-STEEL
2.2	Mounting sheet	1	LC-STEEL
2.3	Rectangle for clamp	4	LC-STEEL
2.4	Stopper angle	1	LC-STEEL
2.5	clamp washer	1	LC-STEEL
2.6	Eye-bolt	1	304_SS
2.7	Location Washer	4	LC-STEEL
2.8	Hinge bottom	2	LC-STEEL
2.9	Rubber stopper	1	RUBBER
2.10	B18.2.3.5M - Hex bolt M12 x 1.75 x 55 --55S	2	HT_STEEL
2.11	B18.2.4.6M - Heavy hex nut, M16 x 2 --W-S	1	HT_STEEL
2.12	B18.2.2.4M - Hex flange nut, M16 x 2 --S	1	HT_STEEL
2.13	B18.2.3.6M - Heavy hex bolt M16 x 2.0 x 65 --38S	1	HT_STEEL

A4 Landscape	University of Cape Town Department of Mechanical Engineering			
	Title: Shaft Gaurd			
Assembly Drawing	Scale: 1:10	Date: 2015/07/08	Sheet	of 10
	Drawn By: Timothy Cole King		Drawing Number 2 (b)	

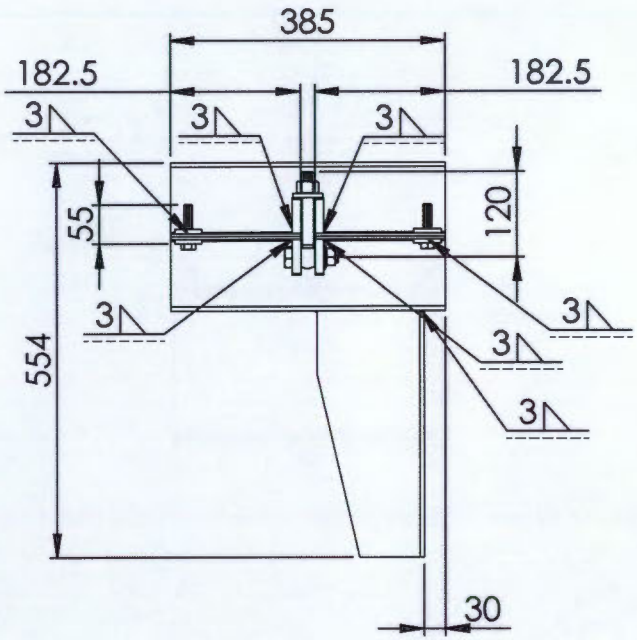

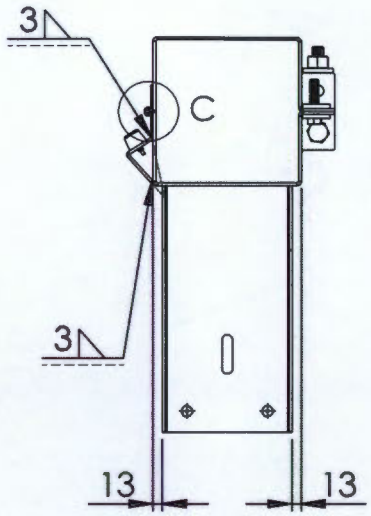

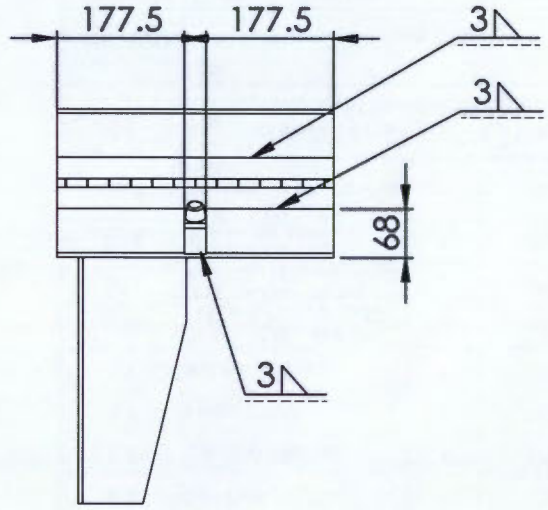

Assembly instructions: 3mm fillet welds

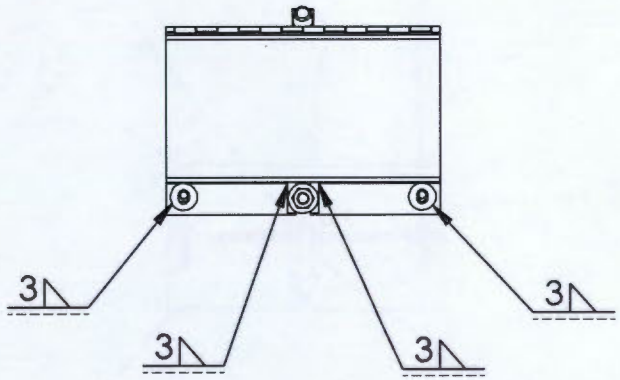

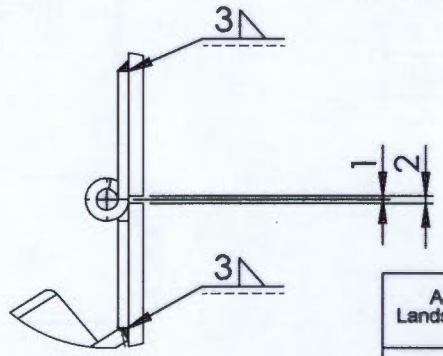

DETAIL C
SCALE 1 : 2

1 10 Sheet

A4 Landscape	University of Cape Town Department of Mechanical Engineering			
	Title: Shaft Gaurd			
Assembly Drawing	Scale: 1:10	Date: 2015/07/08		of
	Drawn By: Timothy Cole King		Drawing Number 2 (b)	

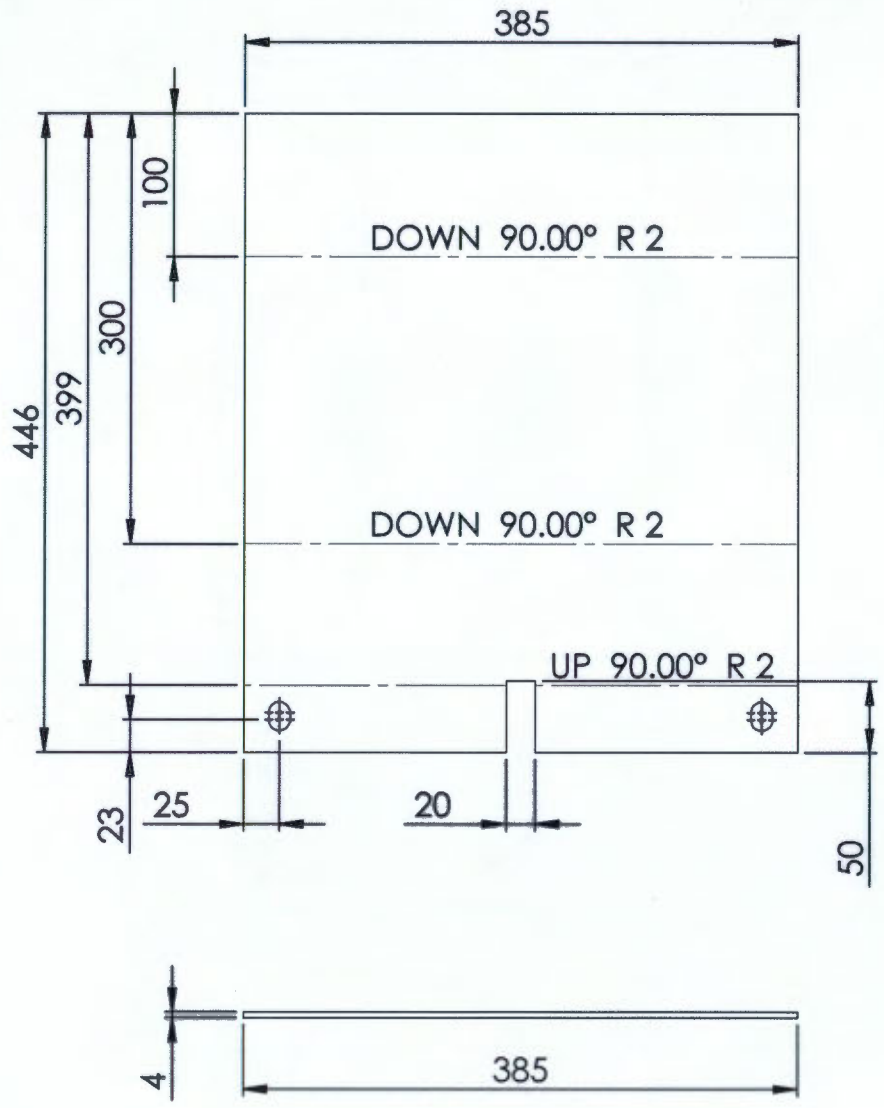

Flattened view: lazer cutting

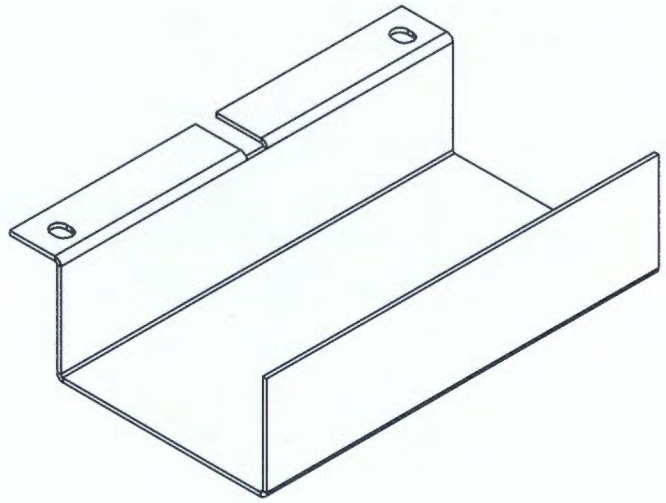

Isometric view of finished part after lazer cutting and bending

A4 Landscape	University of Cape Town Department of Mechanical Engineering			
	Title: Cover_Top and bottom flattened view			
Part Finish	Scale: 1:10	Date: 2015/07/08		of 10
Material: LC Steel	Drawn By: Timothy Cole King		Drawing Number 2.1(a)	

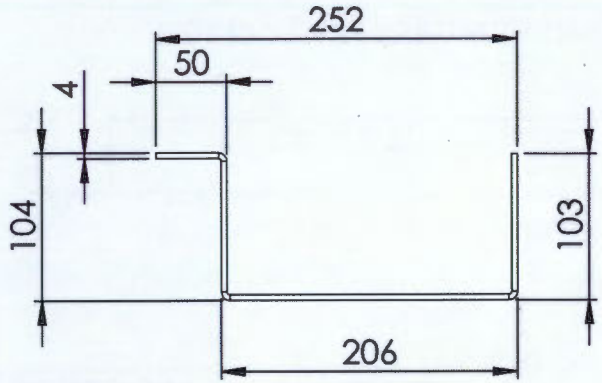

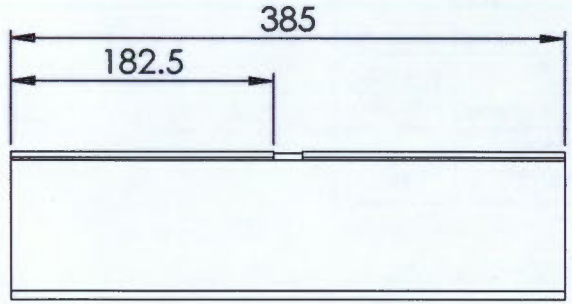

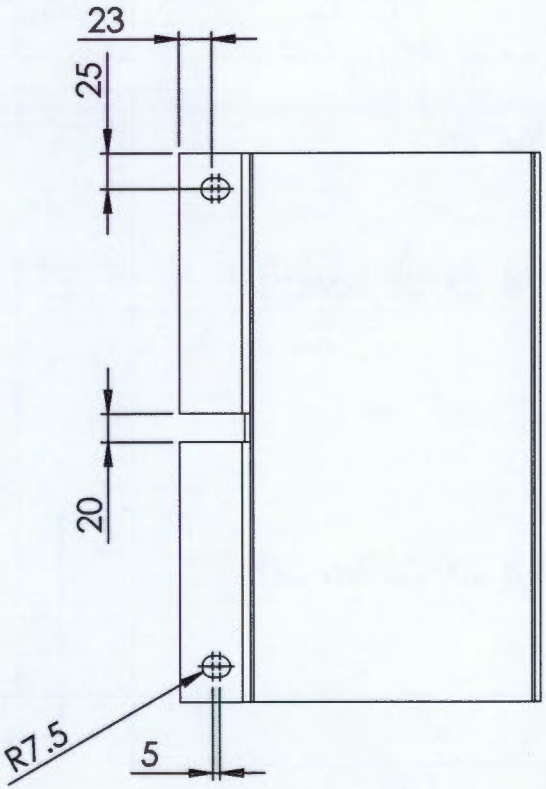

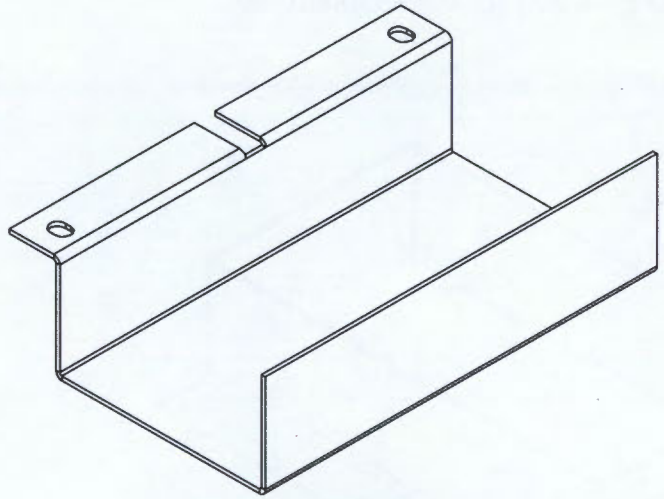

Isometric view

All bends have a radius of 2mm
Plate is 4mm thick

A4 Landscape	University of Cape Town Department of Mechanical Engineering			
	Title: Cover_ Top and Bottom			
Part Finish	Scale:	Date: 2015/07/08		of 10
Material: LC Steel	Drawn By: Timothy Cole King		Drawing Number 2.1(b)	

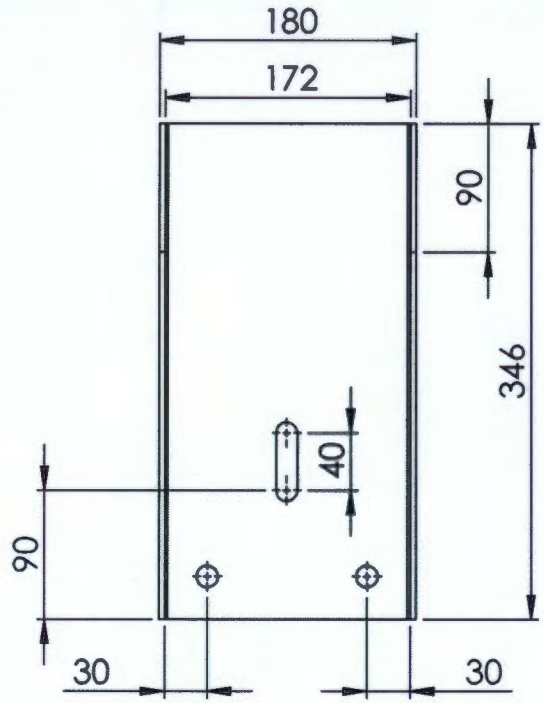

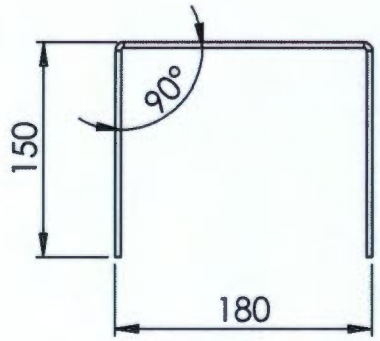

Bent view: CNC bending

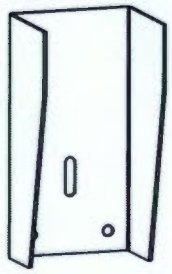

Isometric drawing of final part

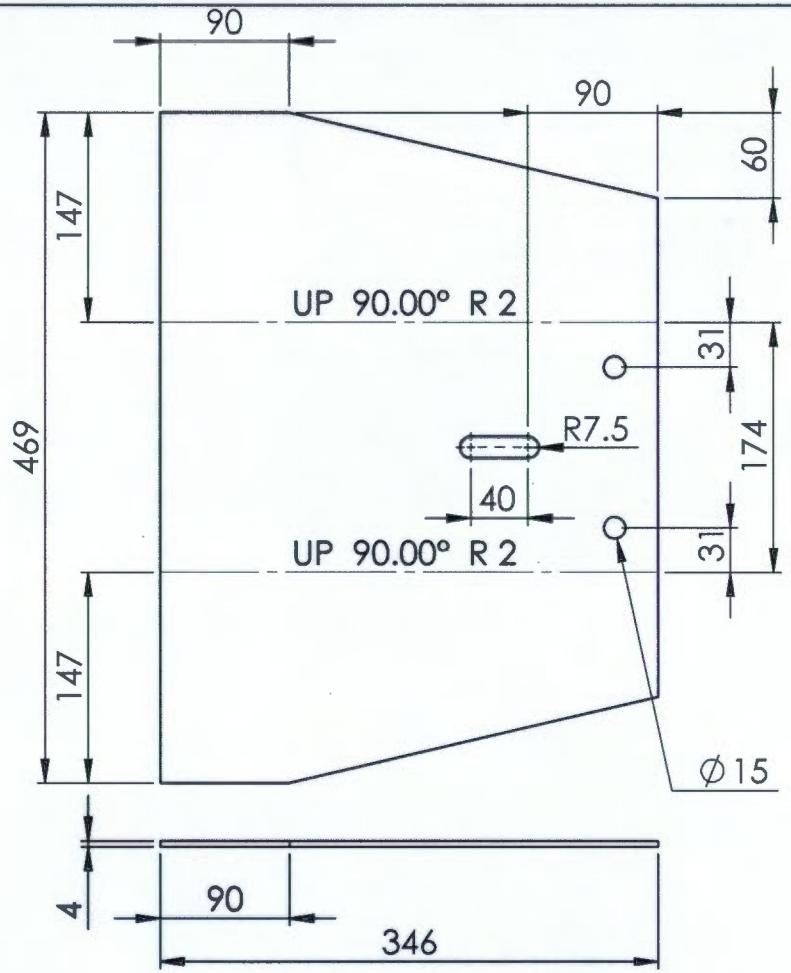

Flattened view: lazer cutting

A4 Landscape	University of Cape Town Department of Mechanical Engineering			
	Title: Mounting sheet			
Part Finish	Scale: 1:5	Date: 2015/07/08		of 10
Material: LC Steel	Drawn By: Timothy Cole King		Drawing Number 2.2	

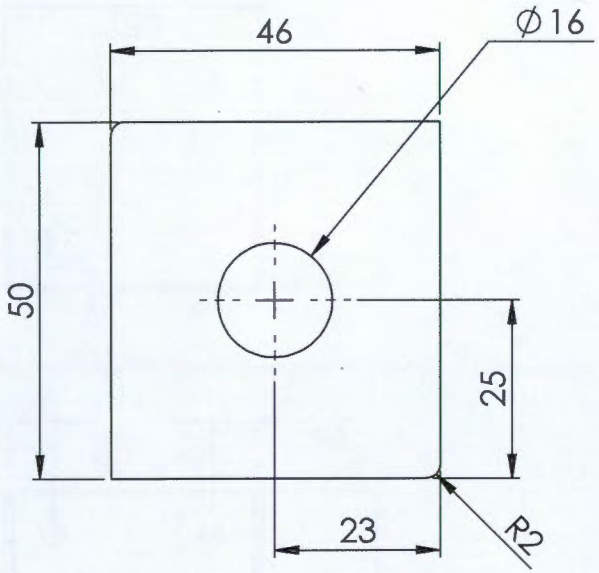

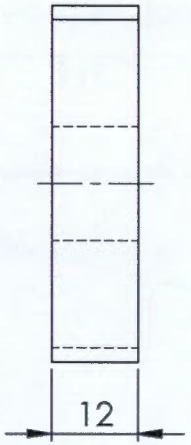

A4 Landscape	University of Cape Town Department of Mechanical Engineering			
	Title: Rectangle for clamp			
Part Finish	Scale: 1:1	Date: 2015/07/08		of 10
Material: LC Steel	Drawn By: Timothy Cole King		Drawing Number 2.3	

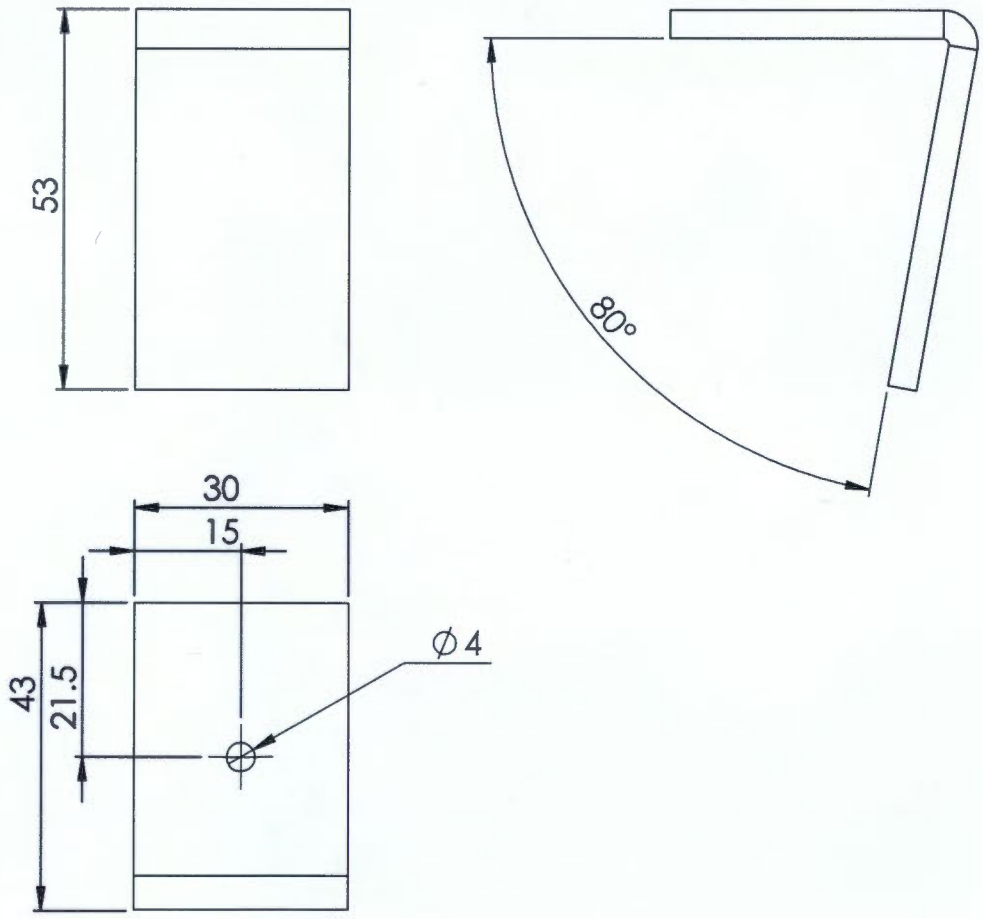

Bent view: CNC bending

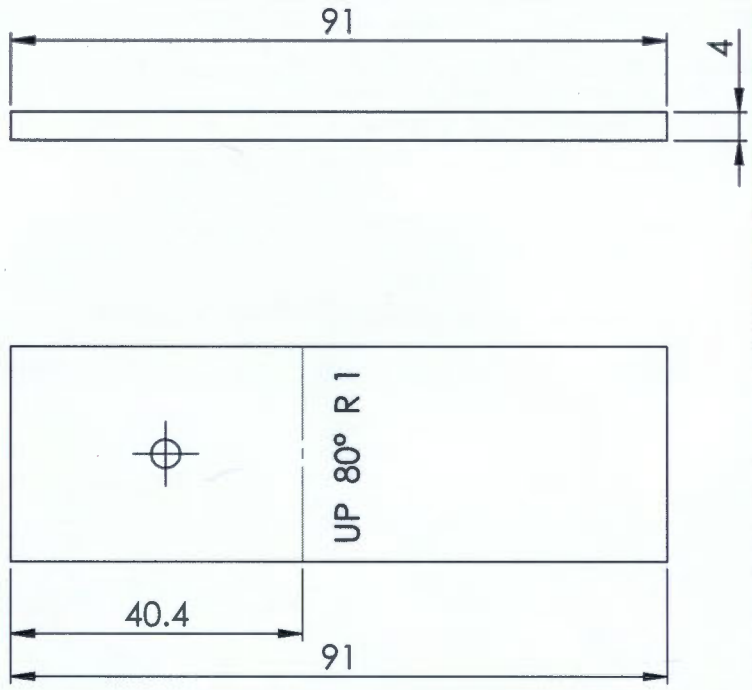

Flattened view: to be laser-cut

A4 Landscape	University of Cape Town Department of Mechanical Engineering			
	Title: Stopper angle			
QTY 1	Scale: 1:1	Date: 2015/07/08	sheet7	of 10
Material: LC STEEL	Drawn By: Timothy Cole King		Drawing Number 2.4	

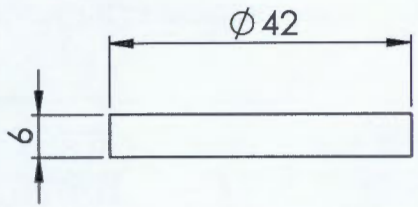

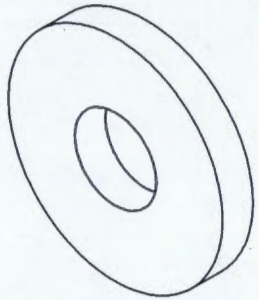

Isometric view

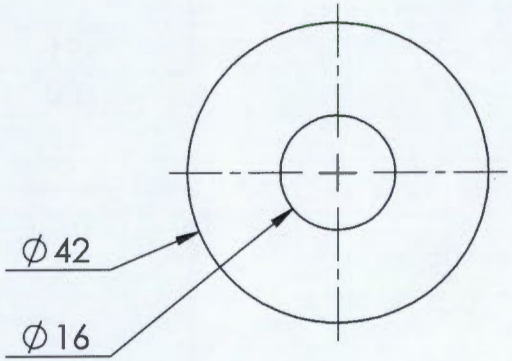

A4 Landscape	University of Cape Town Department of Mechanical Engineering			
	Title: clamp washer			
QTY 1	Scale: 1:1	Date: 2015/07/08	sheet8	of 10
Material: LC_Steel	Drawn By: Timothy Cole King		Drawing Number 2.5	

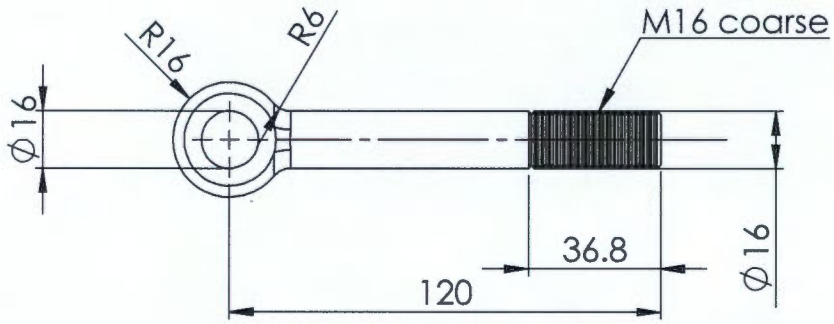

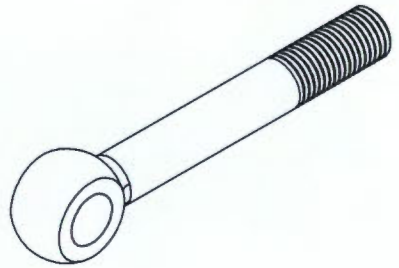

Isometric view

A4 Landscape	University of Cape Town Department of Mechanical Engineering			
	Title: eyebolt_din			
QTY 1	Scale: 1:2	Date: 2015/07/08		of
Material: 304 SS	Drawn By: Timothy Cole King		Drawing Number 2.6	

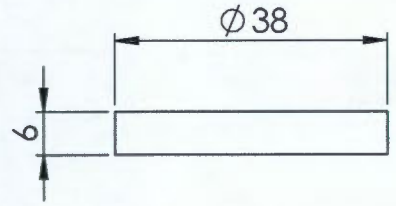

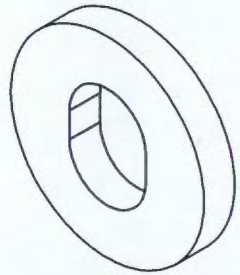

Isometric view

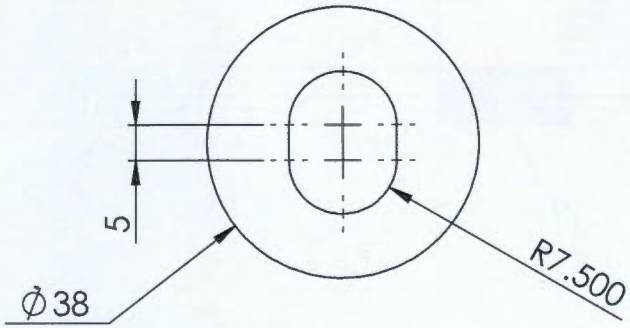

A4 Landscape	University of Cape Town Department of Mechanical Engineering			
	Title: Location Washer			
QTY 4	Scale: 1:2	Date: 2015/07/08		of 10
Material: LC STEEL	Drawn By: Timothy Cole King		Drawing Number 2.7	

F.3 Instrument stand

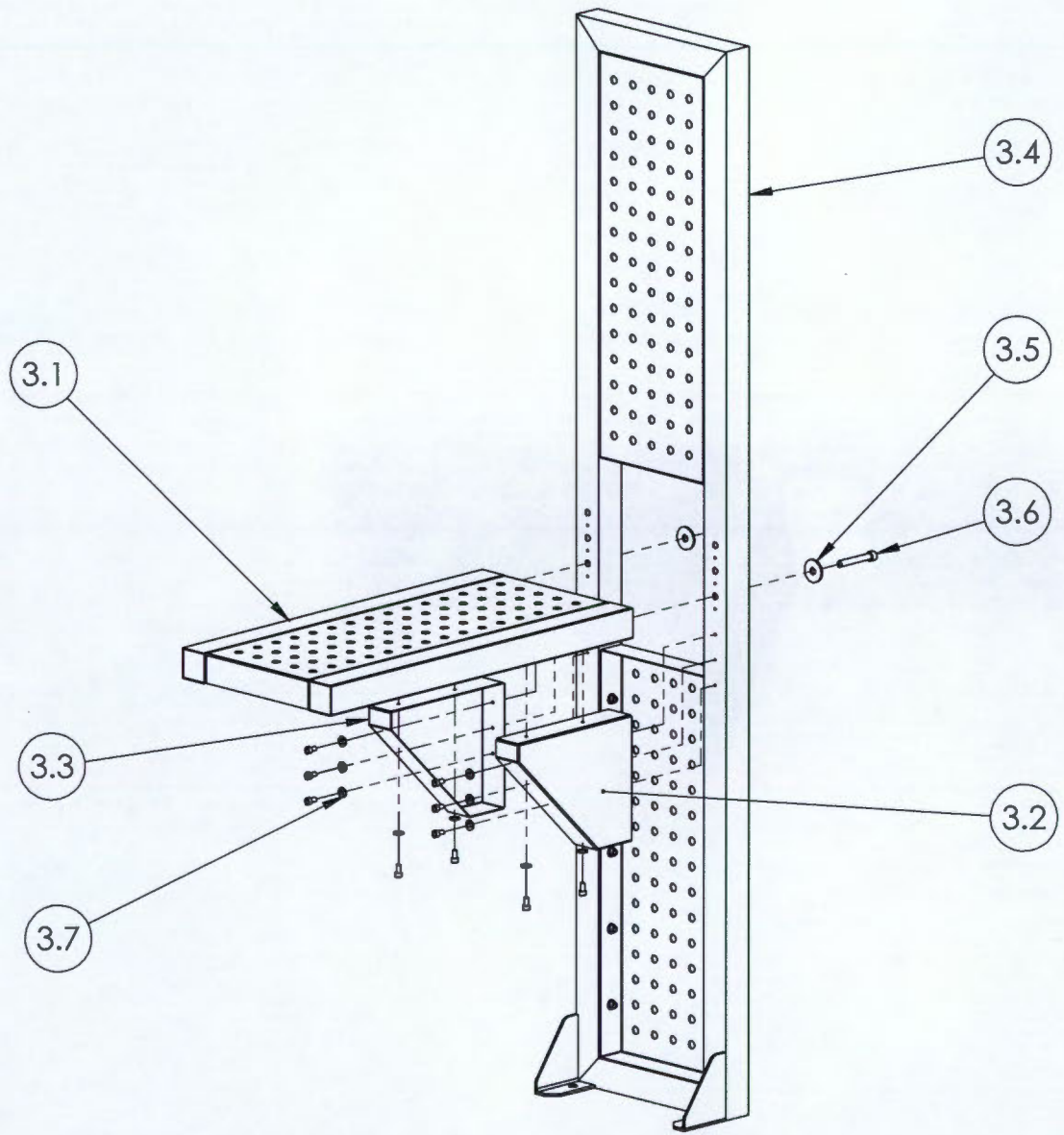

ITEM NO.	PART NUMBER	QTY.	Material
3.1	Shelf	1	
3.2	Shelf to frame support left	1	
3.3	Shelf to frame support right	1	
3.4	Frame verticle Asssembly	1	
3.5	B18.22M - Plain washer, 12 mm, wide	2	
3.6	B18.3.1M - 8 x 1.25 x 16 Hex SHCS -- 16NHX	12	
3.7	B18.22M - Plain washer, 8 mm, narrow	10	

A4 Landscape	University of Cape Town Department of Mechanical Engineering			
	Title: Pedestal_15_07_09			
Part Finish	Scale:	Date: 2015/07/09	sheet1	of 21
	Drawn By: Timothy Cole King		Drawing Number 3(a)	

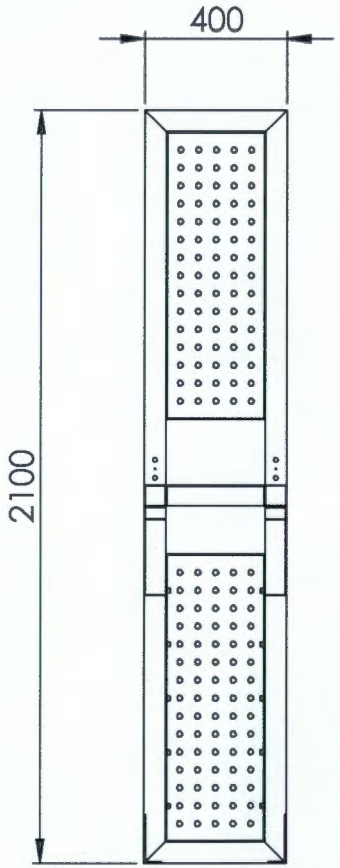

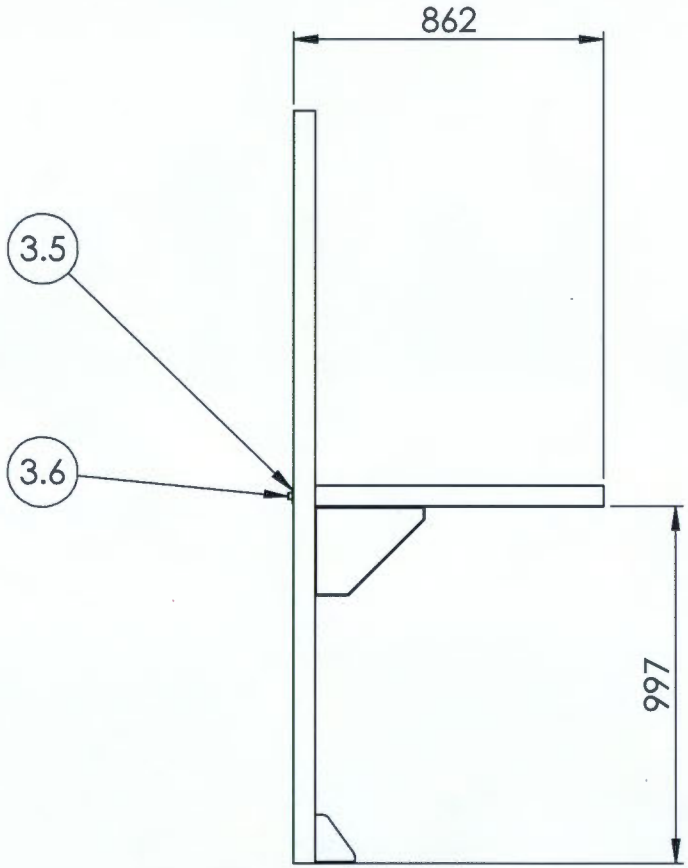

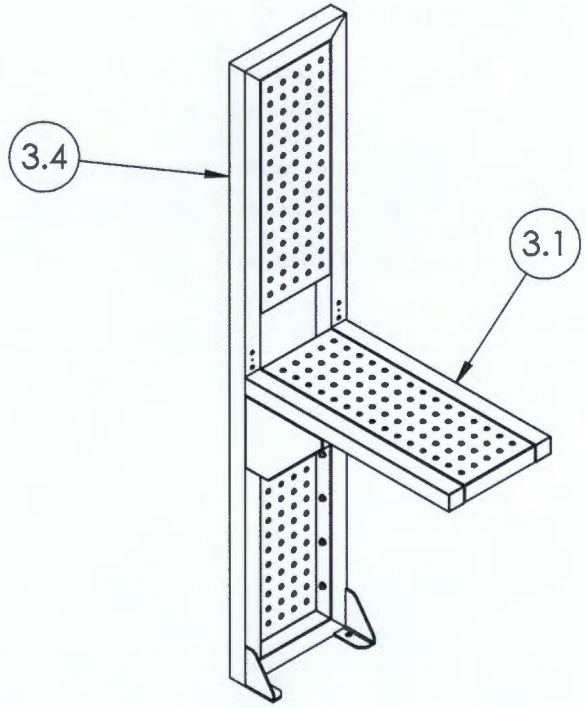

Isometric view

ITEM NO.	PART NUMBER	QTY.	Material
3.1	Shelf	1	
3.2	Shelf to frame support left	1	
3.3	Shelf to frame support right	1	
3.4	Frame verticle Asssembly	1	
3.5	B18.22M - Plain washer, 12 mm, wide	2	
3.6	B18.3.1M - 8 x 1.25 x 16 Hex SHCS -- 16NHX	12	
3.7	B18.22M - Plain washer, 8 mm, narrow	10	

A4 Landscape	University of Cape Town Department of Mechanical Engineering			
	Title: Pedestal_15_07_09			
Part Finish	Scale: 1:10	Date: 2015/07/09	sheet2	of 21
	Drawn By: Timothy Cole King		Drawing Number 3(b)	

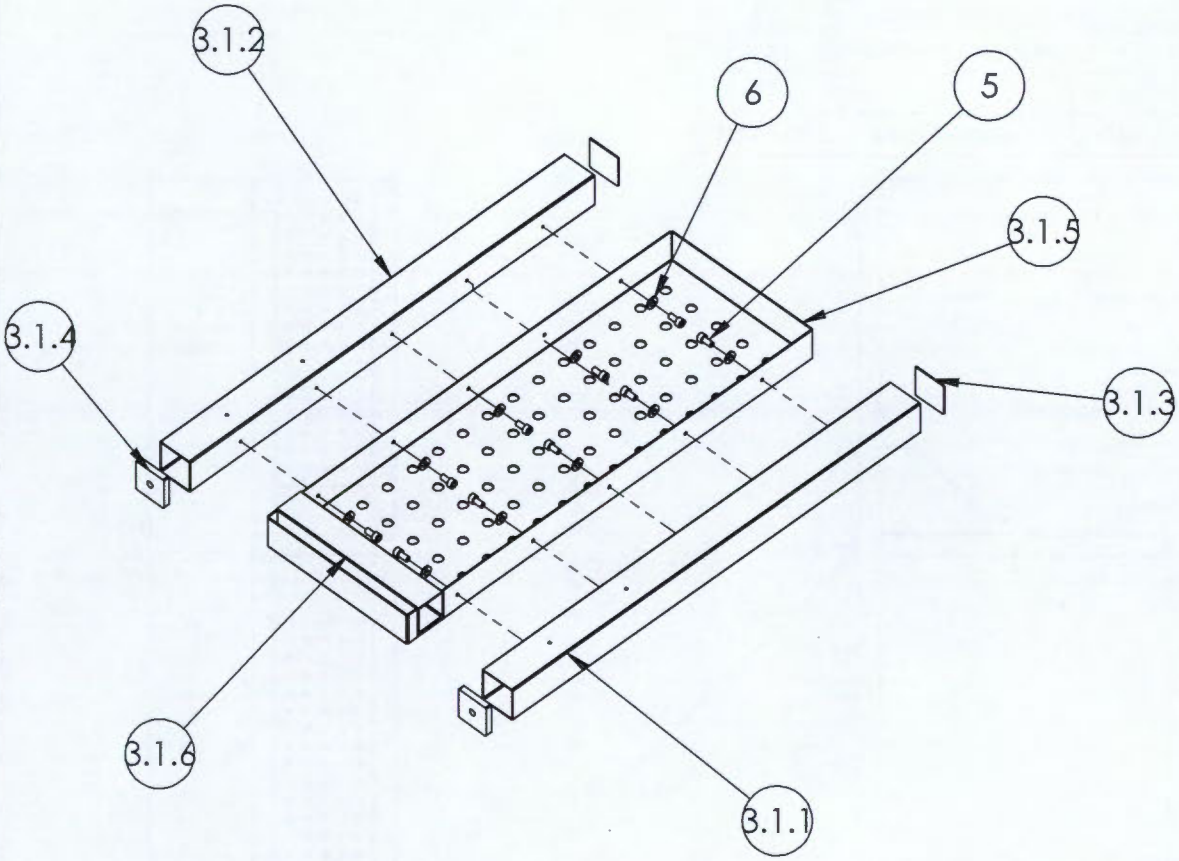

Exploded view of shelf

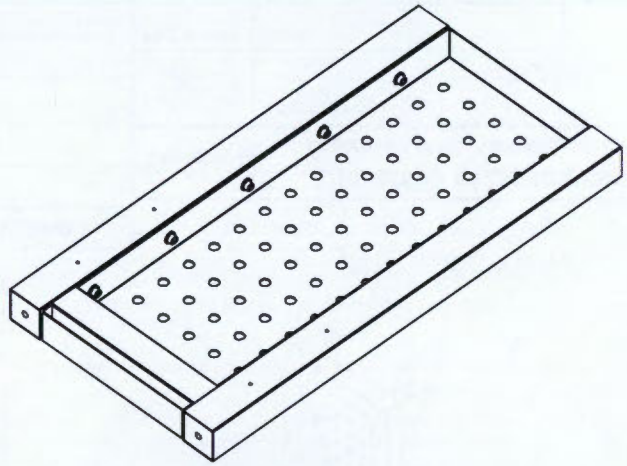

Isometric view
Welding and fastening assembly process

ITEM NO.	PART NUMBER	QTY.	Material
3.1.1	Shelf square tubing left	1	
3.1.2	Shelf square tubing right	1	
3.1.3	Shelf square tubing end cap	2	
3.1.4	Shelf square tubing threaded cap	2	
3.1.5	Shelf perforated plate OLD	1	
3.1.6	Spacing square tubing	1	
5	B18.3.1M - 8 x 1.25 x 16 Hex SHCS – 16NHX	10	
6	B18.22M - Plain washer, 8 mm, narrow	10	

A4 Landscape	University of Cape Town Department of Mechanical Engineering			
	Title: Shelf			
Part Finish	Scale: 1:10	Date: 2015/07/09	sheet3	of 21
	Drawn By: Timothy Cole King		Drawing Number 3.1(a)	

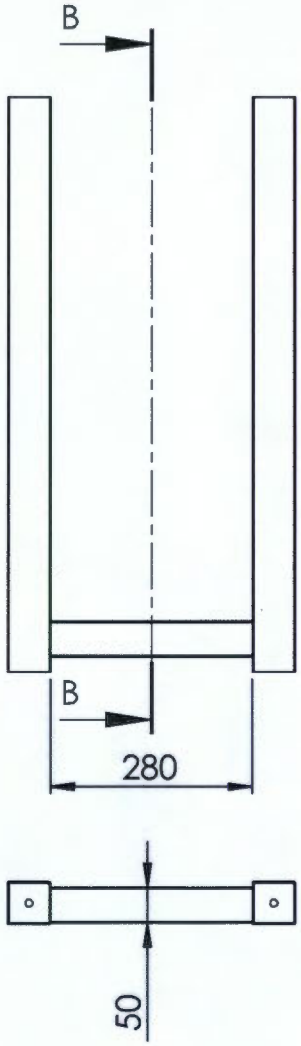

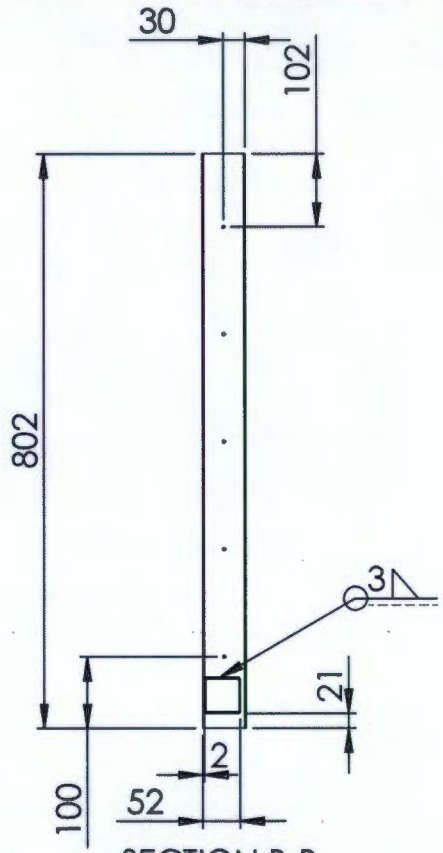

SECTION B-B
SCALE 1 : 10

A4 Landscape	University of Cape Town Department of Mechanical Engineering			
	Title: Shelf frame assembly			
QTY 1	Scale: 1:20	Date: 2015/07/09	sheet4	of 21
Material: LC_Steel	Drawn By: Timothy Cole King		Drawing Number 3.1_Frame	

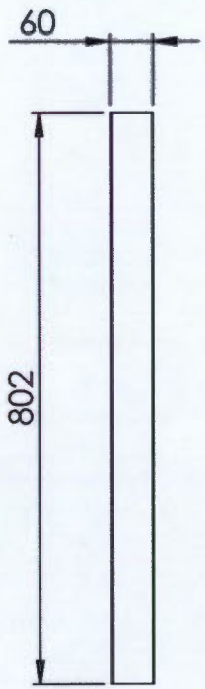

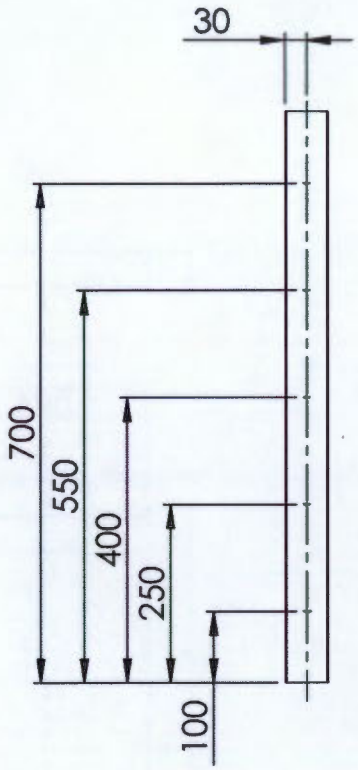

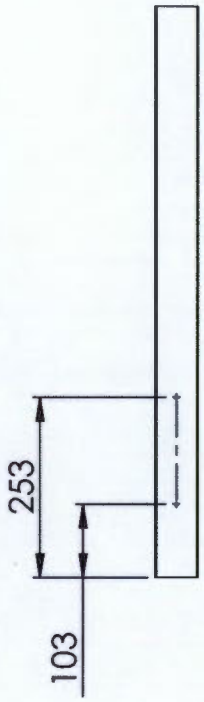

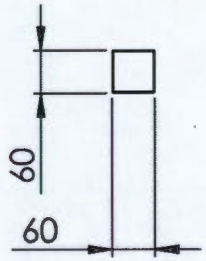

A4 Landscape	University of Cape Town Department of Mechanical Engineering			
	Title: shelf square tubing left			
QTY 1	Scale: 1:20	Date: 2015/07/09	sheet5	of 21
Material: LC_Steel	Drawn By: Timothy Cole King		Drawing Number 3.1.1	

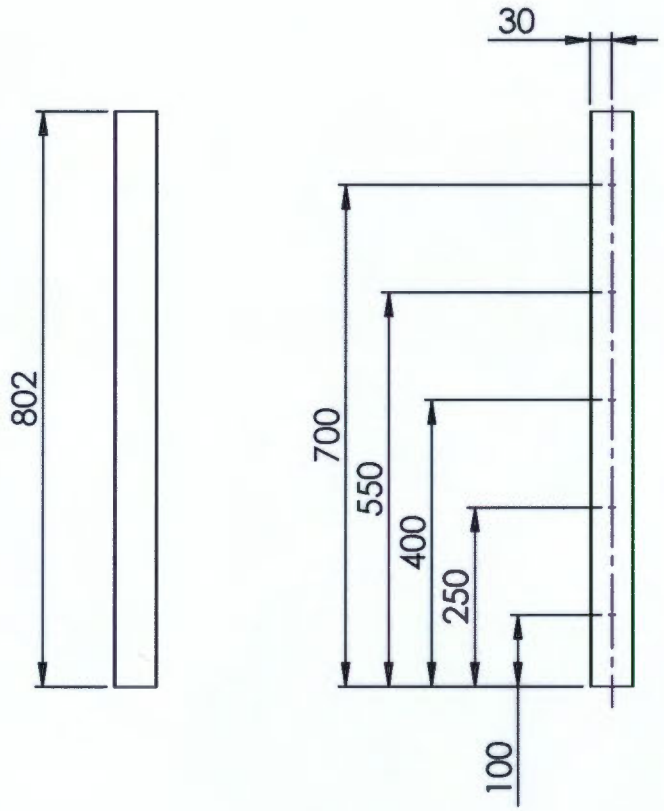

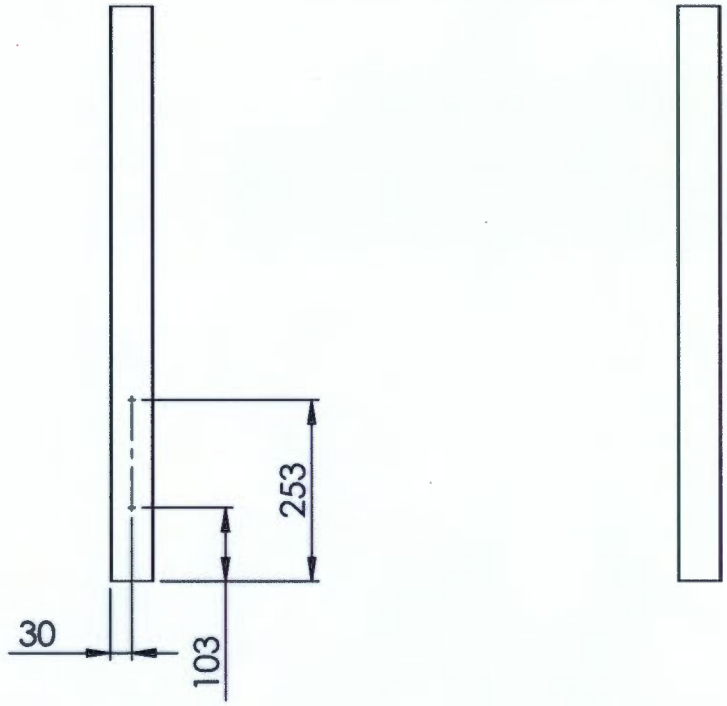

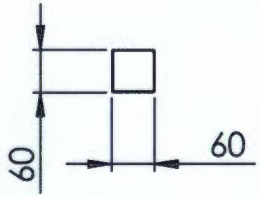

A4 Landscape	University of Cape Town Department of Mechanical Engineering			
	Title: Shelf square tubing right			
QTY 1	Scale: 1:20	Date: 2015/07/09	sheet6	of 21
Material: LC_Steel	Drawn By: Timothy Cole King		Drawing Number 3.1.2	

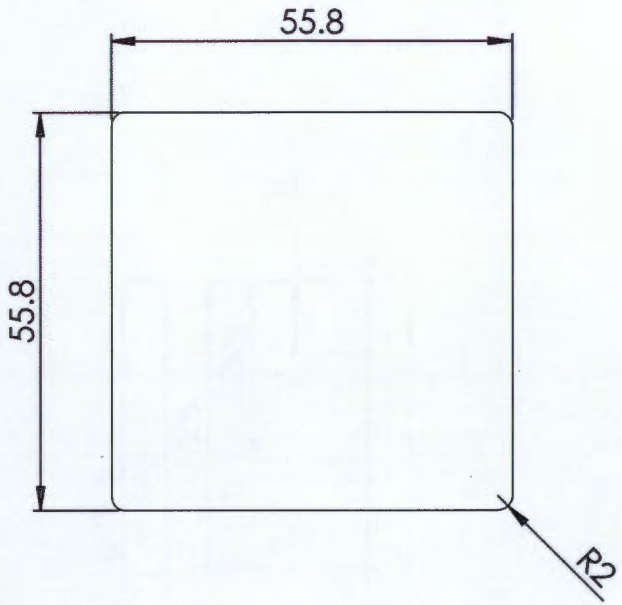

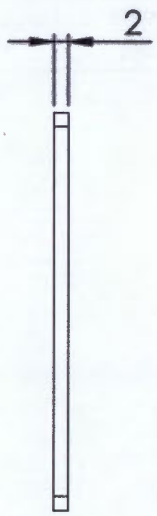

A4 Landscape	University of Cape Town Department of Mechanical Engineering			
	Title: Shelf square tubing end cap			
QTY 2	Scale: 1:20	Date: 2015/07/09	sheet7	of 21
Material: LC_Steel	Drawn By: Timothy Cole King		Drawing Number 3.1.3	

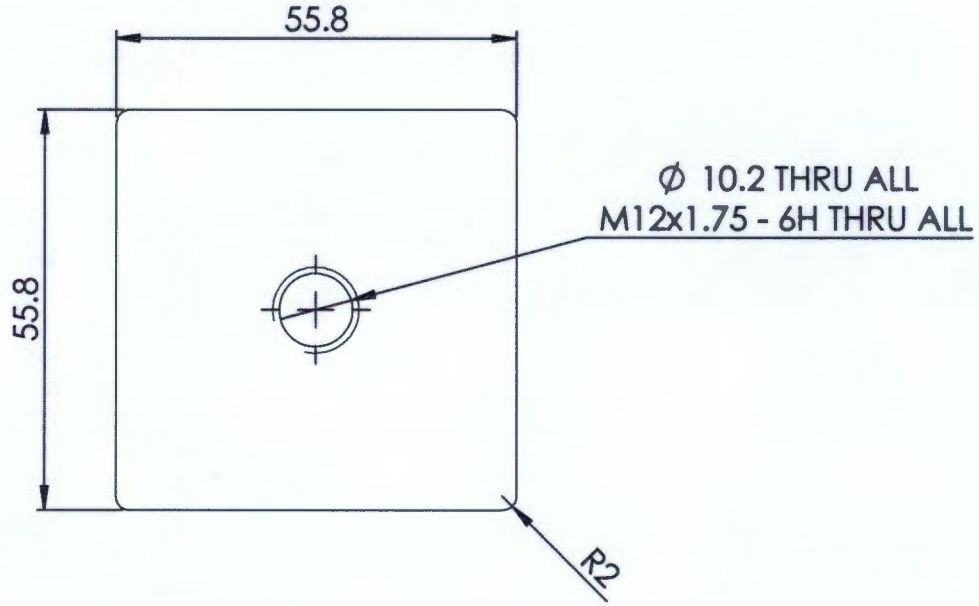

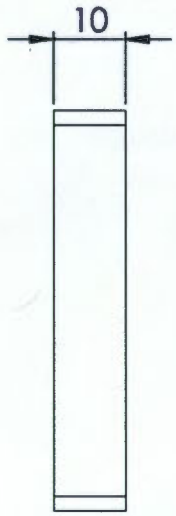

A4 Landscape	University of Cape Town Department of Mechanical Engineering			
	Title: Shelf square tubing threaded cap			
QTY 2	Scale: 1:20	Date: 2015/07/09	sheet8	of 21
Material: LC_Steel	Drawn By: Timothy Cole King		Drawing Number 3.1.4	

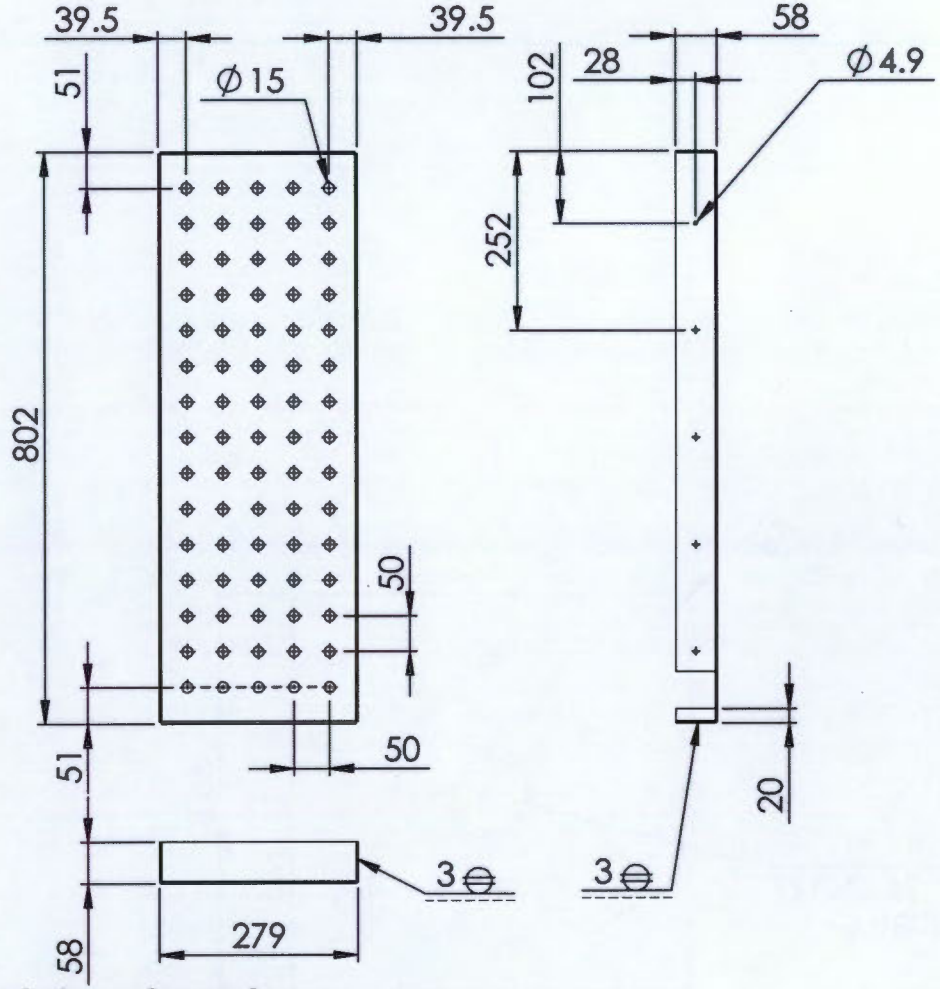

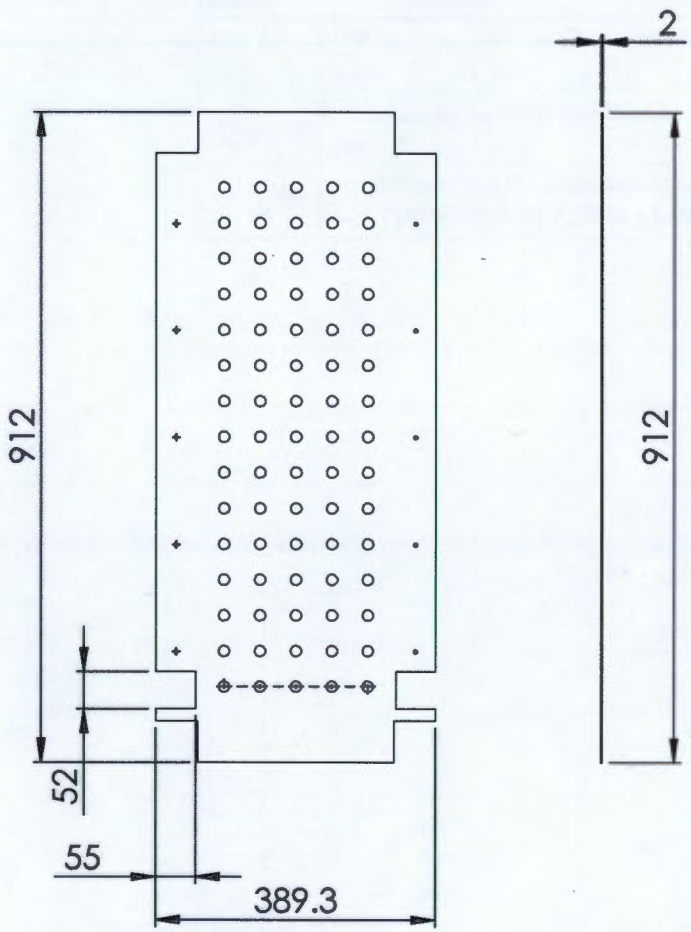

Flat pattern

Bent view of panel:
These dimensions are critical.
All bends are 90° with 1mm bend radius.
All bent edges are to be neatly seam welded together and cleaned if necessary
Note: outside (top) surfaces must have a polished finish

A4 Landscape	University of Cape Town Department of Mechanical Engineering			
	Title: Shelf perferated plate OLD			
QTY 1	Scale: 1:10	Date: 2015/07/09	sheet9	of 21
Material: 304 SS	Drawn By: Timothy Cole King		Drawing Number 3.1.5	

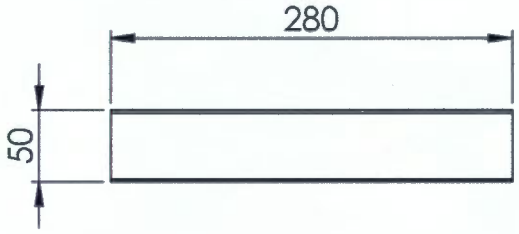

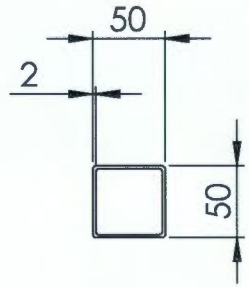

Square tubing: 50mm x 2mm profile

A4 Landscape	University of Cape Town Department of Mechanical Engineering			
	Title: Spacing square tubing			
QTY 2	Scale: 1:20	Date: 2015/07/09	sheet10	of 21
Material: LC_Steel	Drawn By: Timothy Cole King		Drawing Number 3.1.6	

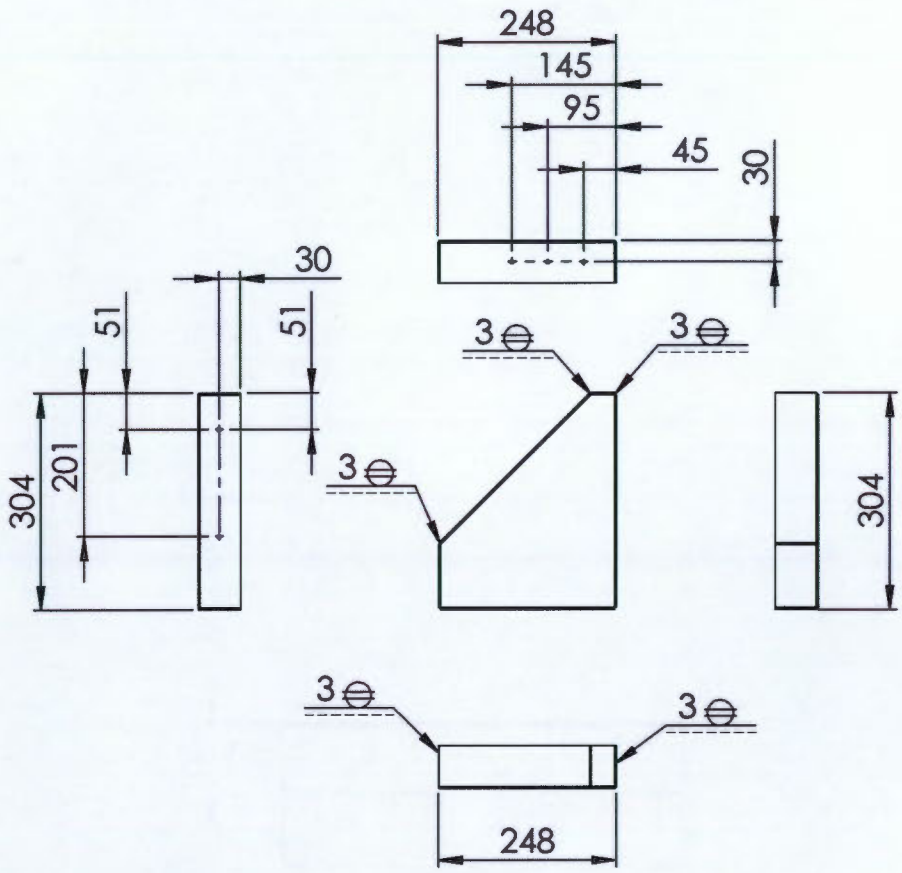

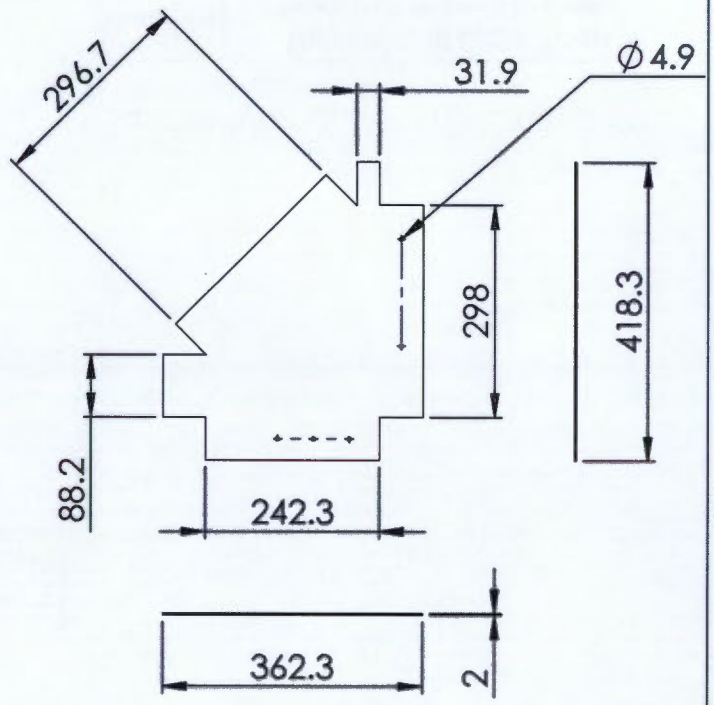

Flat pattern

Bent view of panel:
These dimensions are critical.
All bends are 90° with 1mm bend radius.
All bent edges are to be neatly seam welded together and cleaned if necessary.
All holes are Ø4.9
Note: outside (top) surfaces must have a polished finish

A4 Landscape	University of Cape Town Department of Mechanical Engineering			
	Title: Shelf to frame support left			
QTY 1	Scale: 1:10	Date: 2015/07/09	sheet11	of 21
Material: 304 SS	Drawn By: Timothy Cole King		Drawing Number 3.2	

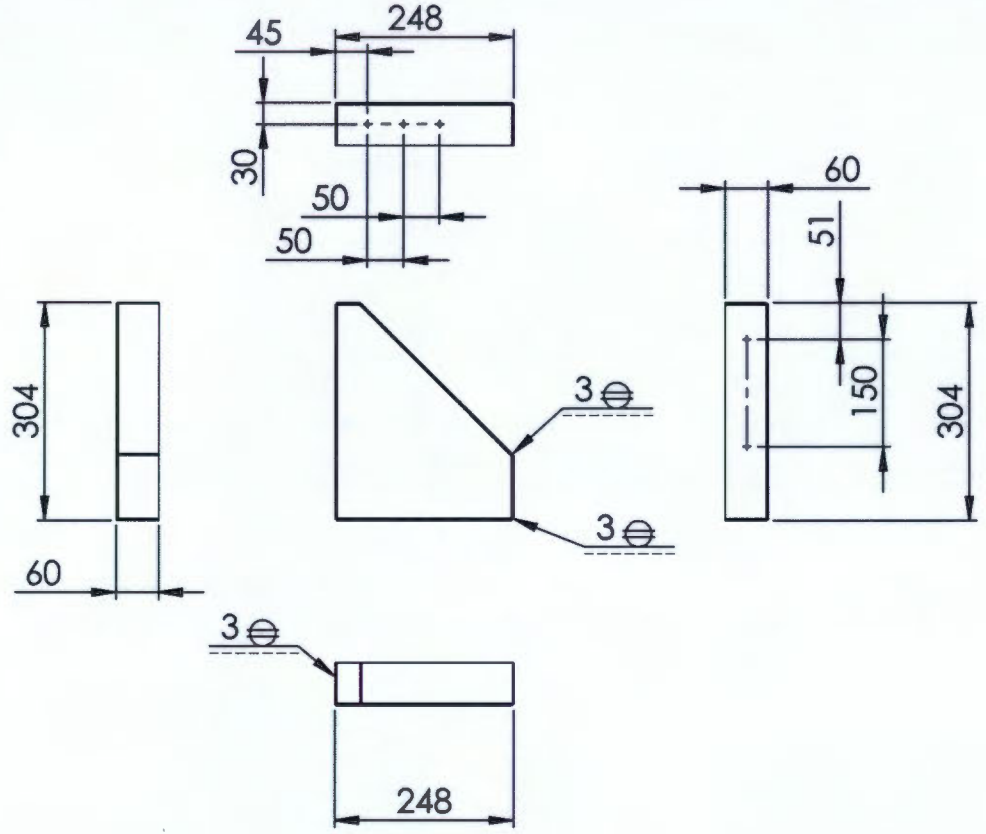

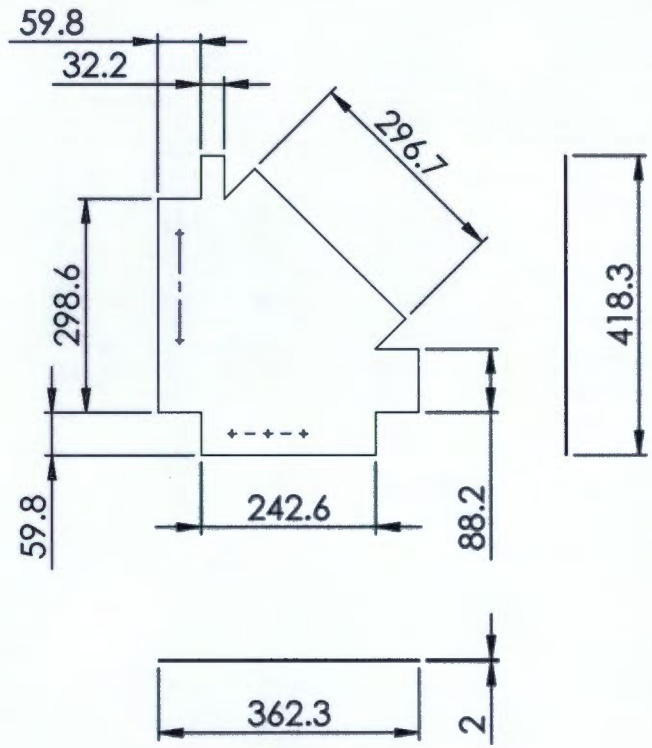

Flat pattern

Bent view of part:
These dimensions are critical.
All bends are 90° with 1mm bend radius.
All bent edges are to be neatly seam welded together and cleaned if necessary
All holes are ∅4.9
Note: outside (top) surfaces must have a polished finish

A4 Landscape	University of Cape Town Department of Mechanical Engineering			
	Title: Shelf to frame support right			
QTY 1	Scale: 1:10	Date: 2015/07/09	sheet12	of 21
Material: 304 SS	Drawn By: Timothy Cole King		Drawing Number 3.3	

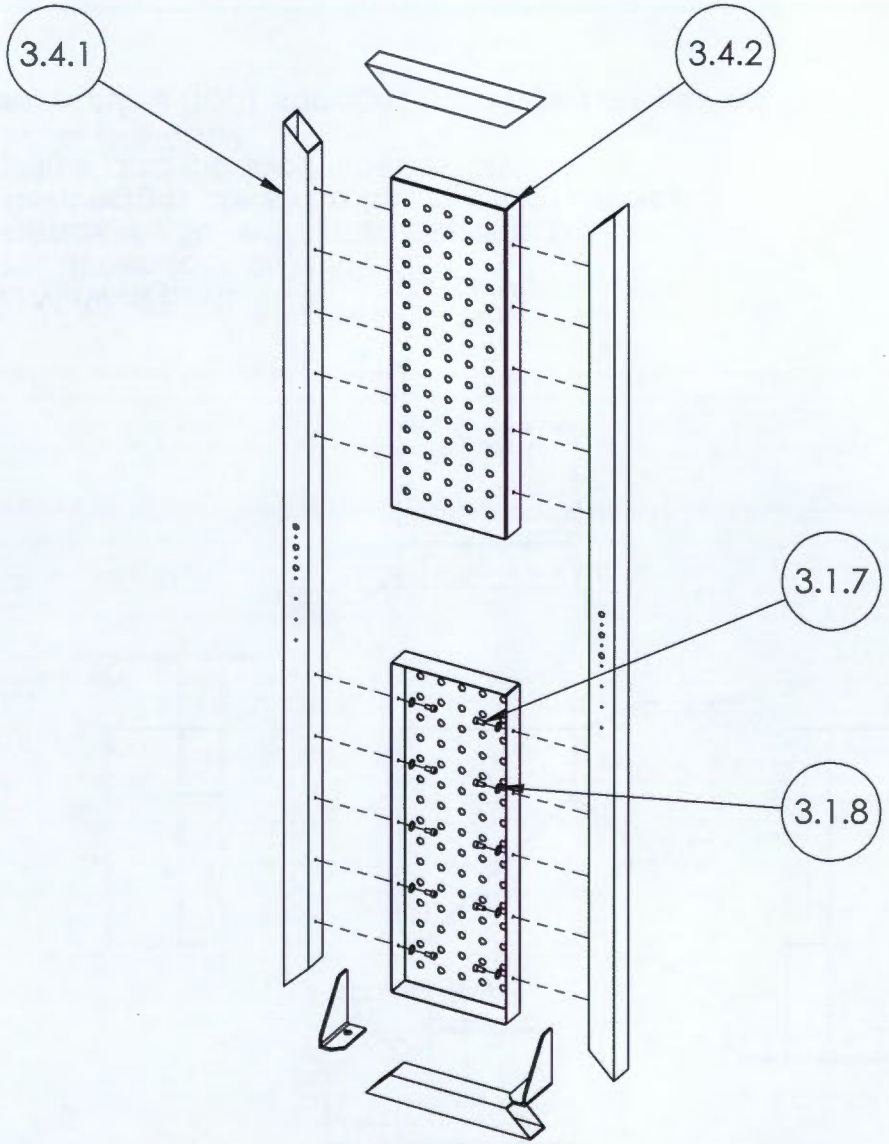

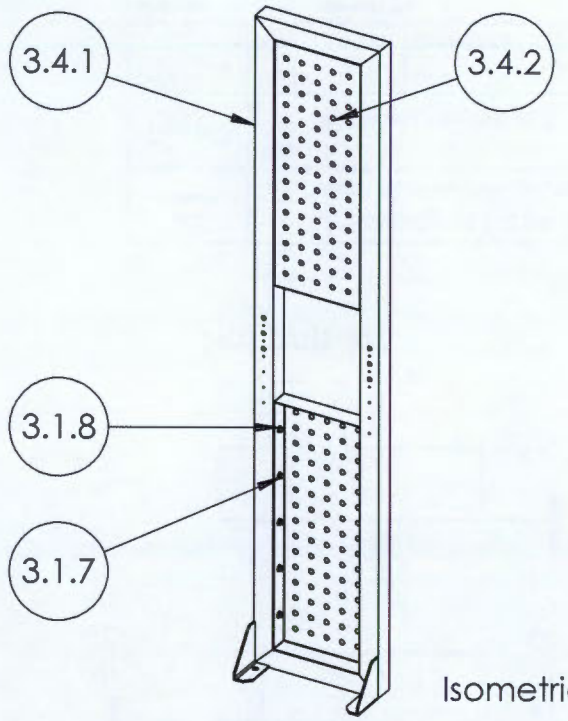

Isometric view

ITEM NO.	PART NUMBER	Explode/QTY.	Material
3.4.1	frame assembly	1	
3.4.2	Perferated panel	2	
3.1.7	B18.3.1M - 8 x 1.25 x 16 Hex SHCS – 16NHX	20	
3.1.8	B18.22M - Plain washer, 8 mm, narrow	19	

A4 Landscape	University of Cape Town Department of Mechanical Engineering			
	Title: Frame verticle			
Part Finish	Scale: 1:13	Date: 2015/07/09	sheet13	of 21
Material:	Drawn By: Timothy Cole King		Drawing Number 3.4(a)	

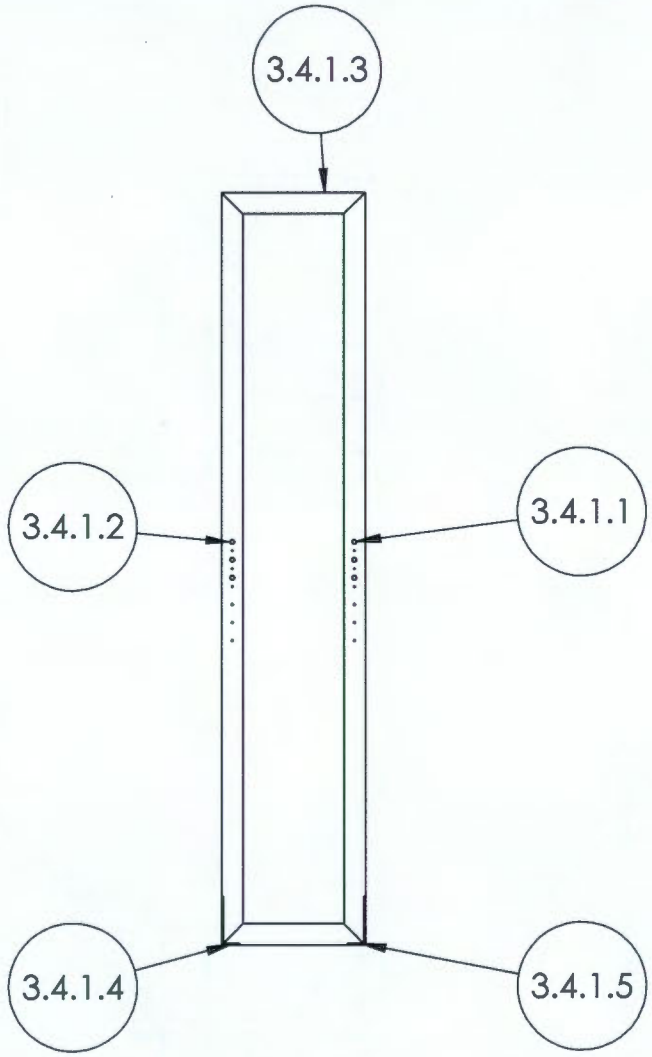

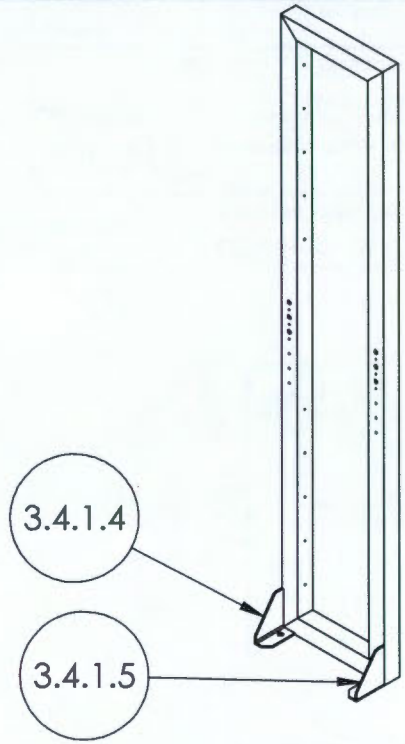

Isometric view

ITEM NO.	PART NUMBER	QTY.	Material
3.4.1.1	2. Frame verticle square tubing right	1	
3.4.1.2	1. Frame verticle square tubing left	1	
3.4.1.3	3 Frame top and bottom slat	2	
3.4.1.4	Frame mounting foot assembly left	1	
3.4.1.5	Frame mounting foot assembly right	1	

A4 Landscape	University of Cape Town Department of Mechanical Engineering			
	Title: Square tube frame_BOM			
QTY 1	Scale: 1:20	Date: 2015/07/09		of 21
Material:	Drawn By: Timothy Cole King		Drawing Number 3.4.1(a)	

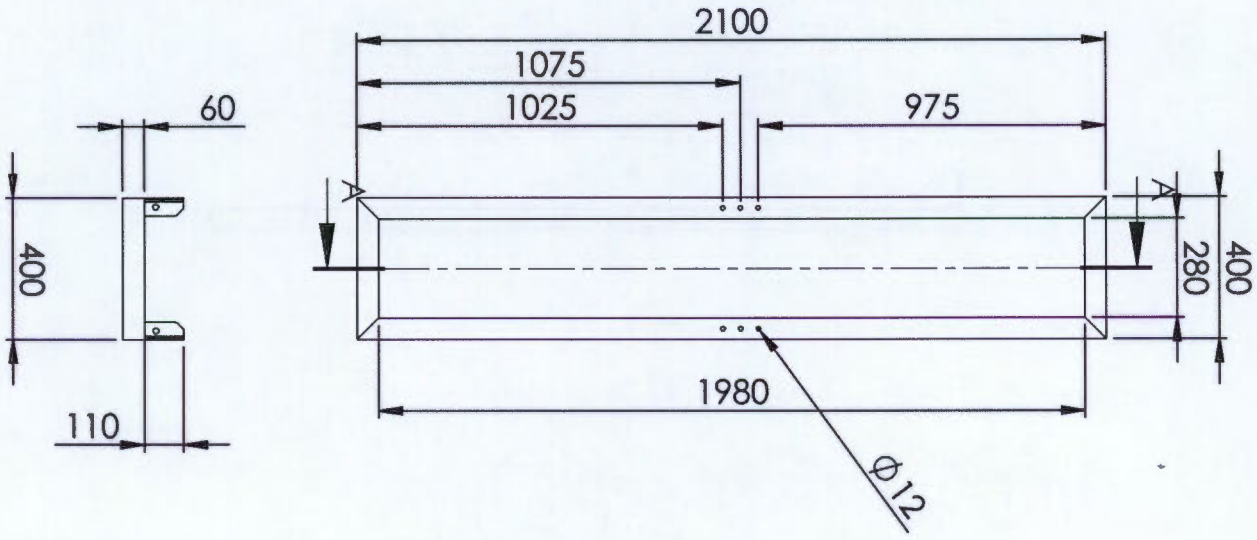

SECTION A-A

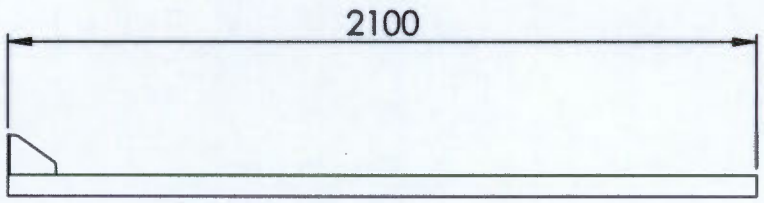

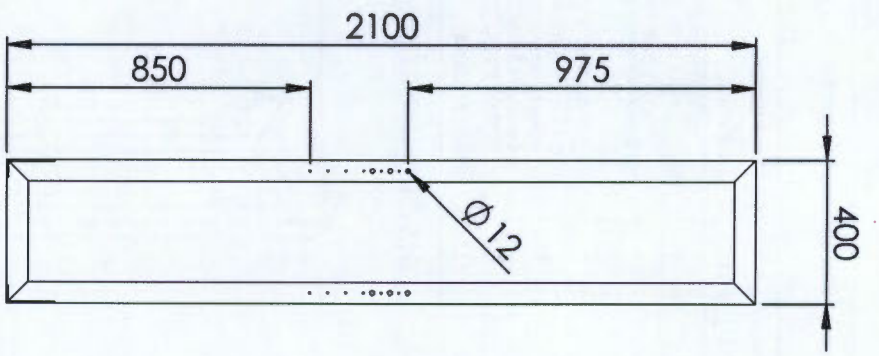

A4 Landscape	University of Cape Town Department of Mechanical Engineering		
QTY: 1	Title: Square tube frame_Assembly		
Material: 304 SS	Scale: 1:20	Date: 2015/07/09	
Drawn By: Timothy Cole King	Drawing Number 3.4.1 (b)	sheet 15	of 21

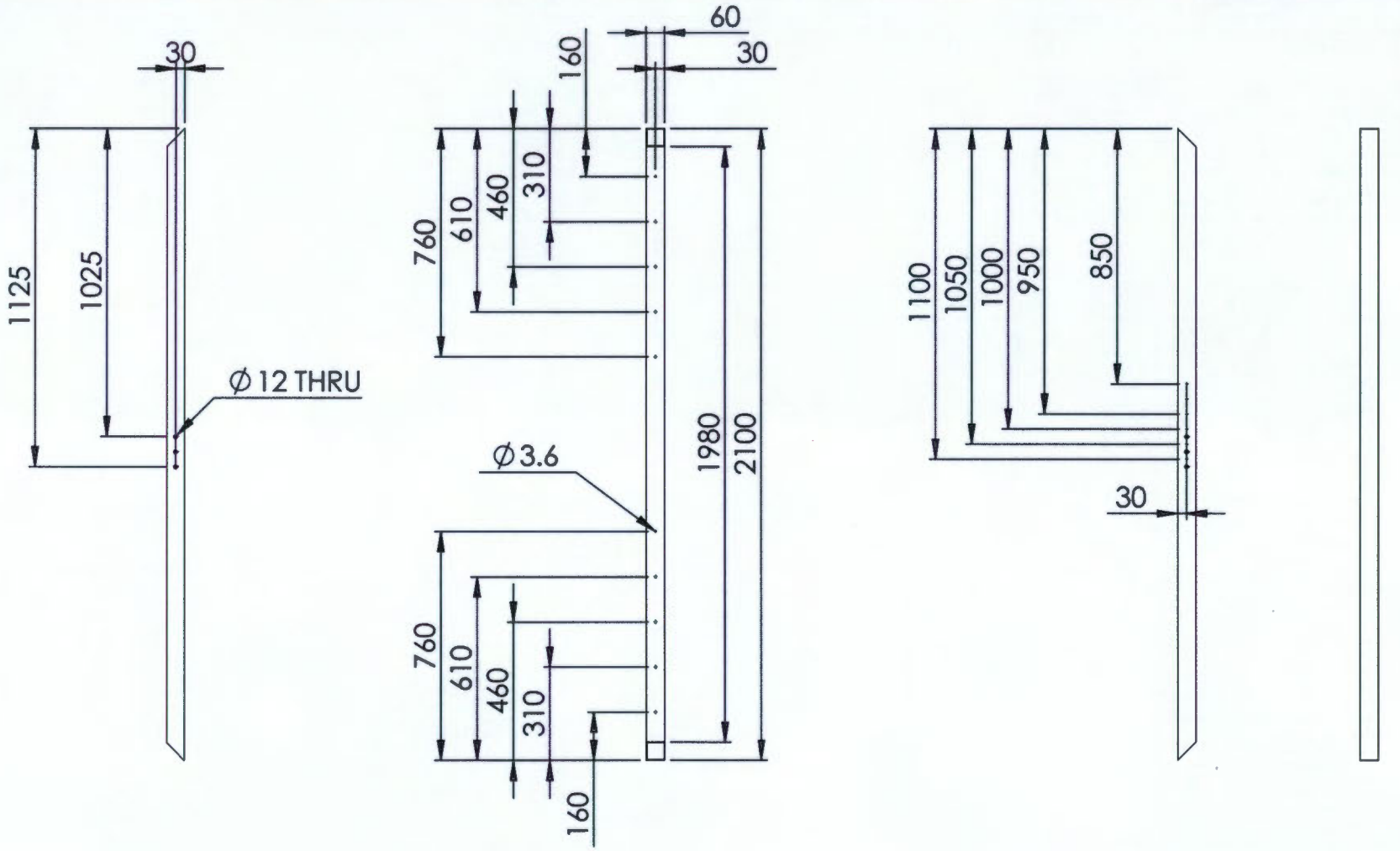

A4 Landscape	University of Cape Town Department of Mechanical Engineering			
	Title: 2. Frame verticle square tubing right			
QTY 1	Scale: 1:20	Date: 2015/07/09	sheet16	of 21
Material: LC_Steel	Drawn By: Timothy Cole King		Drawing Number 3.4.1.1	

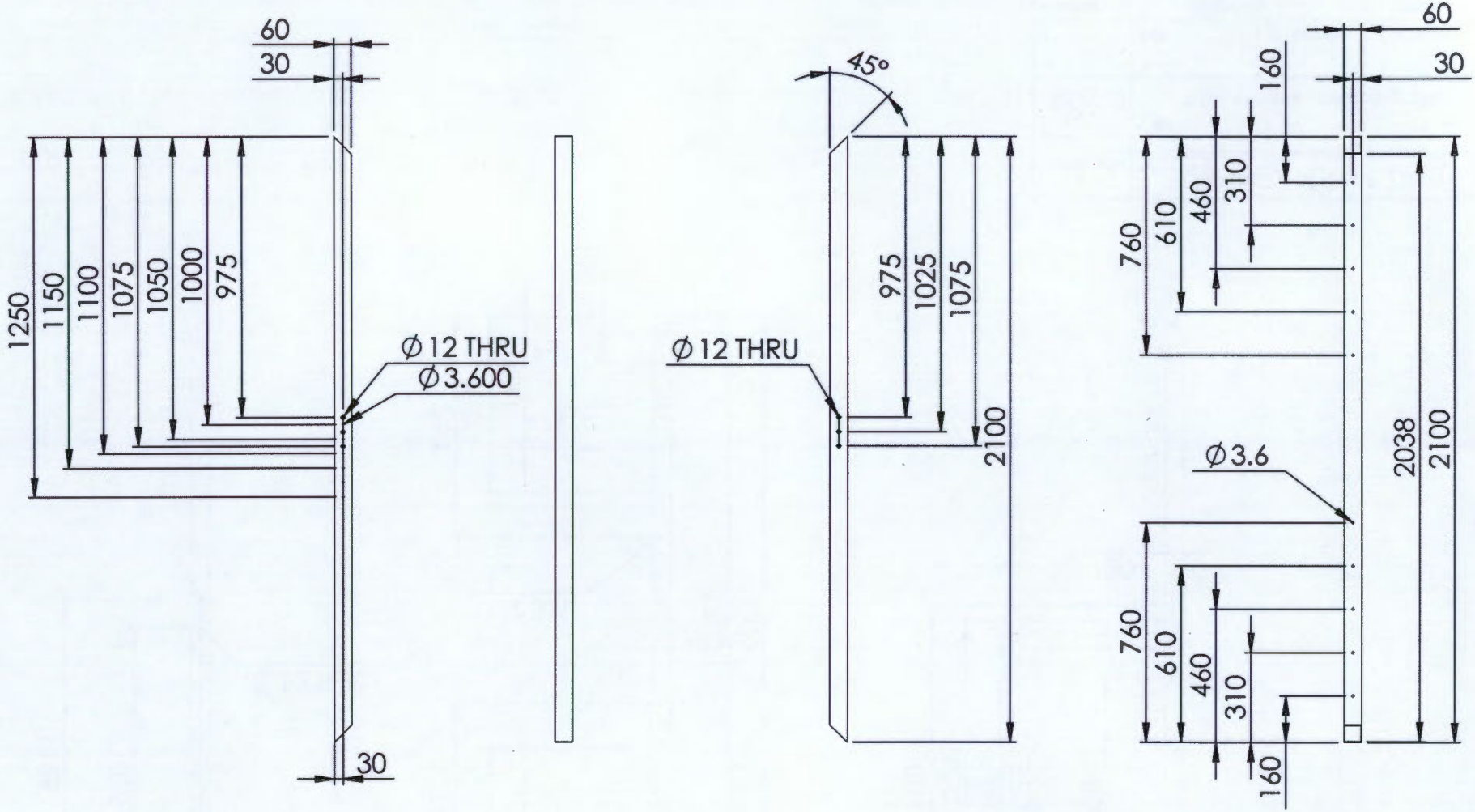

A4 Landscape	University of Cape Town Department of Mechanical Engineering			
	Title: 1. Frame verticle square tubing left			
QTY 1	Scale: 1:20	Date: 2015/07/09	sheet17	of 21
Material: LC_Steel	Drawn By: Timothy Cole King		Drawing Number 3.4.1.2	

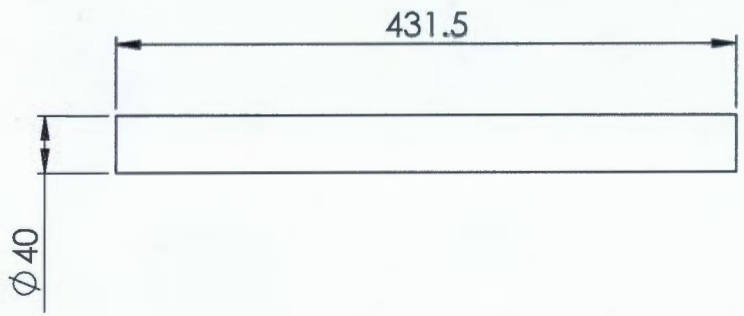

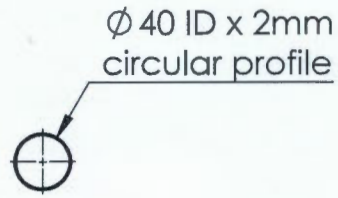

A4 Landscape	University of Cape Town Department of Mechanical Engineering			
	Title: Oil filling pipe			
QTY 1	Scale: 1:5	Date: 2015/07/10	Sheet14	of 14
Material: 304 SS	Drawn By: Timothy Cole King		Drawing Number 7.7.4	

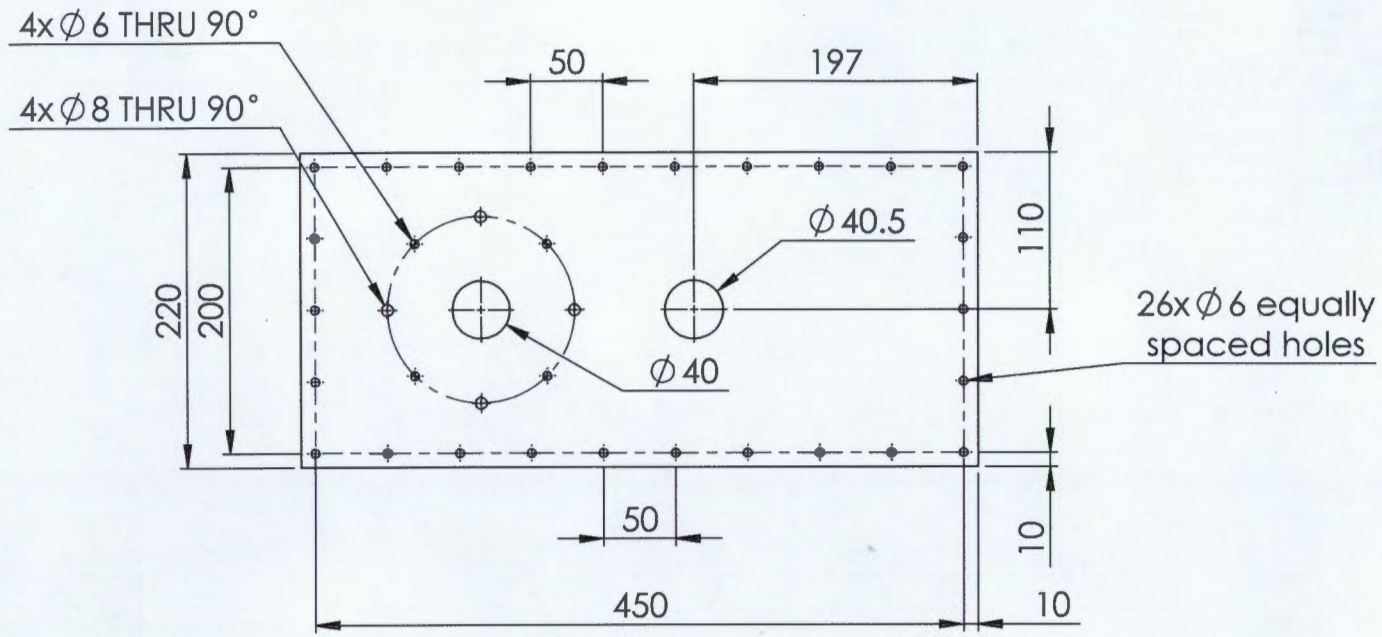

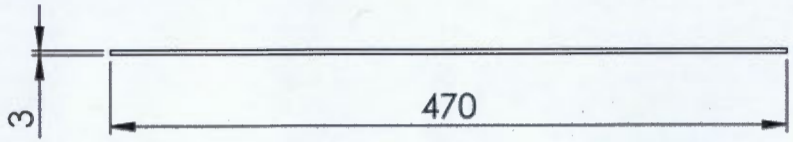

Part no. 7.7.3 to be laser-cut from 3mm 304_SS plate.

A4 Landscape	University of Cape Town Department of Mechanical Engineering			
	Title: oil sump lid new			
QTY 1	Scale:	Date: 2015/07/10	Sheet13	of 14
Material: 304 SS	Drawn By: Timothy Cole King		Drawing Number 7.7.3	

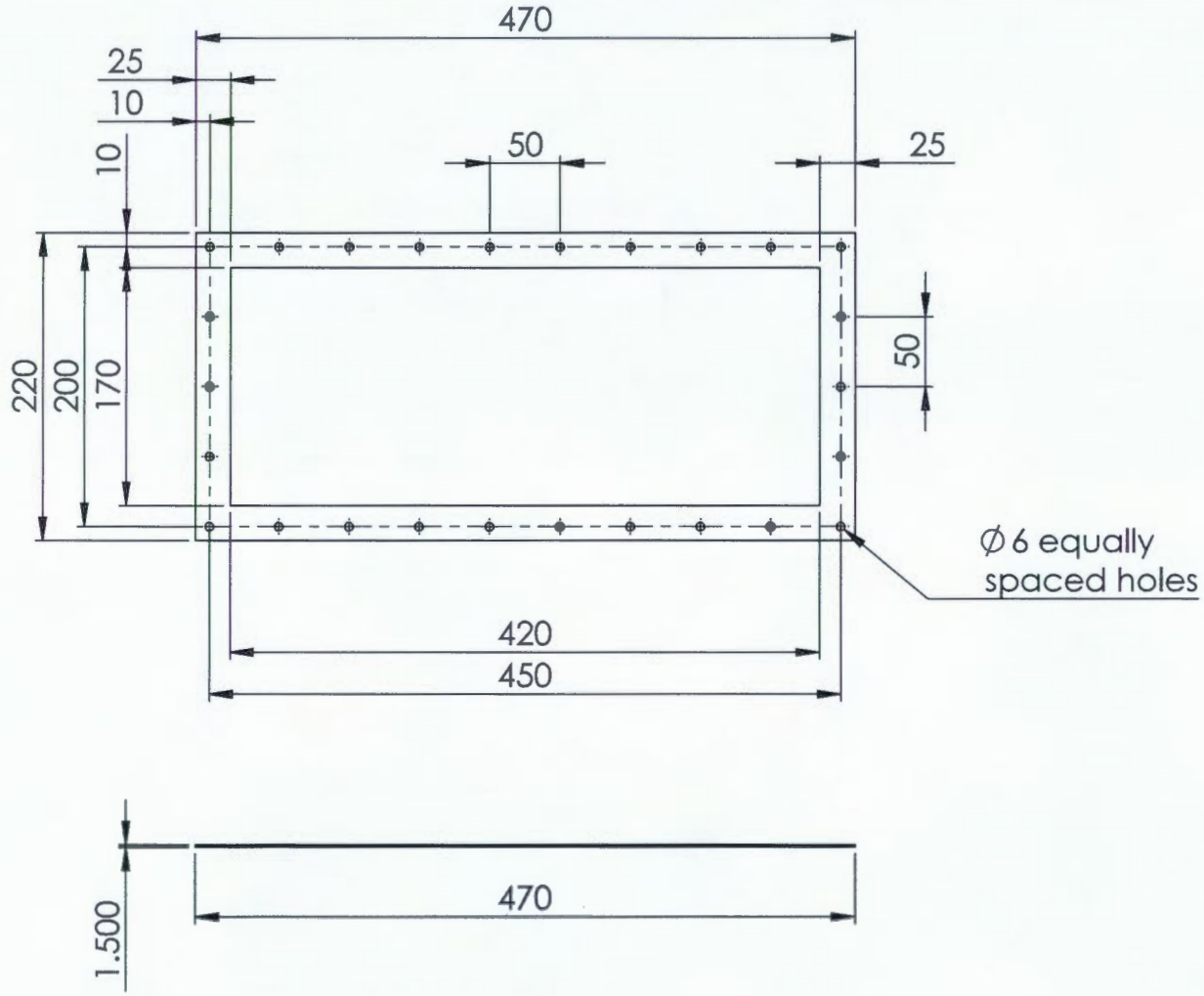

A4 Landscape	University of Cape Town Department of Mechanical Engineering			
	Title: oil sump gaskit new			
QTY 1	Scale:	Date: 2015/07/10	Sheet12	of 14
Material: NBR	Drawn By: Timothy Cole King		Drawing Number 7.7.2	

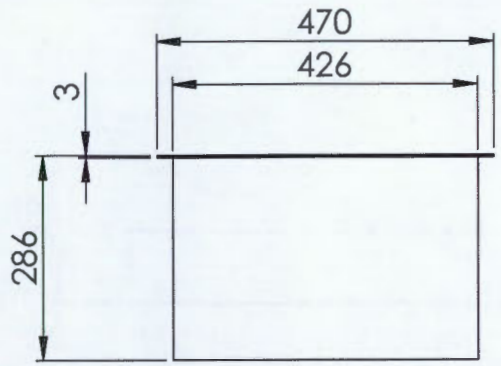

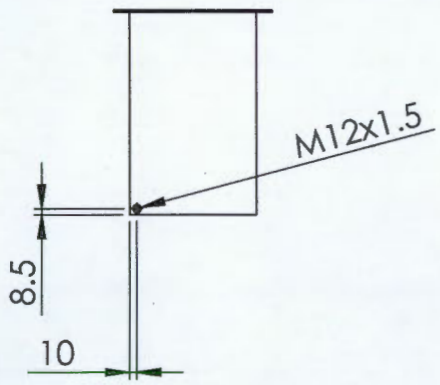

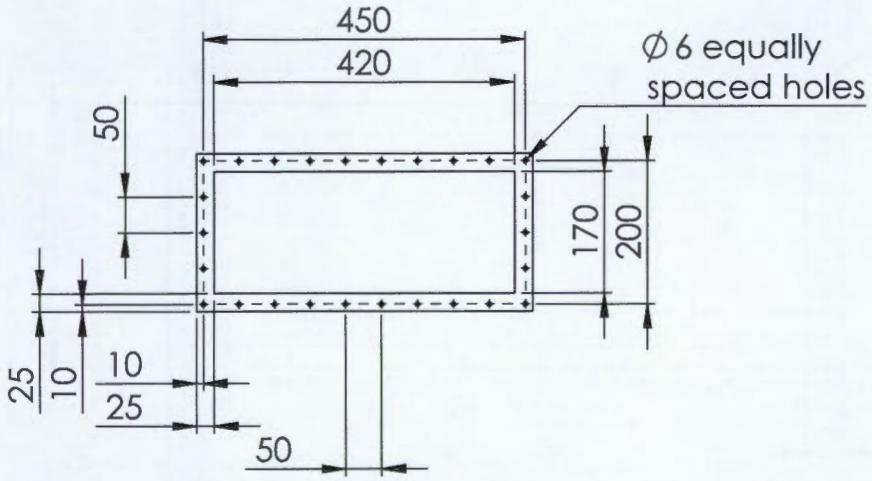

Part no, 7.7.1 to be constructed from 3mm Al plate and TIG welded together

A4 Landscape	University of Cape Town Department of Mechanical Engineering			
	Title: Oil sump box new			
QTY 1	Scale:	Date: 2015/07/10	Sheet11	of 14
Material: Al	Drawn By: Timothy Cole King		Drawing Number 7.7.1	

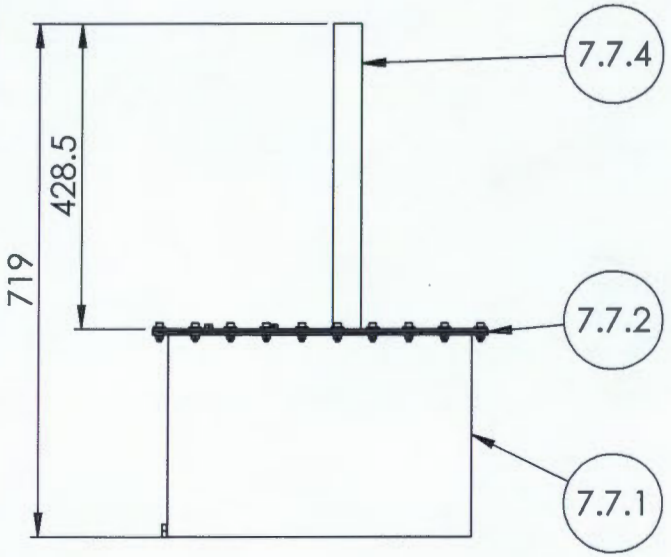

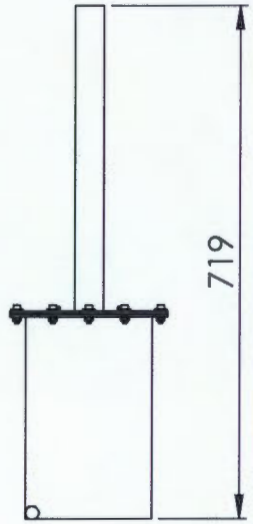

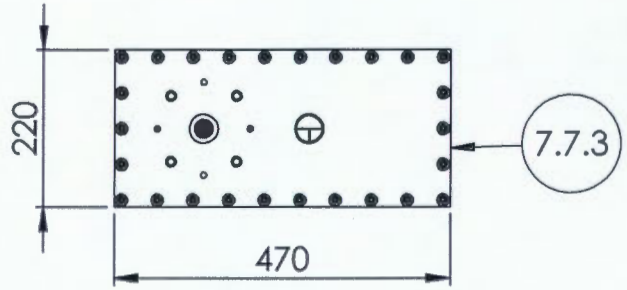

ITEM NO.	PART NUMBER	QTY.	Material
7.7.1	Oil sump box new	1	Al
7.7.2	oil sump gaskit new	1	NBR
7.7.3	oil sump lid new	1	304_SS
7.7.4	Oil filling pipe	1	SS_304
7.7.5	bellhousing new	1	
7.7.6	Vivolo Oil pump internal drainage new	1	
7.7.7	pressure relief valve new	1	
7.7.8	Piping_sump	1	304_SS
7.7.9	ISO 4017 - M12 x 25-N	1	
7.7.10	DIN 6340-6.4	26	
7.7.11	DIN 912 M6 x 20 — 20N	26	
7.7.12	Hexagon Flange Nut DIN 6923 - M6 - N	30	
7.7.13	DIN 6921 - M6 x 25 x 25-N	4	

A4 Landscape	University of Cape Town Department of Mechanical Engineering			
	Title: Oil sump_Assembly			
Assembly Drawing	Scale:	Date: 2015/07/10	Sheet10	of
	Drawn By: Timothy Cole King		Drawing Number 7.7(a)	

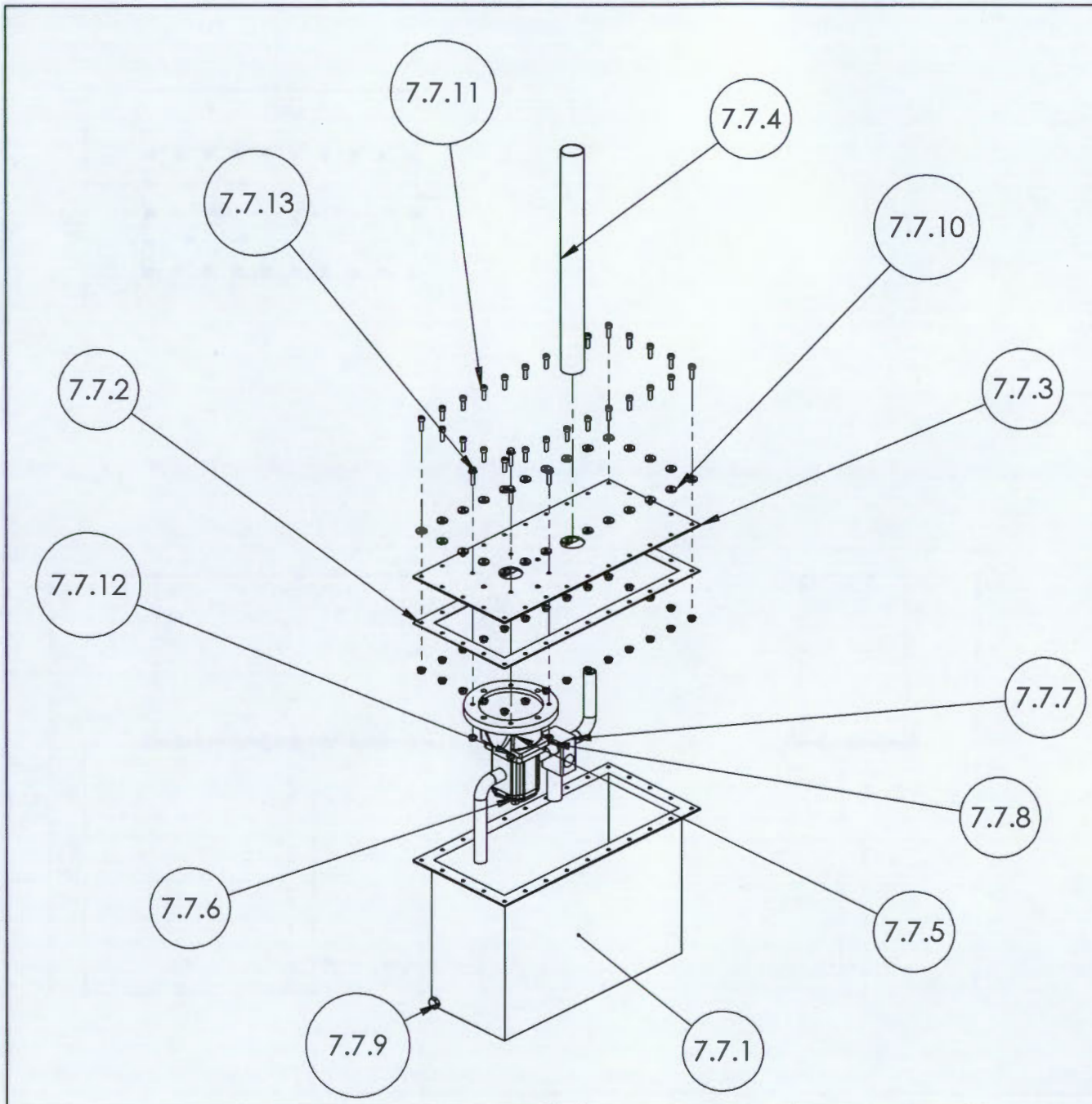

ITEM NO.	PART NUMBER	QTY.	Material
7.7.1	Oil sump box new	1	Al
7.7.2	oil sump gaskit new	1	NBR
7.7.3	oil sump lid new	1	304_SS
7.7.4	Oil filling pipe	1	SS_304
7.7.5	bellhousing new	1	
7.7.6	Vivolo Oil pump internal drainage new	1	
7.7.7	pressure relief valve new	1	
7.7.8	Piping_sump	1	304_SS
7.7.9	ISO 4017 - M12 x 25-N	1	
7.7.10	DIN 6340-6.4	26	
7.7.11	DIN 912 M6 x 20 — 20N	26	
7.7.12	Hexagon Flange Nut DIN 6923 - M6 - N	30	
7.7.13	DIN 6921 - M6 x 25 x 25-N	4	

A4 Landscape	University of Cape Town Department of Mechanical Engineering			
	Title: Oil sump_BOM			
Assembly Drawing	Scale: 1:10	Date: 2015/07/10		of
	Drawn By: Timothy Cole King		Drawing Number 7.7(a)	

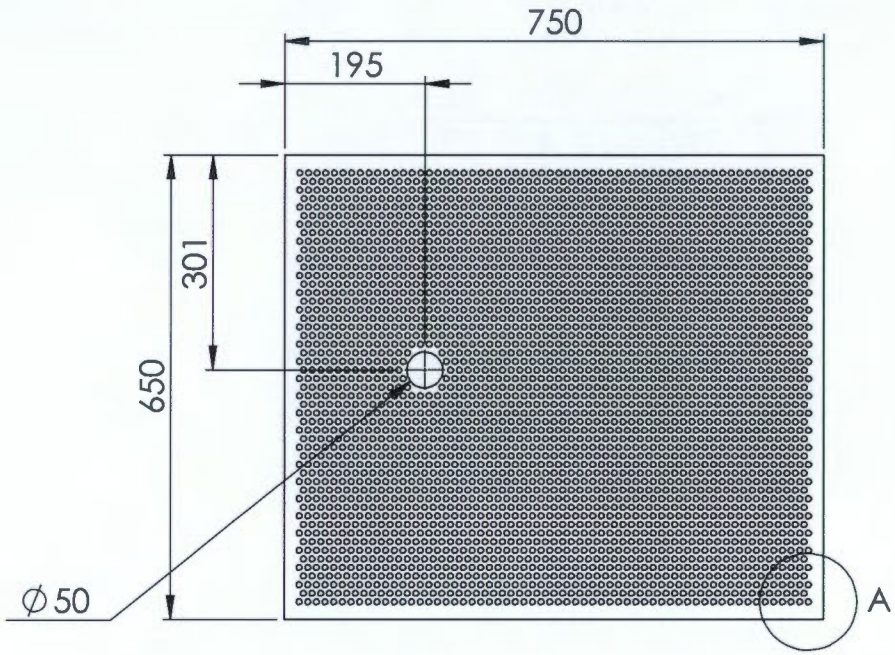

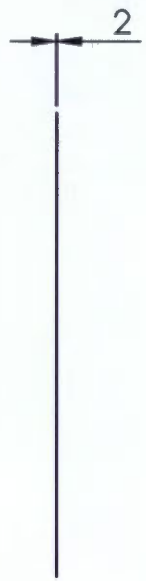

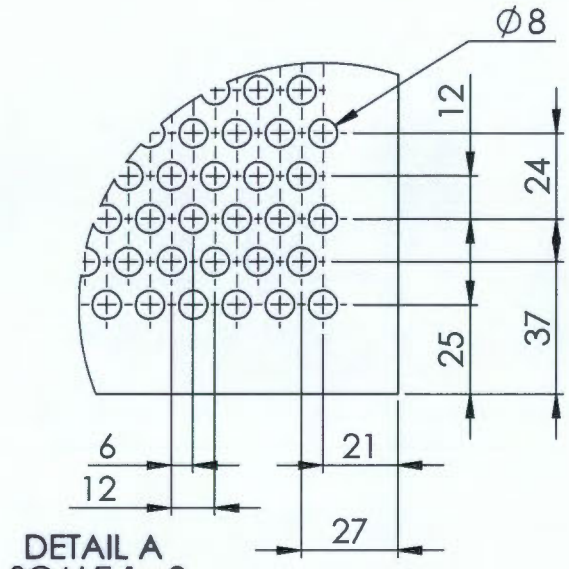

DETAIL A
SCALE 1 : 2

Holes to be punched

A4 Landscape	University of Cape Town Department of Mechanical Engineering			
	Title: Top perforated plate			
QTY 1	Scale: 1:5	Date: 2015/07/10	Sheet8	of 14
Material: LC_Steel	Drawn By: Timothy Cole King		Drawing Number 7.6	

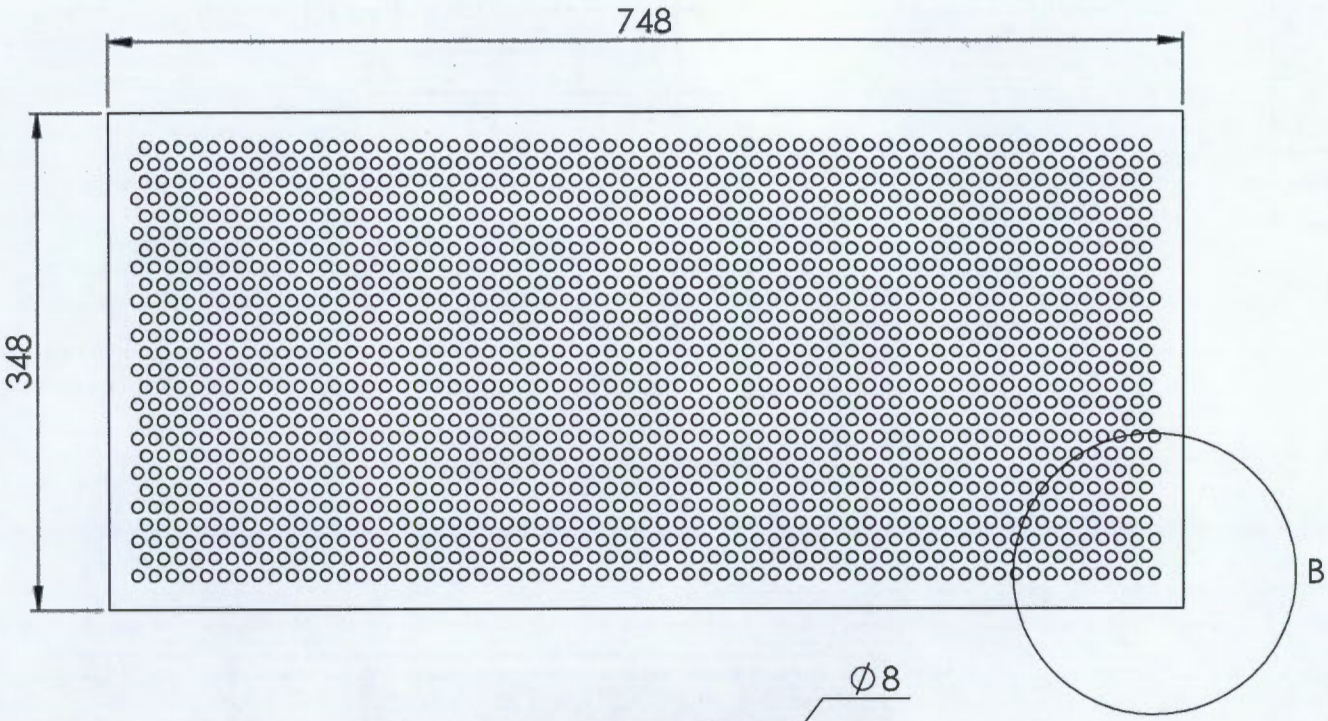

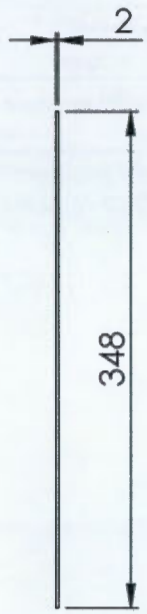

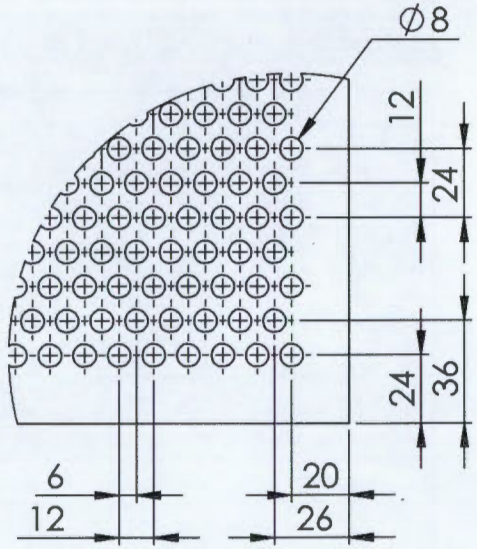

DETAIL B
SCALE 2 : 5

Holes to be punched

A4 Landscape	University of Cape Town Department of Mechanical Engineering			
	Title: Side perforated plate			
QTY 1	Scale:	Date: 2015/07/10	Sheet7	of 14
Material: LC_Steel	Drawn By: Timothy Cole King		Drawing Number 7.5	

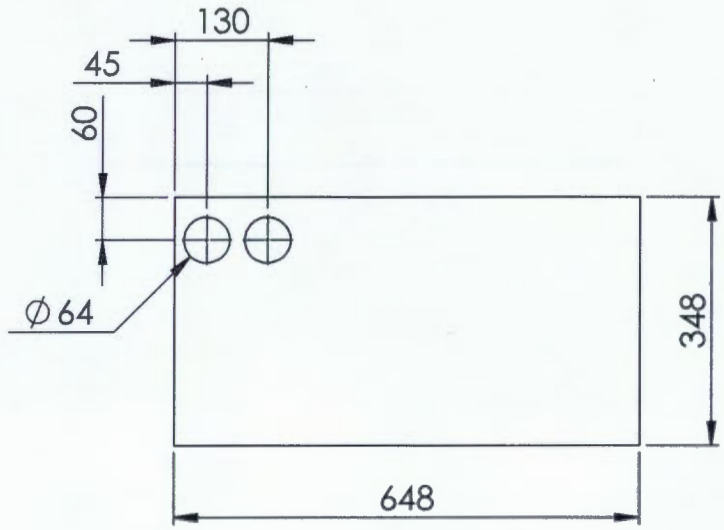

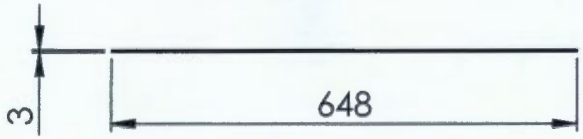

Part no. 7.4 to be welded to part no. 7.1.

A4 Landscape	University of Cape Town Department of Mechanical Engineering			
	Title: Front panel			
QTY 1	Scale:	Date: 2015/07/10	Sheet6	of 14
Material: 304 SS	Drawn By: Timothy Cole King		Drawing Number 7.4	

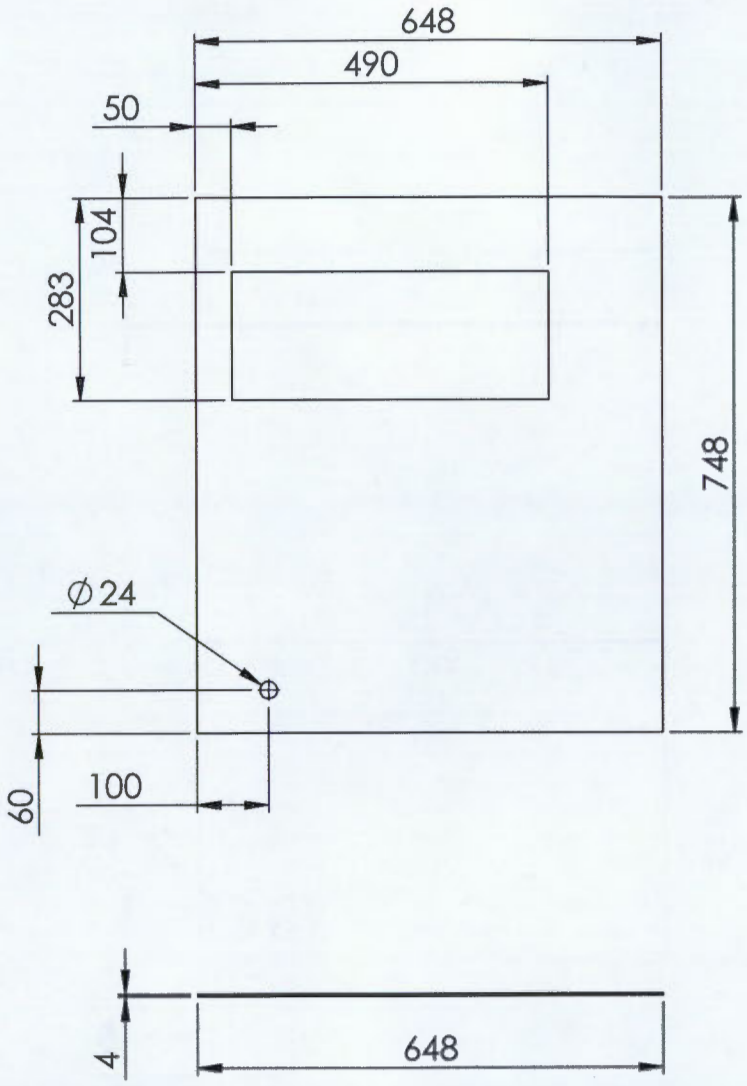

Part no. 7.3 to be welded to part no. 7.1.

A4 Landscape	University of Cape Town Department of Mechanical Engineering			
	Title: Bottom panel			
QTY 1	Scale:	Date: 2015/07/10	Sheet5	of 14
Material: 304 SS	Drawn By: Timothy Cole King		Drawing Number 7.3	

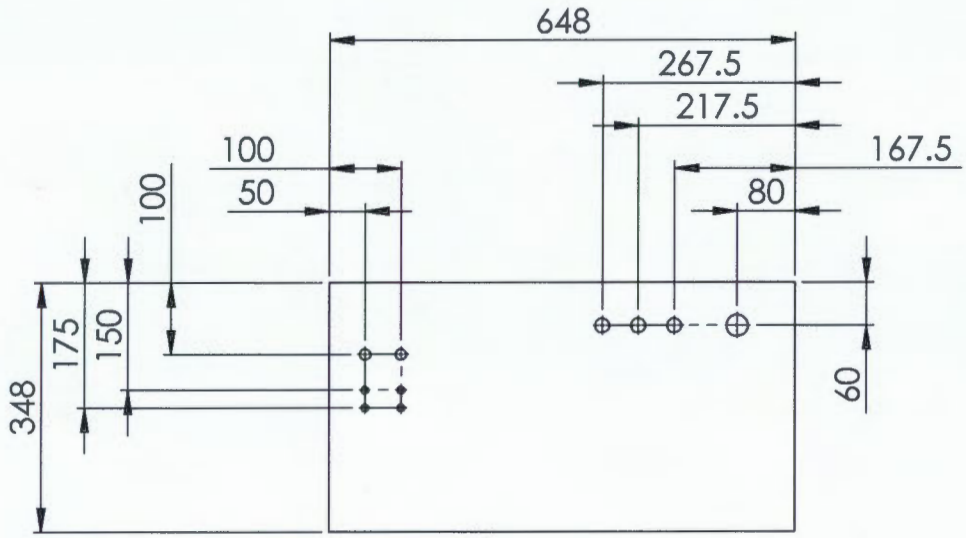

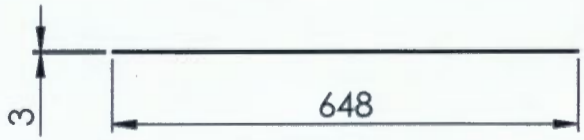

Part no. 7.2 to be welded to part no. 7.1.

A4 Landscape	University of Cape Town Department of Mechanical Engineering			
	Title: Back panel			
QTY 1	Scale:	Date: 2015/07/10	Sheet4	of 14
Material: 304 SS	Drawn By: Timothy Cole King		Drawing Number 7.2	

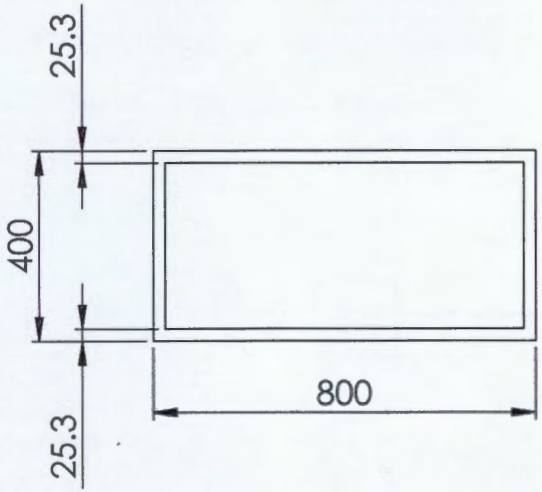

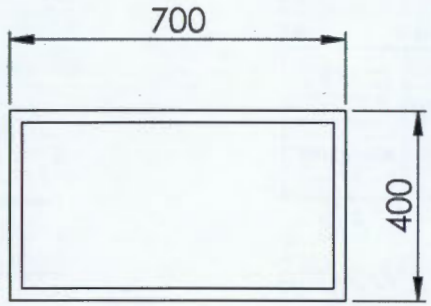

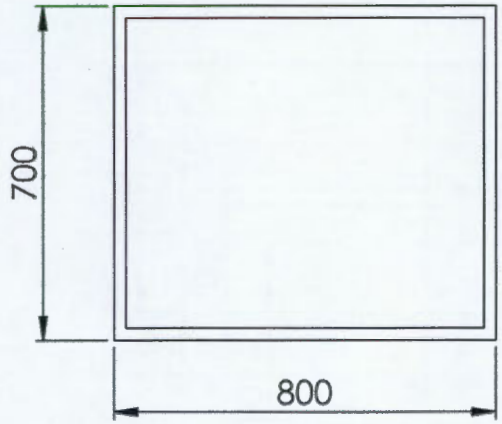

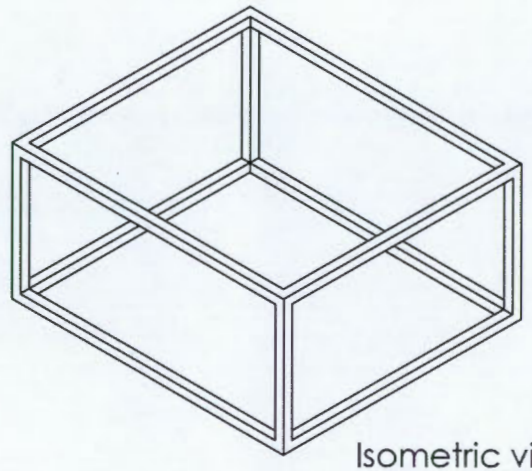

Isometric view

Frame welded together
Square tube profile: 25.3mmx2mm

A4 Landscape	University of Cape Town Department of Mechanical Engineering			
	Title: Frame 800x700x400			
QTY 1	Scale:	Date: 2015/07/10	Sheet3	of 14
Material: 304 SS	Drawn By: Timothy Cole King		Drawing Number 7.1	

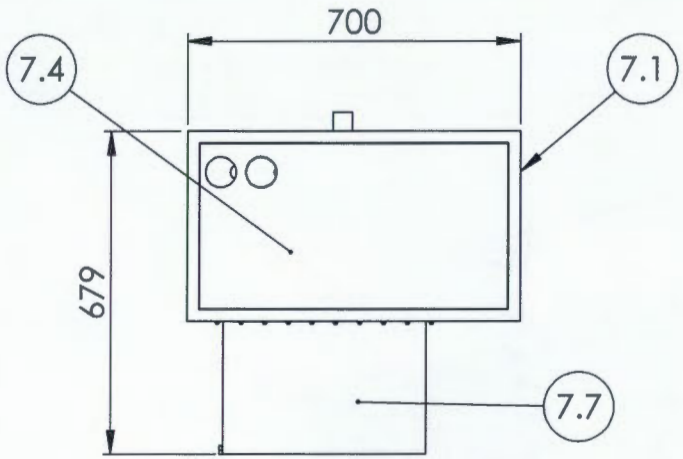

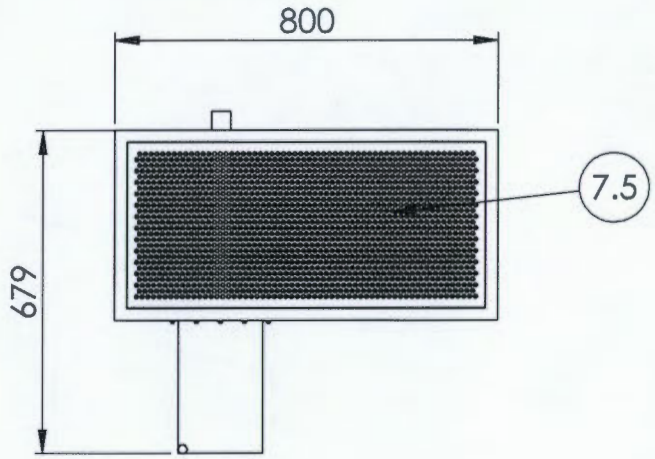

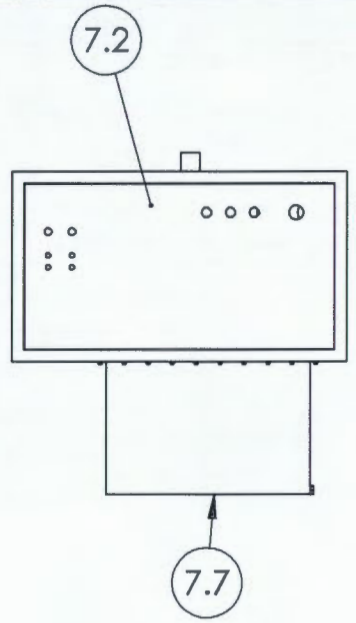

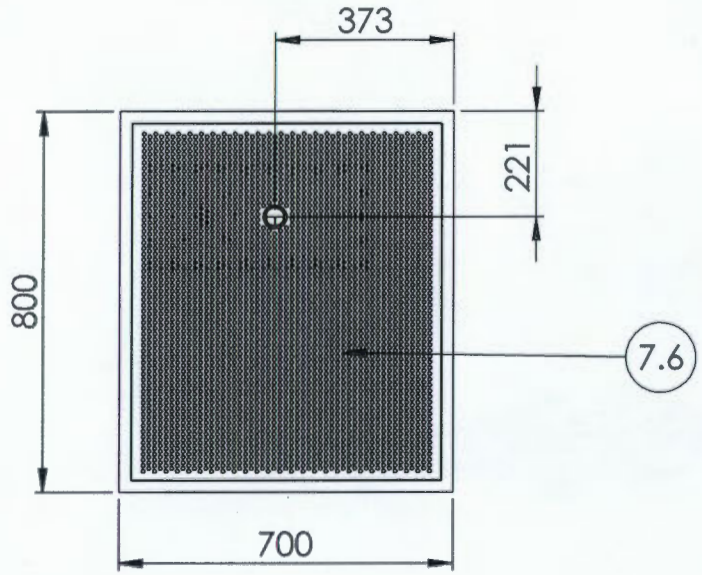

ITEM NO.	PART NUMBER	QTY.	Material
7.1	Frame 800x700x400	1	
7.2	Back panel	1	
7.3	Bottom panel	1	
7.4	Front panel	1	
7.5	Side perforated plate	2	
7.6	Top perforated plate	1	
7.7	Oil sump assembly new	1	

A4 Landscape	University of Cape Town Department of Mechanical Engineering			
	Title: Conditioning unit_Assemb ly			
Assembly Drawing	Scale:	Date: 2015/07/10	Sheet2	of
	Drawn By: Timothy Cole King		Drawing Number 7(b)	

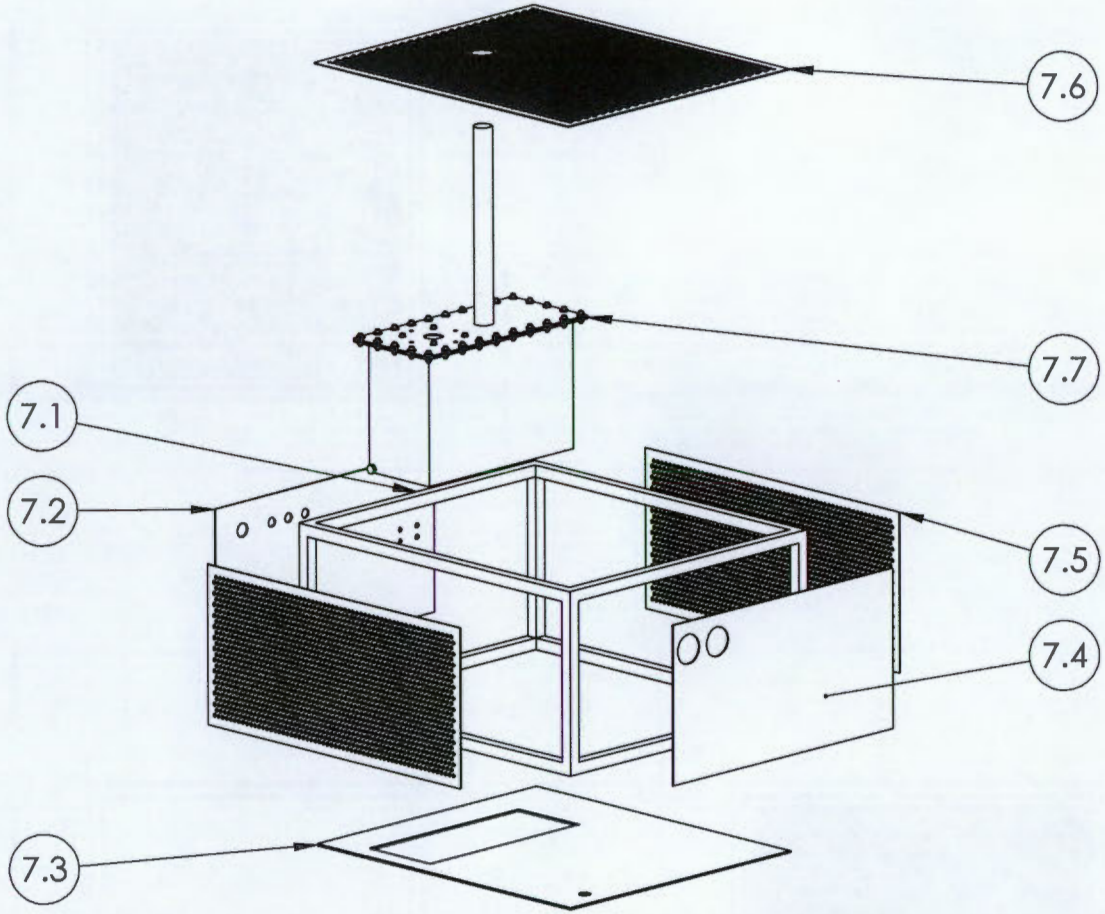

ITEM NO.	PART NUMBER	QTY.	Material
7.1	Frame 800x700x400	1	304_ss
7.2	Back panel	1	304_ss
7.3	Bottom panel	1	304_ss
7.4	Front panel	1	304_ss
7.5	Side perforated plate	2	LC_Steel
7.6	Top perforated plate	1	LC_Steel
7.7	Oil sump assembly new	1	

A4 Landscape	University of Cape Town Department of Mechanical Engineering			
	Title: Conditioning unit final_BOM			
Assembly Drawing	Scale:	Date: 2015/07/10	Sheet1	of
	Drawn By: Timothy Cole King		Drawing Number 7(a)	

F.7 Conditioning unit

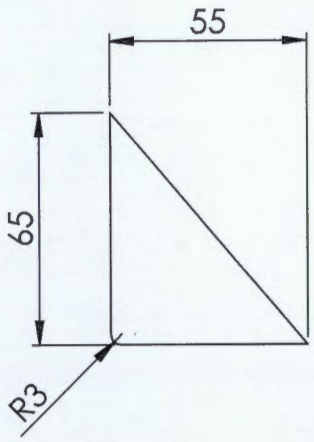

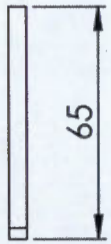

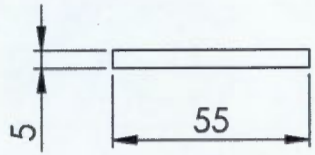

A4 Landscape	University of Cape Town Department of Mechanical Engineering			
	Title: Rib_mounting bracket			
QTY 2	Scale:	Date: 2015/07/10	sheet9	of 9
Material: 304 SS	Drawn By: Timothy Cole King		Drawing Number 6.6.2	

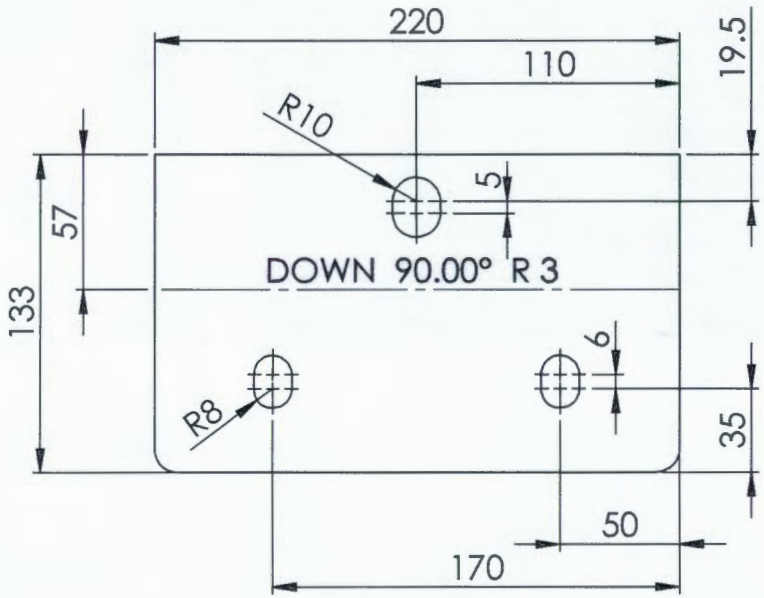

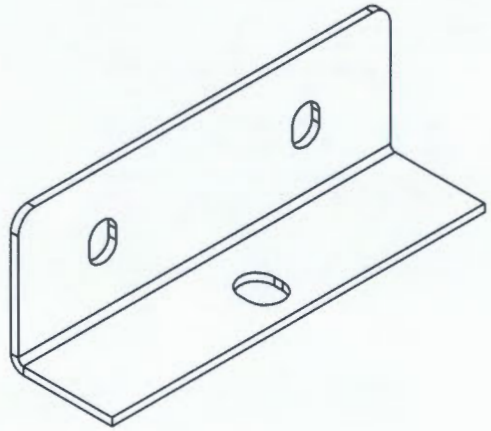

Isometric view

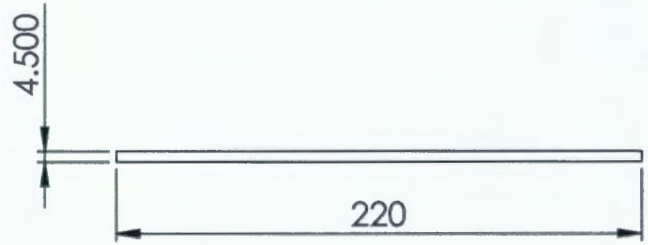

A4 Landscape	University of Cape Town Department of Mechanical Engineering			
	Title: Mounting bracket 2_Pulsation vessel stand			
QTY 1	Scale:	Date: 2015/07/10	sheet8	of 9
Material: 304 SS	Drawn By: Timothy Cole King		Drawing Number 6.6.1	

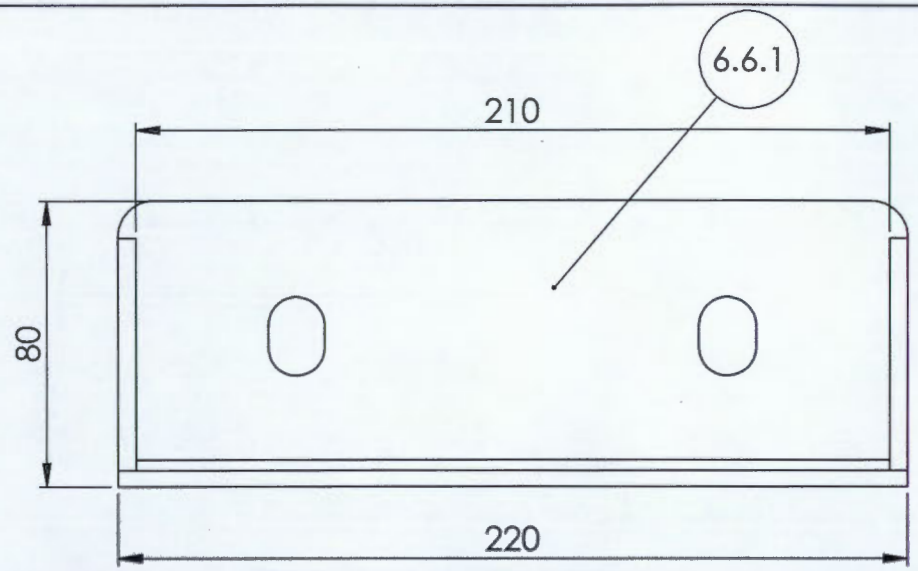

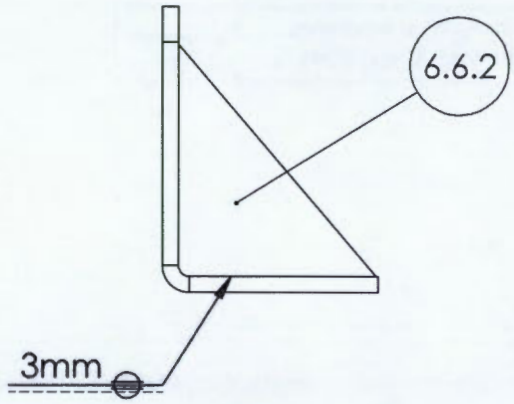

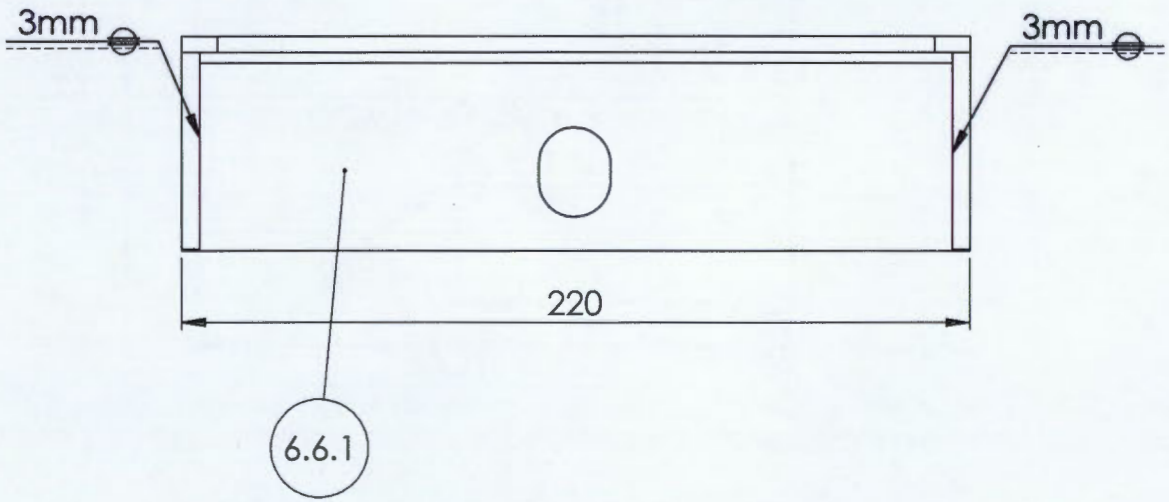

3 x Mounting brackets to be made

Part no. 6.6.1 to be laser cut and CNC bent. 2x Part no. 6.6.2 to be laser cut and welded to part no. 6.6.1

ITEM NO.	PART NUMBER	QTY.	Material
6.6.1	Mounting bracket 2_Pulsation vessel stand	1	304_SS
6.6.2	Rib_mounting bracket	2	304_SS

A4 Landscape	University of Cape Town Department of Mechanical Engineering			
	Title: Mounting bracket assembly 2_Pulsation vessel stand			
Assembly Drawing	Scale: 1:2	Date: 2015/07/10	Sheet7	of
	Drawn By: Timothy Cole King		Drawing Number	

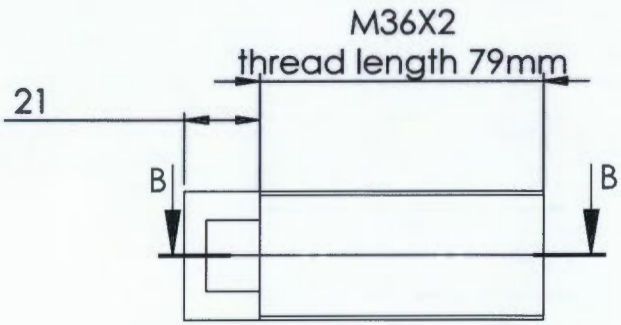

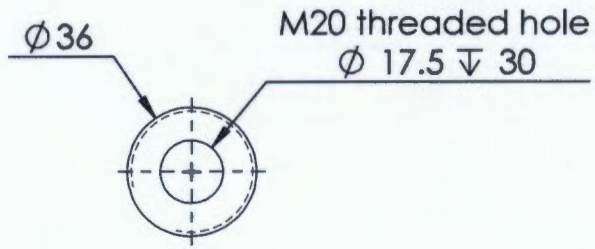

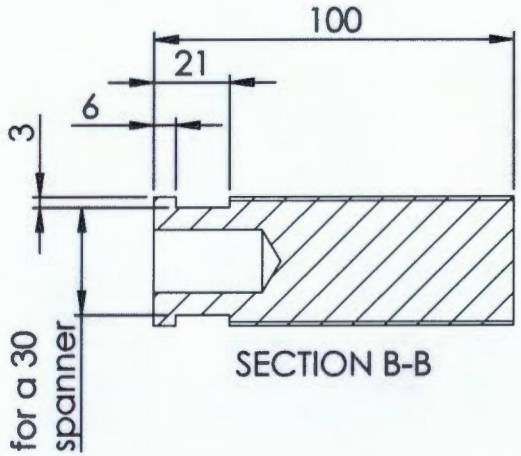

A4 Landscape	University of Cape Town Department of Mechanical Engineering			
	Title: Threaded bar_Pulsation vessel stand			
QTY 3	Scale: 1:2	Date: 2015/07/10	sheet6	of 9
Material: M300	Drawn By: Timothy Cole King		Drawing Number 6.5	

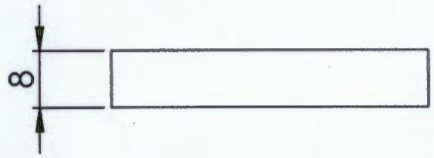

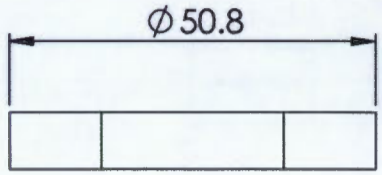

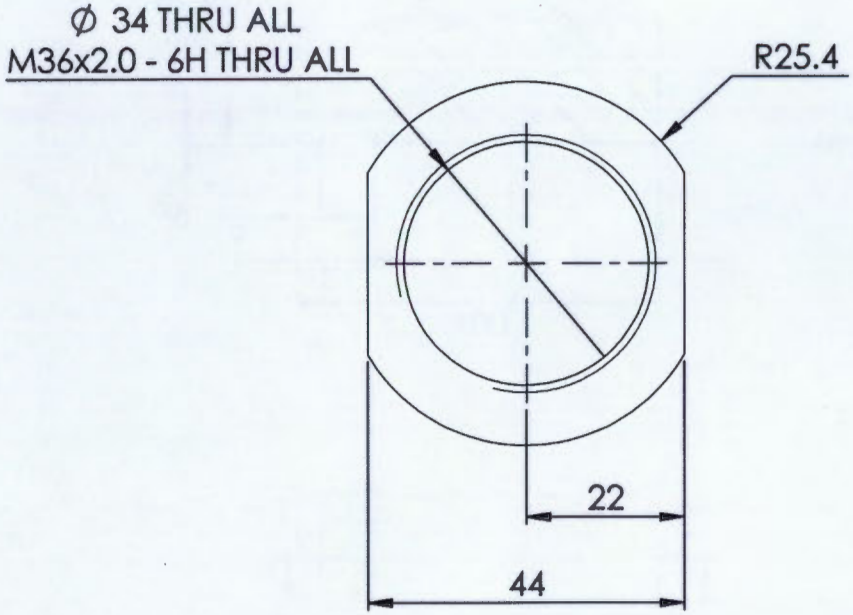

A4 Landscape	University of Cape Town Department of Mechanical Engineering			
	Title: Nut_thread tensioner			
QTY 3	Scale: 1:1	Date: 2015/07/10	sheet5	of 9
Material: 304 SS	Drawn By: Timothy Cole King		Drawing Number 6.4	

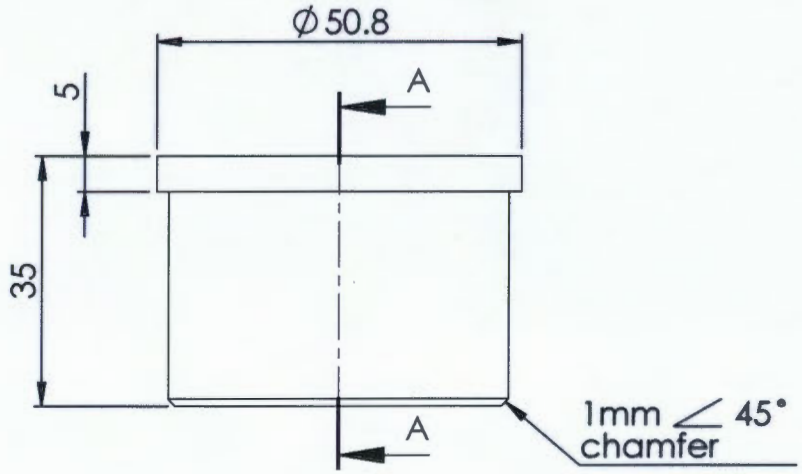

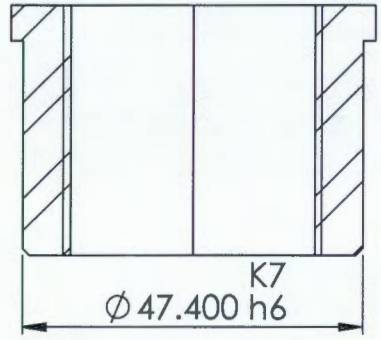

SECTION A-A

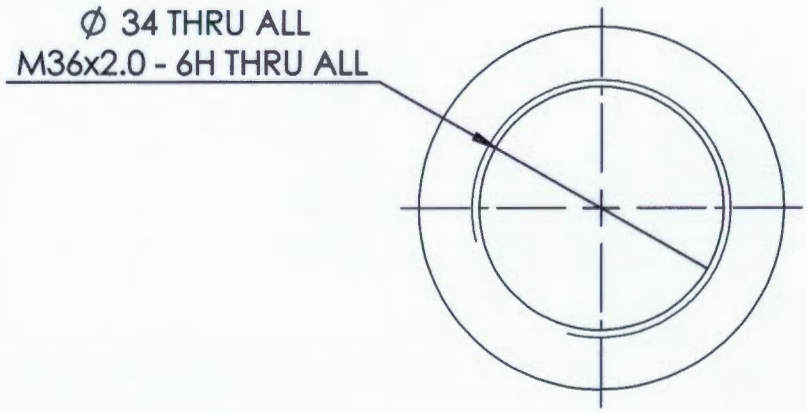

A4 Landscape	University of Cape Town Department of Mechanical Engineering			
	Title: Adaptor plug type 2_EGR loop valve stand			
QTY 3	Scale: 1:1	Date: 2015/07/10		of 9
Material: 304SS	Drawn By: Timothy Cole King		Drawing Number 6.3	

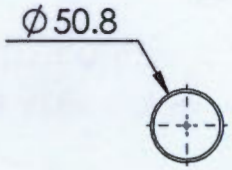

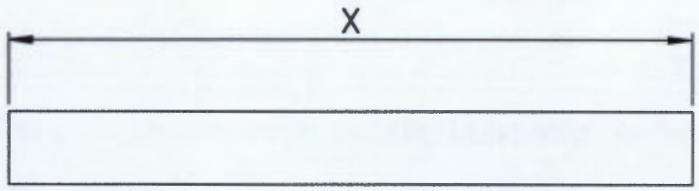

Lengths of 2" pipe to be parted on lathe for pulsation vessel stands

Part #	Size(x)mm	Qty
1	480	2
2	350	1

A4 Landscape	University of Cape Town Department of Mechanical Engineering			
	Title: Pipes_Pulsation vessel stand			
QTY 3	Scale: 1:5	Date: 2015/07/10		of 9
Material: 304 SS	Drawn By: Timothy Cole King		Drawing Number 6.2	

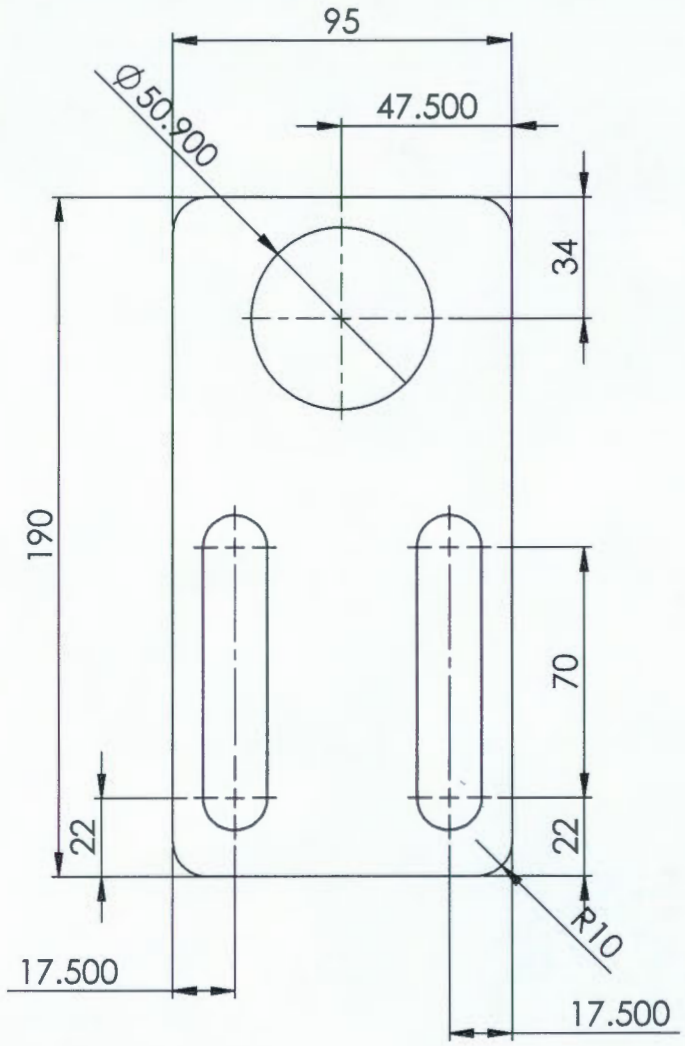

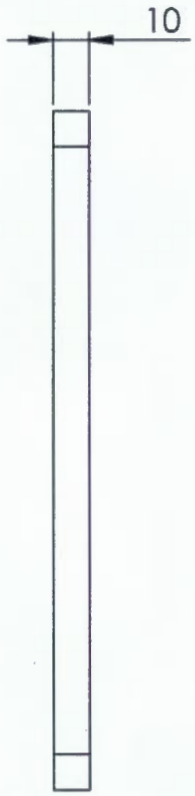

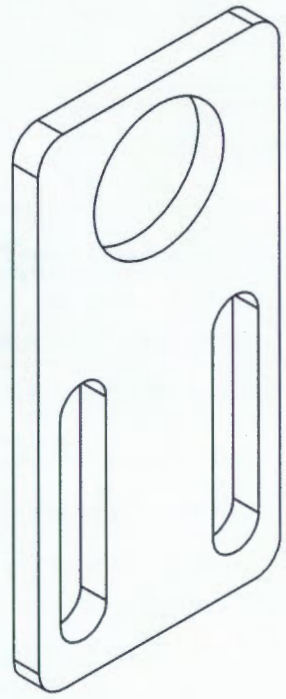

Isometric view

A4 Landscape	University of Cape Town Department of Mechanical Engineering			
	Title: base plate 2b_pulsation vessel stand			
QTY 3	Scale: 1:2	Date: 2015/07/10	sheet2	of 9
Material: 304 SS	Drawn By: Timothy Cole King		Drawing Number 3.1.5	

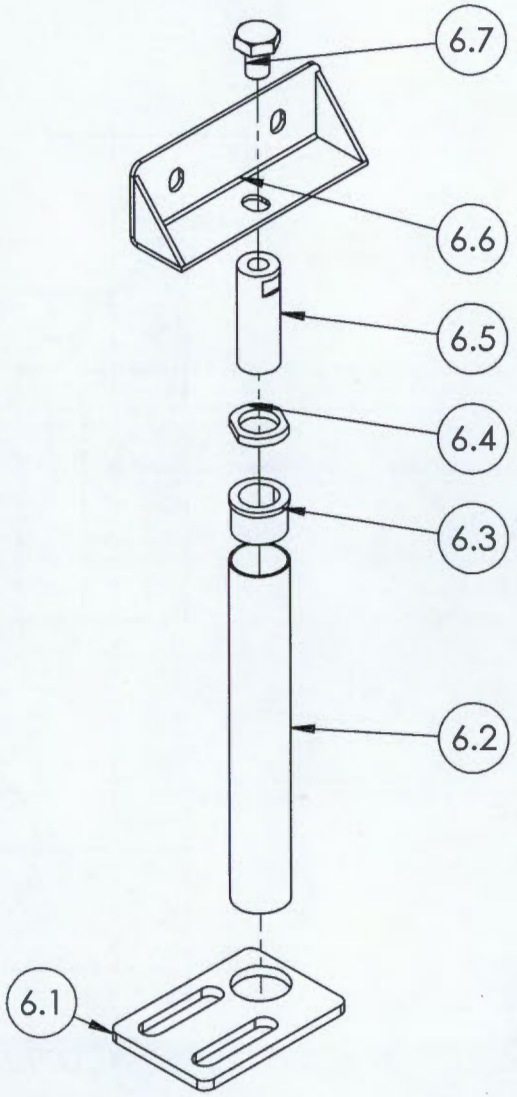

3x 'Stand_pulsation vessel' to be manufactured. Part no. 6.2 is the only part in the assembly that differs between assemblies. See drawing number 6.2 for more details.

ITEM NO.	PART NUMBER	QTY.	Material
6.1	base plate 3_pulsation vessel stand	3	
6.2	Pipe 3_Pulsation Vessel stand	3	
6.3	Adaptor plug type 2_EGR loop valve stand	3	304SS
6.4	Nut_thread tensioner	3	
6.5	Threaded bar_Pulsation vessel stand	3	M300
6.6	Mounting bracket assembly 2_Pulsation vessel stand	3	
6.7	B18.2.3.3M - Heavy hex screw, M20 x 2.5 x 30 --30N	3	

A4 Landscape	University of Cape Town Department of Mechanical Engineering			
	Title: Stand_pulsation vessel			
Assembly Drawing	Scale: 1:2	Date: 2015/07/10	Sheet1	of 9
	Drawn By: Timothy Cole King		Drawing Number 6	

F.6 Pulsation vessel stand

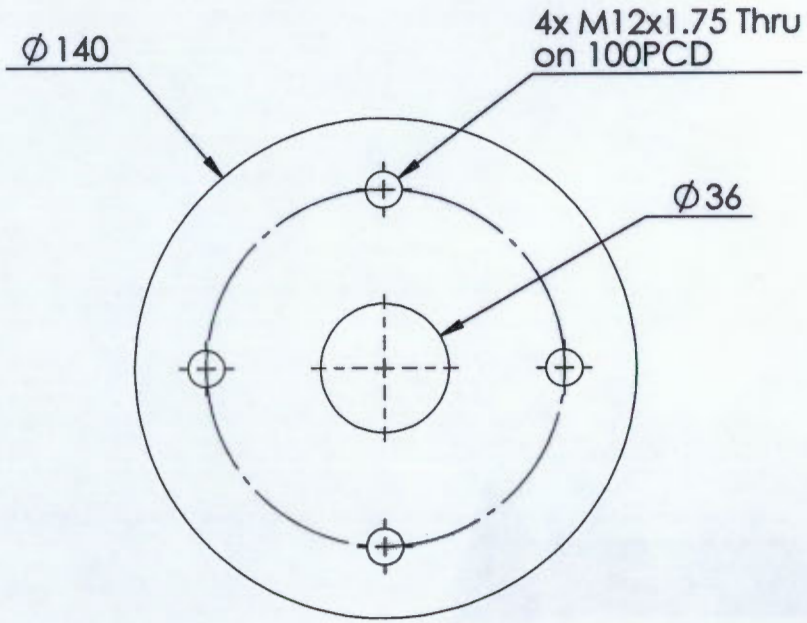

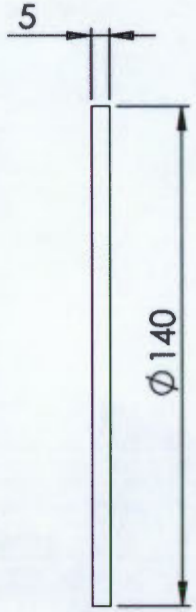

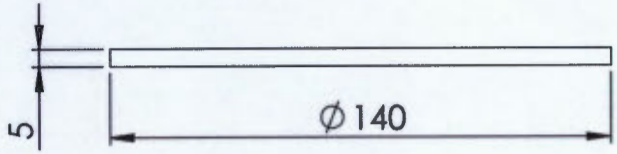

CNC laser cut at Vulcan
from solid model, thus dimensioning
isn't critical.

A4 Landscape	University of Cape Town Department of Mechanical Engineering			
	Title: Plate_Mounting bracket attachment to stand			
QTY 1	Scale: 1:2	Date: 2013/05/08	Sheet8	of 9
Material: 304 SS	Drawn By: Timothy Cole King		Drawing Number 5.6.2	

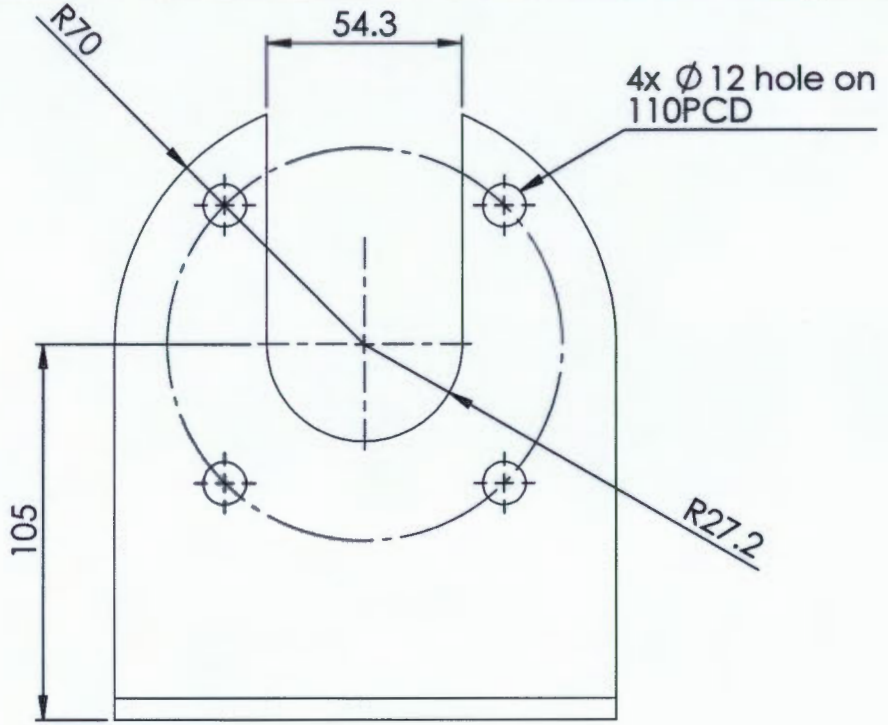

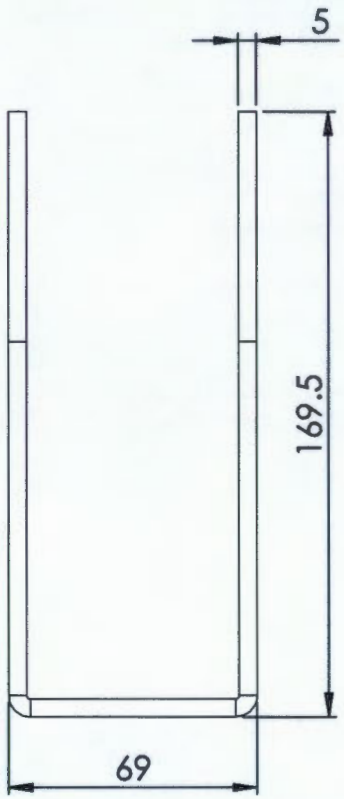

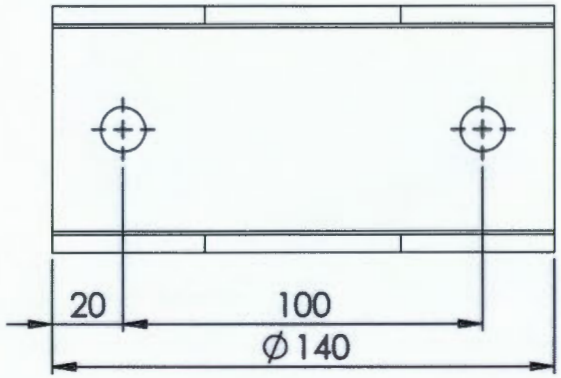

CNC laser cut and bent at Vulcan from solid model, thus dimensioning isn't critical

A4 Landscape	University of Cape Town Department of Mechanical Engineering			
	Title: Mounting bracket			
QTY 1	Scale: 1:5	Date: 2013/05/08	Sheet7	of 9
Material: 304 SS	Drawn By: Timothy Cole King		Drawing Number 5.6.1	

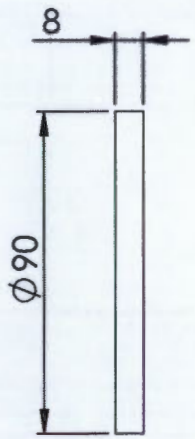

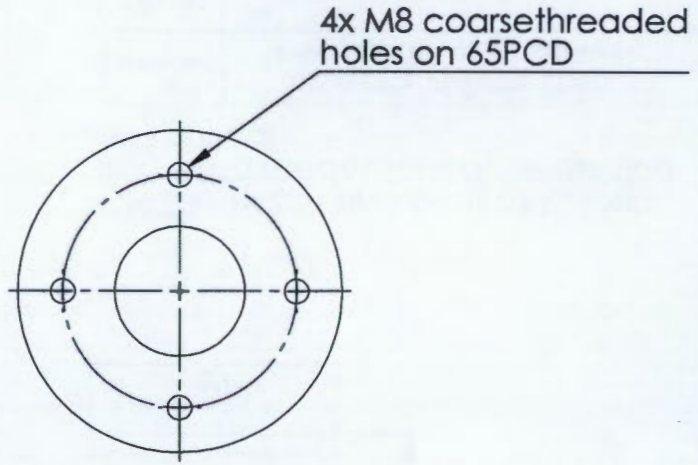

CNC laser cut at Vulcan
from solid model, thus dimensioning isn't critical.
Holes to be laser-cut undersized, then drilled and tapped in the workshop.

A4 Landscape	University of Cape Town Department of Mechanical Engineering			
	Title: Plate_Round attachment to stand			
QTY 2	Scale: 1:2	Date: 2013/05/08	Sheet6	of 9
Material: 304 SS	Drawn By: Timothy Cole King		Drawing Number 5.5.2	

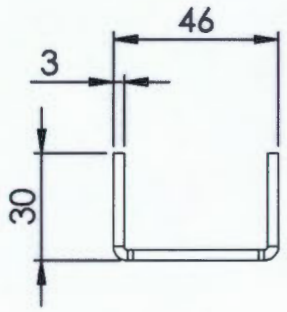

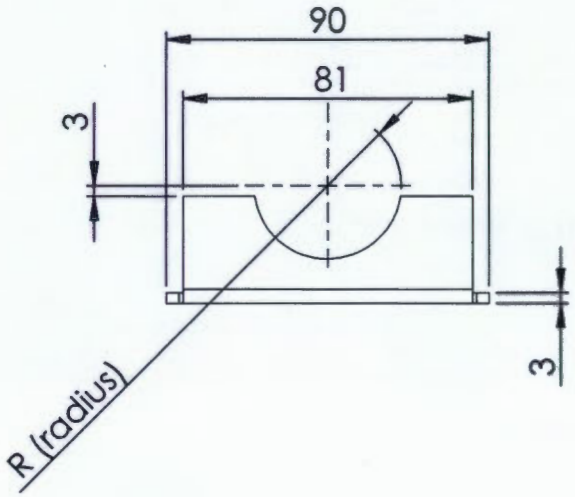

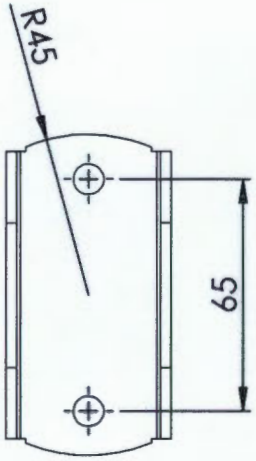

CNC laser cut and bent at Vulcan from solid model, thus dimensioning isn't critical

Clamp part		
Pipe no.	**Radius (R)**	**Qty**
1	20.5	2
2	25.5	2

A4 Landscape	University of Cape Town Department of Mechanical Engineering			
	Title: Clamp			
QTY 4	Scale: 1:2	Date: 2013/05/08	Sheet5	of 9
Material: 304 SS	Drawn By: Timothy Cole King		Drawing Number 5.5.1	

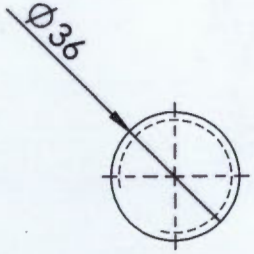

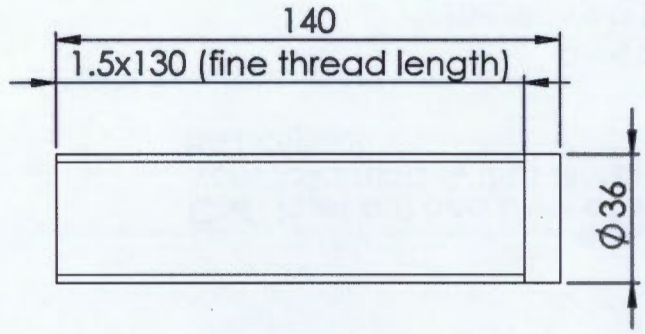

Glen has a 400mm length of M300 round bar

A4 Landscape	University of Cape Town Department of Mechanical Engineering			
	Title: Threaded bar new			
QTY 3	Scale: 1:2	Date: 2013/05/08	Sheet4	of 9
Material: M300	Drawn By: Timothy Cole King		Drawing Number 5.4	

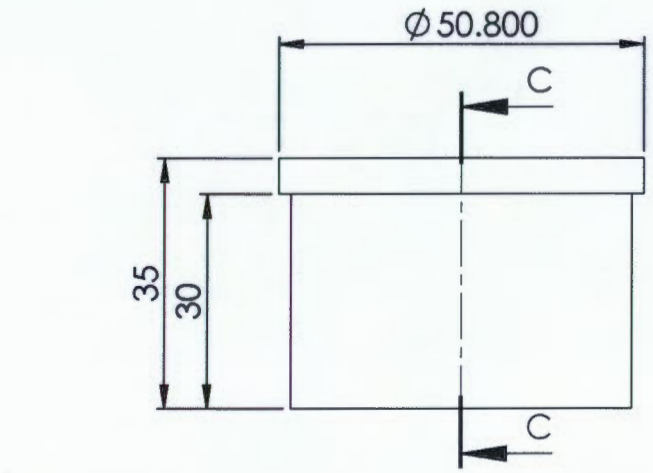

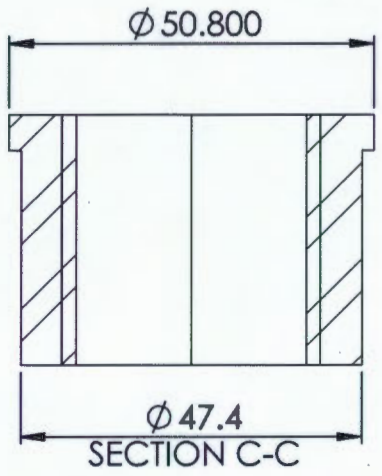

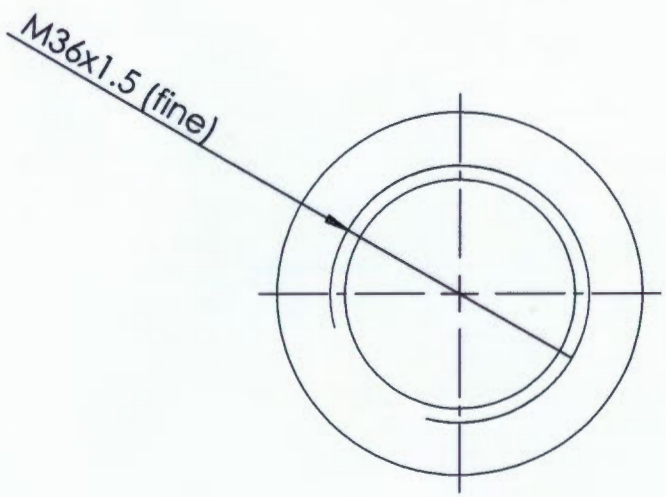

A4 Landscape	University of Cape Town Department of Mechanical Engineering			
	Title: Adaptor plug type 2			
QTY 3	Scale: 1:1	Date: 2013/05/08	Sheet9	of 9
Material: 304 SS	Drawn By: Timothy Cole King		Drawing Number 5.3	

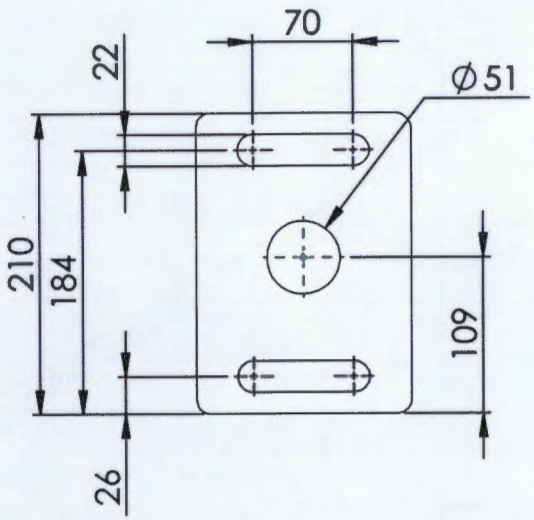

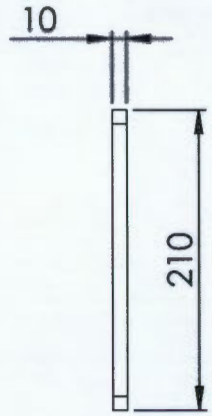

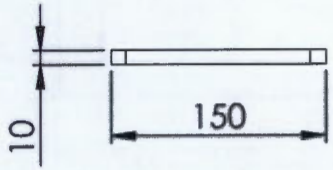

CNC laser cut at Vulcan from solid model, thus dimensioning isn't critical

A4 Landscape	University of Cape Town Department of Mechanical Engineering			
	Title: Exhaust stand base plate type 2			
QTY 3	Scale: 1:5	Date: 2013/05/08	Sheet3	of 9
Material: 304 SS	Drawn By: Timothy Cole King		Drawing Number 5.2	

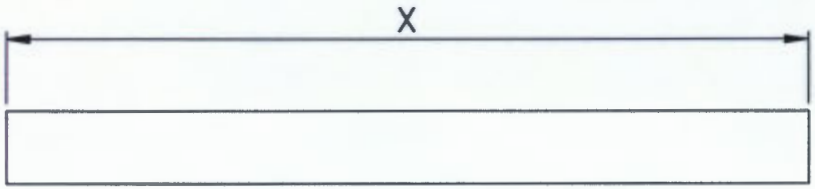

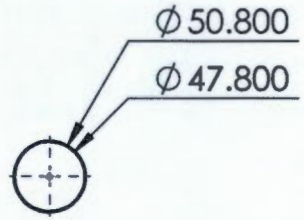

Exhaust stand pipe length		
Pipe no.	**Length (X)**	**Qty**
2	560	2
1	640	1

A4 Landscape	University of Cape Town Department of Mechanical Engineering			
	Title: Exhaust stand tubing			
QTY 3	Scale: 1:5	Date: 2013/05/08	Sheet2	of 9
Material: 304 SS	Drawn By: Timothy Cole King		Drawing Number 5.1	

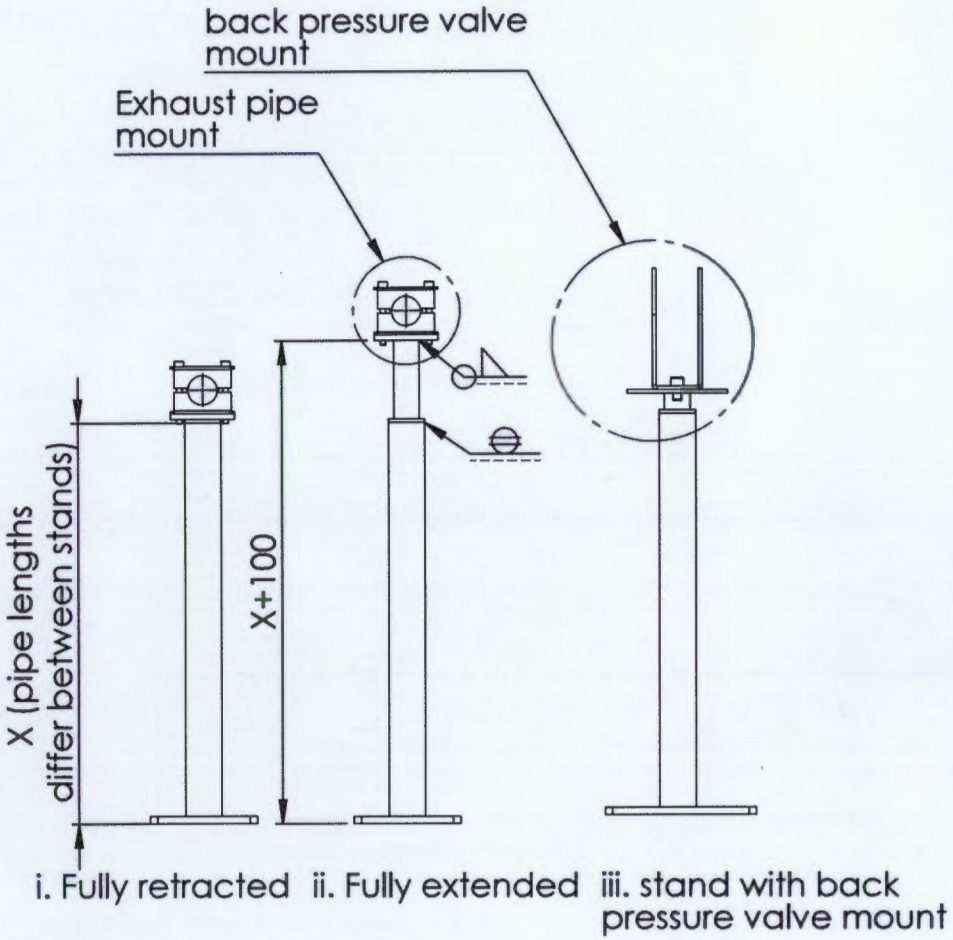

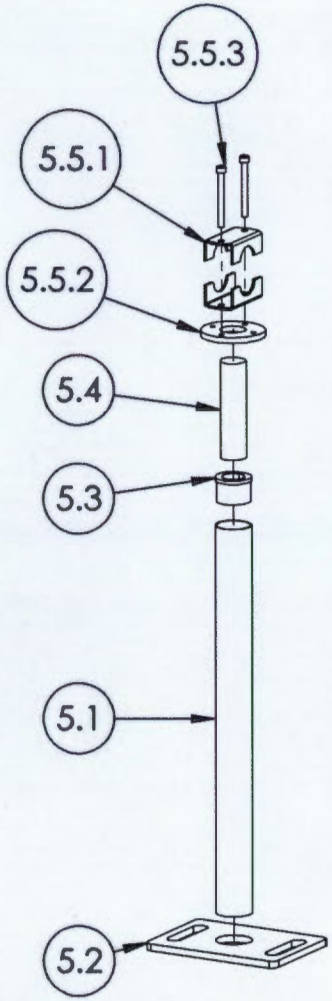

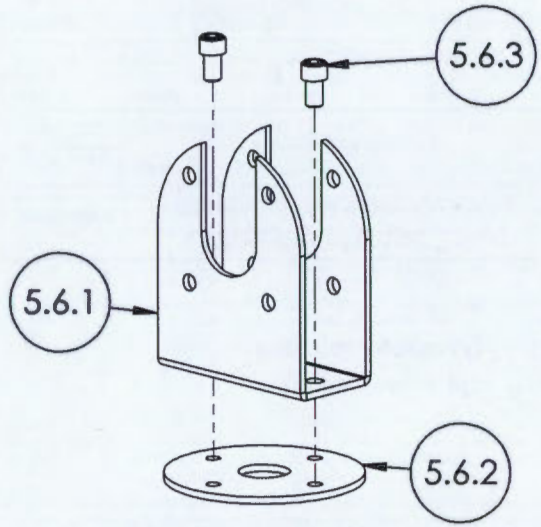

Back pressure valve mount

ITEM NO.	PART NUMBER	Default /QTY.	Material
5.1	Exhaust stand_Pipe	3	304SS NDE dairy grade
5.2	exhaust stand base plate type 2	3	304SS
5.3	Adaptor plug type 2	3	304SS
5.4	Threaded bar new	3	M300
5.5.1	Clamp part type 2	4	304SS
5.5.2	Plate_Round attachment to stand	1	304SS
5.5.3	B18.3.1M - 8 x 1.25 x 80 Hex SHCS – 28NHX	2	SS
5.6.1	Mounting bracket	1	304SS
5.6.2	Plate_mounting bracket attachment to stand	1	304SS
5.6.3	Hex cap M12x10	2	SS

A4 Landscape	University of Cape Town Department of Mechanical Engineering			
	Title: Exhaust stands			
QTY 1	Scale: 1:10	Date: 2013/05/08	Sheet1	of 9
Material:	Drawn By: Timothy Cole King		Drawing Number 3.1.5	

F.5 Back pressure valve and exhaust pipe stands

NOZZL.	ITEM	QUANT.	DESCRIPTION	CERT.	MATERIAL SPEC.
	11	1	NAMEPLATE: 170 x 150 x 3 THK.	2.2	SA-240 GR. 304
	10B	1	NAMEPLATE BRACKET: 180 x 160 x 6 THK.	2.2	SA-387 GR.12-1
	10A	1	NAMEPLATE CLIP: 160 x 75 x 6 THK.	3.1	SA-387 GR.12-1
	9	3	SUPPORT BRACKET: 360 x 70 x 6 THK.	3.1	SA-387 GR.12-1
RV1	8	1	HALF COUPLING: 2" CL.3000 NPT	3.1	SA-182 GR.F 12-2
P1	7	1	HALF COUPLING: 2" CL.3000 NPT	3.1	SA-182 GR.F 12-2
D1	6C	1	BALL VALVE: 1" THREADED NPT CL.800	3.1	SA-182 GR.F 12-2
	6B	1	HEX. NIPPLE: 1" CL.3000 NPT	3.1	SA-182 GR.F 12-2
	6A	1	HALF COUPLING: 1" CL.3000 NPT	3.1	SA-182 GR.F 12-2
N2	5B	1	NOZZLE: 2" SCH.80 x 61 LG.	3.1	SA-335 GR.P12
	5A	1	FLANGE: 160 OD x 49 ID x 32 THK. (SEE DETAIL)	3.1	SA-182 GR.F 12-2
N1	4B	1	NOZZLE: 2" SCH.80 x 61 LG.	3.1	SA-335 GR.P12
	4A	1	FLANGE: 160 OD x 49 ID x 32 THK. (SEE DETAIL)	3.1	SA-182 GR.F 12-2
	3	1	BAFFLE PLATE: 433 x 310 x 6 THK.	3.1	SA-387 GR.12-1
	2	2	HEAD: TORISPHERICAL HEAD x CROWN RADIUS 446 ID x 45 KNUCKLE RADIUS x 6 THK.	3.1	SA-387 GR.12-1
	1	1	SHELL: 446 OD x 6 THK. x 270 LG.	3.1	SA-387 GR.12-1

MATERIAL LIST

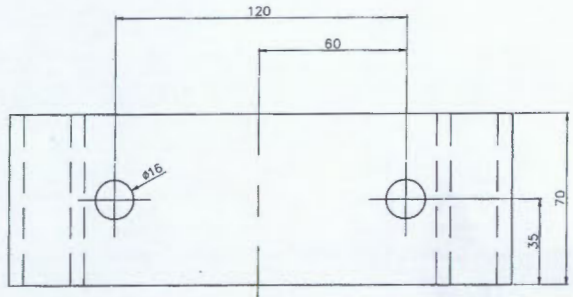

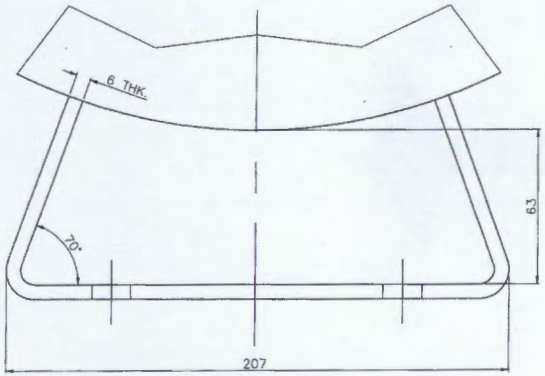

SUPPORT BRACKET
ITEM 9

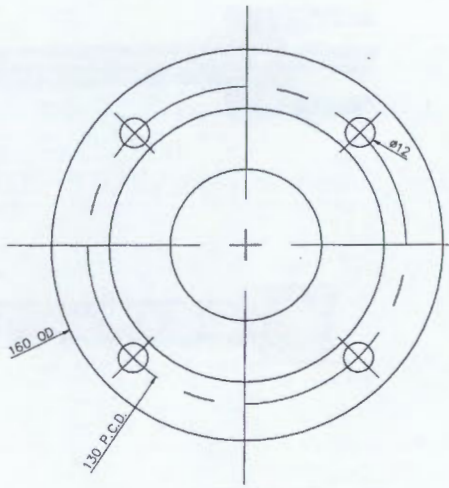

NOZZLE N1 AND N2 FLANGE
ITEM 4A&5A

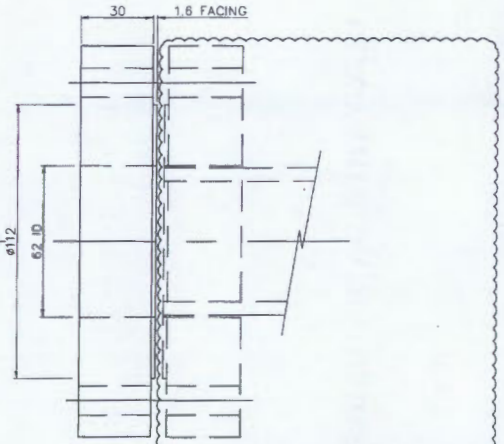

REQUIRED MATING FLANGE TO BE SUPPLIED BY OTHER.
REQUIRED MATING FLANGE MATERIAL MUST BE SA-182 GR.F 12.2
GASKET DIMENSIONS TO BE 112 OD x 62 ID x 3 THK.
GASKET MATERIAL TO BE KLINGERGRAPH SLS

JF Schoeman 970068

REFERENCE DOCUMENTS		
CLIENT DOC. No.	APEX PROCESS DOC. No.	DESCRIPTION
-	AP645-DME-001_01	GENERAL ARRANGEMENT

REV.	REVISION DESCRIPTION	DRAUGHT.	CHECKED	LEAD ENGINEER	PROCESS ENGINEER	MECHANICAL ENGINEER	CIVIL ENGINEER	PIPING ENGINEER	INSTRUM. ENGINEER	ELECTR. ENGINEER	PROJECT MANAGER	DATE
A	ISSUE FOR COMMENTS	WFB	JHK		HVD	JHK					HVD	-

VBV HOLDINGS
20 WILLIAMS STOW STREET
SASOLBURG
TEL.: +27-16-976-2582

PROJECT No. : AP645
DRAWN : W.A. PRETORIUS — DATE 2013/08/07
CHECKED : H. VAN DER MERWE — DATE -
ENGINEER : J.H. KOEKEMOER — DATE -
SCALE : 1:1 PROJ. — DWG. SIZE : A1

APEX PROCESS
TEL.: +27-16-971 4401
FAX TO E-MAIL : +27-86-501 8422
E-MAIL : hsm@apexprocess.co.za
RIEBLAND OFFICE PARK BLOCK E
VANDIJK 1945
SOUTH AFRICA

VBV HOLDINGS
PULSATION VESSEL
DETAIL AND MATERIAL LIST DRAWING

		INTER. No.	REV. No.
CLIENT DWG No. :	-		
APEX DWG.No. :	AP645-DME-001_02	A3	A
CLIENT ORDER No. :	12529		

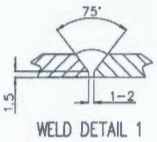

WELD DETAIL 1

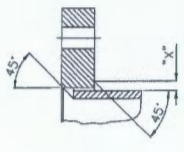

WELD DETAIL 2

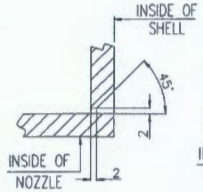

WELD DETAIL 3

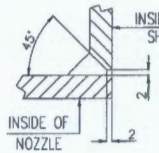

WELD DETAIL 4

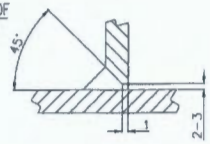

WELD DETAIL 5

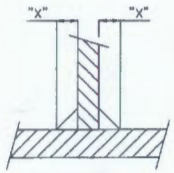

WELD DETAIL 6

JOINT. No.	DETAIL No.	BASE MATERIAL	BASE MATERIAL	MATERIAL THK.		FILLET WELD "X"
CW1	1	SA-387 GR.12-1	SA-387 GR.12-1	6	6	
CW2	1	SA-387 GR.12-1	SA-387 GR.12-1	6	6	
LW 1	1	SA-387 GR.12-1	SA-387 GR.12-1	6	6	
FW N1	2	SA-182 GR.F 12-2	SA-335 GR.P12	5.54	5.54	
FW N2	2	SA-182 GR.F 12-2	SA-335 GR.P12	5.54	5.54	
NW N1	3	SA-335 GR.P12	SA-387 GR.12-1	5.54	6	6
NW N2	3	SA-335 GR.P12	SA-387 GR.12-1	5.54	6	6
NW P1	4	SA-182 GR.F 12-2	SA-387 GR.12-1	8.2	6	4
NW RV1	4	SA-182 GR.F 12-2	SA-387 GR.12-1	9.3	6	6
NW D1	4	SA-182 GR.F 12-2	SA-387 GR.12-1	9.3	6	6
AW 1.1-6	3	SA-387 GR.12-1	SA-387 GR.12-1	6	6	6
AW 2.1-2	3	SA-387 GR.12-1	SA-387 GR.12-1	6	6	6
AW 3	3	SA-387 GR.12-1	SA-387 GR.12-1	6	6	6
AW 4	4	SA-387 GR.12-1	SA-387 GR.12-1	6	6	6

SUPPORT BRACKET TO SHELL
BAFFLE PLATE TO SHELL
NAME PLATE CLIP TO SHELL
NAME PLATE BRACKET TO CLIP

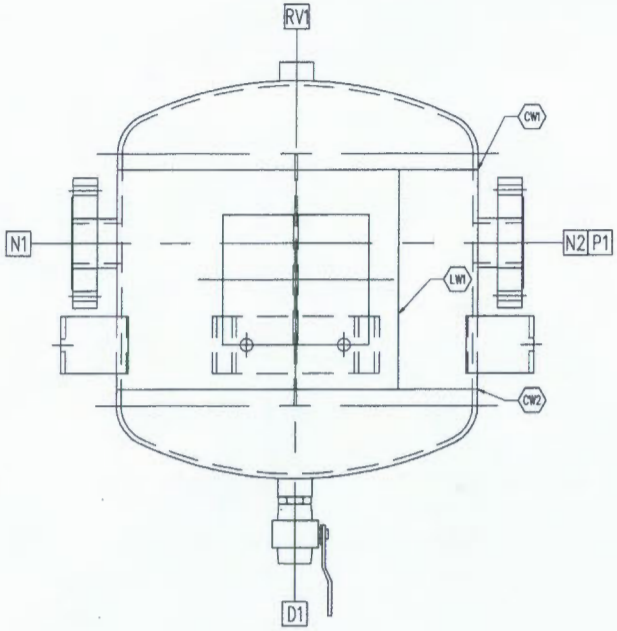

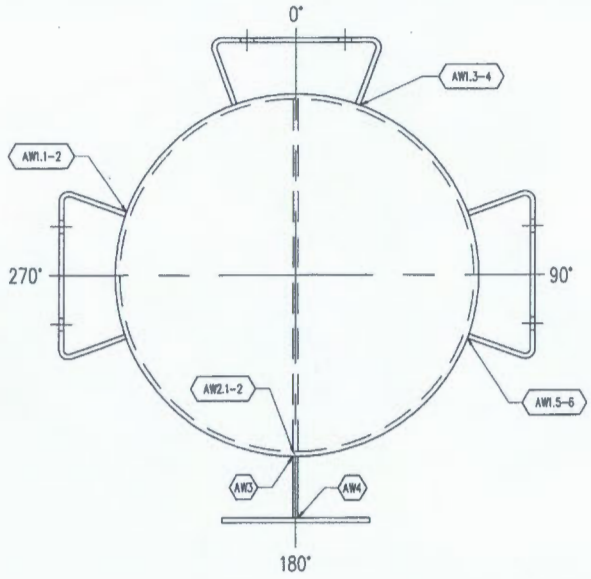

JF Schoultz
970648
16/10/13

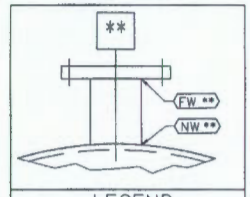

LEGEND

NW = NOZZLE WELD
FW = FLANGE WELD
CW = CIRCUMFERENTIAL WELD
AW = ATTACHMENT WELD

TH = NOMINAL THK. OF HEAD.
TN = NOMINAL THK. OF NOZZLE WALL.
TS = NOMINAL THK. OF SHELL.
'X' = FILLET WELD SIZE IN mm
T = NOMINAL THICKNESS.

REFERENCE DOCUMENTS		
CLIENT DOC. No.	APEX PROCESS DOC. No.	DESCRIPTION
-	AP645-DME-001_01	GENERAL ARRANGEMENT

REV	REVISION DESCRIPTION	DRAWN	CHECKED	LEAD ENGINEER	PROCESS ENGINEER	MECHANICAL ENGINEER	CIVIL ENGINEER	PIPING ENGINEER	INSTRUMENT ENGINEER	ELECTRICAL ENGINEER	PROJECT MANAGER	DATE
A	ISSUE FOR COMMENTS	WPH	JHK		HVD	JHK					HVD	-

VBV HOLDINGS
39 WILLIAMS STOW STREET
SASOLBURG
TEL.: +27-16-976-2582

PROJECT No. : AP645
DRAWN : M.A. PRETORIUS — DATE 2013/08/07
CHECKED : H. VAN DER MERWE — DATE -
ENGINEER : J.H. KOEKEMOER — DATE -
SCALE : 1:1 — PROJ. — DWG. SIZE : A1

APEX PROCESS
TEL.: +27-16-971 4481
FAX TO E-MAIL : +27-86-501 8422
E-MAIL : hank@apexprocess.co.za
HEALAND OFFICE PARK BLOCK E
VAALPARK 1945
SOUTH AFRICA

VBV HOLDINGS
PULSATION VESSEL
WELD MAP

CLIENT DWG No. : -		
APEX. DWG.No. :	AP645-DME-001_03	
CLIENT ORDER No. :	12529	A2 A

NOZZLE SCHEDULE

ITEM	NOZZ. No.	SIZE	SCH.	TYPE	FACING	CLASS	PROJECTION	DESCRIPTION
4	N1	2"	80	PLT.	RF	–	279 FROM C.L.	INLET
5	N2	2"	80	PLT.	RF	–	279 FROM C.L.	OUTLET
6	D1	1"		HALF COUPLING		3000		DRAIN
7	P1	3/4"		HALF COUPLING		3000		PRESSURE GAUGE
8	RV1	1"		HALF COUPLING		3000		RELIEF VALVE

PRESSURE VESSEL DESIGN DATA

DESIGN CODE:		ASME VIII DIV. 1 2010A ED. ADDENDA '11a
HAZARD CATEGORY (SANS 347:2010):		III
VESSEL TYPE:		PULSATION VESSEL
DESIGN PRESSURE:	kPa(g)	350
DESIGN TEMPERATURE (MIN/MAX):	°C	15/500
OPERATING PRESSURE:	kPa(g)	300
OPERATING TEMPERATURE (MIN/MAX):	°C	477
MAX. ALLOWABLE EXTERNAL PRESSURE:	kPa(g)	0
DESIGN TEMPERATURE FOR EXTERNAL PRESSURE:	°C	
INITIAL HYDROSTATIC TEST PRESSURE (TOP/BOT.):	kPa(g)	800/805
FUTURE HYDROSTATIC TEST PRESSURE (TOP/BOT.):	kPa(g)	535/540
CORROSION ALLOWANCE:	mm	2
JOINT EFFICIENCY:		100%
MEDIUM:		DEISEL EXHAUST GAS (CO)
MEDIUM SPECIFIC GRAVITY:		0
RADIOGRAPHY:		RTI
POST WELD HEAT TREATMENT:		YES
VOLUME:	m^3	0.063
MASS EMPTY:	kg	62
MASS FILLED WITH WATER:	kg	125
MASS OPERATING:	kg	62
INSULATION:	mm	ls(40 THK.)
PAINTING: (OUTSIDE ONLY,PRIMER ONLY)		YES
PICKLE AND PASSIVATION:		NO

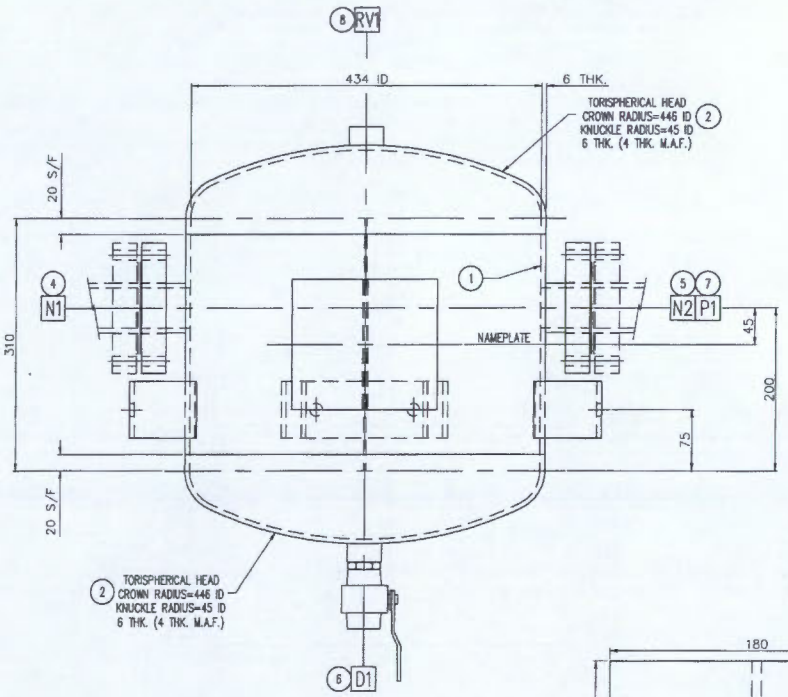

ELEVATION

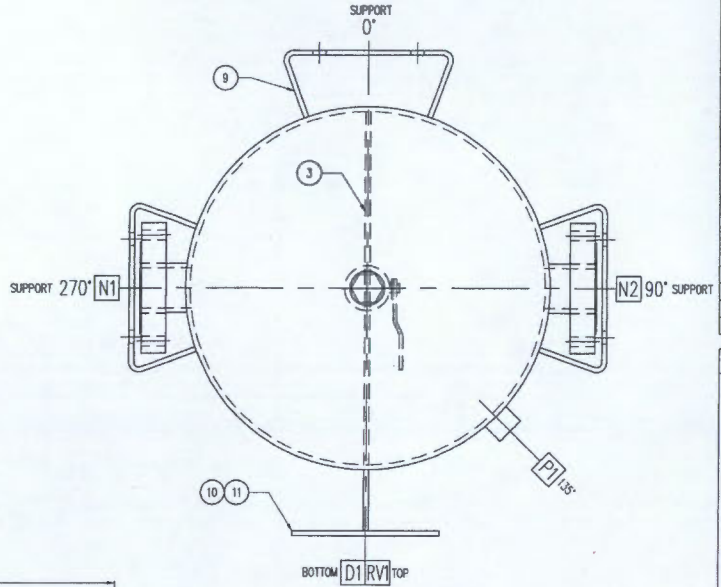

180°
NAMEPLATE
ORIENTATION

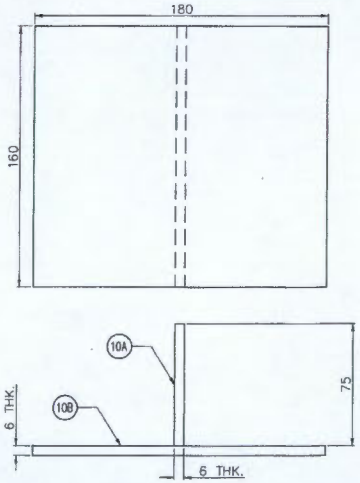

NAMEPLATE BRACKET

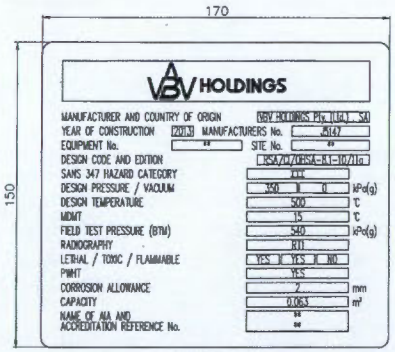

NAMEPLATE
**-TO BE COMPLETED BY MANUFACTURER

Reviewed by JF Schwalk 9700648 16/10/13
on behalf of Apex

GENERAL NOTES

1. INSPECTION DURING MANUFACTURING BY AN APPROVED INSPECTION AUTHORITY.
2. ALL MATERIALS TO BE STRICTLY IN ACCORDANCE WITH THE SPECIFICATIONS IN THE PART LIST. MANUFACTURER MUST ENSURE THAT ALL MATERIALS SPECIFIED AVAILABLE, OR OFFER ALTERNATIVES AT TENDER STAGE.ANY PROPOSED MATERIAL SUBSTITUTION IS SUBJECT TO APPROVAL OF APPROVED INSPECTION AUTHORITY.
3. NO MATERIAL CONCESSIONS WILL BE GRANTED AFTER THE ACCEPTANCE OF ORDER OR CONTRACT.
4. ALL VESSEL FITTINGS TO BE ATLEAST 50mm FROM ANY SEAM WELD. WHERE THIS IS NOT POSSIBLE, APPROVAL SHALL BE OBTAINED FROM SCI INSPECTION AUTHORITY.
5. SADDLES, SKIDS AND SUPPORTING DETAILS TO BE POSITIONED CLEAR IF MAIN SHELL WELD SEAMS.
6. ALL FLANGE BOLT HOLES TO STRADDLE NATURAL HORIZONTAL AND VERTICAL CENTRE LINES OF VESSEL, UNLESS OTHERWISE STATED.
7. MINIMUM WATER TEMPERATURE FOR HYDRAULIC PRESSURE TEST: CARBON STEEL = 15°C. STAINLESS STEEL: FABRICATOR TO SUPPLY TEST PROCEDURE TO APPROVED INSPECTION AUTHORITY FOR APPROVAL.
8. THE FOLLOWING MUST BE SUPPLIED IN DUPLICATE FOR APPROVAL BEFORE COMMENCING WORK:
   a) A WELD MAP SHOWING ALL WELDS & REFERENCE WELD PROCEDURE No's.
   b) WELDING PROCEDURES, INCLUDING PREP. & WELD SIZES.
   c) QUALITY ASSURANCE STEP PROCEDURE INDICATING MANUFACTURER & INSPECTION HOLD POINTS.
9. VESSEL TO COMPLY IN ALL RESPECTS WITH REQUIREMENTS OF OCCUPATIONAL HEALTH AND SAFETY ACT No. 85 (1993).
10. PRESSURE WELDS TO BE FULL PENETRATION WELDS UNLESS OTHERWISE STATED.
11. A 1/4" NPT TELL-TALE HOLE TO BE DRILLED IN EACH SECTION OF ALL DOUBLING PLATES AT LOWEST POINT. ALL DOUBLE PLATES TO BE SUBJECTED TO A SOAP-AIR TEST OF 100kPa. ALL TELL-TALE HOLES TO BE OPEN AND CLEAR DURING HEAT TREATMENT & HYDRAULIC PRESSURE TEST.
12. PRESSURE TEST BLANKS AND TWO SETS OF GASKETS TO BE SUPPLIED BY CONTRACTOR.
13. AFTER TEST VESSEL MUST BE FULLY DRIED OUT AND ALL OPENINGS BLANKED OFF TO PREVENT INGRESS OF MOISTURE.
14. ALL UNDERCUT/EDGES STRESS RAISERS TO BE DRESSED TO THE SATISFACTION OF SCI INSPECTION AUTHORITY.
15. ALL PIPE & PIPE FITTINGS TO BE SEAMLESS TYPE UNLESS OTHERWISE STATED.
16. HARD STAMP PLANT ITEM No. ON ALL REMOVABLE PARTS.

REFERENCE DOCUMENTS			
CLIENT DOC. No.	APEX PROCESS DOC. No.	REV.	DESCRIPTION
	AP645-DME-001_01	A	GENERAL ARRANGEMENT
	AP645-DME-001_02	A	DETAIL DRAWING
	AP645-DME-001_03	A	WELD MAP
	AP645-DMC-001	A2	MECHANICAL CALCULATIONS
			PULSATION VESSEL CONCEPT 3

REV	REVISION DESCRIPTION	DRAWN	CHECKED	LEAD ENGINEER	PROCESS ENGINEER	MECHANICAL ENGINEER	CIVIL ENGINEER	PIPING ENGINEER	INSTRUMENT ENGINEER	ELECTRIL ENGINEER	PROJECT MANAGER	DATE
A	ISSUE FOR COMMENTS	WPR	JVK		NVD	JVK					NVD	2013/10/04

VBV HOLDINGS
30 WILLIAMS STOW STREET
SASOLBURG
TEL.: +27-16-976-2582

PROJECT No. : AP645
DRAWN : W.PRETORIUS — DATE 2013/08/07
CHECKED : R. VAN DER MERWE — DATE
ENGINEER : J.H. KOEKEMOER — DATE
SCALE : 1:1 PROJ. — DWG. SIZE : A1

APEX PROCESS
TEL : +27-16-971 4480
FAX TO E-MAIL : +27-86-501 8422
E-MAIL : heidi@apexprocess.co.za
RIEKLAND OFFICE PARK BLOCK E
VAALPARK 1945
SOUTH AFRICA

VBV HOLDINGS
PULSATION VESSEL
GENERAL ARRANGEMENT

CLIENT DWG No. :	–	INTER. No.	REV. No.
APEX DWG.No. :	AP645-DME-001_01		
CLIENT ORDER No. :	12529	A3	A

F.4.2 Final design by VBV Holdings

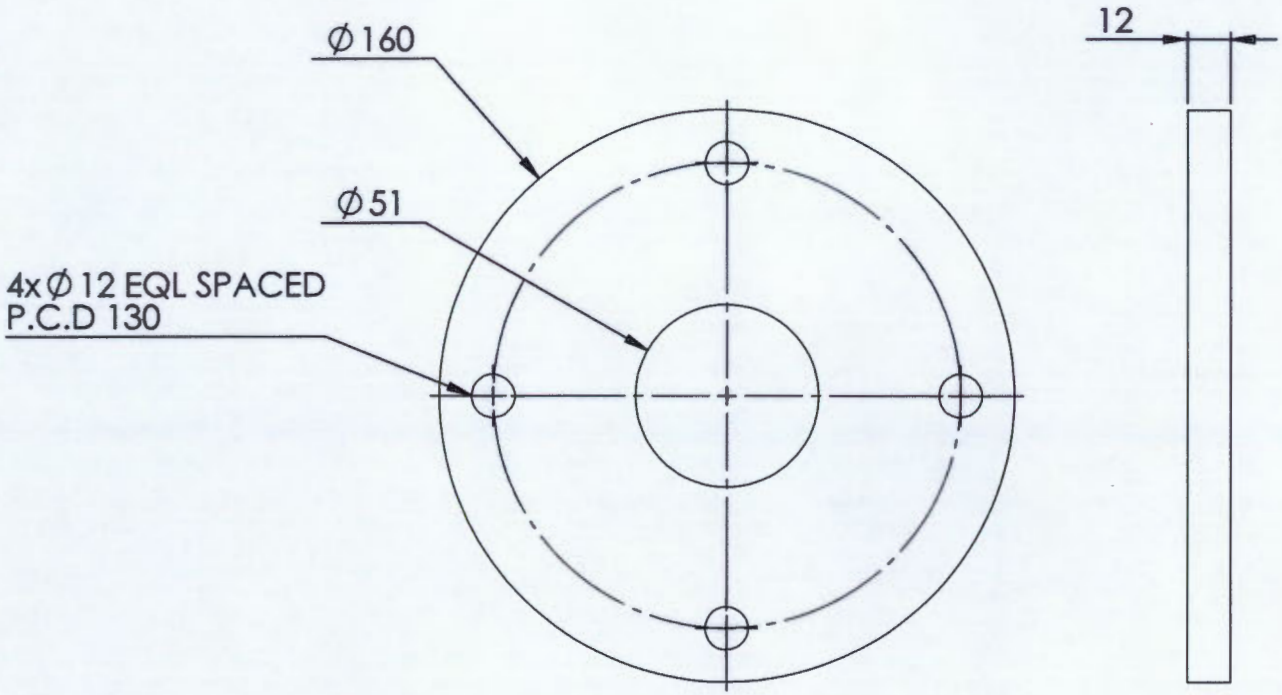

Critical Dimensions
All dimensions, excluding the flange thickness, are critical

Ideal flange design, mating back pressure valve uses a flange of this type.

A4 Landscape	University of Cape Town Department of Mechanical Engineering			
	Title: Flange Back pressure 160OD			
QTY 1	Scale: 1:20	Date: 2015/07/09	sheet4	of 4
Material: Boiler steel	Drawn By: Timothy Cole King		Drawing Number 4.3	

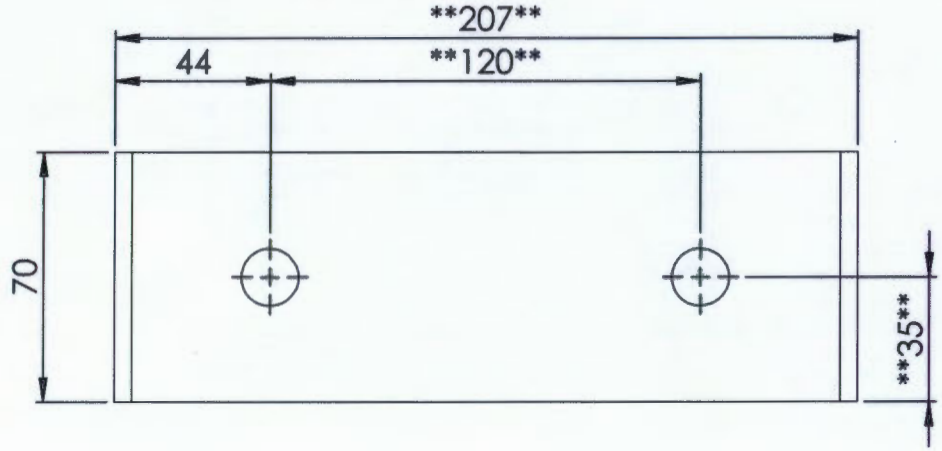

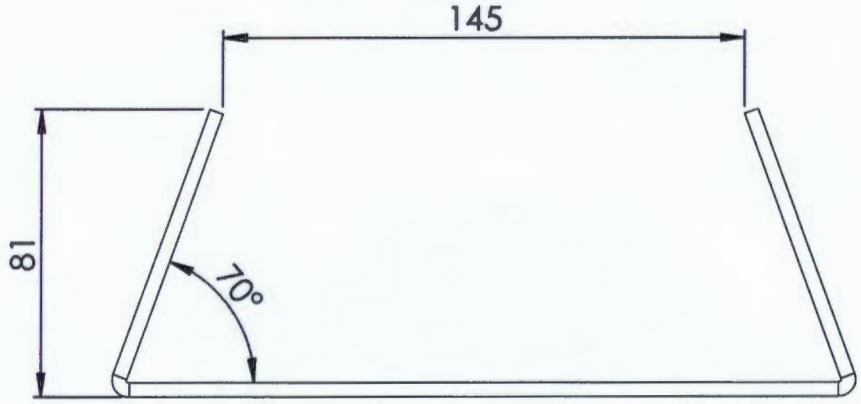

Critical Dimensions *(indicated by **dim**)*
Hole spacing:120mm

Hole vertical position from bottom: 35mm

Bracket length must be a maximum of 207mm due to stand bracket design.

Plate thickness to be used for mounting brackets to be detertmined at VBVholding's discretion depending on what the gross mass of the vessel comes out at. However, please insure that if the thickness is subjected to change the critical dimensions are kept the same.

A4 Landscape	University of Cape Town Department of Mechanical Engineering			
	Title: vessel mounting bracket			
QTY 1	Scale: 1:2	Date: 2015/07/09	sheet3	of 4
Material: Boiler steel	Drawn By: Timothy Cole King		Drawing Number 4.2	

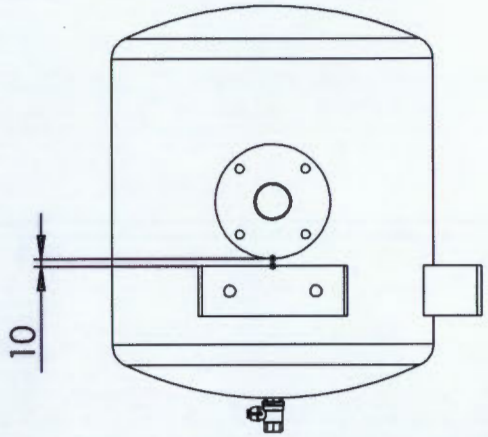

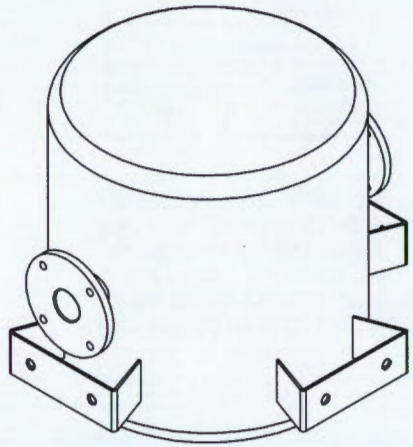

Isometric view of pulsation vessel

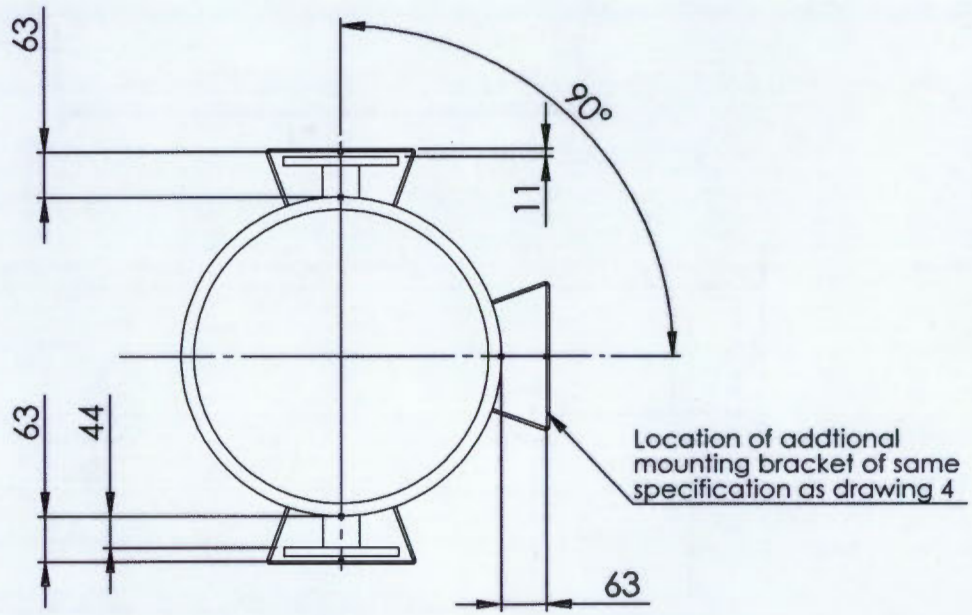

A4 Landscape	University of Cape Town Department of Mechanical Engineering			
	Title: Pulasation vessel Concept 3			
QTY 1	Scale: 1:20	Date: 2015/07/09	sheet2	of 4
Material: Boiler steel	Drawn By: Timothy Cole King		Drawing Number 4.1(b)	

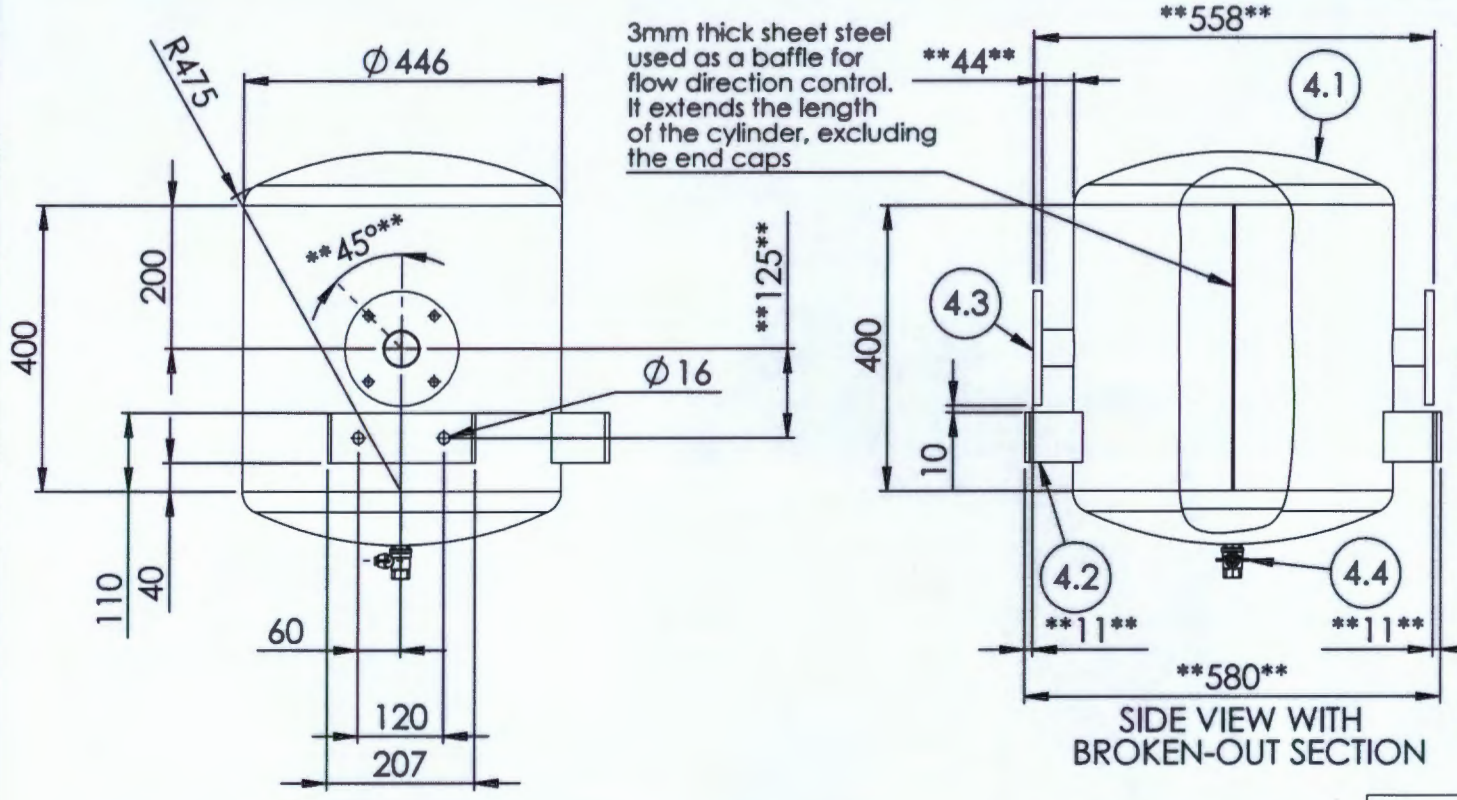

Critical Dimensions *(indicated by **dim**)*
Horizontal distance between flange and mounting bracket must be 11mm

Distance between flange and vessel must be at least 44mm

Flange hole positions relative to vessel must be as shown on drawing, note 45° dimension

Flange to flange distance: 558mm

Mounting bracket to mounting bracket: 580mm

Intake (and exhaust) centre line to mounting bracket hole: 125mm

Drawing changes
Vertical distance between flange perimeter and mounting bracket now indicated and increased to 10mm as per Gareth's instructions.

Addition of third mounting bracket at the same vertical height on vessel as the other two.

Note:
The volume of the vessel must be approximately 61L. Must have a drainage point indicated on the drawing by "2", the ball valve. The vessel must be able to withstand an operating pressure of 3 bar. The vessel must be usable at temperatures of approximately 750K as specified by Dr Floweday.
The tubing used on the inlet and outlet is standard 2" dairy type from NDE. The rest of the exhaust system will use the same tubing.

ITEM NO.	PART NUMBER	QTY.	Material
4.1	Pulsation Vessel concept 3	1	
4.2	vessel mounting bracket	3	
4.3	Flange Back pressure 160OD	2	
4.4	Ball valve	1	

A4 Landscape	University of Cape Town Department of Mechanical Engineering			
	Title: Pulasation vessel Concept 3			
QTY 1	Scale: 1:10	Date: 2015/07/09	sheet1	of 4
Material: Boiler steel	Drawn By: Timothy Cole King		Drawing Number 4.1(a)	

F.4 Pulsation vessel

F.4.1 Preliminary design

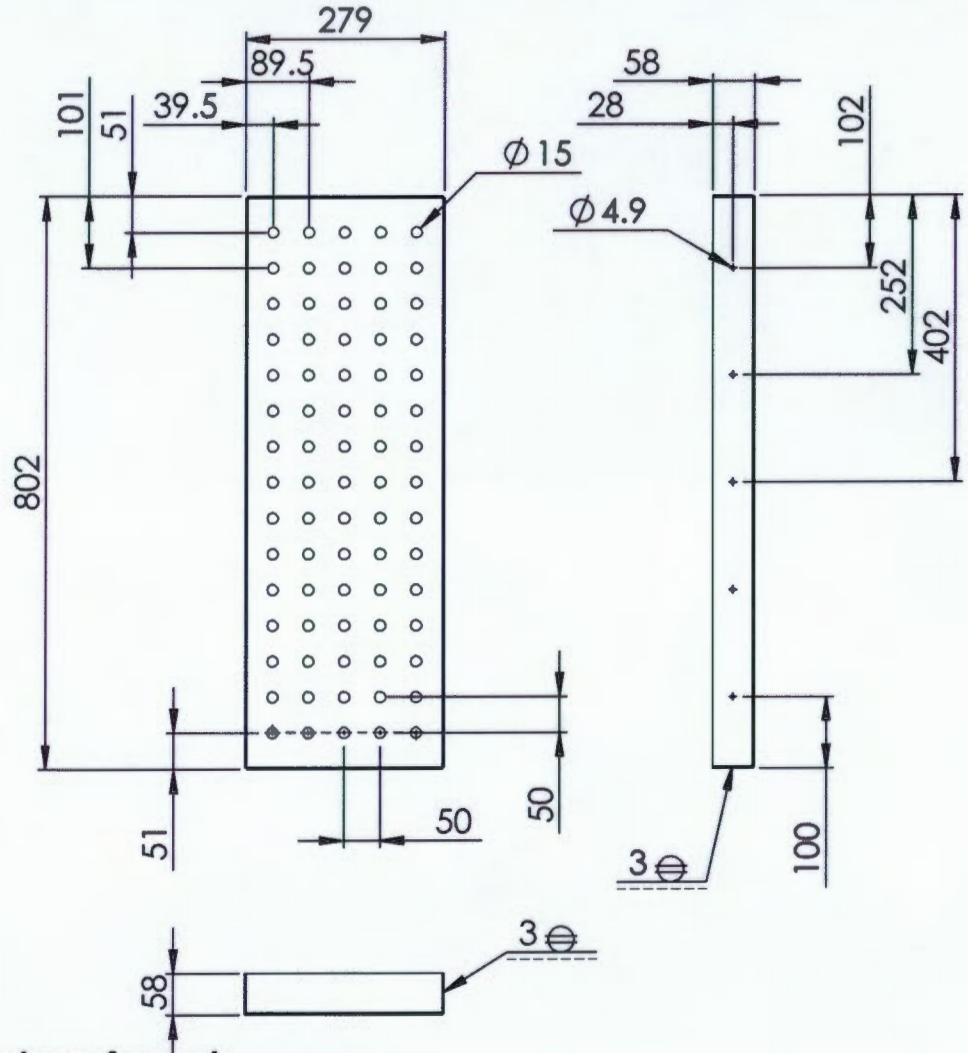

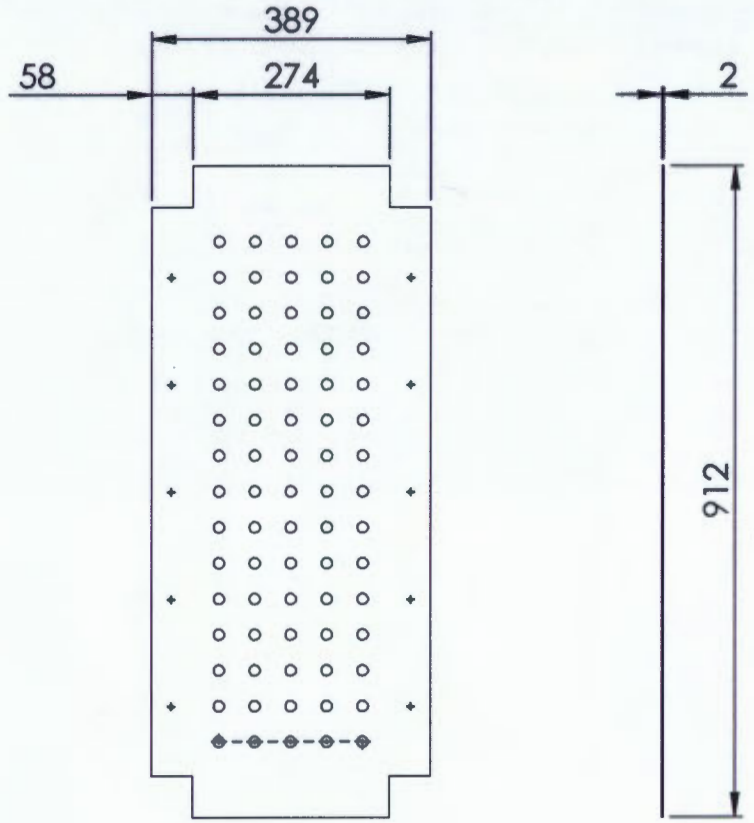

Flat pattern

Bent view of panel:
These dimensions are critical.
All bends are 90° with 1mm bend radius.
All bent edges are to be neatly seam welded together and cleaned if necessary
Note: outside (top) surfaces must have a polished finish

A4 Landscape	University of Cape Town Department of Mechanical Engineering			
	Title: Perferated panel			
QTY 2	Scale: 1:10	Date: 2015/07/09	sheet21	of 21
Material: 304 SS	Drawn By: Timothy Cole King		Drawing Number 3.3	

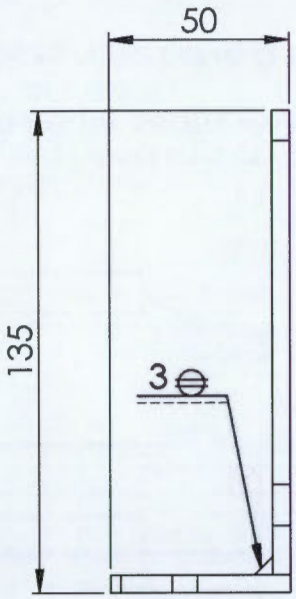

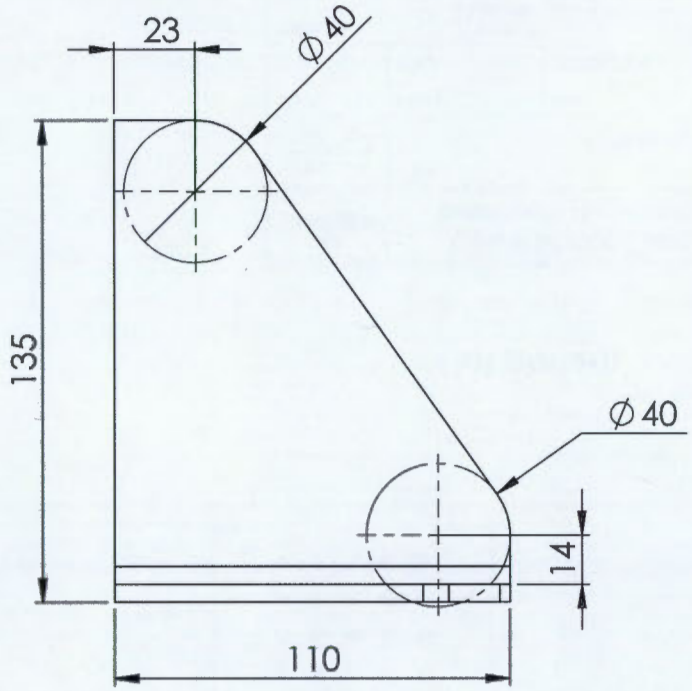

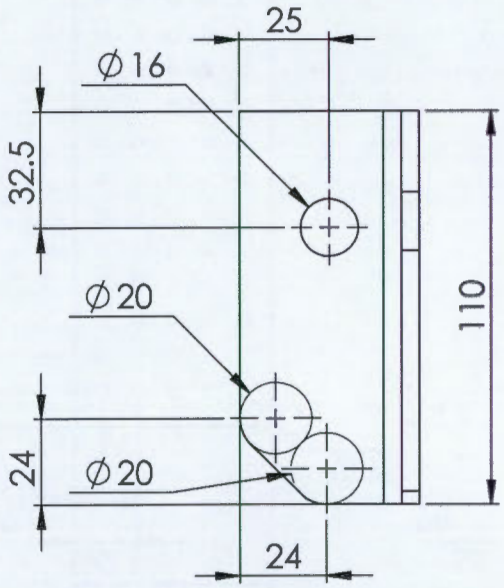

Two plates to be laser-cut and welded together (3mm fillet)

A4 Landscape	University of Cape Town Department of Mechanical Engineering			
	Title: Frame mounting foot assembly right			
QTY 2	Scale: 1:10	Date: 2015/07/09	sheet20	of 21
Material: LC_Steel	Drawn By: Timothy Cole King		Drawing Number 3.4.1.5	

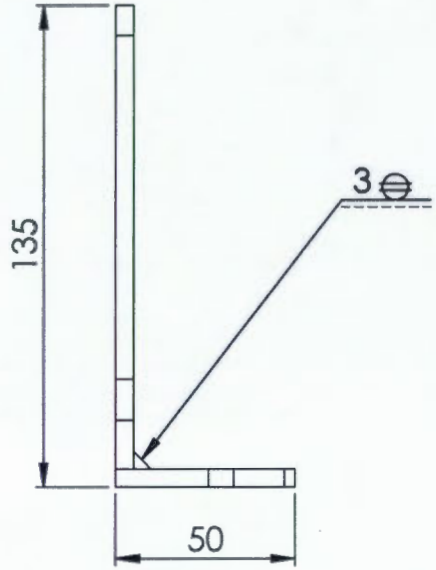

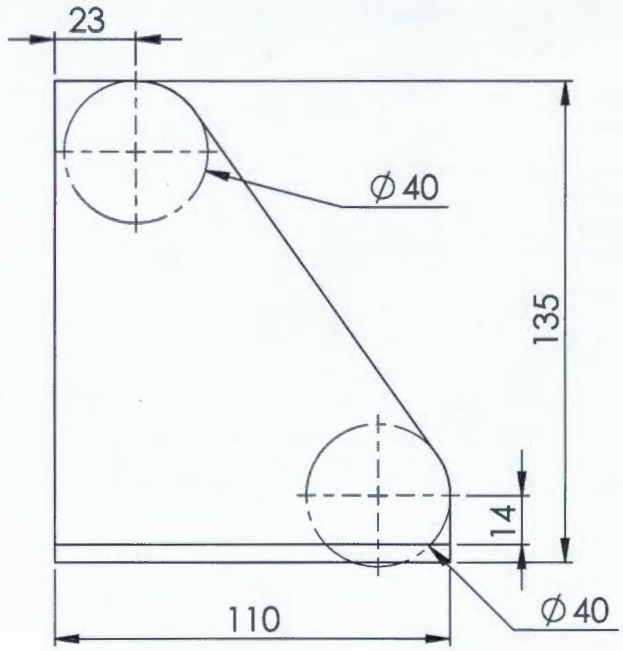

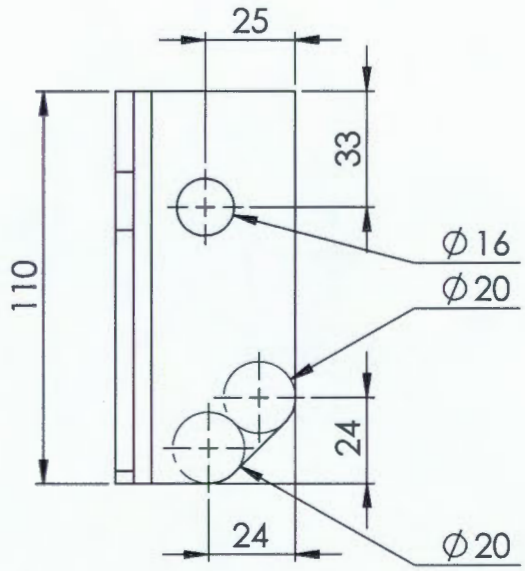

Two plates to be laser-cut and welded together (3mm fillet)

A4 Landscape	University of Cape Town Department of Mechanical Engineering			
	Title: Frame mounting foot assembly left			
QTY 2	Scale: 1:10	Date: 2015/07/09	sheet19	of 21
Material: LC_Steel	Drawn By: Timothy Cole King		Drawing Number 3.4.1.4	

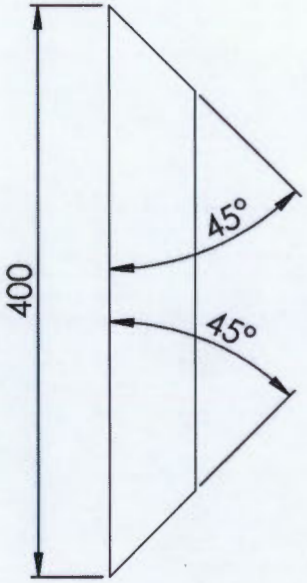

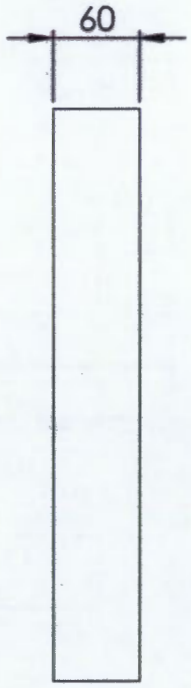

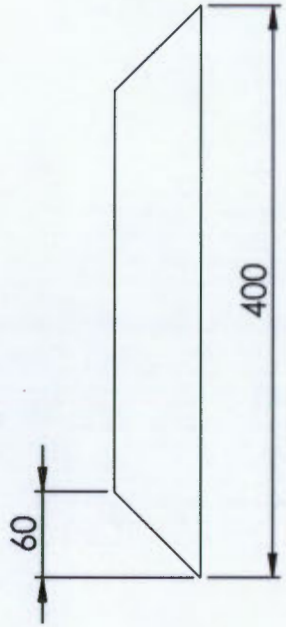

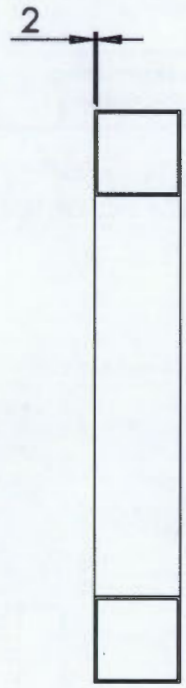

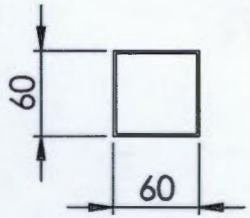

A4 Landscape	University of Cape Town Department of Mechanical Engineering			
	Title: 3 Frame top slat			
QTY 1	Scale: 1:20	Date: 2015/07/09	sheet18	of 21
Material: LC_Steel	Drawn By: Timothy Cole King		Drawing Number 3.4.1.3	